Adsorption of selected organic emerging chemical pollutants from aqueous media using graphene wool composites

by

Adedapo Oluwasanu Adeola

Submitted in partial fulfilment of the requirements for the degree

Doctor of Philosophy in Chemistry

In the Faculty of Natural & Agricultural Sciences
University of Pretoria

Supervisor: Prof P.B.C. Forbes

November 2021

Declaration

I, Adedapo Oluwasanu Adeola, declare that this thesis, which I hereby submit for the degree Doctor of Philosophy (Chemistry) at the University of Pretoria, is my work and has not previously been submitted by me for a degree at this or any other tertiary institution.

Signature: 

Date: November 2021

Acknowledgments

I count it a privilege and I am delighted as well to finally be able to submit this project as my contribution to the advancement of learning and research. To God be the glory!

Firstly, I want to appreciate my supervisor, Professor Patricia Forbes, for the unique opportunity to do my PhD studies with her research group, and for having an enormous faith in me. I am highly honoured for the opportunity to learn from her and for the unflinching support my supervisor has provided throughout the intense academic journey. I would not have wished for a better supervisor and mentor, in this lifetime or the next! I will forever be grateful.

I also want to express my immense gratitude to my family for all the love and support throughout this journey. I am grateful for the love, prayers, and understanding of my beloved wife, Motunrayo Adeola, my parents (Mr and Mrs Adeleke Adeola), and my siblings. I also appreciate the support of very close friends, Ayokunle Ige, Afolabi Afeez, Adeleke Jimoh, Ore Odunayo, Jide Buhari, Omoyajowo Blessing, Ogunyele Chris, Adedibu Sunny, Adetola Adewole, Dr Kabiru Oyedotun, Dr Kyesmen Pannan, Dr Ayodeji Ijagbuji, and others.

I extend my profound gratitude to my colleagues, who are essentially my friends during this program at the University of Pretoria, Dr Sifiso Nsibande, Dr Chiedza Munyeza, Kapambwe, Loreley, Ané, Wilmé, Amanda, Gugu and others. I want to specially thank Genna Schoonraad for developing the protocol for the synthesis of graphene wool and for being a good friend, as well as Dr Jurgens de Lange for assisting with the computational aspect of this project. You all will forever have a place in my heart! Thanks to Dr Yvette Naudé and Dr Madelien Wooding for the technical assistance I received while I was using the GC-MS and LC-MS instruments. You are all part of this success story.

In conclusion, I want to specifically thank the University of Pretoria Commonwealth Doctoral Scholarship and Rand Water for providing financial support for this project.

Summary

Polycyclic aromatic hydrocarbons (PAHs) and antiretroviral drugs (ARVDs) are emerging chemical pollutants that continue to pose significant health and ecotoxicological risks. Anthropogenic activities contribute to the release of these hazardous compounds into the environment and the adverse effects caused by these contaminants, even at low concentration and acute exposure, make them priority pollutants. There is a need for the development of novel materials and optimization of existing methods for the remediation of these pollutants, as conventional water treatment plants have not been able to satisfactorily deal with emerging organic chemical pollutants. Advances in remediation technologies and material science have allowed for the design of efficient and ecofriendly materials suitable for removal of organic pollutants even at trace concentration levels.

In this project, a comprehensive review of existing and emerging technologies for the mitigation of PAH pollution in water was conducted. Furthermore, the status of antiretroviral drugs in African surface water, toxicological impacts, and potential remediation strategies were assessed. Through these reviews, the current status of carbon-based/graphene-based materials as an efficient alternative adsorbent for the removal of antiretroviral drugs and PAHs from water was evaluated. It was discovered that there is scanty/no report on the development of adsorbents for the removal of ARVDs, especially those prevalent in Africa- namely efavirenz (EFV) and nevirapine (NVP). The underlying mechanisms of interaction between ARVDs and carbon-based materials has not been reported. Other knowledge gaps include the fact that regeneration and reusability is a major challenge for those adsorbents which have been tested for adsorption of PAHs, due to loss of active sites, difficulty in clean-up and retrieval of many nano-scale materials. Graphene wool is a novel material which was applied for the adsorption of chemical pollutants in water in this study for the first time.

Graphene is two-dimensional (2D) with sp^2 hybridized carbon atoms arranged hexagonally in a closely packed crystal lattice structure containing σ- and π-bonds. The large specific surface area, thermal stability, thermal conductivity, high tensile strength, chemical robustness, charge mobility, flexibility, and thin film thickness provide the

basis for the vast applications of graphene and its composites in many fields of science. In this study, a graphene wool composite was utilized for the adsorption of selected PAHs and ARVDs under variable conditions such as pH, concentration, ionic strength, and temperature. Sorption isotherms and sorption kinetic models were used to fit experimental data to elucidate the mechanism of interactions and predict conditions for optimum adsorption efficiency of the composites. The role of natural organic matter (NOM), which is a ubiquitous component of aquatic systems, was also studied and its impact on the mechanism of interaction and efficiency of the material was evaluated.

Generally, adsorption of PAHs by GW is best described by the Sips (Freundlich-Langmuir) model and the Freundlich multilayer adsorption mechanism for single-solute and competitive batch adsorption studies, and is mainly controlled by hydrophobic and π-π interactions. Thermodynamic studies of PAH adsorption revealed that the process is spontaneous and endothermic, with a negative value of Gibb's free energy (ΔG) and a positive value of adsorption enthalpy (ΔH). On the contrary, the adsorption of antiretroviral drugs, specifically EFV and NVP, is slightly more complex and the nature of interaction may vary for different types of ARVD due to the variations in chemical structure thereof. Similar to PAHs, ARVD adsorption onto GW was best described by Sips (EFV) and Freundlich (NVP) models. However, while GW-EFV interaction was endothermic, GW-NVP was exothermic. Several mechanisms such as hydrophobic, π-π, covalent, van der Waal's, and hydrogen bonding interactions are possible, depending on the molecular properties and conformations of the ARVD as revealed by supporting computational studies.

Furthermore, the study carried out on the influence of NOM on the adsorption of pyrene revealed that the mineral-rich fraction of NOM significantly diminished the removal efficiency of graphene wool, as both adsorption capacity (K_d) and efficiency reduced from 16.9 L g^{-1} and 95.4% to 0.3 L g^{-1} and 18.5%, respectively. Fractions with higher % organic carbon (natural sediment, black carbon and mineral deficient fractions) had higher maximum adsorption capacities for several PAHs. Aromaticity and hydrophobic moieties of the different PAHs and NOM significantly influenced the π-π and hydrophobic–organophilic interactions between sorbates and sorbents that may have occurred, which led to some degree of irreversible sorption as shown by hysteresis indices. Adsorption isotherm parameters suggested that GW adsorbed NVP slightly

better with stronger binding strength than EFV, with removal efficiencies of 84% (NVP) and 80% (EFV) under optimum conditions. The overall GW removal efficiencies of the target compounds (PAHs and ARVDs) in this project ranged from 81 – 100% under optimum conditions. It was reported that the removal efficiency is dependent on the choice of operational parameters, such as concentration of adsorbate and adsorbent dosage, etc.

Graphene wool doped with stabilized silver nanoparticles (GW-αAgNP) was synthesized and its adsorption capacity was evaluated using benzo(a)pyrene contaminated water. GW-αAgNP were found to have an adsorption capacity (K_d) and Sips maximum adsorption capacity (q_m) of 2.75 L g^{-1} and 97.62 μg g^{-1} respectively, much higher than GW with 0.93 L g^{-1} and 59.76 μg g^{-1} respectively. Furthermore, GW-αAgNP and GW were tested against Gram-negative and Gram-positive bacteria (*Pseudomonas aeruginosa* and *Bacillus subtilis*). While GW showed no significant inhibition at the concentrations tested, 1000 mg L^{-1} dosage of GW-αAgNP significantly inhibited the growth of both bacteria. This hybrid material thus has the potential to serve as a smart solution to chemical and microbiological water pollution.

This project demonstrated how advancement in material sciences could be harnessed for the development of novel solutions to environmental challenges and pollution remediation.

Publications

This thesis is based on the following papers:

1. Adeola, A.O., Forbes, P.B.C. (2021). Antiretroviral drugs in African surface waters: prevalence, analysis and potential remediation. Environmental Toxicology and Chemistry. https://doi.org/10.1002/etc.5127
2. Adeola, A.O., Forbes, P.B.C. (2021). Advances in water treatment technologies for removal of polycyclic aromatic hydrocarbons: Existing concepts, emerging trends, and future prospects. Water Environment Research, 93(3): 343-359. DOI: https://doi.org/10.1002/wer.1420 ***(Journal paper was selected as Editor's Choice- Appendix- page 226)***
3. Adeola, A.O., Forbes, P.B.C. (2019). Optimization of sorption of selected polycyclic aromatic hydrocarbons by regenerable graphene wool. Water Science and Technology, 80(10): 1931-1943. DOI: https://doi.org/10.2166/wst.2020.011
4. Adeola, A.O., Forbes, P.B.C. (2020). Assessment of reusable graphene wool adsorbent for the simultaneous removal of selected 2-6 ringed polycyclic aromatic hydrocarbons from aqueous solution. Environmental Technology. DOI: https://doi.org/10.1080/09593330.2020.1824024
5. Adeola, A.O., Forbes, P.B.C. (2021). Influence of natural organic matter fractions on PAH sorption by stream sediments and a synthetic graphene wool adsorbent. Environmental Technology and innovations, 21, 101202. DOI: https://doi.org/10.1016/j.eti.2020.101202
6. Adeola, A.O., de Lange, J., Forbes, P.B.C. Adsorption of antiretroviral drugs, efavirenz and nevirapine from aqueous solution by graphene wool: kinetic, equilibrium and thermodynamic studies. *Applied Surface Science Advances,* 6, 100157. https://doi.org/10.1016/j.apsadv.2021.100157
7. Adeola, A.O., Kubheka, G., Chirwa, E.M.N., Forbes, P.B.C Facile synthesis of graphene wool doped with oleylamine-capped silver nanoparticles (GW-αAgNPs) for water treatment applications. *Applied Water Science,* 11(11), 172. https://doi.org/10.1007/s13201-021-01493-3

Conference presentation

Adedapo O. Adeola and Patricia B.C. Forbes "Regenerable graphene wool for the removal of selected polycyclic aromatic hydrocarbons from contaminated water", 2nd Commonwealth Chemistry Posters - Building Networks to Address the Goals, Royal Society of Chemistry, 30 September - 1 October 2021, United Kingdom, online.

This poster presentation won the "best poster award" in the Water and Environmental Chemistry theme.

List of abbreviations

AgNP	Silver nanoparticle
AIDS	Autoimmune deficiency syndrome
APCVD	Atmospheric pressure chemical vapor deposition
ARVD	Antiretroviral drug
BC	Black carbon
CNS	Central nervous system
CVD	Chemical vapor deposition
DOC	Dissolved organic carbon
DPE	Diphenyl ether
D-R	Dubinin-Radushkevish
EC	Effective concentration
ECP	Emerging chemical pollutant
EFV	Efavirenz
FTIR	Fourier-transform infrared
GBM	Graphene-based material
GC-MS	Gas chromatography-mass spectrometry
GNS	Graphene nanoshell
GO	Graphene oxide
GS	Graphene sheets
GW	Graphene wool
GW-AgNP	Graphene wool-silver nanocomposite
HIV	Human immunodeficiency virus
HMW	High molecular weight
IARC	International Agency for Research on Cancer
IC	Inhibition concentration
IS	Internal standard
LC	Liquid chromatography
LMW	Low molecular weight
LOD	Limit of detection
LOQ	Limit of quantitation

MDF	Mineral-deficient fraction
MIP	Molecularly imprinted polymer
MRF	Mineral-rich fraction
NAS	Natural sediment
nNRTI	Non-nucleoside reverse transcriptase inhibitor
NOM	Natural organic matter
NVP	Nevirapine
OA	Oleic acid
OCP	Organic chemical pollutant
OD	Optical density
OLA	Oleylamine
PAH	Polycyclic aromatic hydrocarbon
PCPP	Pharmaceutical and personal care product
PFOA	Perfluorooctanoic acid
PFOS	Perfluorooctane sulphonate
POP	Persistent organic pollutant
PZNC	Point zero net charge
RGO	Reduced graphene oxide
RSD	Relative standard deviation
SD	Standard deviation
SDG	Sustainable development goal
SEM	Scanning electron microscopy
SOC	Soil organic carbon
TEF	Toxic equivalence factor
TEQ	Toxic equivalence quotient
TEM	Transmission electron microscopy
UPLC-MS	Ultra-performance liquid chromatography-mass spectrometry
US EPA	United States Environmental Protection Agency
US FDA	United States Food and Drug Administration
WHO	World Health Organization
WWTP	Wastewater treatment plant
XPS	X-ray photoelectron spectroscopy
XRD	X-ray diffraction

Table of contents

List of figures

Chapter 2

Chapter 3

Paper 1

Paper 2

Chapter 4

Chapter 5

Chapter 6

Chapter 7

Chapter 8

List of tables

Chapter 2

Chapter 3

Paper 1

Paper 2

Chapter 4

Chapter 5

Chapter 6

Chapter 7

Chapter 8

Appendix

Chapter 1 Background and Motivation

In this chapter, an overview of the problems which motivated this study is given. In addition, the aim and objectives together with the context of the thesis are presented.

1.1 Problem statement and motivation

Clean and potable water is regarded as one of the fundamental needs of life, especially for the sustainance of humans, plants, and animals. This is corroborated by the United Nations Sustainable Development Goals (SDG 6), which affirms that access to safe water, sanitation and efficient management of water resources are pivotal to healthy living, sustainable ecosystems, and economic development (Griggs et al., 2013). The global demand for clean and potable water is on the increase due to the ever-increasing world population, advancement in technology, civilization, and industrialization (Onda et al., 2012). In most developing countries of the world, especially in Sub-Saharan Africa and Asia, there is a shortfall in potable water, due to high demand, poverty, and inadequacies in water treatment technologies.

Emerging chemical pollutants (ECPs) are pollutants existing in different environmental compartments, which are not routinely monitored and are not regulated, however, there are growing concerns regarding the potential hazards caused by these compounds (Liu et al., 2014, Richardson and Kimura, 2017). Emerging chemical pollutants (ECPs) may subject ecosystems to unprecedented strain, due to their mobility and the ability of some ECPs to bioaccumulate in non-target environments. ECPs include polycyclic aromatic hydrocarbons (PAHs), pharmaceuticals, personal care products, industrial additives, pesticides, etc. (Fayiga et al., 2018). PAHs are ubiquitous organic pollutants and their occurrence in environmental compartments is due to several natural and anthropogenic activities, such as pyrolysis of organic matter, industrial effluents, use/burning of fossil fuel, etc. (Abdel-Shafy & Mansour, 2016; Gallego et al., 2008; Manoli & Samara, 1999; Torabian et al., 2010). To date, PAHs do not have a regulatory status in several parts of the world, including South Africa, which is the reason for their classification as emerging chemical pollutants (Pal et al., 2010). Pharmaceutical products, such as antiretroviral drugs (ARVDs), are regarded as emerging chemical pollutants (Gavrilescu et al., 2015; Patel et al., 2019). The concentration of antiretroviral drugs in water bodies has been found to be increasing due to the widespread use of the drugs in HIV treatment (Ngqwala and Muchesa, 2020; Adeola and Forbes, 2021a). Furthermore, high concentrations are reported in wastewater treatment plant (WWTP) effluents leading to concerns about the efficiency thereof (Wood et al., 2016; Russo et al., 2018).

Different adsorbents have been developed for the remediation of PAHs and several pharmaceutical compounds in an aqueous medium. Graphene-based materials (GBMs) have been harnessed as efficient next-generation sorbents for water purification applications because their surface is largely hydrophobic, porous, and they possess high adsorption affinities for a vast number of organic contaminants (OCs) (Ali et al., 2019; Xu et al., 2013, Adeola and Forbes, 2021b). However, the application of graphene wool for PAH remediation and the removal of antiretroviral drugs (ARVDs) using any graphene-based material (GBM) has not been reported until now.

It is almost impracticable to rapidly restore heavily polluted water to its pristine state, thus, the development of a suitable remediation approach based on a detailed risk assessment may prove to be most appropriate for the management of severely polluted water. Emerging technologies must seek to surmount challenges related to removal efficiency, ease of application, reusability, generation of secondary pollutants, etc., in order to develop a sustainable approach for remediation of water contaminated with hazardous pollutants, such as PAHs and ARVDs.

1.2 Aim and objectives of the thesis

1.2.1 General aim

The primary aim of this research was to synthesize graphene wool composites for water treatment applications, with primary focus on the removal of selected polycyclic aromatic hydrocarbons (PAHs) and antiretroviral drugs (ARVDs).

1.2.2 Objectives

i. To synthesize and characterize graphene wool (GW) composites using established analytical methods.
ii. To conduct sorption experiments with selected PAHs and ARVDs (efavirenz and nevirapine) as target aqueous pollutants, and graphene wool as adsorbent.
iii. To establish the optimum process conditions (considering variables such as pH, time, temperature, the initial concentration of pollutants, adsorbent dosage, ionic strength) for optimum adsorption efficiency of the synthesized GW adsorbent.
iv. To isolate different natural organic matter (NOM) fractions from stream sediments and evaluate the influence of NOM on the adsorption of selected PAHs.

v. To carry out the regeneration of the adsorbent and perform reusability tests.
vi. To synthesize and characterize graphene wool doped with lipopeptide-capped silver nanoparticles (GW-αAgNP) for adsorption of benzo(a)pyrene.
vii. To evaluate the antimicrobial activity of the synthesized GW-αAgNP composite for potential dual functionality as an adsorbent and biocide.

1.3 Context of the thesis/Thesis layout

Chapter 2 presents the target environmental pollutants and highlights their environmental significance. This chapter includes a general overview of adsorption, factors influencing adsorption of organic pollutants, and several models of adsorption. Graphene-based materials are discussed, including the synthesis of graphene wool (GW), doped GW, and a brief description of characterization techniques.

Chapter 3 This chapter contains two literature reviews. **Paper 1** focuses on established remediation options available for PAH-contaminated water. A concise outlook is provided into established and emerging technologies such as adsorption, electrokinetic remediation, advanced phytoremediation, green nanoremediation, enhanced remediation using biocatalysts, and integrated approaches. **Paper 2** presents the reported concentrations of antiretroviral drugs (ARVDs) in aquatic systems and toxicity thereof from an African perspective. Moreover, insight was provided into the adsorption of ARVDs using carbon-based adsorbents as a potential remediation strategy, as well as analytical techniques for the determination of ARVDs in different environmental compartments.

Chapter 4 (Paper 3) described the adsorption of phenanthrene (PHEN) and pyrene (PYR) onto graphene wool (GW). The paper investigated the optimum conditions for PAH adsorption onto GW in a single-solute batch sorption experiment and efficiency was compared with different adsorbents used for PHEN and/or PYR adsorption in literature. The reusability of the novel adsorbent was also examined via several cycles of regeneration and reuse.

Chapter 5 (Paper 4) reported the simultaneous sorption of fifteen polycyclic aromatic hydrocarbons (PAHs) onto graphene wool (GW) in a competitive adsorption

environment via multi-solute experiments. Specific attention was directed towards the role of adsorbent dosage and PAH hydrophobicity on the adsorption capacity of GW.

Chapter 6 (**Paper 5)** reported the isolation and characterization of fractions of natural organic matter (NOM) recovered from stream sediment. The sorption of selected PAHs onto different fractions of NOM was evaluated. The impact of NOM on solution chemistry and the inhibitory influence of NOM on the PAH removal efficiency of graphene wool (GW) was reported.

In **Chapter 7 (Paper 6)**, the adsorption of selected ARVDs (efavirenz and nevirapine) using the synthesized graphene wool adsorbent was studied under different concentrations, pH, and temperature. The plausible mechanisms of interaction between the different antiretroviral drugs and graphene wool adsorbent was evaluated using experimental and computational studies.

In **Chapter 8 (Paper 7)** graphene wool (GW) was doped with lipopeptide-stabilized silver nanoparticles (AgNP) and characterized. GW-αAgNP was applied to remove benzo(a)pyrene (often regarded as the most carcinogenic PAH) from water. Furthermore, due to the antimicrobial properties of AgNPs and adsorption capacity of GW, the potential dual application of GW-αAgNP as an adsorbent and microbial growth inhibitor/biocide was evaluated.

In **Chapter 9,** the overall conclusion and future work was presented.
Note: The chapters where the work has been published are presented in journal article format, i.e. as published.

1.4 References

Abdel-Shafy, H.I., Mansour, M.S.M., 2016. A review on polycyclic aromatic hydrocarbons: Source, environmental impact, effect on human health and remediation. Egyptian Journal of Petroleum, 25, 107-123. https://doi.org/10.1016/j.ejpe.2015.03.011

Adeola, A.O., Forbes, P.B.C, 2021a. Antiretroviral drugs in African surface waters: prevalence, analysis and potential remediation, Environmental Toxicology and Chemistry. https://doi.org/10.1002/etc.5127

Adeola, A.O., Forbes, P.B.C, 2021b. Advances in water treatment technologies for removal of polycyclic aromatic hydrocarbons: Existing concepts, emerging trends, and future prospects. Water Environment Research. 93 (3), 342-359. https://doi.org/10.1002/wer.1420.

Ali, I., Basheer, A.A., Mbianda, X.Y., Burakov, A., Galunin, E., Burakova, I., Mkrtchyan, E., Tkachev, A., Grachev, V., 2019. Graphene based adsorbents for remediation of noxious pollutants from wastewater. Environment International, 127, 160-180. https://doi.org/10.1016/j.envint.2019.03.029

Fayiga, A.O., Ipinmoroti, M.O., Chirenje, T. 2018. Environmental pollution in Africa. Environment Development and Sustainability, 20, 41–73. https://doi.org/10.1007/s10668-016-9894-4

Gallego, E., Roca, F.J., Perales, J.F., Guardino, X., Berenguer, M.J., 2008. VOCs and PAHs emissions from creosote-treated wood in a field storage area. Science of The Total Environment, 402, 130-138. https://doi.org/10.1016/j.scitotenv.2008.04.008

Gavrilescu, M., Demnerová, K., Aamand, J., Agathos, S., Fava, F., 2015. Emerging pollutants in the environment: present and future challenges in biomonitoring, ecological risks and bioremediation. New Biotechnology, 32, 147-156. https://doi.org/10.1016/j.nbt.2014.01.001

Griggs, D., Stafford-Smith, M., Gaffney, O., Rockström, J., Öhman, M.C., Shyamsundar, P., Steffen, W., Glaser, G., Kanie, N., Noble, I., 2013. Sustainable development goals for people and planet. Nature, 495, 305-307. https://doi.org/10.1038/495305a

Liu, Q., Zhou, Q., Jiang, G., 2014. Nanomaterials for analysis and monitoring of emerging chemical pollutants. TrAC Trends in Analytical Chemistry, 58, 10-22. https://doi.org/10.1016/j.trac.2014.02.014

Manoli, E., Samara, C., 1999. Polycyclic aromatic hydrocarbons in natural waters: sources, occurrence and analysis. TrAC Trends in Analytical Chemistry, 18, 417-428. https://doi.org/10.1016/S0165-9936(99)00111-9

Ngqwala, N.P, Muchesa, P. 2020. Occurrence of pharmaceuticals in aquatic environments: A review and potential impacts in South Africa. South African Journal of Science, 116(7/8). https://doi.org/10.17159/sajs.2020/5730

Onda, K., LoBuglio, J., Bartram, J., 2012. Global Access to Safe Water: Accounting for Water Quality and the Resulting Impact on MDG Progress. International Journal of Environmental Research and Public Health, 9(3), 880-894. https://doi.org/10.12927/whp.2013.23437

Pal, A., Gin, KY-H., Lin, AY-C., Reinhard, M., 2010. Impacts of emerging organic contaminants on freshwater resources: Review of recent occurrences, sources, fate and effects. Science of The Total Environment 408, 6062-6069. https://doi.org/10.1016/j.scitotenv.2010.09.026

Patel, M., Kumar, R., Kishor, K., Mlsna, T., Pittman, C.U., Mohan, D. 2019. Pharmaceuticals of Emerging Concern in Aquatic Systems: Chemistry, Occurrence, Effects, and Removal Methods. Chemical Reviews, 119, 3510-3673. https://doi.org/10.1021/acs.chemrev.8b00299

Richardson, S.D., Kimura, S.Y., 2017. Emerging environmental contaminants: Challenges facing our next generation and potential engineering solutions. Environmental Technology & Innovation, 8, 40-56. https://doi.org/10.1016/j.eti.2017.04.002

Russo, D., Siciliano, A., Guida, M., Andreozzi, R., Reis, N.M., Li Puma, G., Marotta, R., 2018. Removal of antiretroviral drugs stavudine and zidovudine in water under UV254 and UV_{254}/H_2O_2 processes: Quantum yields, kinetics and ecotoxicology assessment. Journal of Hazardous Materials, 349, 195-204.

Torabian, A., Kazemian, H., Seifi, L., Bidhendi, G.N., Azimi, A.A., Ghadiri, S.K., 2010. Removal of Petroleum Aromatic Hydrocarbons by Surfactant-modified Natural Zeolite: The Effect of Surfactant. CLEAN – Soil, Air, Water, 38, 77-83. https://doi.org/10.1002/clen.200900157

Wood, T.P., Basson, A.E., Duvenage, C., Rohwer, E.R., 2016. The chlorination behaviour and environmental fate of the antiretroviral drug nevirapine in South African surface water. Water Research, 104, 349-360. https://doi.org/10.1016/j.watres.2016.08.038

Wooding, M., Rohwer, E.R., Naudé, Y., 2017. Determination of endocrine disrupting chemicals and antiretroviral compounds in surface water: A disposable sorptive sampler with comprehensive gas chromatography – Time-of-flight mass spectrometry and large volume injection with ultra-high performance liquid chromatography–tandem mass spectrometry. Journal of Chromatography A, 1496, 122-132. https://doi.org/10.1016/j.chroma.2017.03.057

Xu, J., Lv, H., Yang, S.-T., Luo, J., 2013. Preparation of graphene adsorbents and their applications in water purification. Reviews in Inorganic Chemistry, 33, 139-160. https://doi.org/10.1515/revic-2013-0007

Chapter 2 Introduction

This chapter provides a general overview of the sources, fate, and toxicities of the target pollutants relevant to this study. Furthermore, principles of adsorption, adsorption models, and factors influencing the adsorption of organic chemical pollutants are presented. Finally, the synthesis and characterization of the graphene wool composites used in this project are briefly described.

2.1 Background

Emerging chemical pollutants (ECPs) include a wide spectrum of chemicals which do not have a regulatory status, but may adversely affect human health and the environment (Liu et al., 2014). They include polycyclic aromatic hydrocarbons (PAHs), flame retardants, industrial additives, perfluorinated compounds (PFOS/PFAS), personal care products and pharmaceuticals, such as antiretroviral drugs (Richardson and Kimura, 2017).

The occurrence of ECPs in environmental compartments has become an area of concern in environmental science. PAHs have been monitored in different environmental matrices such as water, air, soil, food, and beverages, yet continue to be of concern (Forbes and Rohwer, 2009; Munyeza et al., 2018; Zelinkova and Wenzl, 2015). PAHs are ubiquitous environmental pollutants that are potentially carcinogenic and mutagenic. They are widely distributed in the environment thus making human exposure almost unavoidable (IARC, 2010). Antiretroviral drugs (ARVDs) are therapeutic agents for the treatment of retroviral infections, primarily the human immunodeficiency virus type 1 (HIV-1) (Wood et al., 2015; Abafe et al., 2018; Ncube et al., 2018). ARVDs are of environmental concern due to the lack of a comprehensive ecotoxicological profile and regulatory measures, and they may impact water quality, flora, fauna, and human health.

Contaminated water can be treated in several ways based on the target pollutant, however, adsorption processes have been widely applied and possess several advantages over other techniques, such as ease of operation, less sludge and secondary pollutant formation, reduced chemical usage, easy recovery of adsorbents, reusability, etc. (Cohen-Tanugi and Grossman, 2012; Kemp et al., 2013; Shannon et al., 2008). Previous attempts have been made to remove PAHs from contaminated water but there are challenges such as chemical fouling, cost-effectiveness, loss of efficiency, and regeneration challenges (Zhang et al., 2013; Zheng et al., 2016). ARVDs have been detected in surface water and wastewater in South Africa and other parts of the world (Wood et al., 2015), yet there is no report to date on how to efficiently remove ARVDs from water.

The adsorption process is a surface phenomenon that involves the adherence of pollutants onto the surface of an adsorbent via physical, chemical, and/or electrostatic attraction. Adsorption of organic compounds can be influenced by many process variables such as temperature, pH, the concentration of sorbate, contact time, sorbent particle and pore size, and other physicochemical properties of the adsorbate and adsorbent (Adeola and Forbes, 2019, 2020; Site, 2001). Several materials have been developed over the last two decades for the sorption of PAHs from aqueous systems, many of which are discussed and compared in **Chapter 3.**

2.2 Environmental significance of polycyclic aromatic hydrocarbons (PAHs)

2.2.1 Sources of PAHs

PAHs are ubiquitous organic environmental contaminants that can be found in different environmental compartments. PAHs are generated mainly through the combustion of organic compounds (e.g. petrochemicals, coal, oil, and wood). Some PAHs emanate from natural occurrences, such as bush/forest fires, volcanic eruption/emissions, seepage from petroleum and coal deposits **(Figure 1)** (Hussain et al., 2018). However, emissions due to anthropogenic activities such as coal gasification, mineral exploration/mining, production of coal-tar and carbon black, catalytic cracking of asphalt and coke, petroleum refining, and other related activities, as well as motor vehicle exhausts, are responsible for a larger percentage of environmental pollution caused by PAHs (Abdel-Shafy and Mansour, 2016). Transformation derivatives with nitro-, oxy- and hydroxy-groups may also contribute a large fraction to the total PAHs in the air (Lammel, 2015).

PAHs are classified into three broad classes based on their sources namely, pyrogenic, petrogenic and biological (Hussain et al., 2018). ***Pyrogenic*** PAHs are formed by pyrolysis of organic materials at high temperatures under conditions of little or no oxygen (Balmer et al., 2019). Pyrogenic PAHs are generated during the destructive distillation of coal, cracking of petroleum, incomplete combustion of fuels in vehicle engines and household cooking devices (Hussain et al., 2018; Munyeza et al., 2020). ***Petrogenic*** PAHs are formed during the generation of crude oil and gas from organic matter under suitable pressure and temperature (crude oil maturation). The environment is exposed to these PAHs as a result of the transportation, leakage of storage tanks, and the use of crude oil and petrochemical products (Zakaria et al., 2002). Furthermore, there have been strong indications that PAHs are produced ***biologically***

as well (Wilcke et al., 2000; 2002). For example, they can be synthesized by certain plants and bacteria or are formed during the degradation of vegetative matter. Termites have been reported to generate PAHs in relatively small quantity, and the occurrence of selected PAHs, such as naphthalene, phenanthrene, and perylene in termite nests and plants corroborates the assumption that PAHs are produced biologically (Krauss et al., 2005).

Accidental oil spills have taken place in several parts of the world, leading to the release of large amounts of crude oil into the highly susceptible aquatic environment. Worthy of note is the infamous Deepwater Horizon Oil Spill, in which over 4.9 million barrels of crude oil was released into the Gulf of Mexico between 20 April and 15 July 2010 (McNutt et al., 2012; Romero et al., 2018).

2.2.2 Fate and toxicity of PAHs

Polycyclic aromatic hydrocarbons possess two or more fused aromatic rings with a pair of carbon atoms shared between rings and arranged in linear, angular, and cluster orientations (Arey and Atkinson, 2003; Abdel-Shafy and Mansour, 2016). Generally, PAHs are characterized by low vapor pressures, low solubility in water, high melting point and boiling points; with direct proportionality of these properties to the molecular weight of the PAHs (Balmer et al., 2019). The environmental fate of PAHs includes volatilization, adsorption, photodegradation, biodegradation, etc., which are controlled by several biotic and abiotic factors (**Figure 1**) (Ghosal et al., 2016). The distance travelled by PAHs in the particulate and vapor phase in air is influenced by chemical reactions and climatic factors (Harrison et al., 1996). For example, in South Africa, airborne PAHs were analyzed in platinum mines and higher concentrations in the range of 0.01 – 18 μg m^{-3} was reported in the gaseous phase than particle phase (0.47 to 260 ng m^{-3}) (Geldenhuys et al., 2015). The average gaseous PAH concentration in rural households in Kenya, ranged from 0.81 to 6.09 μg m^{-3}, much lower than urban homes (ranging from <LOD to 2.59 μg m^{-3}), while ambient air PAH concentrations were higher in urban environments, which can be attributed to increased anthropogenic activities (Fang et al., 2004; Munyeza et al., 2020).

Marine environments receive PAHs from wastewater treatment plants, stormwater runoff, petroleum spills, natural seeps, commercial ships, sewage effluents, volcanoes,

and atmospheric deposition by the action of rainfall, etc. Degradation of PAHs in water occurs via photooxidation and chemical oxidation (Abde-Shafy and Monsour, 2016). Photodegradation of PAHs also occurs in water via direct and indirect photolysis, or photocatalyzed reactions in the presence of excited species such as singlet-state oxygen ($^1O_2$), hydroxyl radical ($^{\cdot}OH$), and other reactive species found in natural waters (Fasnacht and Blough, 2002). Dissolved organic carbon (DOC) also promotes the photodegradation of low molecular weight (LMW) PAHs by ensuring the formation of suitable intermediates (Shang et al., 2015). PAHs strongly interact with organic matter and soot-like carbon, thus contributing to their sequestration, mobility, and persistence in the terrestrial compartment. The mobility of PAHs in soils is influenced by soil organic carbon (SOC) (Luo et al., 2012).

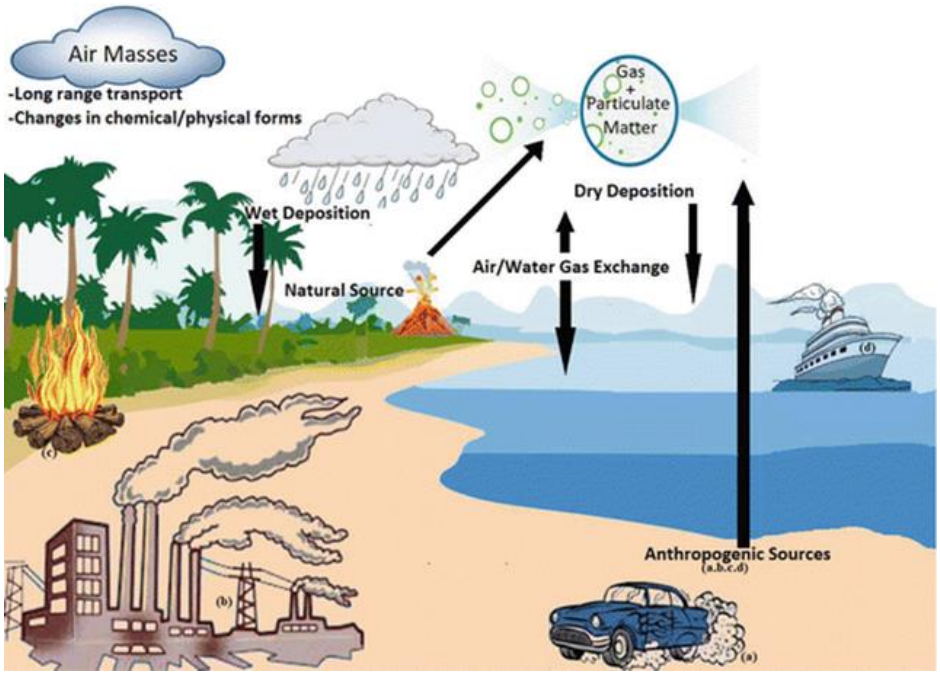

Figure 1. *The fate of PAHs in the environment (Hussain et al., 2018)*

Some marine microorganisms, plants, and animals can metabolize ingested PAHs (Abde-Shafy and Monsour, 2016). Bioaccumulation of PAHs in aquatic species occurs due to poor metabolic abilities, high lipid content, and high concentrations of PAHs (Abdel-Shafy and Mansour, 2016). Recalcitrance to biological transformation is more common with high molecular weight (HMW) PAHs with 4 – 7 rings, and due to their hydrophobic nature, they tend to bind to sediments (Lukić et al., 2016). Turbulence and agitation by boating, explorations, and shoreline activities, may lead to desorption of

PAHs from sediments and re-entry of recently deposited or concentrated PAHs to the aqueous phase (Balmer et al., 2019). Residence time for PAHs in sediments could be several decades, much longer than in air, if the sediment is undisturbed. This implies that PAHs are more persistent in the marine environment than in the atmosphere.

PAHs and their derivatives have harmful effects on aquatic plants and animals when they bioaccumulate according to the United States Environmental Protection Agency (US EPA) (USEPA, 2010). PAHs are nonpolar hydrocarbons which are highly soluble in lipids, and thus readily transport within the gastrointestinal tract of animals and humans (Balcıoğlu, 2016; Honda and Suzuki, 2020). The distribution of PAHs in body tissues is rapid with high potential to bioaccumulate in body fat (Abdel-Shafy and Mansour, 2016). PAHs are metabolized in mammals, with the first step being oxidation or hydroxylation via the cytochrome P450-enhanced mixed-function oxidase system (Bekki et al., 2013). Some PAHs cause mutations, reproductive defects, cancerous growth, etc. (Malakahmad et al., 2016). In humans, toxicities such as immunotoxicity, teratogenicity, cardiotoxicity, and mutagenicity, have been attributed to prolonged exposures to PAHs according to International Agency for Research on Cancer (IARC) (IARC, 2010). The toxic equivalency factors (TEF) of six high molecular weight PAHs and their relative cancer potency are shown in **Table 1**.

Table 1. Relative toxicity and cancer potency of selected PAHs according to US EPA and IARC (Nisbet and LaGoy, 1992; Patra 2003)

PAH compounds	Toxic equivalency factors	Relative cancer potency
Benzo (a)pyrene	1.0000	1.0000
Chrysene	0.0100	0.0044
Benzo(k)fluoranthene	0.1000	0.0200
Benzo(a)anthracene	0.1000	0.1450
Benzo(a)fluoranthene	0.1000	0.1670
Dibenzo(a,h)anthracene	5.0000	1.1100

2.3 Antiretroviral drugs (ARVDs) in the environment

The United States Food and Drug Administration (US FDA) has approved over 20 antiretroviral drugs, and many more are in clinical trials (Jain et al., 2011). The different classes of ARVDs currently in use, generic and brand names as of 2020 are presented in **Appendix-table 1. Table 2** presents the basic properties of efavirenz and nevirapine selected as target pollutants in this research, due to their established presence in surface waters in South Africa (Adeola and Forbes, 2021a).

Table 2. Compound names, CAS numbers, mass to charge ratio of ions, collision energies, and predicted Log Kow and pKa values of antiretroviral drugs (ARVDs) of relevance to this research (Wood et al., 2015)

Name (CAS No.)	Structure	m/z (collision energy eV)	Log Kow	pKa
Efavirenz (154598-52-4)	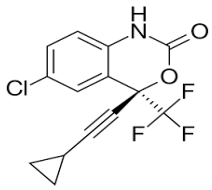	299.1 (0)	4.15	12.52
Nevirapine (129618-40-2)	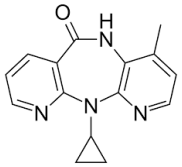	226 (24)	3.89	10.37

pKa: acid-dissociation constant of a weak acid; Log Kow: octanol-water partition coefficient

Different antiretroviral drugs have been detected in several surface waters in South Africa (**Appendix-table 2**). Effluents from wastewater treatment plants (**Table 3**) are regarded as a major aquatic source of several antiretroviral drugs (Wood et al., 2015). Furthermore, indiscriminate waste disposal along river channels and coastal areas are also routes via which ARVDs may enter water bodies. Coastal landfill sites provide a pathway for ARVDs disposed with municipal and clinical wastes to enter aquatic environments (Schoeman et al., 2017). The presence of these specialized compounds in the aquatic environment, and the inability of existing wastewater treatment plants to satisfactorily handle organic contaminants is worrisome due to the activity of the pharmaceuticals, even at low concentrations (Deblonde et al., 2011; Deblonde and Hartemann, 2013; Petrie et al., 2015; Rasheed et al., 2019). As emerging chemical pollutants (ECPs), there is rarity of reports on the ecotoxicity of antiretroviral drugs,

However, available information on the fate and toxicity of selected antiretroviral drugs are comprehensively discussed in **Chapter 3 (Paper 2).**

Table 3. Levels of ARVDs reported in WWTP influents and effluents situated in some African countries and other parts of the world

ARVD	Country	Concentration in Influents (ng L^{-1})	Concentration in Effluents (ng L^{-1})	Reference
Zidovudine	Kenya	12100-20130	90-110	(K'Oreje et al., 2016)
	South Africa	6900-53000	87-500	(Abafe et al., 2018)
	Germany	564	380	(Prasse et al., 2010)
	Finland	22-37	46-62	(Ngumba et al., 2016)
Nevirapine	Finland	13-19	8-10	(Ngumba et al., 2016)
	Germany	32	22	(Prasse et al., 2010)
	South Africa	670-2800	540-1900	(Abafe et al., 2018)
	Kenya	850-3300	1030-2080	(K'Oreje et al., 2016)
Lamivudine	Finland	37-55	20-22	(Ngumba et al., 2016)
	Belgium	507	ND	(Vergeynst et al., 2015)
	Germany	720	ND	(Prasse et al., 2010)
	South Africa	840-2200	≤ LOD-130	(Abafe et al., 2018)
	Kenya	30300-60680	19900-31070	(K'Oreje et al., 2016)
Efavirenz	South Africa	24000-34000	20000-34000	(Abafe et al., 2018)
		17400	7100	(Schoeman C, 2015)
	Kenya	460-1020	100-110	(K'Oreje et al., 2016)
Abacavir	France	-	33	(Aminot et al., 2018)
	Greece	13.6	10	(Terzopoulou et al., 2016)

2.4 Adsorption of organic chemical pollutants (OCPs)

Adsorption science and technology have proven very helpful in meeting the global demand for clean and safe water. The adsorption process and related technology have been widely studied, improved, and applied for the adsorption of organic pollutants in surface waters, and the provision of potable water around the world. Many cutting-edge scientific research, which has resulted in high-impact publications, patents and industrial/field-scale applications, have been recorded in the field of adsorption and material science in the last few decades (Unuabonah et al., 2019). The adsorption method for the decontamination of water polluted with organics has advantages and

benefits such as simplicity in design and operation, low operational cost, easy adaptability, and minimal tendency of generating secondary pollutants or undesirable by-products (Singh et al., 2018). The nature of adsorbent and optimal process conditions is vital towards sorptive removal of OCPs, such as PAHs and ARVDs, from water.

Furthermore, several laboratory-scale studies have reported that the adsorption technique has the potential of improving water quality across the world (Adeola and Forbes, 2019; Apul et al., 2013; Ternes et al., 2002). However, there is a need to scale-up research via modeling and pilot studies for large-scale water treatment applications. A comprehensive understanding of the equilibrium adsorption capacity, kinetics (rate of uptake), and thermodynamic conditions for optimal performance of the adsorption process are vital, to inform decision making for industrial-scale treatment of water (Lamichhane et al., 2016; Unuabonah et al., 2019).

2.4.1 Factors affecting sorption of OCPs

Sorption of organic chemical pollutants is often controlled by two or more mechanisms, especially for compounds and adsorbents with different functionalities or functional groups. Fundamental factors controlling the adsorption behavior of organic pollutants are discussed in this section.

2.4.1.1 Morphology of the adsorbent

The specific surface area, pore size, pore-volume, pore structure, and pore distribution of the sorbent are vital morphological characteristics which control the interaction between adsorbents and organic pollutants (Yuan et al., 2018). Mostly adsorbents possess micropores and mesopores, thus the surface and pore structure of the adsorbent could limit the amount of pollutant adsorbed via size exclusion (Menéndez-Díaz and Martín-Gullón, 2006, Adeola and Forbes, 2019). Pore structure also influences accessibility and packing of the pollutant molecules in the pores, for example slit-shaped micropores will prove inaccessible to compounds of spherical geometry, with diameter larger than the pore width (Ghasemzadeh et al., 2019; Wang et al., 2019).

2.4.1.2 Surface chemistry of the adsorbent

Surface chemistry is defined by the functional groups present on the surface of the adsorbent, which influences the binding capacity and nature of the interaction between the sorbate and sorbent (Yu et al., 2020). The presence of oxygen-containing functional groups is related to acidity, while the presence of nitrogen-containing groups promotes the basicity of the surface of carbonaceous materials like graphene, granular activated carbon, and carbon nanotubes (Tessmer et al., 1997; Ye et al., 2020). Surface chemistry is also affected by the pH of the sorption medium, as the surface of the adsorbent can become either positively or negatively charged at pH values before or after the point zero net charge (PZNC) of the material. Furthermore, the buildup of water clusters around hydrophilic oxygen groups also limits the adsorption capacity of adsorbents via oxidation (Fang et al., 2014; Khan and Sarwar, 2007).

2.4.1.3 Physicochemical properties of target pollutants

The adsorption capacity, rate of adsorption, and mechanism of adsorption of pollutants are significantly influenced by the physicochemical properties and nature of the sorbate molecules (Guo et al., 2012). The molecular dimension and arrangement/conformation control the accessibility of the compounds to the sorbent pores. Solubility of the pollutant controls the hydrophobic sorbent-sorbate interactions and partitioning between the solid-liquid interface (Site, 2001). The conformation of the adsorbate may lead to either close interaction, favorable for π-π interaction, as is the case for most planar molecules. Steric hindrance may occur due to the inability of the nonplanar molecules to draw closer to the adsorbent, leading to weak interactions (Cornelissen, 2005; Cornelissen et al., 2005; Jonker and Koelmans, 2002).

Hydrophilicity and polarity of pollutants also play significant roles in the adsorption process. Several reports suggest that adsorption is enhanced with increasing hydrophobicity of the compounds, as it becomes easier to partition away from polar/aqueous medium (Adeola and Forbes, 2019; Li et al., 2018; Ololade et al., 2018; Villacañas et al., 2006). Other interactions such as interactions with surface groups leading to hydrogen bonding, covalent bonding, electrostatic interactions, dipole-dipole interactions, etc., are all affected by the sorbate and sorbent physicochemical properties and electronic structure (Fraga et al., 2019).

Other factors capable of influencing adsorption of organic pollutants are pH, ionic strength, temperature and other physicochemical parameters related to the contaminated media to be treated. The presence of natural organic matter (NOM) and competing ions/molecules, different from the target pollutant, have widely been reported to also alter solution chemistry, block sorption sites and ultimately influence the adsorption performance of adsorbents and the mechanism of the sorption process (Adeola and Forbes, 2019; 2021b; Huang et al., 2003).

2.5 Models of adsorption

Several researchers have developed, validated, and applied several adsorption models which describe sorption equilibria and kinetics. The elucidation of adsorbate-adsorbent interactions is vital towards decisions regarding the choice of adsorbent and target-specific strategies required in adsorption processes. Furthermore, modeling adsorption experimental data is salient in describing the influence of process variables/environmental conditions on adsorption performance and treatment efficiency (Wang et al., 2020). Empirical adsorption models can be a single- or multi-parameter model, depending on the number of constants obtainable from the model equation. But it will suffice to say that using complex models such as three- or four-parameter models is not necessary when two-parameter models give a good fitting for adsorption data (Unuabonah et al., 2019; Yousef et al., 2016).

The principal relevance of sorption models includes; understanding mechanisms of adsorption, equilibrium dynamics, predicting the influence of operational changes, and optimization of the adsorption process. Adsorption models in batch flow experiments can be used to deduce the adsorption capacity of natural and synthetic adsorbents, and provide dependable adsorption parameters for quantitative comparison of sorption interactions in single-solute and multi-solute adsorptive systems (Adeola and Forbes, 2019, 2020; Unuabonah et al., 2019). Sorption isotherm models can be applied via both linear and nonlinear regression methods/equations (Adeola and Forbes, 2020; Chowdhury et al., 2011; Wu et al., 2020). The sorption models used in several studies in this thesis are linear, Freundlich, Langmuir, Sips, Temkin, Dubinin-Radushkevich isotherm, pseudo-first-order, pseudo-second-order, and intraparticle diffusion models.

2.5.1 Adsorption isotherm models

2.5.1.1 Langmuir isotherm model

The Langmuir isotherm relates the adsorption of molecules onto an adsorbent, with gas pressure or concentration of the medium above the solid surface at a fixed temperature (Unuabonah et al., 2019). This suggests that the adsorption of the sorbate occurs in one layer and is thus often used to describe chemisorption. The four basic assumptions proposed by the model are:

1. The surface of the adsorbent possesses equivalent and uniform adsorption sites.
2. The amount of sorbate adsorbed does not affect the rate of adsorption per site, as there is no sorbate-sorbate interaction.
3. Adsorption mechanisms for all solutes are the same and the adsorbent complex has a uniform structure.
4. Adsorption only occurs on free sites and only a monolayer is formed even at adsorption maxima. Molecules of sorbates do not deposit on each other, forming multiple layers.

These four assumptions are seldom true in real-life systems. This is because there are always imperfections on the surface of adsorbents, and these conditions will only hold if the surface of the material is ultraclean and homogeneous. Also, adsorbed molecules are not necessarily inert, and the mechanism is not the same for the first and last adsorbed molecules. However, like most foundational theories in science, the Langmuir model is regarded as one of the pillars on which adsorption theory is built for proper conceptual understanding of the process.

The Langmuir model describing a site-limiting sorption equilibrium has the following form

$$Langmuir: q_e = \frac{q_m K_L Ce}{1 + K_L Ce} \qquad (1)$$

where q_{max} is the maximal sorption capacity and K_L is a solute–surface interaction energy-related parameter. The Langmuir equation can be rearranged to a linear form for the convenience of plotting and determination of the Langmuir constant (K_L). The values of q_{max} and K_L can be determined from the linear plot of $1/q_e$ versus $1/C_e$:

$$Linear\ form: \frac{1}{q_e} = \frac{1}{K_L q_{max} C_e} + \frac{1}{q_{max}} \qquad (2)$$

The essential characteristics of the Langmuir isotherm parameters can be used to predict the affinity between the sorbate and the sorbent using the separation factor or dimensionless equilibrium parameter 'R_L', expressed as in the following equation:

$$R_L = \frac{1}{1+K_L C_0} \quad (3)$$

where K_L is the Langmuir constant and C_0 is the initial concentration of the PAHs or ARVDs. The value of the separation factor R_L provides important information about the nature of adsorption. The value of R_L is between 0 and 1 for favorable adsorption, while $R_L>1$ represents unfavorable adsorption and R_L = 1 represents linear adsorption. The adsorption process is irreversible if R_L = 0 (Huang et al., 2003; Rahman and Islam, 2009).

2.5.1.2 Freundlich isotherm model

The Freundlich isotherm describes adsorption processes occurring on multiple sites on the surface of the adsorbent. Unlike Langmuir, multiple layers of adsorbed solute are possible and surface heterogeneity, exponential distribution of active sites, and their energies can be accounted for using the Freundlich model (Van der Bruggen, 2015).

The Freundlich model, which is commonly used for quantifying hydrophobic organic compound sorption equilibria has the following form:

$$\textit{Non-linear form: } q_e = K_f C_e^N \quad (4)$$

where q_e is the solid-phase concentration (ng g^{-1}) and C_e is the liquid-phase equilibrium concentration (mg L^{-1}). K_f is the sorption capacity-related parameter and N is the isotherm non-linearity index, an indicator of site energy heterogeneity determined by linear regression of log-transformed data as shown below:

$$\textit{Linear form: } Log\ q_e = Log\ K_f + \frac{1}{n} Log\ C_e \quad (5)$$

The Freundlich isotherm constants K_f and $1/n$ are evaluated from the intercept, and the slope respectively, of the linear plot of log q_e versus log C_e (Rahman and Islam, 2009).

2.5.1.3 Dubinin–Radushkevich isotherm model

The Dubinin–Radushkevish (D-R) isotherm describes the porosity of adsorbent and a pore-filling adsorption mechanism, rather than the assumption that the adsorption process was related to layer-by-layer adsorption on pore walls (Hu and Zhang, 2019).

The D-R model was also used to fit experimental adsorption data using the equations below:

$$Non\text{-}linear\ form:\ q_e = Q_D\, exp\ (-\ k_{ad} \cdot \varepsilon^2) \quad (6)$$

$$Linear\ form:\ lnq_e = lnQ_D - 2B_D RTln(1 + 1/C_e) \quad (7)$$

where Q_D is the theoretical maximum capacity (mol g^{-1}), B_D is the D-R model constant (kJ mol^{-1} K^{-1}), T is the absolute temperature (K) and R is the gas constant (kJ mol^{-1}). The mean energy of sorption, E (kJ mol^{-1}), is calculated from the relation:

$$E = 1/\sqrt{2B_D} \quad (8)$$

Q_D and B_D can be estimated from the intercept and slope of the plot of ln (q_e) versus ln (1 + $1/C_e$) (Igwe and Augustine, 2007).

2.5.1.4 Temkin isotherm model

Temkin isotherm model describes the role of the heat of reaction (enthalpy of adsorption) on the adsorption process. The model assumes that the enthalpy of adsorption of all molecules in each sorption layer decreases linearly with an increase in surface coverage (Ringot et al., 2007).

The non-linear and linearized forms are expressed by the following equations:

$$Non\text{-}linear:\ q_e = \frac{RT}{b_T} lnK_T\,.\,C_e \quad (9)$$

$$Linear\ form:\ q_e = \frac{RT}{b_T} lnK_T + \frac{RT}{b_T} lnC_e \quad (10)$$

where K_T (L g^{-1}) is the Temkin isotherm constant, b_T (J mol^{-1}) is a constant related to the heat of sorption, and R (8.314 J mol^{-1} K^{-1}) is the gas constant. A plot of q_e versus ln (C_e) gives a straight-line equation from which K_T and b_T can be evaluated from the slope and the intercept (Mahamadi and Nharingo, 2010).

2.5.1.5 Sips isotherm model

The Sips isotherm is used to describe localized adsorption without adsorbate–adsorbate interactions. The Sips isotherm is a hybrid of Freundlich and Langmuir models used to evaluate the adsorption of sorbates and circumventing the limitations of heterogeneous systems and the effect of sorbate concentrations (Tzabar and ter Brake, 2016). The Sips

model can either tend towards the Freundlich model or Langmuir model depending on the value of the sorbate equilibrium concentration (C_e). The Sips equation is given as:

$$\textit{Non-linear form: } q_e = \frac{K_S .Ce^{\beta s}}{1+ \alpha_S .Ce^{\beta s}} \quad (11)$$

$$\textit{Linear form: } \frac{1}{q_e} = \frac{1}{q_{max}K_S}\left(\frac{1}{C_e}\right)^{1/N} + \frac{1}{q_{max}} \quad (12)$$

where K_S (L mg^{-1}) and q_{max} (mg g^{-1}) are the Sips equilibrium constant and maximum adsorption capacity values. The Sips isotherm equation includes the dimensionless heterogeneity factor, N, which describes the system's heterogeneity when its value is between 0 and 1. When N = 1, the Sips equation implies a homogeneous adsorption process (Langmuir) (Allen et al., 2004).

2.5.2 Adsorption kinetics

The kinetics of the adsorption process refers to the time-dependence of sorbent-sorbate interactions, relative to the equilibrium concentration of adsorbate per time and at the end of the process (Worch, 2008). The following steps are involved in the kinetics of adsorption of solute onto solid surfaces (Unuabonah et al., 2019):

1. Solute transfer from solution to the boundary of the hydrodynamic layer around the sorbent.
2. Solute transfer through the boundary layer via diffusion onto the external surface of the adsorbent.
3. Intraparticle and surface diffusion into the pore spaces and internal surfaces of the adsorbent.
4. Energetic interaction between adsorbed molecules and sorption sites.

The first and last steps are believed to be very fast, unlike the rate-determining steps (third and fourth). In other words, the overall rate of reaction/adsorption is controlled by film and/or intraparticle diffusion involving the slowest steps (Worch, 2012). Adsorption kinetics can be modeled, just like adsorption isotherms, and vital information regarding the adsorption mechanism and mode of mass transfer between the solid-liquid interface can be recovered using kinetic models.

2.5.2.1 Pseudo-first-order kinetic model

The pseudo-first-order rate equation was first presented by Lagergren in 1898 (Lagergren, 1898). Over the years, the Lagergren pseudo-first equation has been further explained and applied to describe the mass transfer system, in terms of ion-exchange and/or film diffusion-controlled adsorption. The consensus is that rate constant (k_1) will be inversely proportional to the thickness of boundary film for a film-diffusion controlled sorption kinetics, while rate constant (k_1) will be independent of particle size, but depend solely on temperature and concentrations of ions available in ion-exchange controlled pseudo-first-order adsorption kinetics (Boyd et al., 1947; Ho and McKay, 1999).

The pseudo-first-order adsorption kinetic equations are given as:

$$\textit{Non-linear form: } \frac{dq_t}{dt} = k_1(q_e - q_t) \quad (13)$$

$$q_t = q_e(1 - e^{-Kit}) \quad (14)$$

$$\textit{Linear form: } log(q_e - q_t) = log q_e - \frac{k_1}{2.303} t \quad (15)$$

where q_t and q_e are the amount of solute sorbed per mass of sorbent (mg g^{-1}) at any time and equilibrium, respectively, and k_1 is the rate constant of first-order sorption (min^{-1}). The straight-line plot of log ($q_e - q_t$) against t gives log (q_e) as slope and intercept equal to $k_1/2.303$. Hence, the amount of solute sorbed per gram of sorbent at equilibrium (q_e) and the first-order sorption rate constant (k_1) can be evaluated from the slope and the intercept (Kowanga et al., 2016; Lagergren, 1898).

2.5.2.2 Pseudo-second-order kinetic model

The pseudo-second order model predicts a chemical reaction leading to adsorption of sorbate molecules onto adsorbent (chemisorption). Chemisorption could be as a result of valence electron transfer or sharing during sorbate-sorbent interaction, and the rate-limiting step is controlled by physicochemical interaction between the solution and adsorbent phases (Ho and McKay, 1999; Robati, 2013; Wang et al., 2007).

The model equations are presented as follows:

$$\textit{Non-linear form: } \frac{dq_t}{dt} = K_1(q_e - q_t)^2 \quad (15)$$

$$q_t = \frac{q_e^2 K_2 t}{q_e K_2 t + 1} \quad (16)$$

$$Linear\ form: \frac{t}{q_t} = \frac{1}{k_2 q_{e^2}} + \left(\frac{1}{q_e}\right) t \quad (17)$$

The kinetic parameters can be evaluated with a straight-line plot of t/q_t against t; q_e and k_2 can be deduced from the slope and intercept respectively. The initial sorption rate is defined by the following equation:

$$h = k_2 q_{e^2} \quad (18)$$

where k_2 is the rate constant, and q_t is the PAH or ARVD uptake capacity at any time t (Kalavathy et al., 2005).

2.5.2.3 Weber-Morris intraparticle diffusion model

The intraparticle diffusion model describes sorption interaction, where the adsorption rate is influenced significantly by the rate of diffusion of the sorbate molecules towards the adsorbent in aqueous media (Wu et al., 2009). It is assumed that if intraparticle-diffusion is the rate-determining step in any adsorption process, then a plot of q_t against $t^{0.5}$ will produce a straight line with rate constant k_p as slope and intercept of zero, as the line will pass through the origin. The intra-particle diffusion equation is presented below:

$$q_t = k_p t^{0.5} + C \quad (19)$$

Where k_p is the rate constant of intra-particle diffusion (μg g^{-1} $min^{1/2}$) and C relates to boundary layer thickness. It was reported that when an intra-particle diffusion plot exhibits multiple linearities, it then suggests that several steps (as discussed in Section 2.6.2) occurred during the adsorption process (Anthony et al., 2020; Weber and Smith, 1987).

2.6 Graphene-based materials

Graphene possesses a two-dimensional (2D) structure, with sp^2 hybridized carbon atoms arranged in a closely packed lattice structure, containing both sigma- and pi-bonds (Ali et al., 2019). Graphene is a carbon-based material and has been reported in many forms in literature such as pristine graphene, graphene sheets (GS), graphene oxide (GO), reduced graphene oxide (RGO), graphene nanoshell (GNS), graphene quantum dots, graphene wool, graphene-based composites, and functionalized

graphene (**Figure 2**) (Adeola and Forbes, 2019; Apul et al., 2013; Oyedotun et al., 2019; Sun et al., 2013; Wang et al., 2017; Wang et al., 2014b).

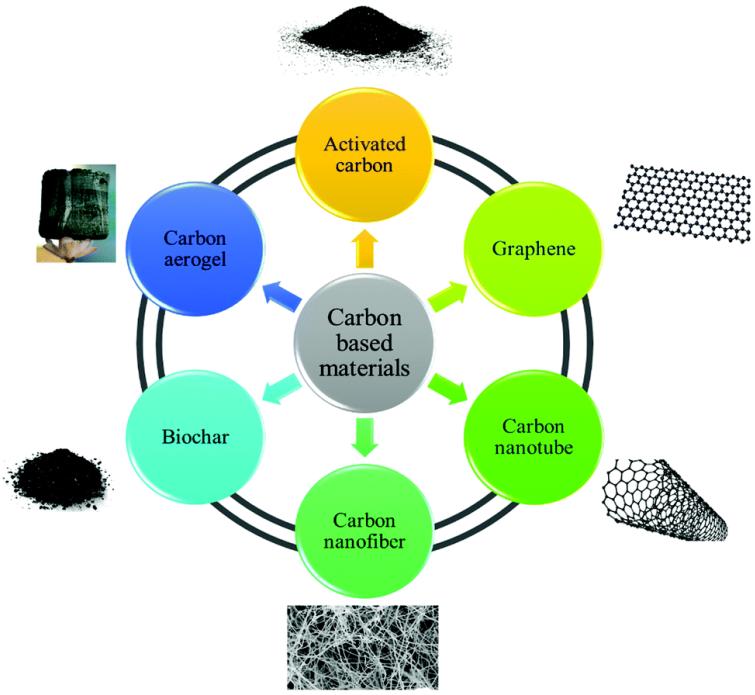

***Figure 2**. Different forms of carbon-based adsorbents (Sabzehmeidani et al., 2021).*

A number of reports suggest the potential application of graphene as an efficient adsorbent for water treatment (Adeola and Forbes, 2021c; Ali et al., 2019; Ersan et al., 2017; Wang et al., 2014a; Zhao et al., 2011). Several attempts have been made to functionalize carbon-based adsorbents, which includes graphene, towards enhancement of physicochemical properties such as specific surface area, stability, tensile strength, chemical robustness, electronic charge mobility, flexibility, thin-film thickness; and promoting high adsorption capacity, antimicrobial properties and electrochemical activity (**Figure 3**) (Dreyer et al., 2010; Geim, 2009; Novoselov et al., 2012; Mayavan et al., 2012, Yang et al., 2019).

2.6.1 Synthesis of graphene wool composites

Graphene adsorbents can be synthesized via two main routes, which are the 'top-down' and 'bottom-up' approaches. The top-down approach requires the reduction of macroscopic carbonaceous materials (e.g. graphite, carbon fibers, graphene oxide, metal-organic frameworks, etc.) into small graphene particles, usually through thermal reduction treatments. Also, the use of molecular or atomic carbon precursors (e.g.

glucose, methane, and even PAHs) under suitable reaction conditions can be used to synthesize graphene, and this route is regarded as a bottom-up approach (Adeola and Forbes, 2020; Bhuyan et al., 2016; Liu et al., 2011).

Graphene wool (GW), as used in this project, was synthesized using an established method reported by Schoonraad et al. (2020). The novel graphene wool was synthesized onto a quartz wool substrate using the atmospheric pressure chemical vapor deposition (APCVD) method with the aid of high temperature equipment (specifically using chemical vapor deposition, with temperatures up to 1200 ^{o}C) and regulated gas flow (argon, hydrogen and methane) (**Figure 3**). The quartz wool fibres provided solid support for the graphene. In other words, the 'graphene wool (GW)' used in this thesis refers to graphene coated on quartz wool (Schoonraad et al., 2020). Other information regarding the synthesis of GW is presented in **Chapters 4-8**.

Several studies have established the antimicrobial action of AgNPs and composites thereof (**Figure 4**), with different minimum inhibitory concentrations against bacterial infections and drug-resistant microbes (Mukherjee et al. 2001; Padilla-Cruz et al. 2021). Consequently, graphene wool (GW) was doped with lipopeptide-coated silver nanoparticles (AgNP) to form a GW-AgNP composite, in order to introduce antimicrobial properties to the material in addition to the adsorption potential of graphene wool. Lipopeptide-coated silver nanoparticles was synthesized via reduction of $AgNO_3$ in phenyl ether, and oleylamine served as a capping agent (Bezza et al., 2020). Oleic acid and oleylamine provided the required functionalities for stabilization on the surface of graphene wool fibers (Liu et al., 2011).

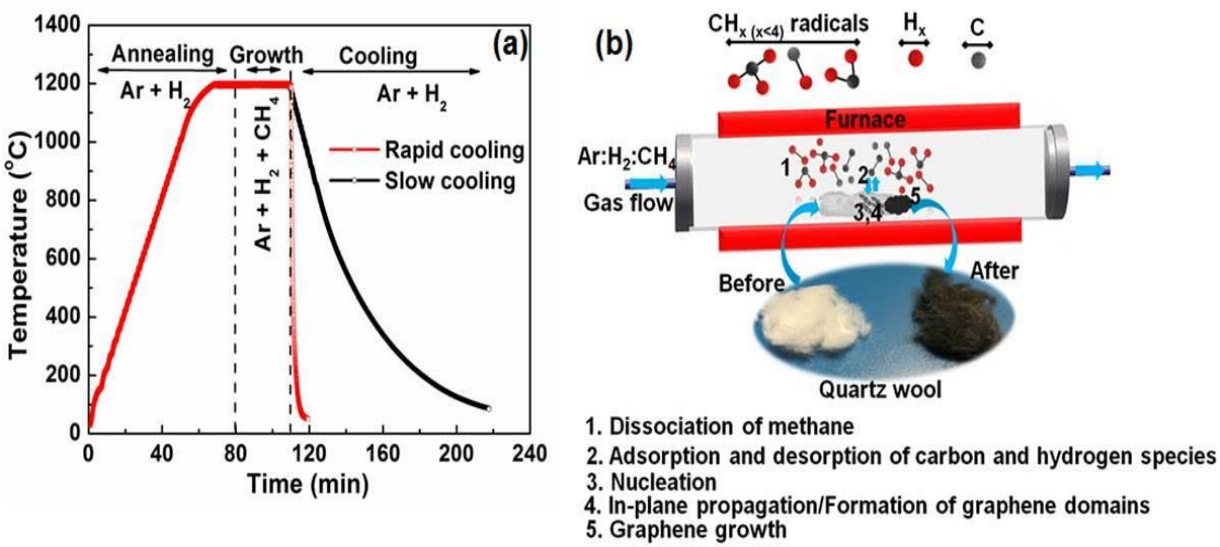

Figure 3. *(a) Temperature profile of the CVD process as measured by a series of thermocouples and (b) schematic of the non-catalytic direct growth mechanism of CVD graphene on quartz wool substrate (Schoonraad et al. 2020)*

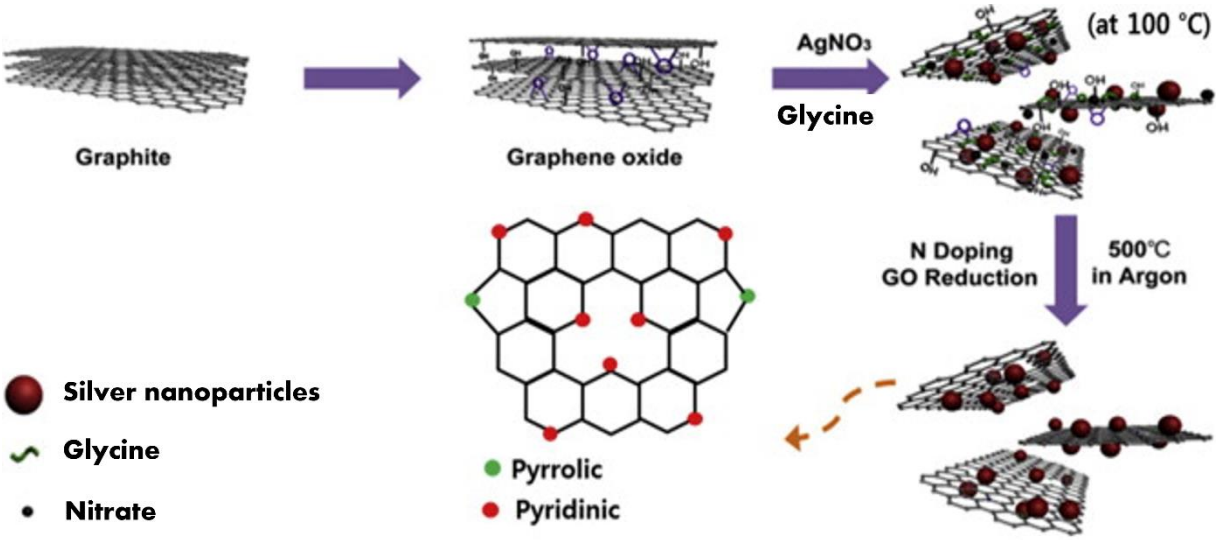

Figure 4. *Doping of graphene with silver nanoparticles and nitrogen (Mayavan et al., 2012).*

2.6.2 Structural and morphological characterization

To elucidate the structure of graphene wool (GW and GW-αAgNP), imaging and spectroscopic techniques can be adopted. A summary of the basic techniques often used for the analysis of graphene-based materials is briefly discussed here, and the results of these analyses are reported in subsequent chapters of this thesis.

High-resolution transmission microscopy (HRTEM) involves the use of a beam of short-wavelength electrons to illuminate a sample under vacuum. The transmission of part of the beam through the material of interest onto a charge-coupled device camera ensures the capture of images that can be used to study the morphology of GW (Adeola and Forbes, 2020; Schoonraad et al., 2020; Warner et al., 2009).

X-ray diffraction (XRD) spectroscopy is a non-destructive tool involving the application of an X-ray beam to irradiate samples, in order to obtain diffraction patterns that reveals information on the crystallinity, lattice structure and grain size of a material. The elemental/mineral composition of a sample can also be identified with a fair degree of accuracy using diffraction patterns in comparison with standard references (International Centre for Diffraction Data) (Mourdikoudis et al., 2018). Doped graphene and graphene composites (such as GW) are mostly amorphous with a very limited crystalline phase (Das et al., 2020; Stankovich et al., 2006).

Fourier-transform infrared (FTIR) spectroscopy is a useful technique for examining the surface chemistry of materials. FTIR spectroscopy operates on the principle of absorption of light in the infra-red region (4000 – 400 cm^{-1}) by a sample, and the consequent modification of its dipole. The FTIR spectrum gives information on the nature of functional groups and bonds a material possesses on its surface, and standard FTIR tables are normally used to infer this information (Mohamed et al., 2017). Also, the adsorption of organic compounds onto the surface of an adsorbent is often confirmed by FTIR spectra, as it reveals either new peaks or stronger intensity of existing peaks (Chen et al., 2017).

Raman spectroscopy is a useful imaging technique used to study the molecular interactions and structure of materials, including graphene. The technique involves the scattering of an incident monochromatic laser beam by the sample at a different wavelength from that of the incident beam. A Raman spectrum is generated via light

scattering, and the intensity and wavelength positions of the scattered light provide fingerprint information on the collective vibrational, rotational, and other low-frequency transitions that are present in the sample (Gouadec and Colomban, 2007). The G, D, and 2D peaks are attributed to Raman spectra are attributed to graphene and varying intensity of the peaks can be used to infer monolayer or multilayer graphene coverage of substrates (Hong et al., 2013; Schoonraad et al., 2020).

X-ray photoelectron spectroscopy (XPS) is a technique used to identify the functional states of elements existing on the surface of a material. XPS is based on photoemission as a result of bombardment of a sample by a fast-moving beam of X-rays, and the unique emissions generated through the sample bears fingerprint information that can be used to elucidate structures within a material or coverage up to a thickness of 2 - 5 nm (Burke et al., 1992; Schoonraad et al., 2020; Steffen, 2013; Susi et al., 2015).

Brunauer–Emmett–Teller (BET) analysis is a technique used to determine the specific surface area, pore size and distribution of solids. The principle is based on the correlation of the amount of gas adsorbed (N_2 gas was used in this project) with the specific surface area of the adsorbent (Ambroz et al., 2018). Generally, adsorbents with pore diameter < 2 nm are microporous, between 2 – 50 nm are mesoporous and > 50 nm are regarded as microporous (Table 4). Paper 4 reports Sear's titrimetric method for the estimation of the surface area (also called Sear's number) of materials using acid, base and salt (Sear, 1956; Oyelude et al., 2017). The BET method may be more accurate because it takes into account possible variables such as temperature, pressure, volume of gas and mass of adsorbents. However, Sear's method can be useful in comparative estimation between two or more samples and for analysis of complex materials such as fibers, rods and composites (Heinroth et al. 2008). The BET analyser works best for the analysis of pulverized solids, given the nature of the sample holder and expected homogeneity and active sites of samples. However, tiny fragments of GW and pulverized fractions of NOM were analysed successfully in this project (Paper 6 and 7).

Table 4: Summary of the properties of the graphene wool adsorbent used in this project

Characterisation/Parameters	Results	Reference
pH (in water and $CaCl_2$)	7.1 and 6.1	Adeola and Forbes (2019)
BET surface area analysis		Adeola et al. (2021b)
Pore diameter	1.37 nm	
Pore volume	0.039 cc g^{-1}	
Type of pores	Micropores and mesopores	
BET isotherm-hysteresis type	H4-isotherm: associated with molecular clustering followed by pore filling. H4 is common in composites and complex materials (Ambroz et al., 2018)	
BET specific surface area	29.6 m^2 g^{-1}	
Sear's surface area (Estimated value)	279 m^2 g^{-1}	Adeola and Forbes (2019)
Fourier transformed infrared spectroscopy	sp^2 C = C backbone at 775 cm^{-1}, Si-O–C at 1059 cm^{-1}, sp^2 & sp^3 C–H at 2925 & 2845 cm^{-1}	Adeola and Forbes (2020)
Scanning electron microscopy	Extensive coverage of quartz wool by graphene with a heterogenous and rough surface structure	Schoonraad et al. (2020); Adeola and Forbes (2020)
Transmission electron microscopy	Varying translucence confirms heterogeneous multilayer of graphene flake-like sheets with the presence of interstitial spaces. Diameter of each GW strand 6 – 8 μm	Schoonraad et al. (2020); Adeola and Forbes (2020)
Raman spectroscopy	Average crystallite grain size of 24 nm. D, G and 2D peaks at 1,349, 1,582 and 2,630 cm^{-1} corresponding to vibrations of sp^3 and sp^2 carbon atoms	Schoonraad et al. (2020)
X-ray photoelectron spectroscopy	Strongest peak of sp^2 C=C at 284.4 eV	Schoonraad et al. (2020)

2.7 Conclusion

A concise background to the target pollutants (PAHs and ARVDs) was provided in this chapter in order to highlight their environmental significance. Furthermore, the principles and models of adsorption were discussed, as well as graphene wool composites as adsorbents to be synthesized and applied for the removal of the target pollutants in water. The established synthesis approach and characterization techniques that were used for in-depth morphological elucidation of the adsorbent were highlighted. The occurrence of these pollutants in water bodies, deficiencies in conventional wastewater treatment protocols, poor waste management, as well as lack of regulatory guidelines in developing countries, suggest the need for further research towards the development of efficient, cost-effective and sustainable remediation of these emerging chemical pollutants in water.

2.8 References

Abafe, O.A., Späth, J., Fick, J., Jansson, S., Buckley, C., Stark, A., Pietruschka, B., Martincigh, B.S., 2018. LC-MS/MS determination of antiretroviral drugs in influents and effluents from wastewater treatment plants in KwaZulu-Natal, South Africa. Chemosphere, 200, 660-670. https://doi.org/10.1016/j.chemosphere.2018.02.105

Abdel-Shafy, H.I., Mansour, M.S.M., 2016. A review on polycyclic aromatic hydrocarbons: Source, environmental impact, effect on human health and remediation. Egyptian Journal of Petroleum, 25, 107-123. https://doi.org/10.1016/j.ejpe.2015.03.011

Adeola, A.O., Forbes, P.B.C., 2019. Optimization of the sorption of selected polycyclic aromatic hydrocarbons by regenerable graphene wool. Water Science and Technology, 80, 1931-1943. https://doi.org/10.2166/wst.2020.011

Adeola, A.O., Forbes, P.B.C., 2020. Assessment of reusable graphene wool adsorbent for the simultaneous removal of selected 2–6 ringed polycyclic aromatic hydrocarbons from aqueous solution. Environmental Technology, 1-14. https://doi.org/10.1080/09593330.2020.1824024

Adeola, A.O., Forbes, P.B.C, 2021a. Antiretroviral drugs in African surface waters: prevalence, analysis and potential remediation, Environmental Toxicology and Chemistry. https://doi.org/10.1002/etc.5127

Adeola, A.O., Forbes, P.B.C., 2021b. Influence of natural organic matter fractions on PAH sorption by stream sediments and a synthetic graphene wool adsorbent. Environmental Technology and Innovations, 21, 101202. https://doi.org/10.1016/j.eti.2020.101202

Adeola, A.O., Forbes, P.B.C., 2021c. Advances in water treatment technologies for removal of polycyclic aromatic hydrocarbons: Existing concepts, emerging trends, and future prospects. Water Environment Research, 93(3), 343-359. https://doi.org/10.1002/wer.1420

Ali, I., Basheer, A.A., Mbianda, X.Y., Burakov, A., Galunin, E., Burakova, I., Mkrtchyan, E., Tkachev, A., Grachev, V., 2019. Graphene based adsorbents for remediation of noxious pollutants from wastewater. Environment International, 127, 160-180. https://doi.org/10.1016/j.envint.2019.03.029

Allen, S.J., Mckay, G., Porter, J.F., 2004. Adsorption isotherm models for basic dye adsorption by peat in single and binary component systems. Journal of Colloid and Interface Science, 280(2), 322–333. https://doi.org/10.1016/j.jcis.2004.08.078

Aminot, Y., Fuster, L., Pardon, P., Le Menach, K., Budzinski, H., 2018. Suspended solids moderate the degradation and sorption of waste water-derived pharmaceuticals in estuarine waters. Science of The Total Environment, 612, 39-48.

Ambroz, F., Macdonald, T. J., Martis, V., Parkin, I. P., 2018. Evaluation of the BET Theory for the characterization of meso and microporous MOFs. Small Methods, 2, 1800173.

Anthony, E.T., Ojemaye, M.O., Okoh, A.I., Okoh, O.O., 2020. Synthesis of CeO_2 as promising adsorbent for the management of free-DNA harboring antibiotic resistance genes from tap-water. Chemical Engineering Journal, 401, 125562. https://doi.org/10.1016/j.cej.2020.125562

Apul, O.G., Wang, Q., Zhou, Y., Karanfil, T., 2013. Adsorption of aromatic organic contaminants by graphene nanosheets: comparison with carbon nanotubes and activated carbon. Water Research, 47, 1648-1654. https://doi.org/10.1016/j.watres.2012.12.031

Arey, J., Atkinson, R., 2003. Photochemical Reactions of PAHs in the Atmosphere, in: (eds J.M. Weeks, S.O.H., B.A. Rattner and P.E.T. Douben) (Ed.), PAHs: An Ecotoxicological Perspective, Wiley, pp. 47-63. https://doi.org/10.1002/0470867132.ch4

Balcıoğlu, E.B., 2016. Potential effects of polycyclic aromatic hydrocarbons (PAHs) in marine foods on human health: a critical review. Toxin Reviews, 35, 98-105. https://doi.org/10.1080/15569543.2016.1201513

Balmer, J.E., Hung, H., Yu, Y., Letcher, R.J., Muir, D.C.G., 2019. Sources and environmental fate of pyrogenic polycyclic aromatic hydrocarbons (PAHs) in the Arctic. Emerging Contaminants, 5, 128-142. https://doi.org/10.1016/j.emcon.2019.04.002

Bekki, K., Toriba, A., Tang, N., Kameda, T., Hayakawa, K., 2013. Biological effects of polycyclic aromatic hydrocarbon derivatives. Journal of UOEH, 35, 17-24. https://doi.org/10.7888/juoeh.35.17

Bhuyan, M.S.A., Uddin, M.N., Islam, M.M., Bipasha, F.A., Hossain, S.S., 2016. Synthesis of graphene. International Nano Letters, 6, 65-83. https://doi.org/10.1007/s40089-015-0176-1

Boyd, G.E., Adamson, A.W., Myers, L.S., 1947. The Exchange Adsorption of Ions from Aqueous Solutions by Organic Zeolites. II. Kinetics. Journal of the American Chemical Society, 69, 2836-2848. https://doi.org/10.1021/ja01203a066

Burke, G.M., Wurster, D.E., Berg, M.J., Veng-Pedersen, P., Schottelius, D.D., 1992. Surface Characterization of Activated Charcoal by X-Ray Photoelectron Spectroscopy (XPS): Correlation with Phenobarbital Adsorption Data. Pharmaceutical Research, 9, 126-130. https://doi.org/10.1023/a:1018900431661

Chen, P., Li, H., Song, S., Weng, X., He, D., Zhao, Y., 2017. Adsorption of dodecylamine hydrochloride on graphene oxide in water. Results in Physics, 7, 2281-2288. https://doi.org/10.1016/j.rinp.2017.06.054

Chowdhury, S., Misra, R., Kushwaha, P., Das, P., 2011. Optimum Sorption Isotherm by Linear and Nonlinear Methods for Safranin onto Alkali-Treated Rice Husk. Bioremediation Journal, 15, 77-89. https://doi.org/10.1080/10889868.2011.570282

Cohen-Tanugi, D., Grossman, J.C., 2012. Water Desalination across Nanoporous Graphene. Nano Letters, 12, 3602-3608. https://doi.org/10.1021/nl3012853

Cornelissen, 2005. Importance of Unburned Coal Carbon, Black Carbon, and Amorphous Organic Carbon to Phenanthrene Sorption in Sediments. Environmental Science and Technology, 39, 764-769. https://doi.org/10.1021/es049320z

Cornelissen, G., Gustafsson, Ö., Bucheli, T.D., Jonker, M.T.O., Koelmans, A.A., van Noort, P.C.M., 2005. Extensive sorption of organic compounds to black carbon, coal, and kerogen in sediments and soils: mechanisms and consequences for distribution, bioaccumulation, and biodegradation. Environmental Science & Technology, 39, 6881-6895. https://doi.org/10.1021/es050191b

Das, L., Das, P., Bhowal, A., Bhattachariee, C., 2020. Synthesis of hybrid hydrogel nano-polymer composite using Graphene oxide, Chitosan and PVA and its application in wastewater treatment. Environmental Technology & Innovation, 18, 100664. https://doi.org/10.1016/j.eti.2020.100664

Deblonde, T., Cossu-Leguille, C., Hartemann, P., 2011. Emerging pollutants in wastewater: A review of the literature. International Journal of Hygiene and Environmental Health, 214, 442-448. https://doi.org/10.1016/j.ijheh.2011.08.002

Deblonde, T., Hartemann, P., 2013. Environmental impact of medical prescriptions: assessing the risks and hazards of persistence, bioaccumulation and toxicity of pharmaceuticals. Public Health, 127, 312-317. https://doi.org/10.1016/j.puhe.2013.01.026

Dreyer, D.R., Ruoff, R.S., Bielawski, C.W., 2010. From Conception to Realization: An Historial Account of Graphene and Some Perspectives for Its Future. Angewandte Chemie International Edition 49, 9336-9344. https://doi.org/10.1002/anie.201003024

Ersan, G., Apul, O.G., Perreault, F., Karanfil, T., 2017. Adsorption of organic contaminants by graphene nanosheets: A review. Water Research, 126, 385-398. https://doi.org/10.1016/j.watres.2017.08.010

Fang, G.-C., Chang, K.-F., Lu, C., Bai, H., 2004. Estimation of PAHs dry deposition and BaP toxic equivalency factors (TEFs) study at Urban, Industry Park and rural sampling sites in central Taiwan, Taichung. Chemosphere, 55, 787-796. https://doi.org/10.1016/j.chemosphere.2003.12.012

Fang, Q., Chen, B., Lin, Y., Guan, Y., 2014. Aromatic and hydrophobic surfaces of wood-derived biochar enhance perchlorate adsorption via hydrogen bonding to oxygen-containing organic groups. Environmental Science & Technology, 48, 279-288. https://doi.org/10.1021/es403711y

Fasnacht, M.P., Blough, N.V., 2002. Aqueous photodegradation of polycyclic aromatic hydrocarbons. Environmental Science & Technology, 36, 4364-4369. https://doi.org/10.1021/es025603k

Forbes, P.B.C., Rohwer, E.R., 2009. Investigations into a novel method for atmospheric polycyclic aromatic hydrocarbon monitoring. Environmental Pollution, 157, 2529-2535. https://doi.org/10.1016/j.envpol.2009.03.004

Fraga, T.J.M., Carvalho, M.N., Ghislandi, M.G., Motta Sobrinho, M.A.d., 2019. Functionalized graphene-based materials as innovative adsorbents for organic pollutants: a concise overview. Brazilian Journal of Chemical Engineering, 36, 1-31. https://doi.org/10.1590/0104-6632.20190361s20180283

Geim, A.K., 2009. Graphene: Status and Prospects. Science, 324, 1530-1534. https://doi.org/10.1126/science.1158877

Geldenhuys, G., Rohwer, E.R., Naudé, Y., Forbes, P.B.C., 2015. Monitoring of atmospheric gaseous and particulate polycyclic aromatic hydrocarbons in South African platinum mines utilising portable denuder sampling with analysis by thermal desorption–comprehensive gas chromatography–mass spectrometry. Journal of Chromatography A, 1380, 17-28. https://doi.org/10.1016/j.chroma.2014.12.062

Ghasemzadeh, K., Zeynali, R., Basile, A., 2019. Chapter 13 - Microporous graphene-based membrane: structure, preparation, characterization, and applications, in: Basile, A., Ghasemzadeh, K. (Eds.), Current Trends and Future Developments on (Bio-) Membranes. Elsevier, pp. 301-327.

Ghosal, D., Ghosh, S., Dutta, T.K., Ahn, Y., 2016. Current State of Knowledge in Microbial Degradation of Polycyclic Aromatic Hydrocarbons (PAHs): A Review. Frontiers in Microbiology 7. https://doi.org/10.3389/fmicb.2016.01369

Gouadec, G., Colomban, P., 2007. Raman Spectroscopy of nanomaterials: How spectra relate to disorder, particle size and mechanical properties. Progress in Crystal Growth and Characterization of Materials, 53, 1-56. https://doi.org/10.1016/j.pcrysgrow.2007.01.001

Guo, X., Wang, X., Zhou, X., Kong, X., Tao, S., Xing, B., 2012. Sorption of Four Hydrophobic Organic Compounds by Three Chemically Distinct Polymers: Role of Chemical and Physical Composition. Environmental Science & Technology, 46, 7252-7259. https://doi.org/10.1021/es301386z

Harrison, R.M., Smith, D.J.T., Luhana, L., 1996. Source Apportionment of Atmospheric Polycyclic Aromatic Hydrocarbons Collected from an Urban Location in Birmingham, U.K. Environmental Science & Technology, 30, 825-832. https://doi.org/10.1021/es950252d

Ho, Y.S., McKay, G., 1999. Pseudo-second order model for sorption processes. Process Biochemistry, 34, 451-465. https://doi.org/10.1016/S0032-9592(98)00112-5

Honda, M., Suzuki, N., 2020. Toxicities of Polycyclic Aromatic Hydrocarbons for Aquatic Animals. International Journal of Environmental Research and Public Health, 17(4), 1363. https://dx.doi.org/10.3390%2Fijerph17041363

Hong, J., Park, M.K., Lee, E.J., Lee, D., Hwang, D.S., Ryu, S., 2013. Origin of New Broad Raman D and G Peaks in Annealed Graphene. Scientific Reports, 3, 2700. https://doi.org/10.1038/srep02700

Hu, Q., Zhang, Z., 2019. Application of Dubinin–Radushkevich isotherm model at the solid/solution interface: A theoretical analysis. Journal of Molecular Liquids, 277, 646-648. https://doi.org/10.1016/j.molliq.2019.01.005

Huang, W.L., Peng, P.A., Yu, Z.Q., 2003. Effects of organic matter heterogeneity on sorption and desorption of organic contaminants by soils and sediments. Applied Geochemistry, 18, 995-972. https://doi.org/10.1016/S0883-2927(02)00205-6

Hussain K. et al. 2018. Monitoring and risk analysis of PAHs in the environment. In: Hussain C. (eds) Handbook of Environmental Materials Management. Springer, Cham. https://doi.org/10.1007/978-3-319-58538-3_29-2

IARC, International Agency for Research on Cancer, 2010. IARC Monographs on the Evaluation of Carcinogenic Risks to Humans. (Lyon: World Health Organization), 92, 1–853.

Igwe, J.C., Augustine, A.A., 2007. Equilibrium sorption isotherm studies of Cd(II), Pb(II) and Zn(II) ions detoxification from waste water using unmodified and EDTA-modified maize husk. Electronic Journal of Chemistry, 10, 535-548.

Jonker, M.T.O., Koelmans, A.A., 2002. Extraction of Polycyclic Aromatic Hydrocarbons from Soot and Sediment: Solvent Evaluation and Implications for Sorption Mechanism. Environmental Science & Technology, 36, 4107-4113. https://doi.org/10.1021/es0103290

Kalavathy, M.H., Karthikeyan, T., Rajgopal, S., Miranda, L.R., 2005. Kinetic and isotherm studies of Cu(II) adsorption onto H_3PO_4-activated rubber wood sawdust. Journal of Colloid and Interface Science, 292, 354-362. https://doi.org/10.1016/j.jcis.2005.05.087

Kemp, K.C., Seema, H., Saleh, M., Le, N.H., Mahesh, K., Chandra, V., Kim, K.S., 2013. Environmental applications using graphene composites: water remediation and gas adsorption. Nanoscale, 5, 3149-3171. https://doi.org/10.1039/C3NR33708A

Khan, M.N., Sarwar, A., 2007. Determination of points of zero charge of natural and treated adsorbents. Surface Review and Letters, 14, 461-469. doi:10.1142/S0218625X07009517

K'Oreje, K.O., Vergeynst, L., Ombaka, D., De Wispelaere, P., Okoth, M., Van Langenhove, H., Demeestere, K., 2016. Occurrence patterns of pharmaceutical residues in wastewater, surface water and groundwater of Nairobi and Kisumu city, Kenya. Chemosphere, 149, 238-244. https://doi.org/10.1016/j.chemosphere.2016.01.095

Kowanga, K.D., Gatebe, E., Mauti, G.O., Mauti, E.M., 2016. Kinetic, sorption isotherms, pseudo-first-order model and pseudo-second-order model studies of Cu(II) and Pb(II) using defatted Moringa oleifera seed powder. Journal of Phytopharmacology, 5, 71-78.

Krauss, M., Wilcke, W., Martius, C., Bandeira, A.G., Garcia, M.V.B., Amelung, W., 2005. Atmospheric versus biological sources of polycyclic aromatic hydrocarbons (PAHs) in a tropical rain forest environment. Environmental Pollution, 135, 143-154. https://doi.org/10.1016/j.envpol.2004.09.012

Lagergren, S., 1898. About the theory of so-called adsorption of soluble substances. Kungliga Svenska Veteskapsakademiens Handlingar Band, 24, 1-29.

Lamichhane, S., Bal Krishna, K.C., Sarukkalige, R., 2016. Polycyclic aromatic hydrocarbons (PAHs) removal by sorption: A review. Chemosphere, 148, 336-353. https://doi.org/10.1016/j.chemosphere.2016.01.036

Lammel, G., 2015. Polycyclic Aromatic Compounds in the Atmosphere – A Review Identifying Research Needs. Polycyclic Aromatic Compounds, 35, 316-329. https://doi.org/10.1080/10406638.2014.931870

Li, B., Ou, P., Wei, Y., Zhang, X., Song, J., 2018. Polycyclic Aromatic Hydrocarbons Adsorption onto Graphene: A DFT and AIMD Study. Materials (Basel, Switzerland) 11, 726. https://doi.org/10.3390/ma11050726

Liu, Q., Zhou, Q., Jiang, G., 2014. Nanomaterials for analysis and monitoring of emerging chemical pollutants. TrAC Trends in Analytical Chemistry, 58, 10-22. https://doi.org/10.1016/j.trac.2014.02.014

Liu, R., Wu, D., Feng, X., Müllen, K., 2011. Bottom-Up Fabrication of Photoluminescent Graphene Quantum Dots with Uniform Morphology. Journal of the American Chemical Society, 133, 15221-15223. https://doi.org/10.1021/ja204953k

Richardson, S.D., Kimura, S.Y., 2017. Emerging environmental contaminants: Challenges facing our next generation and potential engineering solutions. Environmental Technology & Innovation, 8, 40-56. https://doi.org/10.1016/j.eti.2017.04.002

Lukić, B., Panico, A., Huguenot, D., Fabbricino, M., van Hullebusch, E.D., Esposito, G., 2016. Evaluation of PAH removal efficiency in an artificial soil amended with different types of organic wastes. Euro-Mediterranean Journal for Environmental Integration, 1, 5. https://doi.org/10.1007/s41207-016-0001-x

Luo, L., Lin, S., Huang, H., Zhang, S., 2012. Relationships between aging of PAHs and soil properties. Environmental Pollution, 170, 177-182. https://doi.org/10.1016/j.envpol.2012.07.003

Mahamadi, C., Nharingo, T., 2010. Utilization of water hyacinth weed (Eichhornia crassipes) for the removal of Pb(II), Cd(II) and Zn(II) from aquatic environments: an adsorption isotherm study. Environmental Technology, 31, 1221-1228. https://doi.org/10.1080/09593331003646604

Malakahmad, A., Law, M.X., Ng, K.-W., Manan, T.S.A., 2016. The Fate and Toxicity Assessment of Polycyclic Aromatic Hydrocarbons (PAHs) in Water Streams of Malaysia. Procedia Engineering, 148, 806-811. https://doi.org/10.1016/j.proeng.2016.06.572

Mayavan, S, Sim, J-B, Choi, S-M. 2012. Easy synthesis of nitrogen-doped graphene–silver nanoparticle hybrids by thermal treatment of graphite oxide with glycine and silver nitrate. Carbon, 50, 5148-5155. https://doi.org/10.1016/j.carbon.2012.06.055

McNutt, M.K., Camilli, R., Crone, T.J., Guthrie, G.D., Hsieh, P.A., Ryerson, T.B., Savas, O., Shaffer, F., 2012. Review of flow rate estimates of the Deepwater Horizon oil spill. Proceedings of the National Academy of Sciences of the United States of America, 109, 20260-20267. https://doi.org/10.1073/pnas.1112139108

Menéndez-Díaz, J.A., Martín-Gullón, I., 2006. Chapter 1 Types of carbon adsorbents and their production, in: Bandosz, T.J. (Ed.), Interface Science and Technology. Elsevier, 7, 1-47. https://doi.org/10.1016/S1573-4285(06)80010-4

Mohamed, M.A., Jaafar, J., Ismail, A.F., Othman, M.H.D., Rahman, M.A., 2017. Chapter 1 - Fourier Transform Infrared (FTIR) Spectroscopy, in: N. Hilal, A.F. Ismail, T. Matsuura, D. Oatley-Radcliffe (Eds.) Membrane Characterization, Elsevier, pp. 3-29.

Mourdikoudis, S., Pallares, R.M., Thanh, N.T.K., 2018. Characterization techniques for nanoparticles: comparison and complementarity upon studying nanoparticle properties. Nanoscale, 10, 12871-12934. https://doi.org/10.1039/c8nr02278j

Munyeza, C.F., Dikale, O., Rohwer, E.R., Forbes, P.B.C., 2018. Development and optimization of a plunger assisted solvent extraction method for polycyclic aromatic hydrocarbons sampled onto multi-channel silicone rubber traps. Journal of Chromatography A, 1555, 20-29. https://doi.org/10.1016/j.chroma.2018.04.053

Munyeza, C.F., Osano, A.M., Maghanga, J.K., Forbes, P.B.C., 2020. Polycyclic Aromatic Hydrocarbon Gaseous Emissions from Household Cooking Devices: A Kenyan Case Study. Environmental Toxicology and Chemistry, 39, 538-547. https://doi.org/10.1002/etc.4648

Ncube, S., Madikizela, L.M., Chimuka, L., Nindi, M.M., 2018. Environmental fate and ecotoxicological effects of antiretrovirals: A current global status and future perspectives. Water Research, 145, 231-247. https://doi.org/10.1016/j.watres.2018.08.017

Ngumba, E., Gachanja, A., Tuhkanen, T., 2016. Occurrence of selected antibiotics and antiretroviral drugs in Nairobi River Basin, Kenya. Science of The Total Environment, 539, 206-213. https://doi.org/10.1016/j.scitotenv.2015.08.139

Nisbet, I.C., LaGoy, P.K. 1992. Toxic equivalency factors (TEFs) for polycyclic aromatic hydrocarbons (PAHs). Regulatory Toxicology and Pharmacology, 16, 290-300. https://doi.org/10.1016/0273-2300(92)90009-X

Novoselov, K.S., Fal'ko, V.I., Colombo, L., Gellert, P.R., Schwab, M.G., Kim, K., 2012. A roadmap for graphene. Nature, 490, 192-200. https://doi.org/10.1038/nature11458

Ololade, I.A., Adeola, A.O., Oladoja, N.A., Ololade, O.O., Nwaolisa, S.U., Alabi, A.B., Ogungbe, I.V., 2018. In-situ modification of soil organic matter towards adsorption and desorption of phenol and its chlorinated derivatives. Journal of Environmental Chemical Engineering, 6, 3485-3494. https://doi.org/10.1016/j.jece.2018.05.034

Oyedotun, K.O., Masikhwa, T.M., Lindberg, S., Matic, A., Johansson, P., Manyala, N., 2019. Comparison of ionic liquid electrolyte to aqueous electrolytes on carbon nanofibres supercapacitor electrode derived from oxygen-functionalized graphene. Chemical Engineering Journal, 375, 121906. https://doi.org/10.1016/j.cej.2019.121906

Oyelude, E.O., Awudza, J.A.M. & Twumasi, S.K. 2017. Equilibrium, kinetic and thermodynamic study of removal of Eosin Yellow from aqueous solution using Teak Leaf litter powder. Scientific Report, 7, 12198. https://doi.org/10.1038/s41598-017-12424-1

Patra, D. 2003. Applications and new developments in fluorescence spectroscopic techniques for the analysis of polycyclic aromatic hydrocarbons. Applied Spectroscopy Reviews, 38(2), 155-185. https://doi.org/10.1081/ASR-120021166

Petrie, B., Barden, R., Kasprzyk-Hordern, B., 2015. A review on emerging contaminants in wastewaters and the environment: Current knowledge, understudied areas and recommendations for future monitoring. Water Research, 72, 3-27. https://doi.org/10.1016/j.watres.2014.08.053

Prasse, C., Schlüsener, M.P., Schulz, R., Ternes, T.A., 2010. Antiviral Drugs in Wastewater and Surface Waters: A New Pharmaceutical Class of Environmental Relevance? Environmental Science & Technology, 44, 1728-1735. https://doi.org/10.1021/es903216p

Rahman, M.S., Islam, M.R., 2009. Effects of pH on isotherms modeling for Cu (II) ions adsorption using maple wood sawdust. Chemical Engineering Journal, 149, 273–280. https://doi.org/10.1016/j.cej.2008.11.029

Ringot, D., Lerzy, B., Chaplain, K., Bonhoure, J.-P., Auclair, E., Larondelle, Y., 2007. In vitro biosorption of ochratoxin A on the yeast industry by-products: Comparison of isotherm models. Bioresource Technology, 98, 1812-1821. https://doi.org/10.1016/j.biortech.2006.06.015

Robati, D., 2013. Pseudo-second-order kinetic equations for modeling adsorption systems for removal of lead ions using multi-walled carbon nanotube. Journal of Nanostructure in Chemistry, 3, 55. https://doi.org/10.1186/2193-8865-3-55

Romero, I.C., Sutton, T., Carr, B., Quintana-Rizzo, E., Ross, S.W., Hollander, D.J., Torres, J.J., 2018. Decadal Assessment of Polycyclic Aromatic Hydrocarbons in Mesopelagic Fishes from the Gulf of Mexico Reveals Exposure to Oil-Derived Sources. Environmental Science and Technology, 52, 10985-10996. https://doi.org/10.1021/acs.est.8b02243

Sabzehmeidani, M.M, Mahnaee, S., Ghaedi, M., Heidari, H., Roy, V.A.L. 2021. Carbon based materials: a review of adsorbents for inorganic and organic compounds. Materials Advances, 2, 598-627. https://doi.org/10.1039/D0MA00087F

Sapkota, A., Sapkota, A.R., Kucharski, M., Burke, J., McKenzie, S., Walker, P., Lawrence, R., 2008. Aquaculture practices and potential human health risks: current knowledge and future priorities. Environment International, 34, 1215-1226. https://doi.org/10.1016/j.envint.2008.04.009

Schoeman, C., Dlamini, M., Okonkwo, O.J., 2015. Quantification of Selected Antiretroviral Drugs in a Wastewater Treatment Works in South Africa Using GC-TOFMS. Journal of Chromatography Seperation Techniques, 6, 272. https://doi.org/10.4172/2157-7064.1000272

Schoeman, C., Dlamini, M., Okonkwo, O.J., 2017. The impact of a Wastewater Treatment Works in Southern Gauteng, South Africa on efavirenz and nevirapine discharges into the aquatic environment. Emerging Contaminants, 3, 95-106. https://doi.org/10.1016/j.emcon.2017.09.001

Schoonraad, G.-L., Madito, M.J., Manyala, N., Forbes, P., 2020. Synthesis and optimisation of a novel graphene wool material by atmospheric pressure chemical vapour deposition. Journal of Materials Science, 55, 545-564. https://doi.org/10.1007/s10853-019-03948-0

Sears, G. W. 1956. Determination of specific surface area of colloidal silica by titration with sodium hydroxide. Analytical Chemistry 28 (12), 1981–1983.

Shang, J., Chen, J., Shen, Z., Xiao, X., Yang, H., Wang, Y., Ruan, A., 2015. Photochemical degradation of PAHs in estuarine surface water: effects of DOM, salinity, and suspended particulate matter. Environmental Science and Pollution Research, 22, 12374-12383. https://doi.org/10.1007/s11356-015-4543-2

Shannon, M.A., Bohn, P.W., Elimelech, M., Georgiadis, J.G., Mariñas, B.J., Mayes, A.M., 2008. Science and technology for water purification in the coming decades. Nature, 452, 301-310. https://doi.org/10.1038/nature06599

Singh, N.B., Nagpal, G., Agrawal, S., Rachna, 2018. Water purification by using Adsorbents: A Review. Environmental Technology & Innovation, 11, 187-240. https://doi.org/10.1016/j.eti.2018.05.006

Site, A.D., 2001. Factors Affecting Sorption of Organic Compounds in Natural Sorbent/Water Systems and Sorption Coefficients for Selected Pollutants. A Review. Journal of Physical and Chemical Reference Data, 30, 187-439. https://doi.org/10.1063/1.1347984

Stankovich, S., Dikin, D.A., Dommett, G.H.B., Kohlhaas, K.M., Zimney, E.J., Stach, E.A., Piner, R.D., Nguyen, S.T., Ruoff, R.S., 2006. Graphene-based composite materials. Nature, 442, 282-286. https://doi.org/10.1038/nature04969

Steffen, O., 2013. X-Ray Photoelectron Spectroscopy in Analysis of Surfaces Update based on the original article, Encyclopedia of Analytical Chemistry, John Wiley & Sons, Ltd. https://doi.org/10.1002/9780470027318.a2517.pub2

Sun, Y., Yang, S., Zhao, G., Wang, Q., Wang, X., 2013. Adsorption of polycyclic aromatic hydrocarbons on graphene oxides and reduced graphene oxides. Chemistry- an Asian Journal, 8, 2755-2761. https://doi.org/10.1002/asia.201300496

Susi, T., Pichler, T., Ayala, P., 2015. X-ray photoelectron spectroscopy of graphitic carbon nanomaterials doped with heteroatoms. Beilstein Journal of Nanotechnology, 6, 177-192. https://doi.org/10.3762/bjnano.6.17

Jain, S., Vyas, R.K., Prabhat, P., Sangeeta, V., 2011. A review on fate of antiviral drugs in environment and detection techniques. International Journal of Environmental Sciences, 1, 1526-1541.

Ternes, T.A., Meisenheimer, M., McDowell, D., Sacher, F., Brauch, H.J., HaistGulde, B., Preuss, G., Wilme, U., ZuleiSeiberts, N., 2002. Removal of pharmaceuticals during drinking water

treatment. Environmental Science & Technology, 36, 3855-3863. https://doi.org/10.1021/es015757k

Terzopoulou, Z., Papageorgiou, M., Kyzas, G.Z., Bikiaris, D.N., Lambropoulou, D.A., 2016. Preparation of molecularly imprinted solid-phase microextraction fiber for the selective removal and extraction of the antiviral drug abacavir in environmental and biological matrices. Analytica Chimica Acta, 913, 63-75. https://doi.org/10.1016/j.aca.2016.01.059

Tessmer, C.H., Vidic, R.D., Uranowski, L.J., 1997. Impact of Oxygen-Containing Surface Functional Groups on Activated Carbon Adsorption of Phenols. Environmental Science & Technology, 31, 1872-1878. https://doi.org/10.1021/es960474r

Tzabar, N., ter Brake, H.J.M., 2016. Adsorption isotherms and Sips models of nitrogen, methane, ethane, and propane on commercial activated carbons and polyvinylidene chloride. Adsorption, 22, 901-914. https://doi.org/10.1007/s10450-016-9794-9

Unuabonah, E.I., Omorogie, M.O., Oladoja, N.A., 2019. 5 - Modeling in Adsorption: Fundamentals and Applications, in: Kyzas, G.Z., Mitropoulos, A.C. (Eds.), Composite Nanoadsorbents. Elsevier, pp. 85-118. https://doi.org/10.1016/B978-0-12-814132-8.00005-8

USEPA, United State Environmental Protection Agency, 2000. Toxic release inventory public data release. Washington, D.C.: Office of Environmental Information, United States Environmental Protection Agency. hppt://www.epa.gov/triinter/tridata/index.htm. [Online Resource]

USFDA, Antiretroviral drugs used in the treatment of HIV infection. https://aidsinfo.nih.gov/understanding-hiv-aids/fact-sheets/21/58/fda-approved-hiv-medicines last reviewed on 30 January 2020.

Van der Bruggen, B., 2015. Freundlich Isotherm, in: Drioli, E., Giorno, L. (Eds.), Encyclopedia of Membranes. Springer Berlin Heidelberg, Berlin, Heidelberg, pp. 1-2. https://doi.org/10.1007/978-3-642-40872-4_254-3

Vergeynst, L., Haeck, A., De Wispelaere, P., Van Langenhove, H., Demeestere, K., 2015. Multi-residue analysis of pharmaceuticals in wastewater by liquid chromatography–magnetic sector mass spectrometry: Method quality assessment and application in a Belgian case study. Chemosphere, 119, S2-S8. https://doi.org/10.1016/j.chemosphere.2014.03.069

Villacañas, F., Pereira, M.F., Orfão, J.J., Figueiredo, J.L., 2006. Adsorption of simple aromatic compounds on activated carbons. Journal of Colloid and Interface Science, 293, 128-136. https://doi.org/10.1016/j.jcis.2005.06.032

Wang, H., Zhou, A., Peng, F., Yu, H., Yang, J., 2007. Mechanism study on adsorption of acidified multiwalled carbon nanotubes to Pb(II). Journal of Colloid and Interface Science, 316, 277-283. https://doi.org/10.1016/j.jcis.2007.07.075

Wang, J., Chen, Z., Chen, B., 2014a. Adsorption of Polycyclic Aromatic Hydrocarbons by Graphene and Graphene Oxide Nanosheets. Environmental Science & Technology 48, 4817-4825. https://doi.org/10.1021/es405227u

Wang, L., Shi, C., Wang, L., Pan, L., Zhang, X., Zou, J.-J., 2020. Rational design, synthesis, adsorption principles and applications of metal oxide adsorbents: a review. Nanoscale, 12, 4790-4815. https://doi.org/10.1039/C9NR09274A

Wang, W., Wang, Z., Liu, J., Zhang, Z., Sun, L., 2017. Single-step One-pot Synthesis of Graphene Foam/TiO2 Nanosheet Hybrids for Effective Water Treatment. Scientific Report, 7, 43755. https://doi.org/10.1038/srep43755

Wang, X., Pei, Y., Lu, M., Lu, X., Du, X., 2014b. Highly efficient adsorption of heavy metals from wastewaters by graphene oxide-ordered mesoporous silica materials. Journal of Materials Science, 50, 2113-2121. https://doi.org/10.1007/s10853-014-8773-3

Wang, Y., Li, Z., Tang, C., Ren, H., Zhang, Q., Xue, M., Xiong, J., Wang, D., Yu, Q., He, Z., Wei, F., Jiang, J., 2019. Few-layered mesoporous graphene for high-performance toluene adsorption and regeneration. Environmental Science: Nano, 6, 3113-3122. https://doi.org/10.1039/C9EN00608G

Warner, J.H., Rümmeli, M.H., Ge, L., Gemming, T., Montanari, B., Harrison, N.M., Büchner, B., Briggs, G.A.D., 2009. Structural transformations in graphene studied with high spatial and temporal resolution. Nature Nanotechnology, 4, 500-504. https://doi.org/10.1038/nnano.2009.194

Weber, W.J., Smith, E.H., 1987. Simulation and design models for adsorption processes. Environmental Science & Technology, 21, 1040-1050. https://doi.org/10.1021/es00164a002

Wilcke, W., Amelung, W., Martius, C., Garcia, M.V.B., Zech, W., 2000. Biological Sources of Polycyclic Aromatic Hydrocarbons (PAHs) in the Amazonian Rain Forest. Journal of Plant Nutrition and Soil Science, 163, 27-30. https://doi.org/10.1002/(SICI)1522-2624(200002)163:1%3C27::AID-JPLN27%3E3.0.CO;2-E

Wilcke, W., Krauss, M., Amelung, W., 2002. Carbon Isotope Signature of Polycyclic Aromatic Hydrocarbons (PAHs): Evidence for Different Sources in Tropical and Temperate Environments? Environmental Science & Technology, 36, 3530-3535. https://doi.org/10.1021/es020032h

Wood, T.P., Duvenage, C.S.J., Rohwer, E., 2015. The occurrence of anti-retroviral compounds used for HIV treatment in South African surface water. Environmental Pollution, 199, 235-243. https://doi.org/10.1016/j.envpol.2015.01.030

Wooding, M., Rohwer, E.R., Naudé, Y., 2017. Determination of endocrine disrupting chemicals and antiretroviral compounds in surface water: A disposable sorptive sampler with

comprehensive gas chromatography – Time-of-flight mass spectrometry and large volume injection with ultra-high performance liquid chromatography–tandem mass spectrometry. Journal of Chromatography A, 1496, 122-132. https://doi.org/10.1016/j.chroma.2017.03.057

Worch, E., 2008. Fixed-bed adsorption in drinking water treatment: a critical review on models and parameter estimation. Journal of Water Supply: Research and Technology-Aqua, 57, 171-183. https://doi.org/10.2166/aqua.2008.100

Worch, E., 2012. Adsorption Technology in Water Treatment. Fundamentals, Processes, and Modeling. De Gruyter, Berlin, Boston. https://doi.org/10.1515/9783110240238

Wu, F.-C., Tseng, R.-L., Juang, R.-S., 2009. Initial behavior of intraparticle diffusion model used in the description of adsorption kinetics. Chemical Engineering Journal, 153, 1-8. https://doi.org/10.1016/j.cej.2009.04.042

Wu, Z., Sun, Z., Liu, P., Li, Q., Yang, R., Yang, X., 2020. Competitive adsorption of naphthalene and phenanthrene on walnut shell based activated carbon and the verification via theoretical calculation. RSC Advances, 10, 10703-10714. https://doi.org/10.1039/C9RA09447D

Yang, X., Wan, Y., Zheng Y, He, F., Yu, Z., Huang, J., Wang, H., Ok, Y.S., Jiang, Y., Gao, B. 2019. Surface functional groups of carbon-based adsorbents and their roles in the removal of heavy metals from aqueous solutions: A critical review. Chemical Engineering Journal, 366, 608-621. https://doi.org/10.1016/j.cej.2019.02.119

Ye, B., Kim, S.-I., Lee, M., Ezazi, M., Kim, H.-D., Kwon, G., Lee, D.H., 2020. Synthesis of oxygen functionalized carbon nanotubes and their application for selective catalytic reduction of NO_x with NH_3. RSC Advances 10, 16700-16708. https://doi.org/10.1039/D0RA01665A

Yousef, N.S., Farouq, R., Hazzaa, R., 2016. Adsorption kinetics and isotherms for the removal of nickel ions from aqueous solutions by an ion-exchange resin: application of two and three parameter isotherm models. Desalination and Water Treatment, 57, 21925-21938. https://doi.org/10.1080/19443994.2015.1132474

Yu, W., Sisi, L., Haiyan, Y., Jie, L., 2020. Progress in the functional modification of graphene/graphene oxide: a review. RSC Advances, 10, 15328-15345. https://doi.org/10.1039/D0RA01068E

Yuan, P., Li, X., Wang, W., Liu, H., Yan, Y., Yang, H., Yue, Y., Bao, X., 2018. Tailored Design of Differently Modified Mesoporous Materials To Deeply Understand the Adsorption Mechanism for Polycyclic Aromatic Hydrocarbons. Langmuir, 34, 15708-15718. https://doi.org/10.1021/acs.langmuir.8b03299

Zakaria, M.P., Takada, H., Tsutsumi, S., Ohno, K., Yamada, J., Kouno, E., Kumata, H., 2002. Distribution of Polycyclic Aromatic Hydrocarbons (PAHs) in Rivers and Estuaries in

Malaysia: A Widespread Input of Petrogenic PAHs. Environmental Science & Technology, 36, 1907-1918. https://doi.org/10.1021/es011278+

Zelinkova, Z., Wenzl, T., 2015. The Occurrence of 16 EPA PAHs in Food - A Review. Polycyclic Aromatic Compounds, 35, 248-284. https://doi.org/10.1080/10406638.2014.918550

Zhang, C., Wu, L., Cai, D., Zhang, C., Wang, N., Zhang, J., Wu, Z., 2013. Adsorption of Polycyclic Aromatic Hydrocarbons (Fluoranthene and Anthracenemethanol) by Functional Graphene Oxide and Removal by pH and Temperature-Sensitive Coagulation. ACS Applied Materials & Interfaces, 5, 4783-4790. https://doi.org/10.1021/am4002666

Zhao, G.X., Li, J.X., Wang, X.K., 2011. Kinetic and thermodynamic study of 1-naphthol adsorption from aqueous solution to sulfonated graphene nanosheets. Chemical Engineering Journal, 173, 185–190. https://doi.org/10.1016/j.cej.2011.07.072

Zheng, J., Chen, B., Thanyamanta, W., Hawboldt, K., Zhang, B., Liu, B., 2016. Offshore produced water management: A review of current practice and challenges in harsh/Arctic environments. Marine Pollution Bulletin, 104, 7-19. https://doi.org/10.1016/j.marpolbul.2016.01.004

Chapter 3 Literature review

Paper 1. Remediation approaches for the decontamination of polycyclic aromatic hydrocarbons in aqueous media

This chapter presents a literature review on several mitigation strategies for polycyclic aromatic hydrocarbon (PAH) pollution in aqueous media. It includes a comprehensive review of existing and emerging technologies for the treatment of PAH-polluted water, and the efforts of many researchers to advance water treatment with new proposals. The review is presented as published in Water Environment Research (Wiley). It was selected as the Editor's Choice article in March 2021.

Article

Adeola, A.O., Forbes, P.B.C. (2021). Advances in water treatment technologies for removal of polycyclic aromatic hydrocarbons: Existing concepts, emerging trends, and future prospects. Water Environment Research, 93(3): 343-359.
DOI: https://doi.org/10.1002/wer.1420

Graphical abstract

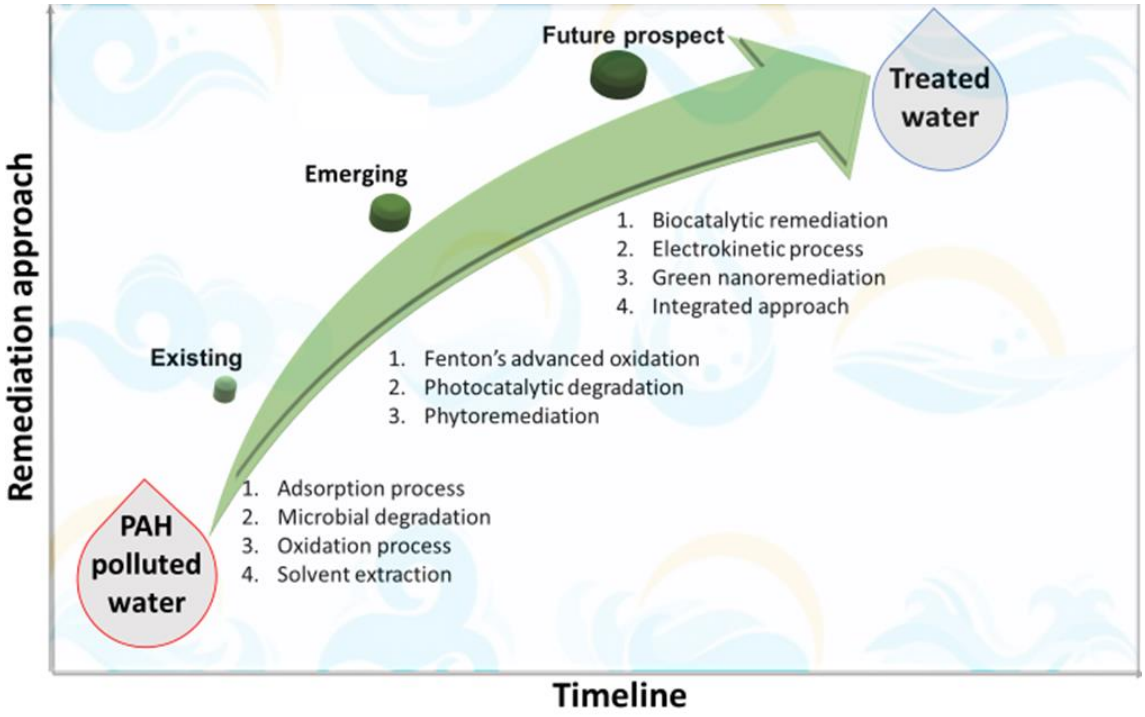

Water Environment Federation
the water quality people™

Advances in water treatment technologies for removal of polycyclic aromatic hydrocarbons: Existing concepts, emerging trends, and future prospects

Adedapo O. Adeola , Patricia B. C. Forbes

Department of Chemistry, Faculty of Natural and Agricultural Sciences, University of Pretoria, Pretoria, South Africa

Received 14 April 2020; Revised 6 July 2020; Accepted 18 July 2020

University of Pretoria

Correspondence to: Patricia B. C. Forbes, Department of Chemistry, Faculty of Natural and Agricultural Sciences, University of Pretoria, Pretoria, South Africa.
Email: patricia.forbes@up.ac.za

Published online 09 August 2020 in Wiley Online Library (wileyonlinelibrary.com)

DOI: 10.1002/wer.1420

Abstract

In the last two decades, environmental experts have focused on the development of several biological, chemical, physical, and thermal methods/technologies for remediation of PAH-polluted water. Some of the findings have been applied to field-scale treatment, while others have remained as prototypes and semi-pilot studies. Existing treatment options include extraction, chemical oxidation, bioremediation, photocatalytic degradation, and adsorption (employing adsorbents such as biomass derivatives, geosorbents, zeolites, mesoporous silica, polymers, nanocomposites, and graphene-based materials). Electrokinetic remediation, advanced phytoremediation, green nanoremediation, enhanced remediation using biocatalysts, and integrated approaches are still at the developmental stage and hold great potential. Water is an essential component of the ecosystem and highly susceptible to PAH contamination due to crude oil exploration and spillage, and improper municipal and industrial waste management, yet comprehensive reviews on PAH remediation are only available for contaminated soils, despite the several treatment methods developed for the remediation of PAH-polluted water. This review seeks to provide a comprehensive overview of existing and emerging methods/technologies, in order to bridge information gaps toward ensuring a green and sustainable remedial approach for PAH-contaminated aqueous systems. © 2020 Water Environment Federation

Practitioner points

- Comprehensive review of existing and emerging technologies for remediation of PAH-polluted water.
- Factors influencing efficiency of various methods, challenges and merits were discussed.
- Green nano-adsorbents, nano-oxidants and bio/phytoremediation are desirous for ecofriendly and economical PAH remediation.
- Adoption of an integrated approach for the efficient and sustainable remediation of PAH-contaminated water is recommended.

Key words

environment; pollution; polycyclic aromatic hydrocarbons; remediation; water treatment

Introduction

PAHs are hydrocarbons containing two or more benzene rings fused together with C–C bonds, which have unique physicochemical characteristics (Mohan, Kisa, Ohkuma, Kanaly, & Shimizu, 2006; Okere, 2011). They are hazardous organic micropollutants, which are ubiquitous and recalcitrant to degradation (Duan, Naidu, Thavamani, Meaklim, & Megharaj, 2015; Ghosal, Ghosh, Dutta, & Ahn, 2016). They are commonly found in water bodies with proximity to crude oil exploration, gas production, and wood/coal processing industries (e.g., Abdel-Shafy & Mansour, 2016; Sun et al., 2009; Zhao,

Jiang, et al., 2011). Some PAHs possess carcinogenic toxicities even at very low concentrations and humans are hazardously exposed through several routes—air (atmospheric deposition, inhalation etc.), water (domestic, recreational use etc.), food, and occupational exposures. However, one of the core routes of human exposure is through polluted water (Wang, Yang, Niu, & Wang, 2009; Wu, Zhang, Zhang, & Cheng, 2011). For simplicity, PAHs can be classified into two groups which are the lower molecular weight (LMW), structurally 2–3 ringed PAHs which are less toxic than the second class, and the higher molecular weight (HMW), 4–7 ring PAHs which are more resistant to degradation and have higher carcinogenicity (Kuppusamy, Thavamani, Megharaj, & Naidu, 2016).

In water bodies, the concentrations of PAHs range widely from 0.03 ng/L {Southeastern Sea, Japan} (Hayakawa et al., 2016) to 753 ng/L {Yellow River Delta, China} (Yuan, Li, Ding, Zhao, & Ye, 2014) to as high as 16.59 mg/L {Limpopo Province, South Africa} (Edokpayi, Odiyo, Popoola, & Msagati, 2016). Furthermore, the bioconcentration of Σ16 PAHs in aquatic animals (fish) ranges from 11.2 ng/g (*Cynoscion guatucupa*, South America) to as high as 4,207.5 ng/g (*Saurida undosquamis*, Egypt) (Mojiri, Zhou, Ohashi, Ozaki, & Kindaichi, 2019). Hundreds of different PAHs and derivatives exist; however, the United States Environmental Protection Agency (US EPA) named 16 PAHs as priority pollutants (USEPA, 2000).

Water is pivotal to the sustenance of life and creation of energy; however, potable water suitable for domestic use, including drinking, was estimated to be around 0.01% of the total (Ritchie & Roser, 2020). Moreover, water is unevenly distributed around the world; as a result, there are regions faced with water shortage, particularly in low latitudes and millions of people globally are suffering due to a shortfall of clean and safe portable water (WHO/UNICEF, 2012). Rapid growth in industrialization, population, and urbanization has significantly spurred severe water pollution. Remediation of PAH-contaminated water systems is important due to the ability of PAHs to bioaccumulate and the risk they pose to human health (Figure 1) (García-Suástegui et al., 2010; Lawal, 2017; Olsson et al., 2010). The United Nations Sustainable Development Goals (SDGs) prioritized the need to address the numerous challenges associated with water, which include flooding, drought, and water pollution. Although some successes have been recorded, there is still a need for the development of efficient, ecofriendly, affordable, and sustainable means to achieve the SDGs by 2030 (United Nations Information Center, 2017).

Polycyclic aromatic hydrocarbons are hydrophobic organic compounds; therefore, they are often deposited on sediments and adhere to solid particles in aquatic environments (Maletic, Beljin, Roncevic, Grgic, & Dalmacija, 2019; Rockne, Shor, Young, Taghon, & Kosson, 2002). Contaminated soil and sediment could potentially contaminate ground and surface water via leaching, runoff, and re-suspension. Therefore, many reviews have been published on the treatment methods and strategies which can be employed for PAH-contaminated soils as well as sediments (de Boer & Wagelmans, 2016; Gan, Lau, & Ng, 2009; Kuppusamy et al., 2017; Maletic et al., 2019; Mohan et al., 2006; Samanta, Singh, & Jain, 2002; Wise, 2000). However, there is no comprehensive literature review which focuses solely on the treatment technologies for PAH-polluted water. This review therefore focuses on target-specific existing and emerging technologies in this regard and highlights successes, limitations, areas of improvement, and the potential field application of the methods. Prospects for the development of innovative approaches to enhance the efficiency of PAH remediation are also explored. This review thus provides holistic insights and a fundamental basis to inform decision making with respect to the development of suitable, ecofriendly, and cost-effective technique(s) that can be adopted for the treatment of PAH-contaminated water.

Extraction and Membrane Technologies

Solid-phase extraction (SE/SPE) is a clean-up technique used for LMW and HMW PAHs based on the preferential solubility of PAHs in organic solvents. The use of basic apparatus such as a separatory funnel and rotary evaporator, along with a suitable nonpolar solvent, such as hexane, dichloromethane, or mixture of both, have been used to isolate PAHs from water (Gong, Wilke, Alef, Li, & Zhou, 2006). This technique often involves SPE or gel permeation chromatography (GPC) with different adsorbent phases, while others include membrane-based extractions such as liquid-phase micro-extractions and membrane-assisted extraction (Egli, Butler, & Bottaro, 2015; Hussain et al., 2018; Martinez, Gros, Lacorte, & Barceló, 2004; Munyeza, Dikale, Rohwer, & Forbes, 2018). The selective removal of PAHs from water has been optimized and over

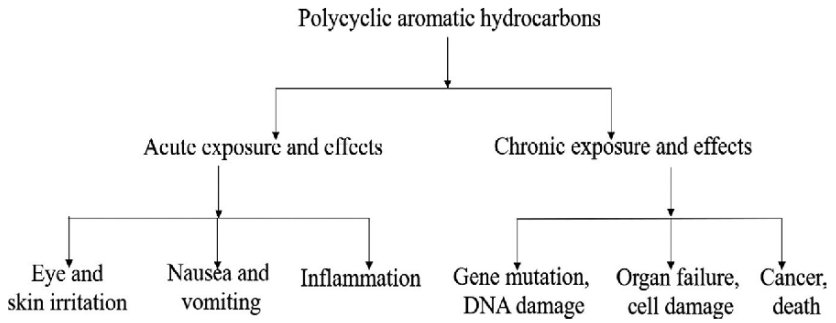

Figure 1. Flowchart showing the effect of acute (short-term) and chronic (long-term) exposure to PAHs.

90 % extraction efficiency has been recorded, as well as the capacity of SPE to isolate target PAHs in trace amounts (Egli et al., 2015). Graphitic carbon nitride derivatives have been reported as sorbents for solid-phase microextraction of PAHs, with recoveries in the range of 83.3%–103.0% (Feng, Huang, Guo, Liu, & Zhang, 2020; Nian, Wang, Wang, & Zuo, 2019). However, SPE and other forms of extraction have only been applied for analytical determination and monitoring of PAHs in water. This is due to its lack of robustness and capacity to deal with a large volume of water; also, the cost of solvents and their environmental impact makes it uneconomical to adopt solid-phase extraction principles forwater resource recovery facility.

Several membrane technologies have been reported in the literature for the treatment of PAH-polluted water, including microfiltration (Klejnowski, Kozielska, Krasa, & Rogula-Kozłowska, 2010), ultrafiltration (Dudziak, Luks-Betlej, & Bodzek, 2003; Smol & Włodarczyk-Makuła, 2012), nanofiltration, and reverse osmosis (Smol, Włodarczyk-Makuła, Mielczarek, & Bohdziewicz, 2014). PAHs have a molecular size smaller than the pore radius of microfiltration and ultrafiltration membranes, but studies have shown that they retain PAHs to a large extent, via hydrophobic effects and adsorption onto the membrane surface (Smol & Włodarczyk-Makuła, 2012). Unlike micro- and ultra-filtration processes, the mechanism of nanofiltration is mainly size exclusion, which indicates that its efficiency is independent of process variables such as discharge or influent pressure, concentration, pH etc. (Smol, Włodarczyk-Makuła, Bohdziewicz, & Mielczarek, 2014). Reverse osmosis has been employed for the treatment of water and landfill leachates and improved efficiencies are found with higher molecular weight PAHs, because the process is controlled by sieving and diffusion mechanisms (Smol, Włodarczyk-Makuła, Mielczarek, Bohdziewicz, & Włóka, 2015). Overall, reports show that PAH removal efficiency increases in the order: microfiltration ‹ ultrafiltration ‹ reverse osmosis ‹ nanofiltration (Dudziak et al., 2003; Smol, Włodarczyk-Makuła, Mielczarek, et al., 2014), although integrated systems such as coagulation-membrane separation provide the best results (>98%) (Smol, Włodarczyk-Makuła, Bohdziewicz, et al., 2014). Membrane fouling and operational costs are drawbacks of these processes, although back-washing assists with fouling, membrane performance often diminishes over time.

Chemical Oxidation Processes

The treatment of PAH contamination in soil and municipal/industrial landfill leachates has been reported using basic and advanced chemical oxidation techniques, and they proved successful with over 90% degradation (Li et al., 2016; Wu, Zhou, et al., 2011; Yap, Gan, & Ng, 2012). Chemical oxidation techniques involve the use of oxidants such as hydrogen peroxide (Flotron, Delteil, Bermond, & Camel, 2005), activated persulfate (Huling & Pivetz, 2006), ozone (Lian et al., 2017; Rivas,

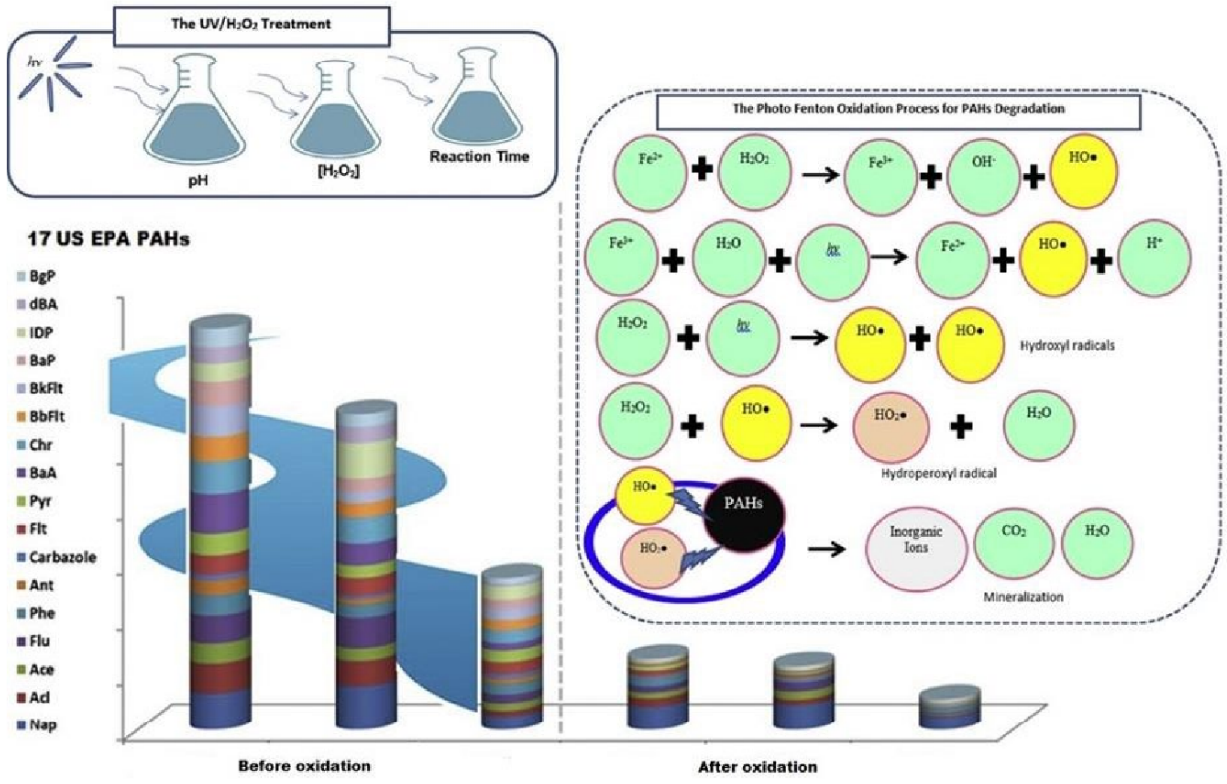

Figure 2. Ultraviolet light-assisted chemical oxidation process for PAH degradation. (Adapted with slight modification from Abd Manan, Beddu, et al., 2019. Copyright 2019 Elsevier).

Gimeno, de la Calle, & Beltrán, 2009), and Fenton's reagent (Zhang, Dong, Zhao, Wang, & Meng, 2019). These techniques involve the generation of very reactive radicals (e.g., ·OH, O_3 and SO_4 $SO_4^{\cdot-}$ $O_3^{\cdot}$ radicals) and other reactive species (e.g., persulfate anion, peroxides), which are responsible for the breakdown of the aromatic rings of PAHs (Figure 2). Merits of chemical oxidation over conventional remediation methods include relatively shorter treatment time, effectiveness for remediation of a broad range of PAHs due to high radical reactivity, and in situ degradation of contaminants. However, the application of very reactive oxidizing agents is complicated due to oxidation of nontarget constituents such as dissolved/particulate organic matter, the volume of water to be decontaminated, and corrosiveness makes it unsuitable for treatment of portable water. Furthermore, H_2O_2 requires careful pH control (i.e., 2.5–4.0) and is quite expensive (Flotron et al., 2005). Cl^- inhibits the destruction of organic contaminants by persulfate-based advanced oxidation processes (AOPs) (Deng & Zhao, 2015). These factors provide constraints to the use of H_2O_2 and persulfate for PAH degradation, thus making these oxidants inappropriate or uneconomical for large-scale water remediation (Huang, Lu, Chen, & Lee, 2003). Advanced methods involving the combination of Fenton oxidative-coagulation and ultraviolet photo-Fenton processes also recorded significant success in the removal of PAHs in solid waste and leachates (Li et al., 2016). However, there are limited reports on the use of chemical oxidation techniques for the remediation of PAHs in water.

Bioremediation

Bioremediation is regarded as an efficient means of degrading organic compounds, including PAHs, in environmental media. The technique involves the use of microorganisms, plants, and enzymatic reactions in the detoxification and degradation of environmental contaminants in water and other environmental compartments (Ghosal et al., 2016; Gouma, Fragoeiro, Bastos, & Magan, 2014). Fungi such as *Peniophora gigantea*, *Phanerochaete chrysosporium*, *Pycnosporus coccineus*, *Trametes versicolor*, and others have been reported to efficiently degrade many organic pollutants, especially PAHs (Silva, Grossman, & Durrant, 2009). Bacterial species (*Aspergillus* sp., *Trichocladium* sp., *Fusarium* sp., and *Pseudomonas* sp.) are also capable of degrading PAHs (Quinn et al., 2009; Soleimani, 2012; Sun et al., 2014; Wu, Chen, Tian, Ding, & Dick, 2013).

A recent study revealed that degradation of PAHs by *Aeromonas hydrophila*, *Bacillus megaterium*, *Raoultella ornithinolytica*, and *Serratia marcescens* recorded over 90% degradation efficiency for fluorene and acenaphthene (Alegbeleye, Opeolu, & Jackson, 2017). However, certain environmental variables such as temperature and pH were reported to have a considerable influence on the efficiency of the bioremediation processes. Specifically, temperatures above room temperature between 30 and 38°C were optimum for degradation of PAHs, due to enhanced microbial growth (Abdou, 2003; Antizar-Ladislao, Spanova, Beck, & Russell, 2008; Moscoso, Ferreira, Deive, Morán, & Sanromán, 2013). However, bioremediation is not a rigid and robust technique, as was evident in a study carried out at slightly higher temperature between 40 and 45°C, which recorded a significant decline in PAH degradation from 92% (37°C) to 73% (45°C). Increase in temperature reduces the solubility of oxygen, which leads to a decrease in dissolved oxygen available for microbial growth in the bioreactor (Alegbeleye et al., 2017; Viñas, Sabaté, Espuny, & Solanas, 2005).

Photocatalytic Degradation

The synergistic role of photocatalysis and chemical catalysts on PAH degradation has been investigated, with the aid of UV irradiation and a titanium oxide (TiO_2) catalyst (Zhang, Li, Gong, & Li, 2008). The photocatalytic degradation of phenanthrene, pyrene, and benzo(a)pyrene under UV irradiation followed the pseudo-first-order kinetics pathway and was accelerated by the addition of TiO_2, due to its established catalytic activity (Garg et al., 2019; Wu, Chang-Chien, & Lee, 2004; Zertal, Molnár-Gábor, Malouki, Sehili, & Boule, 2004). Different PAHs degrade to various extents under varying UV radiation intensities while an increase in TiO_2 dosage from 0.5 to 3 wt% had an insignificant effect on PAH photodegradation which was highest under acidic pH conditions (Zhang et al., 2008).

Composites with photocatalytic properties have been synthesized and applied to PAH degradation (e.g., Pt/TiO_2-SiO_2) (Luo et al., 2015). The correlation between molecular structure and photocatalytic degradability of PAHs was also investigated. Naphthalene, fluorene, phenanthrene, pyrene, benzo[a]pyrene, and dibenzo[a,h]anthracene were degraded using a Pt/TiO_2-SiO_2 suspension under UV irradiation. Results revealed improved efficiency of the process for biorefractory HMW PAHs with the inclusion of Pt/TiO_2-SiO_2, while that of LMW PAHs were reduced under the same conditions. A pseudo-first-order equation fit both the photolysis and photocatalysis of fluorene which displayed a different trend, by fitting best to first-order kinetics.

A model involving the use of molecular descriptors was established using the difference between highest occupied molecular orbital (E_{homo}) and lowest unoccupied molecular orbital (E_{lumo}), which equates to GAP (GAP = $E_{lumo} - E_{homo}$). This was compared with the maximum GAP (7.4529 eV) of PAHs (for dibenzo[a,h]anthracene) and the minimum GAP (8.2086 eV) of PAHs (for pyrene) which was degraded. This was further used to predict the photocatalytic degradation of 67 PAHs (Luo et al., 2015). A TiO_2-graphene composite has also been used for photocatalytic treatment of PAHs in water and 80 % efficiency was achieved in 2 hr (Bai, Zhou, Zhang, & Tang, 2017).

Adsorption Processes

Contaminated water can be treated in several ways based on the target pollutant (Cohen-Tanugi & Grossman, 2012; Kemp et al., 2013; Shannon et al., 2008); however, adsorption processes have been widely used and possess several advantages over other techniques (Kemp et al., 2013). The adsorption

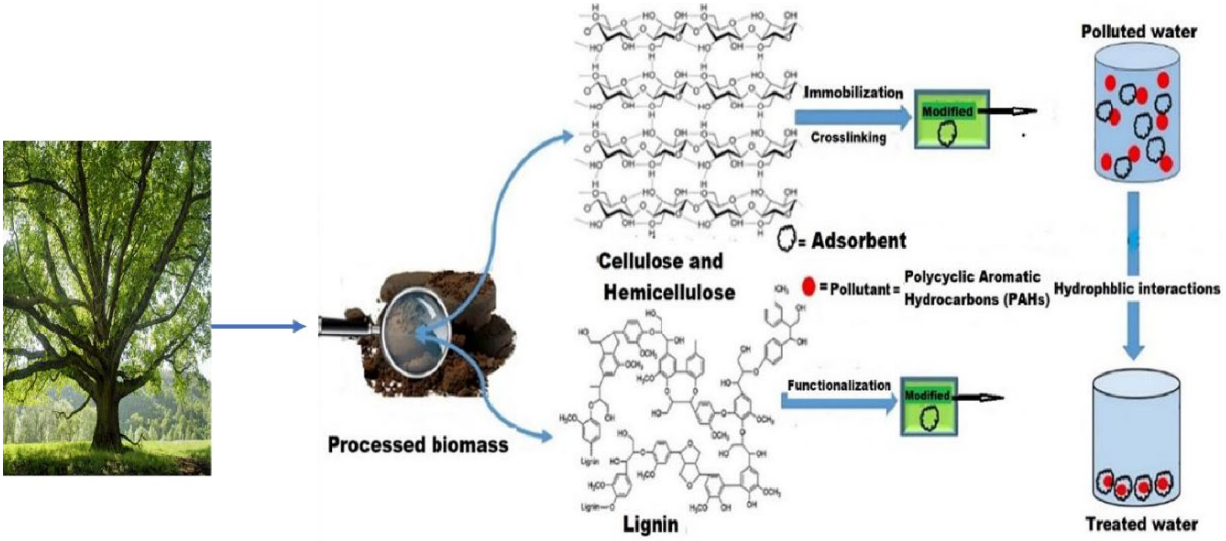

Figure 3. Treatment of PAH-contaminated water using plant derivatives (biomass).

process is a surface phenomenon that involves the adherence of pollutants onto the surface of an adsorbent via physical, chemical, and/or electrostatic attraction. Adsorption of organic compounds can be influenced by many process variables such as temperature, pH, concentration of sorbate, contact time, particle and pore size, temperature, and other physicochemical properties of the adsorbate and adsorbent (Adeola & Forbes, 2019). Several materials have been developed over the last two decades for the sorption of PAHs from aqueous system, many of which are discussed in this section.

Agricultural waste and biomass

Various sorbents for the remediation of PAHs have been derived from agricultural waste such as coconut shells, rice husks, sugar cane bagasse, peat, sawdust etc. (Amstaetter, Eek, & Cornelissen, 2012; Crisafully et al., 2008; Olivella, Jové, & Oliveras, 2011). The decision to explore these materials was driven by the concept of green and sustainable chemistry, which promotes the conversion of "waste to wealth" as an economical path to waste management and ecofriendly material science (Xu, Nasrollahzadeh, Selva, Issaabadi, & Luque, 2019; Xu, Zhan, et al., 2019). Low-cost adsorbents with high porosity and efficiency have been generated from these materials via simple thermal and/or chemical reaction processes, which has led to improved morphology of the biomass-derived sorbents for water treatment applications (Bhatnagar & Sillanpää, 2010; Pérez-Gregorio, García-Falcón, Martínez-Carballo, & Simal-Gándara, 2010).

The remediation performance of activated carbon derived from wheat straw on PAH-contaminated water was reported (Xu, Nasrollahzadeh, et al., 2019; Xu, Zhan, et al., 2019). Results revealed that the PAH adsorption capacity of the adsorbent increased with increase in the number of aromatic rings and the surface area of adsorbent had the greatest influence on removal of both HMW and LMW PAHs with the pseudo-second-order model giving the best fit to kinetic experiments. Adsorption of naphthalene (NAP), phenanthrene (PHEN), and pyrene (PYR) from water was evaluated using activated rice husk (RH) (Yakout & Daifullah, 2013). The Freundlich, generalized and BET isotherms best fit adsorption data for naphthalene, phenanthrene and pyrene. The results suggest that a significant amount of heat was dissipated, as the thermodynamic system was exothermic and spontaneous (Yakout & Daifullah, 2013).

The cross-linkages of starch molecules with epichlorohydrin, 1,6-hexamethylene diisocyanate, 4,4-methylene diphenyl diisocyanate, for the synthesis of a functionalized starch polymer adsorbent for PAHs were reported (Delval, Crini, Bertini, Filiatre, & Torri, 2005; Okoli et al., 2015). The cross-linking process enhanced the morphology, hydrophobicity and incorporated specific functional groups into the starch polymer. Adsorption occurred in multilayers, and diffusion controlled the adsorption kinetics. Thermodynamic variables suggest that the sorption mechanism was endothermic and spontaneous and physisorption occurred via hydrophobic, van der Waals and π–π interactions between sorbent and adsorbate (Okoli et al., 2015).

Plant materials have been used as adsorbent and an indirect form of phytoremediation of PAH-contaminated water (Figure 3). Plant residues, brown seaweed (*Sargassum hemiphyllum*), wood fibers, wood char, fruit cuticles, potato periderm, modified pine bark, tea leaf powders, corn cob etc., have all been reported for the removal of PAHs from aquatic media via adsorption routes (Boving & Zhang, 2004; Chen, Yuan, & Liu, 2011; Chung, Tsui, Cheung, Tam, & Wong, 2007; Crini, 2005; Huang, Boving, & Xing, 2006; Ye, Zeng, et al., 2019). A biochar-based nanocomposite has been synthesized from rice straw and the material exhibited both adsorptive and photodegradation activity, making it suitable for the remediation of water contaminated with organic compounds (Ye, Yan, et al., 2019).

However, the use of biomass in powdered form as column packing material has several limitations, such as difficulty in biomass recovery after sorption, complicated regeneration, low mechanical strength and density, and small particle size. An attempt to address these shortcomings through immobilization of biomass within a polymeric matrix was carried out and an improvement in biomass efficiency, sorption capacity, robustness, ruggedness and recovery of biomass from the pollutant containing solution was reported (Aksu, 2005). This class of adsorbents proved efficient in treatment of simulated and field water samples and thus was regarded as a promising cost-effective alternative for remediation of aqueous PAH pollution (Cabal, Ania, Parra, & Pis, 2009; Zhang et al., 2017). Possible negative environmental impacts of using biomass, such as deforestation and food scarcity, must be considered. Improved biomass recovery through advanced waste management systems is therefore important.

Geosorbents

Geosorbent is generic term for soils, sediments, and natural solid minerals, with different compositions depending on the parent rocks, anthropogenic activities, depth of sample aggregate, particle size, extent of maturation and aging process (Luthy et al., 1997). Combustion residue in particulate form (e.g., char, soot, and ash), clay minerals, silica (sand) and several forms of amorphous and condensed carbon such as kerogen, black carbon, aged carbon etc., are chemically and structurally different in different soils and sediments (Figure 4) (Cornelissen & Gustafsson, 2005; Heijden & Jonker, 2009; Rockne et al., 2002).

Porous carbon derived from petroleum coke (specific surface area (SSA): 562–1,904 m^2/g) was reported for the adsorption of five LMW PAHs (fluoranthene, fluorene, phenanthrene, pyrene and naphthalene) from aqueous solution (Yuan et al., 2014). It was found that the PAH uptake by the sorbent can be described by three successive and complimentary steps: (1) diffusion of molecules of PAHs from contaminated water to the outer walls of porous carbon particles through solid–liquid interphase, also known as film diffusion; (2) intraparticle diffusion of the PAHs within the pores of the carbon, and (3) PAH adsorption onto active sites on the interior surface. Adsorption kinetics is controlled by (1) and (2), while adsorption capacity and binding strength is controlled by step (3) to a very large extent. Furthermore, the petroleum coke derivative provided a removal efficiency of 99% at 1 g/L dosage of the adsorbent and adsorption capacities for the PAHs were >5 mg/g (Yuan et al., 2014).

Leonardite, also known as immature coal, composed of 55% carbon and mainly humic substances, has been studied for the removal of selected PAHs from water (Zeledón-Toruño, Lao-Luque, & de las Heras, F. X. C. & Sole-Sardans, M., 2007). Leonardite adsorbed over 90% of fluorene, pyrene, benzo(k) fluoranthene, benzo(a)pyrene, and benzo(g,h,i)perylene present in solution, after 24 hr of contact at a dosage of 1 g/L, which is quite unique for a material with a relatively low surface area (19.1 m^2/g). The high removal efficiency and adsorption capacity can be attributed to the vast number of hydrophobic functionalities (carboxyl, carbonyl and hydroxyl groups) associated with humic acids and humic-containing geosorbents,

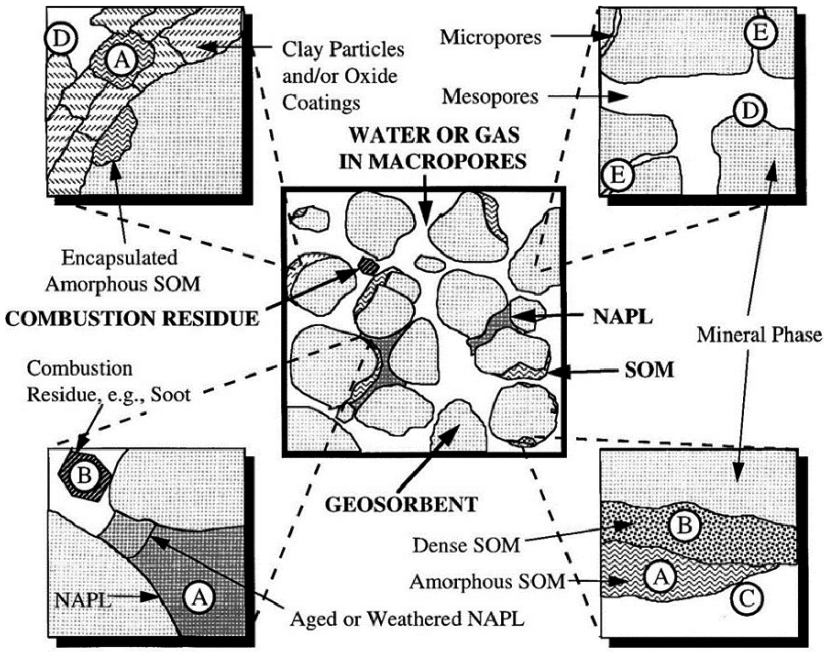

Figure 4. Geosorbent domains which include a mineral and organic matter component (SOM), as well as combustion residues and nonaqueous liquids (NAPL). (a) Absorption to soft natural organic matter or NAPL (b) Adsorption onto hard organic condensed matter (c) Adsorption onto wet-water organic surfaces i.e., soot. (d) Adsorption onto mineral phases e.g., quartz. (Reprinted with permission from Luthy et al., 1997. Copyright 1997 American Chemical Society).

which are readily available for chemical bonding (Lao, Zeledón, Gamisans, & Solé, 2005; Solé, Casas, & Lao, 2003).

Sepiolite is a fibrous clay mineral with a highly porous structure and silanol-surface-active sorption sites. Its molecular sieving and adsorptive abilities have been reported (Sabah & Ouki, 2017). Sepiolite has a relatively high surface area (358 m^2/g,), mean pore diameter (47.3 Å) and total pore volume (0.559 cm^3/g), which makes it a unique material/mineral for PAH remediation of contaminated water (Cobas, Ferreira, Sanromán, & Pazos, 2014). It has a three-dimensional micro-crystalline structure, which makes it rigid, rugged and robust, with no significant change in morphology after adsorption of PAHs (Álvarez, Santarén, Esteban-Cubillo, & Aparicio, 2011). The adsorption of pyrene and naphthalene onto sepiolite and organo-sepiolite occurred via H-type sorption and chemisorption and reached a maximum capacity of 8 mg/g. The process was entirely endothermic with an activation energy between 26.3 and 31.2 kJ/mol and Gibbs free energy (ΔG) of −29.35 kJ/mol, indicating that the process was diffusion controlled and involved weak chemical bonds (Gök, Özcan, & Özcan, 2008).

One major shortcoming of natural geosorbents is the problem attributed to designing a physicochemical sequestration model for the extremely heterogeneous systems found in various geological materials. The practicality of fractionating geosorbents into sorption domains and the establishment of dominant mechanisms of adsorption is questionable given that there is typically insufficient microscopic data. However, it was suggested that predictions can be approached mechanistically by gaining knowledge of simpler systems via study of the components (Ololade et al., 2018; Ran et al., 2002, 2003; Wu & Zhu, 2012), thereby establishing an in-depth knowledge base for prediction of complex, heterogeneous geosorbents in their bulk state.

Zeolites

Zeolites are aluminosilicates with different ratios of Si/Al. They exist naturally and can be synthesized and are important due to their essential physicochemical properties such as specific surface area, mechanical and thermal stability, high ion exchange capacity, adsorption, and sieving properties (Chao & Chen, 2012; Fletcher, Ling, & Slater, 2017). Zeolites have been used as adsorbents, membranes, ion exchangers, and molecular sieves for water and soil remediation. This essential modified clay mineral has been identified as a viable, low-cost, and readily available sorbent (Lee, Kim, Chung, & Jeong, 2004; Lee & Tiwari, 2012; Li & Bowman, 2001).

Zeolite and its modified forms were applied to remove phenanthrene, pyrene and benzo(a)pyrene from water via a sorption process (Müller, Totsche, & Kögel-Knabner, 2007; Torabian et al., 2010; Zhang, Luo, & Zhang, 2011). Using organo-zeolite as adsorbent recorded an average of 98% removal of fluorene, fluoranthene, pyrene, phenanthrene, benzo(a) anthracene from water (Lemić, Tomašević-Čanović, Adamović, Kovačević, & Milićević, 2007). The particle size of zeolites is round 1 mm or greater, and they are not susceptible to contraction and expansion ("shrink-swell") behavior, thus making them suitable for filtration systems as well as adsorption (Vidal et al., 2011; Xi & Chen, 2014).

Polycyclic aromatic hydrocarbons were adsorbed by both zeolites and surfactant-modified zeolites, and the removal efficiency for both sorbents were in the order dibenz[a,h]anthracene > benzo[a]pyrene > anthracene > naphthalene (Wołowiec et al., 2017). The adsorption capacity was highest with higher molecular weight PAHs (HMW), for example dibenz[a,h] anthracene had an adsorption capacity of 0.65 mg/g and was lowest for naphthalene (LMW) (0.058 mg/g). At a concentration of 20 μg/L, the adsorption efficiency for benz[*a*]anthracene by modified zeolite was 100% (Lemić et al., 2007). The removal efficiency depends on the chemical properties of the PAHs (molar weight, molecule structure and dipole interactions) and the properties and morphology of the zeolites (i.e., Si/Al ratio, surface area, particle size, and cation exchange capacity). It was suggested that the sorption mechanism was dominated by penetration/diffusion of PAH molecules into the mesopores of the adsorbent (Wołowiec et al., 2017).

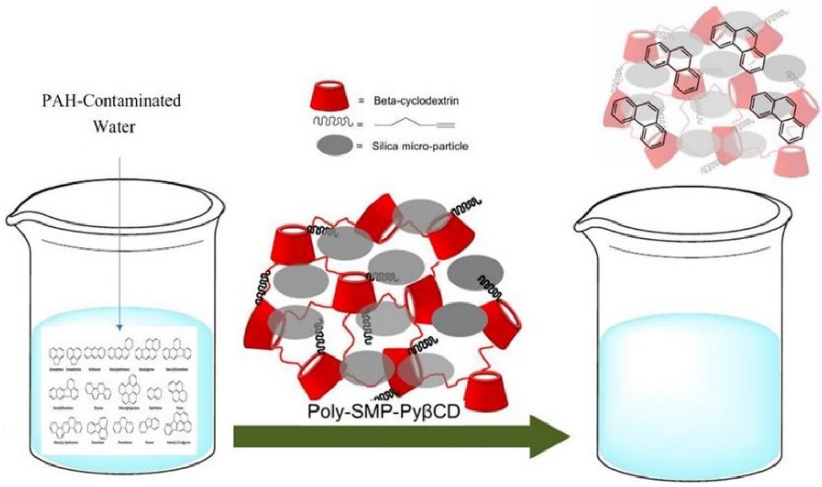

Figure 5. β-cyclodextrin based PMO for PAH decontamination. (Adapted with slight modification from Choi et al., 2017).

Functionalized mesoporous silica

Topuz and Uyar (2017) reported the synthesis of β-cyclodextrin-functionalized periodic mesoporous organosilica (PMO), which was used to adsorb five PAHs from water (Figure 5). The adsorption capacities were in the range of 0.3–1.65 mg/g (Topuz & Uyar, 2017). Pentynyl β-cyclodextrin as an organic moiety for mesoporous silica was used for remediation of phenanthrene and was reported to have an efficiency above 95% (Choi et al., 2017). Several organic reagents prior to β-cyclodextrin have previously been reported, such as macrocyclic tetraazacalix[2]arene[2]triazine which recorded 94%–102% removal efficiencies for five PAHs in water samples (Zhao, Yang, He, & Zhang, 2016).

Functionalized silica with phenyl groups for removal of five PAHs in aqueous solutions was also investigated and adsorption efficiencies and capacities were within the range of 40%–70% and 0.72–1.69 mg/g, respectively (Vidal et al., 2011). Hemoglobin-coated mesoporous silica yielded a PAH removal efficiency of 82% for 11 different PAH compounds in water. Macrocyclic polyamine functionalized with 1,3-dibutylimidazolium bis[(trifluoromethyl)sulfonyl]imide (ionic liquid) achieved an estimated efficiency ranging from 81% to 120% for the removal of five PAHs from aqueous solution (Liu et al., 2014).

Synthetic polymers

Polymeric adsorbents and supports have presented a useful alternative to the widely used granular/powdered activated carbon (GAC) for polycyclic aromatic hydrocarbon removal from water using permeable/porous reactive barriers (PRB) (Anbia & Moradi, 2009; Schad et al., 2000; Valderrama, Cortina, Farran, Gamisans, & Lao, 2007). The quest to discover appropriate and efficient polymeric adsorbents for PAH removal from aqueous solution have spurred the synthesis of innovative resins, with new functionalities and/or modified polymeric frameworks (cross-links), in order to solve existing problems and shortcomings. A functionalized adsorbent called Macronet Hypersol, made up of a macroporous hyper-reticulated network of styrene–divinylbenzene has been evaluated and reported (Valderrama et al., 2007). Due to its adsorptive properties, it has been considered as an economical reactive sorbent for water remediation (Streat & Sweetland, 1997). Batch experiments were carried out to determine the kinetics of adsorption of naphthalene, fluorene, anthracene, acenaphthene, pyrene, and fluoranthene from water. The study showed that sorption systems followed a pseudo-first-order reaction pathway (chemisorption). It was recommended that sorption media thickness of 0.1–1 m will be sufficient to treat PAH-polluted water and the medium would withstand a high-water flux of 0.1–2 $m^3\ m^{-2}\ day^{-1}$ (Valderrama et al., 2007).

The molecular imprinting technique has been used to synthesize nanoporous polymers for PAH remediation of polluted water (Augusto et al., 2010; Hassan, Sayour, El Azab, & Mansour, 2016). Specific molecular materials were synthesized via copolymerization of a monomeric cross linker with the complex derived from template (PAH) and functional monomers. The resultant molecular imprinted material possesses specific affinity for the PAH used as precursor, because its binding sites were of similar shape and size to the target PAH (Figure 6) (Dickert, Tortschanoff, Bulst, & Fischerauer, 1999; Montaseri & Forbes, 2018; Zimmerman, Wendland, Rakow, Zharov, & Suslick, 2002). A study reported the synthesis of a molecular imprinted polymer (MIP) in acetonitrile using a four PAH mix as template, and methacrylic acid and ethylene glycol dimethacrylate as functional monomer and cross-linking monomer (Krupadam, 2012). The microspheric size of the molecularly imprinted polymers (MIPs) generated ranged from 10 to 20 μm and the sorption affinity of the nanoporous polymeric material (NPM) for benzo[a]anthracene, benzo[a]pyrene, benzo[k]fluoranthene, and chrysene were studied via batch sorption experiments. A partition mechanism controlled the sorption interaction between the MIPs and the PAHs (benzo[a]anthracene, benzo[a]pyrene, benzo[k]fluoranthene, and chrysene), with an adsorption capacity of 3.12 μg/g, which was over five times higher than conventional activated carbon (Krupadam, 2012). Regeneration of MIPs was possible with methanol/acetic acid rinsing, with no significant loss in PAH removal efficiency (Baggiani, Anfossi, Baravalle, Giovannoli, & Giraudi, 2007; Krupadam, 2012; Krupadam, Ahuja, & Wate, 2007).

Currently, various adsorbent materials have been studied as remediation materials for PAH decontamination of water. However, it has been difficult to clean-up ultra-trace levels of PAHs, which is achievable via molecular imprinting technology, with high selectivity and specificity. Although costs of chemicals such as monomers and solvents are also factors to consider.

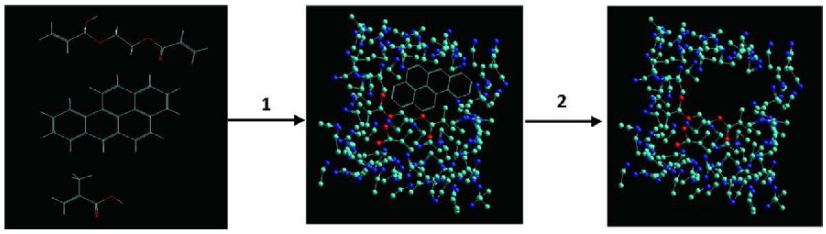

Figure 6. Molecular imprinting of benzo[a]pyrene using methacrylic acid as monomer to generate binding sites. Step (1) involves the polymerization and step (2) involves the removal of the PAHs and creation of binding cites complementary to the specific PAHs. (Reprinted from Polycyclic aromatic hydrocarbons, Volume 32, Krupadam, 2012, with permission from Elsevier).

Table 1. Comparison of different forms of graphene used for remediation of PAH-contaminated water

ADSORBENT	DOSAGE (G/L)	CONTACT TIME (HOURS)	REMOVAL EFFICIENCY (%)	ADSORPTION CAPACITY	REFERENCE
Graphene	1	96	–	1.46 g/g (1-naphthalene-sulfonic acid)	Wu, Cai, et al. (2011)
Graphene nanosheets		168	–	150.2 mg/g (PHEN)	Apul et al., (2013)
Reduced graphene oxide (RGO)	0.4	168	–	5.912 g/g (NAPH), 0.183 g/g (ANT) and 0.979 g/g (PYR)	Sun et al. (2013)
RGO/FeO.Fe_3O_4 composite	1	48	–	2.63 mg/g (NAPH)	Yang, Li, Ren, Huang, and Wang (2013)
Graphene oxide/ brilliant blue (BBGO)	0.025	264	72.7–93.2	1.676 mmol/g (ANTM), 2.212 mmol/g (FLR)	Zhang et al., (2013)
Graphene nanosheets	0.5	90	–	116 mg/g (PHEN), 123 mg/g (PYR)	Wang, Chen, et al. (2014)
Graphene oxide (GO)	0.5	90	–	5.9 mg/g (PHEN), 6.12 mg/g (PYR)	Wang, Chen, et al. (2014)
Exfoliated graphene	1	48	–	24.1 mg/g (PHEN)	Zhao, Wang, Zhao, and Xing (2014)
Graphene coated materials (GCMs)	0.5	36	80	1.74 mg/g (PHEN)	Yang, Chen, and Zhu (2015)
Graphene wool	0.67	24	98.5–99.9	5 mg/g (PHEN), 20 mg/g (PYR)	Adeola and Forbes (2019)

Note. ANT, anthracene; ANTM, anthracenemethanol; FLR, fluoranthene; NAPH, naphthalene; PHEN, Phenanthrene; PYR, pyrene.

Nanoparticles and composites

Nanotechnology has gained immense scientific relevance as a branch of science in the 21st century. It has the capability of generating nano-sized materials with unique properties, which have found application in drug delivery, biosensors as well as in the remediation of different environmental compartments; such as air, water and soil; via clean-up of environmental pollutants (Adeola et al., 2019; Nsibande, Montaseri, & Forbes, 2019). The adsorption of three PAHs, naphthalene (NAP), acenaphthylene (ACN), and phenanthrene (PHEN), from wastewater using a silica-based organic–inorganic nanohybrid material (NH_2-SBA-15) was reported (Balati, Shahbazi, Amini, & Hashemi, 2015). Adsorption kinetics of PAHs by the hybrid followed the pseudo-second-order pathway, providing evidence of chemisorption and pore mass transfer. The adsorption capacities of NH_2-SBA-15 for PAHs studied were 1.67, 1.06, and 0.24 mg/g for NAPH, ACN and PHEN, respectively; and the material was highly reusable for five sequential applications (Balati et al., 2015).

Hydrophobic C_{18}-functionalized iron (III) oxide magnetic nanoparticles (Fe_3O_4@C_{18}) were trapped in a hydrophilic barium alginate (Ba^{2+}-ALG) polymer to generate an adsorbent suitable for solid-phase extraction and treatment of PAH contamination. The sorbents proved very efficient and the magnetic property thereof aided easy recovery and re-use. It was reported that a water-friendly Ba^{2+}-ALG polymer caged Fe_3O_4@C_{18} nanomaterial can be used for extraction or possible remediation of organic pollutants in water on an industrial scale (Zhang, Niu, Cai, & Shi, 2010).

Additionally, tetraethyl orthosilicate magnetized with maghemite (Fe_2O_3) nanoparticles with an adsorption capacity of 0.39 mg/g has been applied for the removal of acenaphthene (ACN) from water with a removal efficiency of 85 % (Huang, Fulton, & Keller, 2016). Hassan, Abdel-Shafy, and Mansour (2018) reported an ecofriendly method for the synthesis of iron oxide nanoparticles (IONPs) for the removal of benzo(a)pyrene and pyrene from contaminated water (also refer to Wang, Jin, Chen, Megharaj, & Naidu, 2014). Factors such as IONPs dosage, pH, temperature, and initial concentration of PAHs were evaluated. The maximum sorption capacities of IONPs toward pyrene and benzo(a)pyrene were 2.8 and 0.029 mg/g, and removal efficiencies were 98.5% and 99%, respectively. The sorption process was exothermic, well defined by a monolayer adsorption mechanism (Langmuir model) and followed the pseudo-second-order kinetic reaction pathway. The study revealed that IONPs are regenerable up to 5 cycles and possess anti-microbial properties (Hassan et al., 2018).

However, there are major drawbacks in the field-based application of nanoparticles for PAH remediation. The fine powdered form of nanomaterials has a very high sorption affinity for PAHs, however, to achieve a reasonable treatment time, a large amount of the nanomaterial is required to treat a large

volume of polluted water. In addition, the resulting nanomaterial residue dispersed or suspended in the treated water may cause toxicity if it is not properly recovered, due to the composition of the nanomaterial (metal poisoning) and/or the small particle size thereof, which aids mobility into tissues when ingested. Membrane separation protocols have been developed to separate fine suspended or dispersed solids from water, however, this increases operational costs. Nanomaterials may also have limited re-use potential, as they tend to lose activity with time as a result of aggregation, fouling, or side reactions.

Graphene and its composites

Graphene as a term was first proposed in 1986 and introduced to the International Union of Pure and Applied Chemistry (IUPAC) in 1995 (Boehm, Setton, & Stumpp, 1994; Fitzer, Kochling, Boehm, & Marsh, 1995; Katsnelson, 2007; Peng, Li, Liu, & Song, 2017). Graphene is two-dimensional (2D), with sp^2 hybridized carbon atoms arranged hexagonally with a closed packed crystal lattice structure containing sigma- and π-bonds (Ali et al., 2019). Graphene is presented in different forms such as pristine graphene, graphene oxide (GO), reduced graphene oxide (RGO), graphene nanoshell (GNS), graphene quantum dots, graphene wool, graphene-based composites and functionalized graphene (Adegoke, Montaseri, Nsibande, & Forbes, 2017; Apul, Wang, Zhou, & Karanfil, 2013; Nsibande & Forbes, 2020; Oyedotun et al., 2019; Schoonraad, Madito, Manyala, & Forbes, 2020; Sun, Yang, Zhao, Wang, & Wang, 2013; Wang, Wang, Liu, Zhang, & Sun, 2017). The large specific surface area, thermal stability, thermal conductivity, high tensile strength, chemical robustness, charge mobility, flexibility, and thin-film thickness provide the basis for the vast applications of graphene and its composites in many fields of science (Dreyer, Ruoff, & Bielawski, 2010; Geim, 2009; Novoselov et al., 2012). Graphene has been utilized as an efficient sorbent for water remediation purposes, such as removal of contamination involving toxic organic and inorganic species (Ali et al., 2019; Ersan, Apul, Perreault, & Karanfil, 2017; Wang, Chen, & Chen, 2014; Zhao, Li, & Wang, 2011).

The mechanism of interaction between PAHs and different forms of graphene in water is described mainly by partitioning and adsorption, and generally follows second order reaction kinetics. From the studies presented in Table 1, it is evident that the efficiency of different forms of graphene is largely dependent on the dosage and concentration of PAHs and is also influenced by temperature of the reaction and ionic strength of the solution (Lamichhane, Bal Krishna, & Sarukkalige, 2016). The effect of pH is typically negligible due to the lack of specific functional groups in PAHs (Adeola & Forbes, 2019; Su, Zhu, Sheng, & Chiou, 2006), if they are not derivatized as in the case of 1-naphthalenesulfonic acid (Wu, Cai, et al., 2011).

Several factors influence the choice of adsorbent for water treatment applications, such as efficiency of the material, non-toxicity, availability of the material, flexibility, robustness and reusability, to mention a few. Graphene wool holds a competitive advantage over other forms of graphene tested for water treatment applications, due to its high PAH removal efficiency >98%, wool-associated flexibility and reusability. GW has a very high volume to mass ratio and porosity which makes it a suitable packing material for membrane separations/filters, as well as a good polishing tool for water remediation (Adeola & Forbes, 2019).

Emerging Trends and Prospects

It is evident that adsorption using various efficient and cost-effective materials as well as bioremediation are the most widely used remedial approaches, however, bioremediation still has limitations such as accumulation of metabolites or degradation products which could be more harmful; as in the case of dichlorodiphenyltrichloroethane (DDT) and its metabolite dichlorodiphenyldichloroethylene (DDE) (ATSDR, 1994); longer duration requirements for treatment procedures and cost. Therefore, to address these challenges or limitations, hyphenated methods or integrated systems have been suggested (Kuppusamy et al., 2017). These may involve chemical–physical (such as chemical oxidation and solvent extraction), biological-physical (e.g., bioremediation and solvent extraction), and biological-chemical (such as bioremediation and chemical oxidation) processes. The bioaugmentation technique is an integrated system which can potentially be used for PAH remediation of polluted water, if the bacteria employed are not harmful to humans, or are easily recovered or removed by a simple chlorination step during the treatment of potable water. Commercial materials developed in line with bioaugmentation include SediMite and AquaGate + GAC. The bio-amendment of granular activated carbon (GAC) with anaerobic and aerobic bacteria as degradants has been reported for the in situ treatment of organic contamination, where the pore water concentration of polychlorinated biphenyls (PCBs) reduced by 94%–97% (Payne, Ghosh, May, Marshall, & Sowers, 2017).

Phytoremediation, which is plant aided bioremediation, is a remedial approach that can potentially address PAH contamination on a large scale (Jeelani et al., 2017; Petruzzelli, Pedron, Rosellini, Grifoni, & Barbafieri, 2016). Plant degradation of PAHs in water is worthy of investigation, because plants possess the ability to sequester, accumulate and chemically transform chemical pollutants. They can secrete enzymes that can play the role of surfactants and enhance the bioavailability of the pollutant in solution. In addition, rhizospheric microbes have xenobiotic-degrading capabilities (Gan et al., 2009). The application of specific plants (such as lichens) for bioaccumulation and phytoremediation of metals, metalloids and PAHs from the surrounding environment have been reported (Kroukamp, Wondimu, & Forbes, 2016; Van der Wat & Forbes, 2019). Phytoremediation of a PAH and heavy metal contaminated brownfield site was also reported by Roy et al. (2005). These are case studies with proven hypotheses toward successful plant-based remediation, and with the existence of aquatic plants, phytoremediation of PAH-polluted water is worth exploring. Plants with long roots and large surface area are highly adaptable to unfriendly environmental conditions (i.e., drought) and are preferred for in situ treatment of contaminated water (Alagić et al., 2016). Intercropping of different plants infuses desired physiological attributes and vast microbial groups in

Table 2. Examples of commercially available water treatment technologies which are applicable to PAH removal, including materials, scale of application and brand names

TREATMENT MATERIAL	TREATMENT PROCESS	SCALE OF APPLICATION	COMMERCIAL/BRAND NAME	SOURCE
Granular activated carbon (GAC) and aeration	Adsorption and filtration	Drinking water and industrial wastewater	Evoqua water technologies CECO Mefiag filters	www.evoqua.com/en/brands/IPS/Pages/Organic-Chemicals-Removal-from-Groundwater https://www.environmental-expert.com/products/ceco-mefiag-activated-carbon-filter-tubes-638430
Polyethersulfone (PES)	Direct nanofiltration	Potable water, surface water and industrial wastewater	Nxfiltration (dNf membrane)	https://nxfiltration.com/technology
Zeolite, activated alumina	Filtration, adsorption	Domestic and industrial wastewater	Zhulin	https://www.zhulincarbon.com/products/filter-media/
Copper & zinc alloy/GAC	Reverse osmosis	Potable water, industrial and surface water	KDF-GAC Filtration	https://www.ampac1.com/emergency-portable-reverse-osmosis-20000-gpd
Silver impregnated coconut activated carbon (Ag/GAC)	Adsorption	Portable water	Zhulin carbon	https://www.zhulincarbon.com/products/special-activated-carbon/25.html
Powdered activated carbon (PAC) from wood and coal	Adsorption	Industrial wastewater	Zhulin carbon	https://www.zhulincarbon.com/products/powdered-activated-carbon/
PAC + PAH degrading microbes	Bioaugmentation	Navigable water and wetland treatments	Bio-amended sediMite	http://www.sedimite.com/sedimite
PAC, bentonite (clay), cellulose-based polymer	Adsorption and capping	Aquatic environments	AquaGate + PAC™	https://www.environmental-expert.com/products/aquagate-pac-activated-carbon-for-active-capping-or-in-situ-treatment-169605
Wetlands and gravel filter	Geo-sorption, sedimentation	Domestic wastewater	Prototype	Fountoulakis, Terzakis, Kalogerakis, and Manios (2009)
Graphene membrane H_2O_2:$FeSO_4$/UV irradiation	Advanced reverse osmosis Advanced oxidation process	Portable water Potable water	Prototype Prototype	Homaeigohar and Elbahri (2017) Abd Manan, Khan, et al. (2019)

the rhizosphere of plants with a commensurate impact on PAH remediation (Meng, Qiao, & Arp, 2011; Sun et al., 2011; Sun & Zhou, 2016). Enhanced phytoremediation can be obtained with the aid of plant growth promoting rhizobacteria (PGPR) such as *Azospirillum brasilense*, *Enterobacter cloacae* and *Pseudomona putida*, for stimulating physiological development, accelerated plant growth, and survival of remediating plant species (de Boer & Wagelmans, 2016; Huang, El-Alawi, Penrose, Glick, & Greenberg, 2004a, 2004b; Jeelani et al., 2017). Although phytoremediation may offer an added advantage of absorbing excess atmospheric CO_2 and reducing air pollution, it may require several years to achieve PAH treatment objectives.

Electrokinetic remediation is an electrochemical technique involving the application of direct current (DC) through appropriate electrodes for the purpose of remediation. Basically, the concept of electrolysis comes into play as ionic pollutants in solution migrate to their oppositely charged electrodes and electroosmotic movement provides the force for transportation of soluble pollutants (Pazos, Rosales, Alcántara, Gómez, & Sanromán, 2010; Reddy, Ala, Sharma, & Kumar, 2006). Electrokinetic remediation is an established tool for decontamination of soils, although its application in PAH remediation of water has not been investigated on a pilot-, field-, or industrial scale. Application of this method would potentially have its own challenges due to the hydrophobicity/insolubility of PAHs and the fact that they do not readily ionize in water. Therefore, it has been suggested that surfactants designed to minimize the tension between the pollutant molecule and water molecules, co-solvents and cyclodextrins should be considered as additives in order to improve the efficiency of PAH remediation in field water samples using the electrokinetic method (Pourfadakari et al., 2019; Saichek & Reddy, 2005). An integrated system comprising an electrochemical test cell enhanced by a persulfate oxidizing agent has been used for treatment of PAH-contaminated clay with 35% PAH removal efficiency as compared to 12%–20% efficiency recorded for either of the methods alone. This integrated system could potentially be used for remediation of PAH-polluted water. It is noted that the efficiency of the integrated approach depends on the applied voltage, ratio of AC-DC voltage, nature of the electrode, process duration and reagent (oxidizing agent) dosage (Isosaari et al., 2007; Pourfadakari et al., 2019; Wang et al., 2013).

Green nanoremediation is a promising and notable approach to remediation of contaminated aqueous systems, based on the concept of green/ecofriendly and sustainable chemistry. In the last decade, nanoscience and technology has received immense attention with respect to research and development, and it holds great potential for remediation of polluted water/wastewater and environmental protection (Huang et al., 2016; Kuppusamy, Thavamani, Megharaj, & Naidu, 2015). The intrinsic properties of nanoparticles such as their small size (1–100 nm size), good surface-coating ability and large surface area, in comparison with macroscopic materials, make nanoparticles preferable for in situ applications. Thus green nanoremediation should be investigated and functionally integrated with established remedial methods such as the chemical oxidation or Fenton process via synthesis of nano-oxidizers (to allow for PAH oxidation), and most importantly adsorption processes by novel, green, efficient and sustainable nano-adsorbents should be further explored (Basheer, 2018; Guerra, Attia, Whitehead, & Alexis, 2018). Efficient integration of established remediation approaches with green nanoremediation and membrane filtration will potentially improve efficiency and allow for rapid PAH degradation or removal during field or industrial applications.

A few examples of treatment technologies readily available on a commercial scale and those still in the prototype/developmental phase are presented in Table 2. The absence of methods such as advanced oxidation, catalytic degradation and bioremediation, indicates that although these methods have been shown to be promising and efficient on a laboratory scale, they have not been commercialized for field/industrial scale water treatment as yet, unlike membrane technologies, due to high operational cost. This is likely due to the fact that these methods are not easily incorporated into existing water treatment plants or due to possible difficulties in their scale up to treat large volumes of water. Furthermore, some of the treatment methods are not robust enough to deal with heavily polluted water. Future research should be directed toward the development of materials/methods that are more economical, durable, efficient, and adaptable with simple designs for the removal of PAHs and other environmental contaminants from wastewater.

Field Application

The treatment of a PAH-contaminated water system essentially involves three phases: (1) site inspection and risk assessment, (2) choice of treatment method, and (3) treatment and post-treatment assessment/monitoring. Phase 1 simply requires that the level/extent of pollution is determined with respect to permissible levels or thresholds (WHO, 1984).

Phase 2 requires evaluation of existing remediation technologies and choosing the most feasible method, considering the site of pollution and its environment, as well as cost considerations. Laboratory scale experiments may prove useful in determining the most effective method for successful remediation of field contamination. Several factors that affect field-scale remediation of PAH-contaminated water include but are not limited to; (1) physicochemical conditions of the water and sediment (organic matter content, temperature, turbidity, pH, nutrients/mineral content, redox potential, ionic strength/salinity etc.); (2) microbial/biotic community (diversity, population, resistance, activity, symbiosis etc.); (3) target contaminants and co-existing contaminants (concentration, toxicity, bioavailable fraction, solubility, volatility, mass transfer etc.); (4) cost (pretreatment and post-treatment); and other factors which are nontechnical such as government and standard regulations, research funding, human resources, infrastructure etc.

In Phase 3, the chosen remediation strategies are implemented, and treatment efficiency is determined on site. If the pollution persists, the treatment protocol is repeated or another approach may need to be adopted (Duan et al., 2015).

Conclusion

A number of the technologies discussed in this review are still at the prototype stage, awaiting field trials, while others have been used on an industrial-scale and have been found to be effective, although some have limitations including high operational cost, fouling, nonregenerable materials, nonecofriendly processes, long treatment time, generation of a large amount of sludge or secondary pollutants, etc. Therefore, emerging technologies must seek to surmount these challenges and consider all these factors, in order to arrive at a sustainable remediation approach for hazardous pollutants such as PAHs. Adsorption, nanofiltration, and integrated systems are very promising technologies, with further development potential toward commercialization. Frankly, it is almost impossible or impracticable to restore heavily PAH-polluted water to its pristine state rapidly, with its full natural functions restored. Therefore, a purpose-directed, risk-based sustainable remediation approach may prove to be most appropriate for the management of long-term and/or severely PAH-polluted water.

Acknowledgments

Authors acknowledge the University of Pretoria Commonwealth Doctoral Scholarship funding (AA), and Departments of Chemistry and Physics at the University of Pretoria, South Africa for their support.

Conflict of interest

The authors declare that there is no conflict of interest regarding the publication of this article.

References

Abd Manan, T. S. B., Beddu, S., Khan, T., Wan Mohtar, W. H. M., Sarwono, A., Jusoh, H., … Ghanim, A. A. J. (2019). Step by step procedures: Degradation of polycyclic aromatic hydrocarbons in potable water using photo-Fenton oxidation process. *MethodsX*, *6*, 1701–1705. https://doi.org/10.1016/j.mex.2019.07.011

Abd Manan, T. S. B., Khan, T., Sivapalan, S., Jusoh, H., Sapari, N., Sarwono, A., … Malakahmad, A. (2019). Application of response surface methodology for the optimization of polycyclic aromatic hydrocarbons degradation from potable water using photo-Fenton oxidation process. *Science of the Total Environment*, *665*, 196–212. https://doi.org/10.1016/j.scitotenv.2019.02.060

Abdel-Shafy, H. I., & Mansour, M. S. M. (2016). A review on polycyclic aromatic hydrocarbons: Source, environmental impact, effect on human health and remediation. *Egyptian Journal of Petroleum*, *25*, 107–123. https://doi.org/10.1016/j.ejpe.2015.03.011

Abdou, A. M. (2003). Purification and partial characterization of psychrotrophic *Serratia marcescens* lipase. *Journal of Dairy Science*, *86*, 127–132. https://doi.org/10.3168/jds.S0022-0302(03)73591-7

Adegoke, O., Montaseri, H., Nsibande, S. A., & Forbes, P. B. C. (2017). Alloyed quaternary/binary core/shell quantum dot-graphene oxide nanocomposite: Preparation, characterization and application as a fluorescence "switch ON" probe for environmental pollutants. *Journal of Alloys and Compounds*, *720*, 70–78. https://doi.org/10.1016/j.jallcom.2017.05.242

Adeola, A. O., Fapohunda, O., Jimoh, A. T., Toluwaloju, T. I., Ige, A. O., & Ogunyele, A. C. (2019). Scientific application and prospect of nanomaterials: A multidisciplinary review. *African Journal of Biotechnology*, *18*, 946–961. https://doi.org/10.5897/AJB2019.16812

Adeola, A. O., & Forbes, P. B. C. (2019). Optimisation of the sorption of selected polycyclic aromatic hydrocarbons by regenerable graphene wool. *Water Science and Technology*, *80*(10), 1931–1943. https://doi.org/10.2166/wst.2020.011

Aksu, Z. (2005). Application of biosorption for the removal of organic pollutants: A review. *Process Biochemistry*, *40*, 997–1026. https://doi.org/10.1016/j.procbio.2004.04.008

Alagić, S. Č., Jovanović, V. P. S., Mitić, V. D., Cvetković, J. S., Petrović, G. M., & Stojanović, G. S. (2016). Bioaccumulation of HMW PAHs in the roots of wild blackberry from the Bor region (Serbia): Phytoremediation and biomonitoring aspects. *Science of the Total Environment*, *562*, 561–570. https://doi.org/10.1016/j.scitotenv.2016.04.063

Alegbeleye, O. O., Opeolu, B. O., & Jackson, V. (2017). Bioremediation of polycyclic aromatic hydrocarbon (PAH) compounds: (acenaphthene and fluorene) in water using indigenous bacterial species isolated from the Diep and Plankenburg rivers, Western Cape, South Africa. *Brazilian Journal of Microbiology*, *48*, 314–325. https://doi.org/10.1016/j.bjm.2016.07.027

Ali, I., Basheer, A. A., Mbianda, X. Y., Burakov, A., Galunin, E., Burakova, I., … Grachev, V. (2019). Graphene based adsorbents for remediation of noxious pollutants from wastewater. *Environment International*, *127*, 160–180. https://doi.org/10.1016/j.envint.2019.03.029

Álvarez, A., Santarén, J., Esteban-Cubillo, A., & Aparicio, P. (2011). Chapter 12 - Current industrial applications of palygorskite and sepiolite. In E. Galàn, & A. Singer (Eds.), *Developments in clay science* (pp. 281–298). Amsterdam, Netherlands: Elsevier.

Amstaetter, K., Eek, E., & Cornelissen, G. (2012). Sorption of PAHs and PCBs to activated carbon: Coal versus biomass-based quality. *Chemosphere*, *87*, 573–578. https://doi.org/10.1016/j.chemosphere.2012.01.007

Anbia, M., & Moradi, S. E. (2009). Removal of naphthalene from petrochemical wastewater streams using carbon nanoporous adsorbent. *Applied Surface Science*, *255*(9), 5041–5047. https://doi.org/10.1016/j.apsusc.2008.12.065

Antizar-Ladislao, B., Spanova, K., Beck, A. J., & Russell, N. J. (2008). Microbial community structure changes during bioremediation of PAHs in an aged coal-tar contaminated soil by in-vessel composting. *International Biodeterioration & Biodegradation*, *61*, 357–364. https://doi.org/10.1016/j.ibiod.2007.10.002

Apul, O. G., Wang, Q., Zhou, Y., & Karanfil, T. (2013). Adsorption of aromatic organic contaminants by graphene nanosheets: comparison with carbon nanotubes and activated carbon. *Water Research*, *47*, 1648–1654. https://doi.org/10.1016/j.watres.2012.12.031

ATSDR, Agency for Toxic Substances and Disease Registry (1994). *Toxicological Profile for 4,4-DDT, 4,4-DDE, and 4,4-DDD*. Public Health Service, U.S. Department of Health and Human Services, Atlanta, GA.

Augusto, F., Carasek, E., Silva, R. G. C., Rivellino, S. R., Batista, A. D., & Martendal, E. (2010). New sorbents for extraction and microextraction techniques. *Journal of Chromatography A*, *1217*, 2533–2542. https://doi.org/10.1016/j.chroma.2009.12.033

Baggiani, C., Anfossi, L., Baravalle, P., Giovannoli, C., & Giraudi, G. (2007). Molecular recognition of polycyclic aromatic hydrocarbons by pyrene-imprinted microspheres. *Analytical and Bioanalytical Chemistry*, *389*, 413–422. https://doi.org/10.1007/s00216-007-1318-8

Bai, H., Zhou, J., Zhang, H., & Tang, G. (2017). Enhanced adsorbability and photocatalytic activity of TiO2-graphene composite for polycyclic aromatic hydrocarbons removal in aqueous phase. *Colloids and Surfaces B: Biointerfaces*, *150*, 68–77. https://doi.org/10.1016/j.colsurfb.2016.11.017

Balati, A., Shahbazi, A., Amini, M. M., & Hashemi, S. H. (2015). Adsorption of polycyclic aromatic hydrocarbons from wastewater by using silica-based organic–inorganic nanohybrid material. *Journal of Water Reuse and Desalination*, *5*, 50–63. https://doi.org/10.2166/wrd.2014.013

Basheer, A. A. (2018). New generation nano-adsorbents for the removal of emerging contaminants in water. *Journal of Molecular Liquids*, *261*, 583–593. https://doi.org/10.1016/j.molliq.2018.04.021

Bhatnagar, A., & Sillanpää, M. (2010). Utilization of agro-industrial and municipal waste materials as potential adsorbents for water treatment—A review. *Chemical Engineering Journal*, *157*, 277–296. https://doi.org/10.1016/j.cej.2010.01.007

Boehm, H. P., Setton, R., & Stumpp, E. (1994). Nomenclature and terminology of graphite intercalation compounds (IUPAC nomenclature 1994). *Pure and Applied Chemistry*, *66*(9), 1893–1901. https://doi.org/10.1351/pac199466091893

Boving, T. B., & Zhang, W. (2004). Removal of aqueous-phase polynuclear aromatic hydrocarbons using aspen wood fibers. *Chemosphere*, *54*, 831–839. https://doi.org/10.1016/j.chemosphere.2003.07.007

Cabal, B., Ania, C. O., Parra, J. B., & Pis, J. J. (2009). Kinetics of naphthalene adsorption on an activated carbon: Comparison between aqueous and organic media. *Chemosphere*, *76*, 433–438. https://doi.org/10.1016/j.chemosphere.2009.04.002

Chao, H.-P., & Chen, S.-H. (2012). Adsorption characteristics of both cationic and oxyanionic metal ions on hexadecyltrimethylammonium bromide-modified NaY zeolite. *Chemical Engineering Journal*, *193–194*, 283–289. https://doi.org/10.1016/j.cej.2012.04.059

Chen, B., Yuan, M., & Liu, H. (2011). Removal of polycyclic aromatic hydrocarbons from aqueous solution using plant residue materials as a biosorbent. *Journal of Hazardous Materials*, *188*, 436–442. https://doi.org/10.1016/j.jhazmat.2011.01.114

Choi, J. M., Jeong, D., Cho, E., Yu, J.-H., Tahir, M. N., & Jung, S. (2017). Pentynyl ether of β-Cyclodextrin polymer and silica micro-particles: A new hybrid material for adsorption of phenanthrene from water. *Polymers*, *9*(1), 1–11. https://doi.org/10.3390/polym9010010

Chung, M. K., Tsui, M. T. K., Cheung, K. C., Tam, N. F. Y., & Wong, M. H. (2007). Removal of aqueous phenanthrene by brown seaweed *Sargassum hemiphyllum*: Sorption-kinetic and equilibrium studies. *Separation and Purification Technology*, *54*, 355–362. https://doi.org/10.1016/j.seppur.2006.10.008

Cobas, M., Ferreira, L., Sanromán, M. A., & Pazos, M. (2014). Assessment of sepiolite as a low-cost adsorbent for phenanthrene and pyrene removal: Kinetic and equilibrium studies. *Ecological Engineering*, *70*, 287–294. https://doi.org/10.1016/j.ecoleng.2014.06.014

Cohen-Tanugi, D., & Grossman, J. C. (2012). Water Desalination across nanoporous graphene. *Nano Letters*, *12*, 3602–3608. https://doi.org/10.1021/nl3012853

Cornelissen, G., & Gustafsson, O. (2005). Importance of unburned coal carbon, black carbon, and amorphous organic carbon to phenanthrene sorption in sediments.

Environmental Science and Technology, *39*(3), 764–769. https://doi.org/10.1021/es049320z

Crini, G. (2005). Recent developments in polysaccharide-based materials used as adsorbents in wastewater treatment. *Progress in Polymer Science*, *30*, 38–70. https://doi.org/10.1016/j.progpolymsci.2004.11.002

Crisafully, R., Milhome, M. A., Cavalcante, R. M., Silveira, E. R., De Keukeleire, D., & Nascimento, R. F. (2008). Removal of some polycyclic aromatic hydrocarbons from petrochemical wastewater using low-cost adsorbents of natural origin. *Bioresources Technology*, *99*, 4515–4519. https://doi.org/10.1016/j.biortech.2007.08.041

de Boer, J., & Wagelmans, M. (2016). Polycyclic aromatic hydrocarbons in soil – practical options for remediation. *CLEAN - Soil, Air, Water*, *44*, 648–653. https://doi.org/10.1002/clen.201500199

Delval, F., Crini, G., Bertini, S., Filiatre, C., & Torri, G. (2005). Preparation, characterization and sorption properties of crosslinked starch-based exchangers. *Carbohydrate Polymers*, *60*, 67–75. https://doi.org/10.1016/j.carbpol.2004.11.025

Deng, Y., & Zhao, R. (2015). Advanced oxidation processes (AOPs) in wastewater treatment. *Current Pollution Reports*, *1*, 167–176. https://doi.org/10.1007/s40726-015-0015-z

Dickert, F. L., Tortschanoff, M., Bulst, W. E., & Fischerauer, G. (1999). Molecularly imprinted sensor layers for the detection of polycyclic aromatic hydrocarbons in water. *Analytical Chemistry*, *71*(20), 4559–4563. https://doi.org/10.1021/ac990513s

Dreyer, D. R., Ruoff, R. S., & Bielawski, C. W. (2010). From conception to realization: An historial account of graphene and some perspectives for its future. *Angewandte Chemie International Edition*, *49*, 9336–9344. https://doi.org/10.1002/anie.201003024

Duan, L., Naidu, R., Thavamani, P., Meaklim, J., & Megharaj, M. (2015). Managing long-term polycyclic aromatic hydrocarbon contaminated soils: a risk-based approach. *Environmental Science and Pollution Research*, *22*, 8927–8941. https://doi.org/10.1007/s11356-013-2270-0

Dudziak, M., Luks-Betlej, K., & Bodzek, M. (2003). Removal of PAHs from water using membrane processes. *Engineering and Protection of Environment*, *3–4*, 299–311.

Edokpayi, J. N., Odiyo, J. O., Popoola, E. O., & Msagati, A. M. T. (2016). Determination and distribution of polycyclic aromatic hydrocarbons in rivers, sediments and wastewater effluents in Vhembe District, South Africa. *International Journal of Environmental Research and Public Health*, *13*, 387–398. https://doi.org/10.3390/ijerph13040387

Egli, S. N., Butler, E. D., & Bottaro, C. S. (2015). Selective extraction of light polycyclic aromatic hydrocarbons in environmental water samples with pseudo-template thin-film molecularly imprinted polymers. *Analytical Methods*, *7*, 2028–2035. https://doi.org/10.1039/C4AY02849J

Ersan, G., Apul, O. G., Perreault, F., & Karanfil, T. (2017). Adsorption of organic contaminants by graphene nanosheets: A review. *Water Research*, *126*, 385–398. https://doi.org/10.1016/j.watres.2017.08.010

Feng, Z., Huang, C., Guo, Y., Liu, W., & Zhang, L. (2020). Graphitic carbon nitride derivative with large mesopores as sorbent for solid-phase microextraction of polycyclic aromatic hydrocarbons. *Talanta*, *209*, 120541. https://doi.org/10.1016/j.talanta.2019.120541

Fitzer, E., Kochling, K. H., Boehm, H. P., & Marsh, H. (1995). Recommended terminology for the description of carbon as a solid (IUPAC Recommendations 1995). *Pure and Applied Chemistry*, *67*(3), 473–506. https://doi.org/10.1351/pac199567030473

Fletcher, R. E., Ling, S., & Slater, B. (2017). Violations of Löwenstein's rule in zeolites. *Chemical Science*, *8*, 7483–7491. https://doi.org/10.1039/C7SC02531A

Flotron, V., Delteil, C., Bermond, A., & Camel, V. (2005). Degradation of polycyclic aromatic hydrocarbons in sewage sludges by Fenton's reagent. In E. Lichtfouse, J. Schwarzbauer, & D. Robert (Eds.), *Environmental Chemistry: Green Chemistry and Pollutants in Ecosystems* (pp. 449–459). Berlin Heidelberg, Berlin, Heidelberg: Springer.

Fountoulakis, M. S., Terzakis, S., Kalogerakis, N., & Manios, T. (2009). Removal of polycyclic aromatic hydrocarbons and linear alkylbenzene sulfonates from domestic wastewater in pilot constructed wetlands and a gravel filter. *Ecological Engineering*, *35*(12), 1702–1709. https://doi.org/10.1016/j.ecoleng.2009.06.011

Gan, S., Lau, E. V., & Ng, H. K. (2009). Remediation of soils contaminated with polycyclic aromatic hydrocarbons (PAHs). *Journal of Hazardous Materials*, *172*, 532–549. https://doi.org/10.1016/j.jhazmat.2009.07.118

García-Suástegui, W. A., Huerta-Chagoya, A., Carrasco-Colín, K. I., Pratt, M. M., John, K., Petrosyan, P., … Gonsebatt, M. E. (2010). Seasonal variations in the levels of PAH–DNA adducts in young adults living in Mexico City. *Mutagenesis*, *26*, 385–391. https://doi.org/10.1093/mutage/geq104

Garg, A., Singhania, T., Singh, A., Sharma, S., Rani, S., Neogy, A., … Garg, N. (2019). Photocatalytic degradation of bisphenol-A using N, Co codoped TiO_2 catalyst under solar light. *Scientific Reports*, *9*(765), 1–13. https://doi.org/10.1038/s41598-018-38358-w

Geim, A. K. (2009). Graphene: status and prospects. *Science*, *324*, 1530–1534. https://doi.org/10.1126/science.1158877

Ghosal, D., Ghosh, S., Dutta, T. K., & Ahn, Y. (2016). Current state of knowledge in microbial degradation of polycyclic aromatic hydrocarbons (PAHs): A review. *Frontiers in Microbiology*, *7*(1369), 1–27. https://doi.org/10.3389/fmicb.2016.01369

Gök, Ö., Özcan, A. S., & Özcan, A. (2008). Adsorption kinetics of naphthalene onto organo-sepiolite from aqueous solutions. *Desalination*, *220*, 96–107. https://doi.org/10.1016/j.desal.2007.01.025

Gong, Z., Wilke, B. M., Alef, K., Li, P., & Zhou, Q. (2006). Removal of polycyclic aromatic hydrocarbons from manufactured gas plant-contaminated soils using sunflower oil: Laboratory column experiments. *Chemosphere*, *62*, 780–787. https://doi.org/10.1016/j.chemosphere.2005.04.078

Gouma, S., Fragoeiro, S., Bastos, A. C., & Magan, N. (2014). 13 - Bacterial and fungal bioremediation strategies. In S. Das (Ed.), *Microbial biodegradation and bioremediation* (pp. 301–323). Oxford, UK: Elsevier.

Guerra, F. D., Attia, M. F., Whitehead, D. C., & Alexis, F. (2018). Nanotechnology for environmental remediation: materials and applications. *Molecules*, *23*(7), 1760–1783. https://doi.org/10.3390/molecules23071760

Hassan, S. S. M., Abdel-Shafy, H. I., & Mansour, M. S. M. (2018). Removal of pyrene and benzo(a)pyrene micropollutant from water via adsorption by green synthesized iron oxide nanoparticles. *Advances in Natural Sciences: Nanoscience and Nanotechnology*, *9*(015006), 1–15. https://doi.org/10.1088/2043-6254/aaa6f0

Hassan, S., Sayour, H., El Azab, W., & Mansour, M. (2016). Synthesis and characterization of molecularly imprinted nanoparticle polymers for selective separation of anthracene. *Journal of Dispersion Science and Technology*, *37*, 1241–1251. https://doi.org/10.1080/01932691.2015.1089514

Hayakawa, K., Makino, F., Yasuma, M., Yoshida, S., Chondo, Y., Toriba, A., … Koudryashova, Y. (2016). Polycyclic aromatic hydrocarbons in surface water of the southeastern Japan sea. *Chemical and Pharmaceutical Bulletin*, *64*, 625–631. https://doi.org/10.1248/cpb.c16-00063

Heijden, S. A., & Jonker, M. T. O. (2009). PAH bioavailability in field sediments: comparing different methods for predicting in situ bioaccumulation. *Environmental Science and Technology*, *43*(10), 3757–3763. https://doi.org/10.1021/es803329p

Homaeigohar, S., & Elbahri, M. (2017). Graphene membranes for water desalination. *NPG Asia Materials*, *9*(8), e427. https://doi.org/10.1038/am.2017.135

Huang, H.-H., Lu, M.-C., Chen, J.-N., & Lee, C.-T. (2003). Catalytic decomposition of hydrogen peroxide and 4-chlorophenol in the presence of modified activated carbons. *Chemosphere*, *51*(9), 935–943. https://doi.org/10.1016/S0045-6535(03)00042-0

Huang, L., Boving, T. B., & Xing, B. (2006). Sorption of PAHs by aspen wood fibers as affected by chemical alterations. *Environmental Science & Technology*, *40*(10), 3279–3284. https://doi.org/10.1021/es0524651

Huang, X.-D., El-Alawi, Y., Penrose, D. M., Glick, B. R., & Greenberg, B. M. (2004a). A multi-process phytoremediation system for removal of polycyclic aromatic hydrocarbons from contaminated soils. *Environmental Pollution*, *130*, 465–476. https://doi.org/10.1016/j.envpol.2003.09.031

Huang, X.-D., El-Alawi, Y., Penrose, D. M., Glick, B. R., & Greenberg, B. M. (2004b). Responses of three grass species to creosote during phytoremediation. *Environmental Pollution*, *130*(3), 453–463. https://doi.org/10.1016/j.envpol.2003.12.018

Huang, Y., Fulton, A. N., & Keller, A. A. (2016). Simultaneous removal of PAHs and metal contaminants from water using magnetic nanoparticle adsorbents. *Science of the Total Environment*, *571*, 1029–1036. https://doi.org/10.1016/j.scitotenv.2016.07.093

Huling, S. G., & Pivetz, B. E. (2006). *In-situ chemical oxidation In-situ chemical oxidation*. EPA/600th/R-06/072. Cincinnati, OH: United States Environmental Protection Agency.

Hussain, K., Hoque, R. R., Balachandran, S., Medhi, S., Idris, M. G., Rahman, M., & Hussain, F. L. (2018). Monitoring and risk analysis of PAHs in the environment. In C. M. Hussain (Ed.), *Handbook of environmental materials management* (pp. 1–35). New York: Springer International Publishing.

Isosaari, P., Piskonen, R., Ojala, P., Voipio, S., Eilola, K., Lehmus, E., & Itävaara, M. (2007). Integration of electrokinetics and chemical oxidation for the remediation of creosote-contaminated clay. *Journal of Hazardous Materials*, *144*, 538–548. https://doi.org/10.1016/j.jhazmat.2006.10.068

Jeelani, N., Yang, W., Xu, L., Qiao, Y., An, S., & Leng, X. (2017). Phytoremediation potential of *Acorus calamus* in soils co-contaminated with cadmium and polycyclic aromatic hydrocarbons. *Scientific Reports*, *7*(1), 1–9. https://doi.org/10.1038/s41598-017-07831-3

Katsnelson, M. I. (2007). Graphene: carbon in two dimensions. *Materials Today*, *10*(1–2), 20–27. https://doi.org/10.1016/S1369-7021(06)71788-6

Kemp, K. C., Seema, H., Saleh, M., Le, N. H., Mahesh, K., Chandra, V., & Kim, K. S. (2013). Environmental applications using graphene composites: water remediation and gas adsorption. *Nanoscale*, *5*, 3149–3171. https://doi.org/10.1039/C3NR33708A

Klejnowski, K., Kozielska, B., Krasa, A., & Rogula-Kozłowska, W. (2010). Polycyclic aromatic hydrocarbons in PM1, PM2.5, PM10 and tsp in the Upper Silesian agglomeration, Poland. *Archives of Environmnetal Protection*, *36*(2), 65–72.

Kroukamp, E. M., Wondimu, T., & Forbes, P. B. C. (2016). Metal and metalloid speciation in plants: Overview, instrumentation, approaches and commonly assessed elements. *TrAC Trends in Analytical Chemistry*, *77*, 87–99. https://doi.org/10.1016/j.trac.2015.10.007

Krupadam, R. J. (2012). Nanoporous polymeric material for remediation of PAHs polluted water. *Polycyclic Aromatic Compounds*, *32*, 313–333. https://doi.org/10.1080/10406638.2011.633591

Krupadam, R. J., Ahuja, R., & Wate, S. R. (2007). Benzo(a)pyrene imprinted polyacrylate nanosurfaces: Adsorption and binding characteristics. *Sensors and Actuators B: Chemical*, *124*, 444–451. https://doi.org/10.1016/j.snb.2007.01.020

Kuppusamy, S., Thavamani, P., Megharaj, M., & Naidu, R. (2015). Bioremediation potential of natural polyphenol rich green wastes: A review of current research and recommendations for future directions. *Environmental Technology & Innovation*, *4*, 17–28. https://doi.org/10.1016/j.eti.2015.04.001

Kuppusamy, S., Thavamani, P., Megharaj, M., & Naidu, R. (2016). Biodegradation of polycyclic aromatic hydrocarbons (PAHs) by novel bacterial consortia tolerant to diverse physical settings – Assessments in liquid- and slurry-phase systems. *International Biodeterioration & Biodegradation*, *108*, 149–157. https://doi.org/10.1016/j.ibiod.2015.12.013

Kuppusamy, S., Thavamani, P., Venkateswarlu, K., Lee, Y. B., Naidu, R., & Megharaj, M. (2017). Remediation approaches for polycyclic aromatic hydrocarbons (PAHs) contaminated soils: Technological constraints, emerging trends and future directions. *Chemosphere*, *168*, 944–968. https://doi.org/10.1016/j.chemosphere.2016.10.115

Lamichhane, S., Bal Krishna, K. C., & Sarukkalige, R. (2016). Polycyclic aromatic hydrocarbons (PAHs) removal by sorption: A review. *Chemosphere*, *148*, 336–353. https://doi.org/10.1016/j.chemosphere.2016.01.036

Lao, C., Zeledón, Z., Gamisans, X., & Solé, M. (2005). Sorption of Cd(II) and Pb(II) from aqueous solutions by a low-rank coal (leonardite). *Separation and Purification Technology*, *45*, 79–85. https://doi.org/10.1016/j.seppur.2005.02.006

Lawal, A. T. (2017). Polycyclic aromatic hydrocarbons. A review. *Cogent Environmental Science*, *3*(1339841), 1–89. https://doi.org/10.1080/23311843.2017.1339841

Lee, S. Y., Kim, S. J., Chung, S. Y., & Jeong, C. H. (2004). Sorption of hydrophobic organic compounds onto organoclays. *Chemosphere*, *55*, 781–785. https://doi.org/10.1016/j.chemosphere.2003.11.007

Lee, S. M., & Tiwari, D. (2012). Organo and inorgano-organo-modified clays in the remediation of aqueous solutions: An overview. *Applied Clay Science*, *59–60*, 84–102. https://doi.org/10.1016/j.clay.2012.02.006

Lemić, J., Tomašević-Čanović, M., Adamović, M., Kovačević, D., & Milićević, S. (2007). Competitive adsorption of polycyclic aromatic hydrocarbons on organo-zeolites. *Microporous and Mesoporous Materials*, *105*, 317–323. https://doi.org/10.1016/j.micromeso.2007.04.014

Li, J., Zhao, L., Qin, L., Tian, X., Wang, A., Zhou, Y., … Chen, Y. (2016). Removal of refractory organics in nanofiltration concentrates of municipal solid waste leachate treatment plants by combined Fenton oxidative-coagulation with photo – Fenton processes. *Chemosphere*, *146*, 442–449. https://doi.org/10.1016/j.chemosphere.2015.12.069

Li, Z., & Bowman, R. S. (2001). Retention of inorganic oxyanions by organo-kaolinite. *Water Research*, *35*, 3771–3776. https://doi.org/10.1016/S0043-1354(01)00120-8

Lian, L., Yao, B., Hou, S., Fang, J., Yan, S., & Song, W. (2017). Kinetic study of hydroxyl and sulfate radical-mediated oxidation of pharmaceuticals in wastewater effluents. *Environmental Science & Technology*, *51*, 2954–2962. https://doi.org/10.1021/acs.est.6b05536

Liu, L., He, L., Jiang, X., Zhao, W., Xiang, G., & Anderson, J. L. (2014). Macrocyclic polyamine-functionalized silica as a solid-phase extraction material coupled with ionic liquid dispersive liquid–liquid extraction for the enrichment of polycyclic aromatic hydrocarbons. *Journal of Separation Science*, *37*, 1004–1011. https://doi.org/10.1002/jssc.201301062

Luo, Z.-H., Wei, C.-L., He, N.-N., Sun, Z.-G., Li, H.-X., & Chen, D. (2015). Correlation between the photocatalytic degradability of PAHs over Pt/TiO_2-SiO_2 in water and their quantitative molecular structure. *Journal of Nanomaterials*, *284834*, 1–11. https://doi.org/10.1155/2015/284834

Luthy, R. G., Aiken, G. R., Brusseau, M. L., Cunningham, S. D., Gschwend, P. M., Pignatello, J. J., … Westall, J. C. (1997). Sequestration of hydrophobic organic contaminants by geosorbents. *Environmental Science & Technology*, *31*(12), 3341–3347. https://doi.org/10.1021/es970512m

Maletic, S. P., Beljin, J. M., Roncevic, S. D., Grgic, M. G., & Dalmacija, B. D. (2019). State of the art and future challenges for polycyclic aromatic hydrocarbons is sediments: Sources, fate, bioavailability and remediation techniques. *Journal of Hazardous Material*, *365*, 467–482. https://doi.org/10.1016/j.jhazmat.2018.11.020

Martinez, E., Gros, M., Lacorte, S., & Barceló, D. (2004). Simplified procedures for the analysis of polycyclic aromatic hydrocarbons in water, sediments and mussels. *Journal of Chromatography A*, *1047*, 181–188. https://doi.org/10.1016/j.chroma.2004.07.003

Meng, L., Qiao, M., & Arp, H. P. H. (2011). Phytoremediation efficiency of a PAH-contaminated industrial soil using ryegrass, white clover, and celery as mono- and mixed cultures. *Journal of Soils and Sediments*, *11*, 482–490. https://doi.org/10.1007/s11368-010-0319-y

Mohan, S. V., Kisa, T., Ohkuma, T., Kanaly, R. A., & Shimizu, Y. (2006). Bioremediation technologies for treatment of PAH-contaminated soil and strategies to enhance process efficiency. *Reviews in Environmental Science and Bio/Technology*, *5*, 347–374. https://doi.org/10.1007/s11157-006-0004-1

Mojiri, A., Zhou, J. L., Ohashi, A., Ozaki, N., & Kindaichi, T. (2019). Comprehensive review of polycyclic aromatic hydrocarbons in water sources, their effects and treatments. *Science of the Total Environment*, *696*(133971), 1–16. https://doi.org/10.1016/j.scitotenv.2019.133971

Montaseri, H., & Forbes, P. B. C. (2018). Molecularly imprinted polymer coated quantum dots for fluorescence sensing of acetaminophen. *Materials Today Communications*, *17*, 480–492. https://doi.org/10.1016/j.mtcomm.2018.10.007

Moscoso, F., Ferreira, L., Deive, F. J., Morán, P., & Sanromán, M. A. (2013). Viability of phenanthrene biodegradation by an isolated bacterial consortium: Optimization and scale-up. *Bioprocess and Biosystems Engineering*, *36*, 133–141. https://doi.org/10.1007/s00449-012-0768-3

Müller, S., Totsche, K. U., & Kögel-Knabner, I. (2007). Sorption of polycyclic aromatic hydrocarbons to mineral surfaces. *European Journal of Soil Science*, *58*, 918–931. https://doi.org/10.1111/j.1365-2389.2007.00930.x

Munyeza, C. F., Dikale, O., Rohwer, E. R., & Forbes, P. B. C. (2018). Development and optimization of a plunger assisted solvent extraction method for polycyclic aromatic hydrocarbons sampled onto multi-channel silicone rubber traps. *Journal of Chromatography A*, *1555*, 20–29. https://doi.org/10.1016/j.chroma.2018.04.053

Nian, Q., Wang, X., Wang, M., & Zuo, G. (2019). A hybrid material composed of graphitic carbon nitride and magnetite (Fe_3O_4) for magnetic solid-phase extraction of trace levels of hydroxylated polycyclic aromatic hydrocarbons. *Microchimica Acta*, *186*(8), 497–506. https://doi.org/10.1007/s00604-019-3607-2

Novoselov, K. S., Fal'ko, V. I., Colombo, L., Gellert, P. R., Schwab, M. G., & Kim, K. (2012). A roadmap for graphene. *Nature*, *490*, 192–200. https://doi.org/10.1038/nature11458

Nsibande, S. A., & Forbes, P. B. C. (2020). Development of a turn-on graphene quantum dot-based fluorescent probe for sensing of pyrene in water. *RSC Advances*, *10*, 12119–12128. https://doi.org/10.1039/C9RA10153E

Nsibande, S. A., Montaseri, H., & Forbes, P. B. C. (2019). Advances in the application of nanomaterial-based sensors for detection of polycyclic aromatic hydrocarbons in aquatic systems. *TrAC Trends in Analytical Chemistry*, *115*, 52–69. https://doi.org/10.1016/j.trac.2019.03.029

Okere, U. V. (2011). Biodegradation of PAHs in 'pristine' soils from different climatic regions. *Journal of Bioremediation & Biodegradation*, *1*, 1–11. https://doi.org/10.4172/2155-6199.S1-006

Okoli, C. P., Adewuyi, G. O., Zhang, Q., Zhu, G., Wang, C., & Guo, Q. (2015). Aqueous scavenging of polycyclic aromatic hydrocarbons using epichlorohydrin, 1,6-hexamethylene diisocyanate and 4,4-methylene diphenyl diisocyanate modified starch: Pollution remediation approach. *Arabian Journal of Chemistry*, *12*(8), 2760–2773. https://doi.org/10.1016/j.arabjc.2015.06.004

Olivella, M. À., Jové, P., & Oliveras, A. (2011). The use of cork waste as a biosorbent for persistent organic pollutants–Study of adsorption/desorption of polycyclic aromatic hydrocarbons. *Journal of Environmental Science and Health, Part A*, *46*, 824–832. https://doi.org/10.1080/10934529.2011.579845

Ololade, I. A., Adeola, A. O., Oladoja, N. A., Ololade, O. O., Nwaolisa, S. U., Alabi, A. B., & Ogungbe, I. V. (2018). In-situ modification of soil organic matter towards adsorption and desorption of phenol and its chlorinated derivatives. *Journal of Environmental Chemical Engineering*, *6*, 3485–3494. https://doi.org/10.1016/j.jece.2018.05.034

Olsson, A. C., Fevotte, J., Fletcher, T., Cassidy, A., Mannetje, A., Zaridze, D., … Boffetta, P. (2010). Occupational exposure to polycyclic aromatic hydrocarbons and lung cancer risk: A multicenter study in Europe. *Occupational and Environmental Medicine*, *67*(2), 98–103. https://doi.org/10.1136/oem.2009.046680

Oyedotun, K. O., Masikhwa, T. M., Lindberg, S., Matic, A., Johansson, P., & Manyala, N. (2019). Comparison of ionic liquid electrolyte to aqueous electrolytes on carbon nanofibres supercapacitor electrode derived from oxygen-functionalized graphene. *Chemical Engineering Journal*, *375*, 121906. https://doi.org/10.1016/j.cej.2019.121906

Payne, R. B., Ghosh, U., May, H. D., Marshall, C. W., & Sowers, K. R. (2017). Mesocosm studies on the efficacy of bioamended activated carbon for treating PCB-impacted sediment. *Environmental Science & Technology*, *51*, 10691–10699. https://doi.org/10.1021/acs.est.7b01935

Pazos, M., Rosales, E., Alcántara, T., Gómez, J., & Sanromán, M. A. (2010). Decontamination of soils containing PAHs by electroremediation: A review. *Journal of Hazardous Materials*, *177*, 1–11. https://doi.org/10.1016/j.jhazmat.2009.11.055

Peng, W., Li, H., Liu, Y., & Song, S. (2017). A review on heavy metal ions adsorption from water by graphene oxide and its composites. *Journal of Molecular Liquids*, *230*, 496–504. https://doi.org/10.1016/j.molliq.2017.01.064

Pérez-Gregorio, M. R., García-Falcón, M. S., Martínez-Carballo, E., & Simal-Gándara, J. (2010). Removal of polycyclic aromatic hydrocarbons from organic solvents by ashes wastes. *Journal of Hazardous Materials*, *178*, 273–281. https://doi.org/10.1016/j.jhazmat.2010.01.073

Petruzzelli, G., Pedron, F., Rosellini, I., Grifoni, M., & Barbafieri, M. (2016). Polycyclic aromatic hydrocarbons and heavy metal contaminated sites: phytoremediation as a strategy for addressing the complexity of pollution. In A. A. Ansari, S. S. Gill, R. Gill, G. R. Lanza, & L. Newman (Eds.), *Phytoremediation: Management of environmental contaminants*, Vol. *4* (pp. 61–90). New York: Springer International Publishing.

Pourfadakari, S., Ahmadi, M., Jaafarzadeh, N., Takdastan, A., Neisi, A. A., Ghafari, S., & Jorfi, S. (2019). Remediation of PAHs contaminated soil using a sequence of soil washing with biosurfactant produced by *Pseudomonas aeruginosa* strain PF2 and electrokinetic oxidation of desorbed solution, effect of electrode modification with Fe_3O_4 nanoparticles. *Journal of Hazardous Materials*, *379*(120839), 1–14. https://doi.org/10.1016/j.jhazmat.2019.120839

Quinn, L., Pieters, R., Nieuwoudt, C., Borgen, A. R., Kylin, H., & Bouwman, H. (2009). Distribution profiles of selected organic pollutants in soils and sediments of industrial, residential and agricultural areas of South Africa. *Journal of Environmental Monitoring*, *11*, 1647–1657. https://doi.org/10.1039/B905585A

Ran, Y., Huang, W., Rao, P. S. C., Liu, D., Sheng, G., & Fu, J. (2002). The role of condensed organic matter in the nonlinear sorption of hydrophobic organic contaminants by a peat and sediments. *Journal of Environmental Quality*, *31*, 1953–1962. https://doi.org/10.2134/jeq2002.1953

Ran, Y., Xiao, B., Huang, W., Peng, P., Liu, D., Fu, J., & Sheng, G. (2003). Kerogen in an aquifer and its strong sorption for hydrophobic organic contaminants. *Journal of Environmental Quality*, *32*(5), 1701–1709. https://doi.org/10.2134/jeq2003.1701

Reddy, K. R., Ala, P. R., Sharma, S., & Kumar, S. N. (2006). Enhanced electrokinetic remediation of contaminated manufactured gas plant soil. *Engineering Geology*, *85*, 132–146. https://doi.org/10.1016/j.enggeo.2005.09.043

Ritchie, H., & Roser, M. (2020). *"Clean Water"*. Published online at OurWorldInData.org. Retrieved from https://ourworldindata.org/water-access

Rivas, J., Gimeno, O., de la Calle, R. G., & Beltrán, F. J. (2009). Ozone treatment of PAH contaminated soils: Operating variables effect. *Journal of Hazardous Materials*, *169*, 509–515. https://doi.org/10.1016/j.jhazmat.2009.03.136

Rockne, K. J., Shor, L. M., Young, L. Y., Taghon, G. L., & Kosson, D. S. (2002). Distributed sequestration and release of PAHs in weathered sediment: The role of sediment structure and organic carbon properties. *Environmental Science and Technology*, *36*, 2636–2644. https://doi.org/10.1021/es015652h

Roy, S., Labelle, S., Mehta, P., Mihoc, A., Fortin, N., Masson, C., … Greer, C. W. (2005). Phytoremediation of heavy metal and PAH-contaminated brownfield sites. *Plant and Soil*, *272*, 277–290. https://doi.org/10.1007/s11104-004-5295-9

Sabah, E., & Ouki, S. (2017). Adsorption of pyrene from aqueous solutions onto sepiolite. *Clays and Clay Minerals*, *65*, 14–26. https://doi.org/10.1346/CCMN.2016.064046

Saichek, R. E., & Reddy, K. R. (2005). Surfactant-enhanced electrokinetic remediation of polycyclic aromatic hydrocarbons in heterogeneous subsurface environments. *Journal of Environmental Engineering and Science, 4*, 327–339. https://doi.org/10.1139/s04-064

Samanta, S. K., Singh, O. V., & Jain, R. K. (2002). Polycyclic aromatic hydrocarbons: environmental pollution and bioremediation. *Trends in Biotechnology, 20*, 243–248. https://doi.org/10.1016/s0167-7799(02)01943-1

Schad, H., Haist-Gulde, B., Klein, R., Maier, D., Maier, M., & Schulze, B. (2000). *Funnel-and-gate at the former manufactured gas plant site in Karlsruhe: sorption test results, hydraulic and technical design, construction*. Proceedings of the seventh international FZK/TNO conference on contaminated soil 18–22 September 2000, Leipzig, Germany, 951–959.

Schoonraad, G.-L., Madito, M. J., Manyala, N., & Forbes, P. (2020). Synthesis and optimisation of a novel graphene wool material by atmospheric pressure chemical vapour deposition. *Journal of Materials Science, 55*, 545–564. https://doi.org/10.1007/s10853-019-03948-0

Shannon, M. A., Bohn, P. W., Elimelech, M., Georgiadis, J. G., Mariñas, B. J., & Mayes, A. M. (2008). Science and technology for water purification in the coming decades. *Nature, 452*, 301–310. https://doi.org/10.1038/nature06599

Silva, I. S., Grossman, M., & Durrant, L. R. (2009). Degradation of polycyclic aromatic hydrocarbons (2–7 rings) under microaerobic and very-low-oxygen conditions by soil fungi. *International Biodeterioration & Biodegradation, 63*, 224–229. https://doi.org/10.1016/j.ibiod.2008.09.008

Smol, M., & Włodarczyk-Makuła, M. (2012). Effectiveness in the removal of polycyclic aromatic hydrocarbons from industrial wastewater by ultrafiltration technique. *Archives of Environmental Protection, 38*(4), 49–58. https://doi.org/10.2478/v10265-012-0040-6

Smol, M., Włodarczyk-Makuła, M., Bohdziewicz, J., & Mielczarek, K. (2014). The use of integrated membrane systems in the removal of selected pollutants from pre-treated wastewater in coke plant. *Monographs of the Environmental Engineering Committee Polish Academy of Sciences, 119*, 143–152.

Smol, M., Włodarczyk-Makuła, M., Mielczarek, K., & Bohdziewicz, J. (2014). Comparison of the retention of selected PAHs from municipal landfill leachate by RO and UF processes. *Desalination and Water Treatment, 52*(19–21), 3889–3897. https://doi.org/10.1080/19443994.2014.887451

Smol, M., Włodarczyk-Makuła, M., Mielczarek, K., Bohdziewicz, J., & Włóka, D. (2015). The use of reverse osmosis in the removal of PAHs from municipal landfill leachate. *Polycyclic Aromatic Compounds, 36*(1), 20–39. https://doi.org/10.1080/10406638.2014.957403

Solé, M., Casas, J. M., & Lao, C. (2003). Removal of Zn from aqueous solutions by low-rank coal. *Water, Air, and Soil Pollution, 144*, 57–65. https://doi.org/10.1023/A:1022965417124

Soleimani, M. (2012). Bioremediation: An environmental friendly solution for oil contaminated soils. *Journal of Bioremediation and Biodegradation, 3*(4), 1000e109. https://doi.org/10.4172/2155-6199.1000e109

Streat, M., & Swetland, L. A. (1997). Physical and adsorptive properties of Hypersol-Macronet™ polymers. *Reactive and Functional Polymers, 35*, 99–109. https://doi.org/10.1016/S1381-5148(97)00049-7

Su, Y.-H., Zhu, Y.-G., Sheng, G., & Chiou, C. T. (2006). Linear adsorption of nonionic organic compounds from water onto hydrophilic minerals: Silica and alumina. *Environmental Science & Technology, 40*, 6949–6954. https://doi.org/10.1021/es0609809

Sun, J.-H., Wang, G.-L., Chai, Y., Zhang, G., Li, J., & Feng, J. (2009). Distribution of polycyclic aromatic hydrocarbons (PAHs) in Henan Reach of the Yellow River, Middle China. *Ecotoxicology and Environmental Safety, 72*(5), 1614–1624. https://doi.org/10.1016/j.ecoenv.2008.05.010

Sun, K., Liu, J., Gao, Y., Jin, L., Gu, Y., & Wang, W. (2014). Isolation, plant colonization potential and phenanthrene degradation performance of the endophytic bacterium *Pseudomonas sp. Scientific Reports, 4*(5462), 1–9. https://doi.org/10.1038/srep05462

Sun, M., Fu, D., Teng, Y., Shen, Y., Luo, Y., Li, Z., & Christie, P. (2011). In situ phytoremediation of PAH-contaminated soil by intercropping alfalfa (*Medicago sativa* L.) with tall fescue (*Festuca arundinacea* Schreb.) and associated soil microbial activity. *Journal of Soils and Sediments, 11*, 980–989. https://doi.org/10.1007/s11368-011-0382-z

Sun, Y., Yang, S., Zhao, G., Wang, Q., & Wang, X. (2013). Adsorption of polycyclic aromatic hydrocarbons on graphene oxides and reduced graphene oxides. *Chemistry – an Asian Journal, 8*, 2755–2761. https://doi.org/10.1002/asia.201300496

Sun, Y., & Zhou, Q. (2016). Uptake and translocation of benzo[a]pyrene (B[a]P) in two ornamental plants and dissipation in soil. *Ecotoxicology and Environmental Safety, 124*, 74–81. https://doi.org/10.1016/j.ecoenv.2015.09.037

Topuz, F., & Uyar, T. (2017). Cyclodextrin-functionalized mesostructured silica nanoparticles for removal of polycyclic aromatic hydrocarbons. *Journal of Colloid and Interface Science, 497*, 233–241. https://doi.org/10.1016/j.jcis.2017.03.015

Torabian, A., Kazemian, H., Seifi, L., Bidhendi, G. N., Azimi, A. A., & Ghadiri, S. K. (2010). Removal of petroleum aromatic hydrocarbons by surfactant-modified natural zeolite: The effect of surfactant. *CLEAN – Soil, Air, Water, 38*, 77–83. https://doi.org/10.1002/clen.200900157

United Nations Information Centre (2017). *The sustainable development goals report*. Retrieved from https://unstats.un.org/sdgs/files/report/2017/TheSustainableDevelopmentGoalsReport2017.pdf

USEPA, United State Environmental Protection Agency (2000). *Toxic release inventory public data release*. Washington, DC: Office of Environmental Information, United States Environmental Protection Agency. Retrieved from http://www.epa.gov/triinter/tridata/index.htm

Valderrama, C., Cortina, J. L., Farran, A., Gamisans, X., & Lao, C. (2007). Kinetics of sorption of polyaromatic hydrocarbons onto granular activated carbon and Macronet hyper-cross-linked polymers (MN200). *Journal of Colloid and Interface Science, 310*, 35–46. https://doi.org/10.1016/j.jcis.2007.01.039

Van der Wat, L., & Forbes, P. B. C. (2019). Comparison of extraction techniques for polycyclic aromatic hydrocarbons from lichen biomonitors. *Environmental Science and Pollution Research, 26*, 11179–11190. https://doi.org/10.1007/s11356-019-04587-3

Vidal, C. B., Barros, A. L., Moura, C. P., de Lima, A. C. A., Dias, F. S., Vasconcellos, L. C. G., … Nascimento, R. F. (2011). Adsorption of polycyclic aromatic hydrocarbons from aqueous solutions by modified periodic mesoporous organosilica. *Journal of Colloid and Interface Science, 357*, 466–473. https://doi.org/10.1016/j.jcis.2011.02.013

Viñas, M., Sabaté, J., Espuny, M. J., & Solanas, A. M. (2005). Bacterial community dynamics and polycyclic aromatic hydrocarbon degradation during bioremediation of heavily creosote-contaminated soil. *Applied and Environmental Microbiology, 71*, 7008. https://doi.org/10.1128/AEM.71.11.7008-7018.2005

Wang, J., Chen, Z., & Chen, B. (2014). Adsorption of polycyclic aromatic hydrocarbons by graphene and graphene oxide nanosheets. *Environmental Science & Technology, 48*, 4817–4825. https://doi.org/10.1021/es405227u

Wang, J., Li, F., Li, X., Wang, X., Li, X., Su, Z., … Guo, S. (2013). Effects of electrokinetic operation mode on removal of polycyclic aromatic hydrocarbons (PAHs), and the indigenous fungal community in PAH-contaminated soil. *Journal of Environmental Science and Health, Part A, 48*, 1677–1684. https://doi.org/10.1080/10934529.2013.815500

Wang, L., Yang, Z., Niu, J., & Wang, J. (2009). Characterization, ecological risk assessment and source diagnostics of polycyclic aromatic hydrocarbons in water column of the Yellow River Delta, one of the most plenty biodiversity zones in the world. *Journal of Hazardous Materials, 169*, 460–465. https://doi.org/10.1016/j.jhazmat.2009.03.125

Wang, T., Jin, X., Chen, Z., Megharaj, M., & Naidu, R. (2014). Green synthesis of Fe nanoparticles using eucalyptus leaf extracts for treatment of eutrophic wastewater. *Science of the Total Environment, 466*, 210–213. https://doi.org/10.1016/j.scitotenv.2013.07.022

Wang, W., Wang, Z., Liu, J., Zhang, Z., & Sun, L. (2017). Single-step one-pot synthesis of graphene foam/TiO_2 nanosheet hybrids for effective water treatment. *Scientific Reports, 7*(43755), 1–9. https://doi.org/10.1038/srep43755

WHO, UNICEF (2012). *Global water supply and sanitation assessment report*. Geneva: WHO/UNICEF. [Online Resource].

Wise, D. L. (2000). *Remediation engineering of contaminated soils. Series: Environmental Science & Pollution*. Boca Raton: CRC Press, Taylor and Francis Group, United Kingdom.

Wołowiec, M., Muir, B., Zięba, K., Bajda, T., Kowalik, M., & Franus, W. (2017). Experimental study on the removal of VOCs and PAHs by zeolites and surfactant-modified zeolites. *Energy & Fuels, 31*, 8803–8812. https://doi.org/10.1021/acs.energyfuels.7b01124

World Health Organization (WHO) (1984). *Guidelines for Drinking Water Quality*. Geneva.

Wu, B., Zhang, Y., Zhang, X.-X., & Cheng, S.-P. (2011). Health risk assessment of polycyclic aromatic hydrocarbons in the source water and drinking water of China: Quantitative analysis based on published monitoring data. *Science of the Total Environment, 410*, 112–118. https://doi.org/10.1016/j.scitotenv.2011.09.046

Wu, C.-H., Chang-Chien, G.-P., & Lee, W.-S. (2004). Photodegradation of polychlorinated dibenzo-p-dioxins: Comparison of photocatalysts. *Journal of Hazardous Materials, 114*, 191–197. https://doi.org/10.1016/j.jhazmat.2004.08.008

Wu, M., Chen, L., Tian, Y., Ding, Y., & Dick, W. A. (2013). Degradation of polycyclic aromatic hydrocarbons by microbial consortia enriched from three soils using two different culture media. *Environmental Pollution, 178*, 152–158. https://doi.org/10.1016/j.envpol.2013.03.004

Wu, T., Cai, X., Tan, S., Li, H., Liu, J., & Yang, W. (2011). Adsorption characteristics of acrylonitrile, p-toluenesulfonic acid, 1-naphthalenesulfonic acid and methyl blue on graphene in aqueous solutions. *Chemical Engineering Journal, 173*, 144–149. https://doi.org/10.1016/j.cej.2011.07.050

Wu, Y., Zhou, S., Ye, X., Chen, D., Zheng, K., & Qin, F. (2011). Transformation of pollutants in landfill leachate treated by a combined sequence batch reactor, coagulation, Fenton oxidation and biological aerated filter technology. *Process Safety and Environmental Protection, 89*, 112–120. https://doi.org/10.1016/j.psep.2010.10.005

Wu, Z., & Zhu, L. (2012). Removal of polycyclic aromatic hydrocarbons and phenols from coking wastewater by simultaneously synthesized organobentonite in a one-step process. *Journal of Environmental Sciences, 24*, 248–253. https://doi.org/10.1016/s1001-0742(11)60780-8

Xi, Z., & Chen, B. (2014). Removal of polycyclic aromatic hydrocarbons from aqueous solution by raw and modified plant residue materials as biosorbents. *Journal of Environmental Sciences, 26*, 737–748. https://doi.org/10.1016/S1001-0742(13)60501-X

Xu, C., Nasrollahzadeh, M., Selva, M., Issaabadi, Z., & Luque, R. (2019). Waste-to-wealth: biowaste valorization into valuable bio(nano)materials. *Chemical Society Reviews, 48*, 4791–4822. https://doi.org/10.1039/C8CS00543E

Xu, H., Zhan, M.-X., Cai, P.-T., Ji, L.-J., Chen, T., & Li, X.-D. (2019). Adsorption characteristics of polycyclic aromatic hydrocarbons by biomass-activated carbon in flue gas. *Energy & Fuels, 33*, 11477–11485. https://doi.org/10.1021/acs.energyfuels.9b02723

Yakout, S. M., & Daifullah, A. A. M. (2013). Removal of selected polycyclic aromatic hydrocarbons from aqueous solution onto various adsorbent materials. *Desalination and Water Treatment, 51*, 6711–6718. https://doi.org/10.1080/19443994.2013.769916

Yang, K., Chen, B., & Zhu, L. (2015). Graphene-coated materials using silica particles as a framework for highly efficient removal of aromatic pollutants in water. *Scientific Reports, 5*(11641), 1–13. https://doi.org/10.1038/srep11641

Yang, X., Li, J., Ren, X., Huang, Y., & Wang, X. (2013). Adsorption of naphthalene and its derivatives on magnetic graphene composites and the mechanism investigation. *Colloid Surface A., 422*, 118–125. https://doi.org/10.1016/j.colsurfa.2012.11.063

Yap, C. L., Gan, S., & Ng, H. K. (2012). Ethyl lactate-Fenton treatment of soil highly contaminated with polycyclic aromatic hydrocarbons (PAHs). *Chemical Engineering Journal, 200–202*, 247–256. https://doi.org/10.1016/j.cej.2012.06.036

Ye, S., Yan, M., Tan, X., Liang, J., Zeng, G., Wu, H., … Wang, H. (2019). Facile assembled biochar-based nanocomposite with improved graphitization for efficient photocatalytic activity driven by visible light. *Applied Catalysis B: Environmental, 250*, 78–88. https://doi.org/10.1016/j.apcatb.2019.03.004

Ye, S., Zeng, G., Wu, H., Liang, J., Zhang, C., Dai, J., … Yu, J. (2019). The effects of activated biochar addition on remediation efficiency of co-composting with contaminated wetland soil. *Resources, Conservation and Recycling, 140*, 278–285. https://doi.org/10.1016/j.resconrec.2018.10.004

Yuan, H., Li, T., Ding, X., Zhao, G., & Ye, S. (2014). Distribution, sources and potential toxicological significance of polycyclic aromatic hydrocarbons (PAHs) in surface soils of the Yellow River Delta, China. *Marine Pollution Bulletin, 83*, 258–264. https://doi.org/10.1016/j.marpolbul.2014.03.043

Zeledón-Toruño, Z. C., Lao-Luque, C., de las Heras, F. X. C., & Sole-Sardans, M., (2007). Removal of PAHs from water using an immature coal (leonardite). *Chemosphere, 67*, 505–512. https://doi.org/10.1016/j.chemosphere.2006.09.047

Zertal, A., Molnár-Gábor, D., Malouki, M. A., Sehili, T., & Boule, P. (2004). Photocatalytic transformation of 4-chloro-2-methylphenoxyacetic acid (MCPA) on several kinds of TiO_2. *Applied Catalysis B: Environmental, 49*, 83–89. https://doi.org/10.1016/j.apcatb.2003.11.015

Zhang, C., Wu, L., Cai, D., Zhang, C., Wang, N., Zhang, J., & Wu, Z. (2013). Adsorption of polycyclic aromatic hydrocarbons (Fluoranthene and Anthracenemethanol) by functional graphene oxide and removal by pH and temperature-sensitive Coagulation. *ACS Applied Materials & Interfaces, 5*, 4783–4790. https://doi.org/10.1021/am4002666

Zhang, L., Li, P., Gong, Z., & Li, X. (2008). Photocatalytic degradation of polycyclic aromatic hydrocarbons on soil surfaces using TiO_2 under UV light. *Journal of Hazardous Materials, 158*, 478–484. https://doi.org/10.1016/j.jhazmat.2008.01.119

Zhang, L., Luo, L., & Zhang, S. (2011). Adsorption of phenanthrene and 1,3-dinitrobenzene on cation-modified clay minerals. *Colloids and Surfaces A: Physicochemical and Engineering Aspects, 377*, 278–283. https://doi.org/10.1016/j.colsurfa.2011.01.017

Zhang, M.-H., Dong, H., Zhao, L., Wang, D.-X., & Meng, D. (2019). A review on Fenton process for organic wastewater treatment based on optimization perspective. *Science of the Total Environment, 670*, 110–121. https://doi.org/10.1016/j.scitotenv.2019.03.180

Zhang, S., Niu, H., Cai, Y., & Shi, Y. (2010). Barium alginate caged Fe_3O_4@C_{18} magnetic nanoparticles for the pre-concentration of polycyclic aromatic hydrocarbons and phthalate esters from environmental water samples. *Analytica Chimica Acta, 665*, 167–175. https://doi.org/10.1016/j.aca.2010.03.026

Zhang, S., Yao, H., Lu, Y., Yu, X., Wang, J., Sun, S., … Zhang, D. (2017). Uptake and translocation of polycyclic aromatic hydrocarbons (PAHs) and heavy metals by maize from soil irrigated with wastewater. *Scientific Reports, 7*(12165), 1–11. https://doi.org/10.1038/s41598-017-12437-w

Zhao, G., Jiang, L., He, Y., Li, J., Dong, H., Wang, X., & Hu, W. (2011). Sulfonated graphene for persistent aromatic pollutant management. *Advanced Materials, 23*, 3959–3963. https://doi.org/10.1002/adma.201101007

Zhao, G. X., Li, J. X., & Wang, X. K. (2011). Kinetic and thermodynamic study of 1-naphthol adsorption from aqueous solution to sulfonated graphene nanosheets. *Chemical Engineering Journal, 173*, 185–190. https://doi.org/10.1016/j.cej.2011.07.072

Zhao, J., Wang, Z., Zhao, Q., & Xing, B. (2014). Adsorption of phenanthrene on multilayer graphene as affected by surfactant and exfoliation. *Environmental Science & Technology, 48*, 331–339. https://doi.org/10.1021/es403873r

Zhao, W., Yang, L., He, L., & Zhang, S. (2016). Simultaneous enrichment of polycyclic aromatic hydrocarbons and Cu^{2+} in water using tetraazacalix[2]arene[2]triazine as a solid-phase extraction selector. *Journal of Agricultural and Food Chemistry, 64*, 6233–6239. https://doi.org/10.1021/acs.jafc.6b03083

Zimmerman, S. C., Wendland, M. S., Rakow, N. A., Zharov, I., & Suslick, K. S. (2002). Synthetic hosts by monomolecular imprinting inside dendrimers. *Nature, 418*, 399–403. https://doi.org/10.1038/nature00877

Paper 2. Environmental fate, ecotoxicity and possible remediation strategies for antiretroviral drug contaminations

---

This chapter presents an Africa perspective on the occurrence, distribution, method of analysis, and potential mitigation techniques for antiretroviral drugs (ARVDs) present in aqueous systems. This comprehensive review presents the reported concentrations of antiretroviral drugs (ARVDs) in aquatic systems and toxicity thereof from an African perspective. Moreover, insight into the adsorption of ARVDs using carbon-based adsorbents as a potential remediation strategy was evaluated, as well as analytical techniques for the determination of ARVDs in different environmental compartments were briefly presented. This chapter is presented in the corrected proof format of Environmental Toxicology and Chemistry, as it is part of a special issue that will be published at a later date.

Article

Adedapo O. Adeola, Patricia B. C. Forbes (2021). Antiretroviral drugs in African surface waters: prevalence, analysis and potential remediation, Environmental Toxicology and Chemistry. https://doi.org/10.1002/etc.5127

Antiretroviral drugs in African surface waters: prevalence, analysis and potential remediation

Adedapo O. Adeola [a] and Patricia B.C. Forbes [a*]

[a]*Department of Chemistry, Faculty of Natural and Agricultural Sciences, University of Pretoria, Lynnwood Road, Hatfield, Pretoria 0002, South Africa.*

Corresponding author email address: patricia.forbes@up.ac.za

Graphical abstract

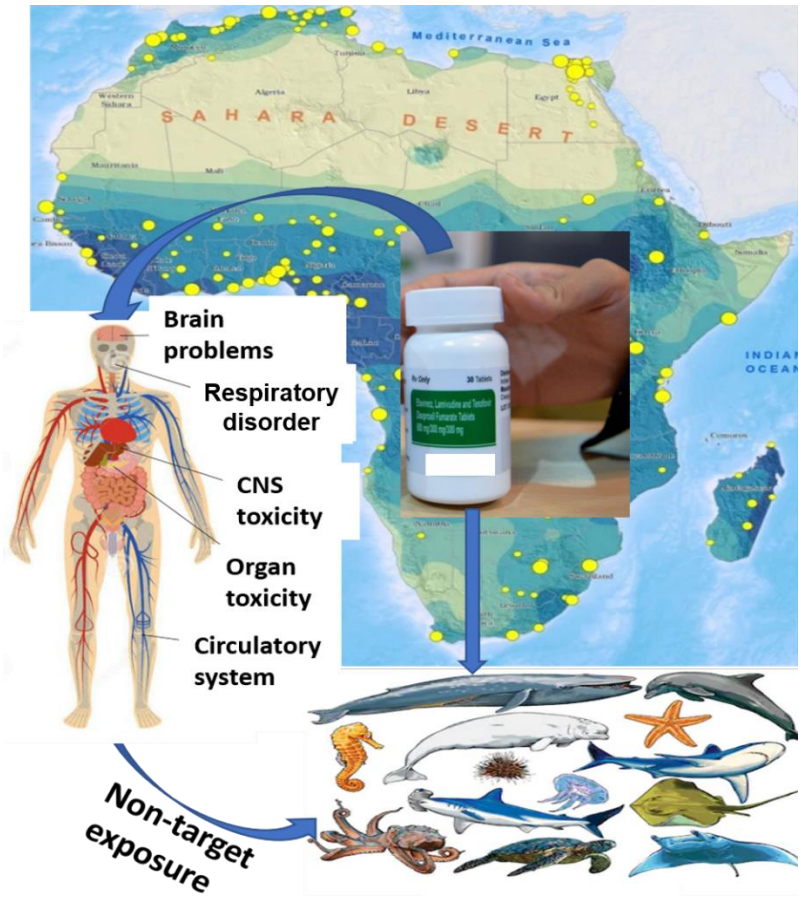

Distribution and ecotoxicity of antiretroviral drug contamination in the African environment.

Highlights

- Relatively high usage of ARVDs in Africa has the potential to lead to water contamination.
- Efavirenz and nevirapine have been detected in wastewater treatment plant effluents and surface water in Africa.
- ARVD concentrations of up to 34,000 ng L^{-1} have been found in WWTP effluents in South Africa.
- LC-MS/MS and GC-TOFMS are efficient methods for analysis of ARVDs in surface waters.
- Carbon-based adsorbents offer a possible means to remediate ARVD contaminated water.

Environmental Toxicology and Chemistry—Volume 00, Number 00—pp. 1–16, 2021
Received: 25 February 2021 | Revised: 24 April 2021 | Accepted: 18 May 2021

Critical Review

Antiretroviral Drugs in African Surface Waters: Prevalence, Analysis, and Potential Remediation

Adedapo O. Adeola and Patricia B.C. Forbes*

Department of Chemistry, Faculty of Natural and Agricultural Sciences, University of Pretoria, Hatfield, Pretoria, South Africa

Abstract: The sources, ecotoxicological impact, and potential remediation strategies of antiretroviral drugs (ARVDs) as emerging contaminants in surface waters are reviewed based on recent literature. The occurrence of ARVDs in water bodies raises concern because many communities in Africa depend on rivers for water resources. Southern Africa is a potential hotspot regarding ARVD contamination due to relatively high therapeutic application and detection thereof in water bodies. Efavirenz and nevirapine are the most persistent in effluents and are prevalent in surface water based on environmental concentrations. Whereas the highest concentration of efavirenz reported in Kenya was 12.4 $\mu g\ L^{-1}$, concentrations as high as 119 and 140 $\mu g\ L^{-1}$ have been reported in Zambia and South Africa, respectively. Concentrations of ARVDs ranging from 670 to 34 000 $ng\ L^{-1}$ (influents) and 540 to 34 000 $ng\ L^{-1}$ (effluents) were determined in wastewater treatment plants in South Africa, compared with Europe, where reported concentrations range from less than limit of detection (LOD) to 32 $ng\ L^{-1}$ (influents) and less than LOD to 22 $ng\ L^{-1}$ (effluents). The present African-based review suggests the need for comprehensive toxicological and risk assessment of these emerging pollutants in Africa, with the intent of averting environmental hazards and the development of sustainable remediation strategies. *Environ Toxicol Chem* 2021;00:1–16. © 2021 SETAC

Keywords: Antiretroviral drugs; Africa; Emerging chemical pollutants; Remediation; Wastewater treatment; Water pollution

INTRODUCTION

Human immunodeficiency virus/autoimmune deficiency (HIV/AIDS) has caused >15 million deaths in Africa, according to the report of the Joint United Nations Programme on HIV/AIDS (2020), and the viral infection has raised major public health concerns and attracted global attention. Africa holds >15% of the world's population, and reports indicate that two-thirds of the global population living with HIV/AIDS are residents of Sub-Saharan Africa (Buvé et al. 2002; World Health Organization 2019). There are countries with very successful antiretroviral therapy programs, in terms of the percentage of infected people on antiretroviral treatment, for example, Australia (90%), Sweden and Botswana (both 83%), Rwanda, Italy, Cambodia, and Switzerland (80% each; Joint United Nations Programme on HIV/AIDS 2020). Other countries with ≥70% of its infected population on antiretroviral treatment programs as of 2019 were Swaziland (79%), France (78%), Spain and Ireland (77%), Algeria (76%), Zimbabwe (75%), and South Africa (70%; World Health Organization 2019; Joint United Nations Programme on HIV/AIDS 2020). In South Africa, 62% of approximately 7.7 million people living with HIV had commenced antiretroviral treatment therapy as of 2018 (Joint United Nations Programme on HIV/AIDS 2020). Swaziland (now Eswatini) has had the highest HIV/AIDS prevalence and reports the most successful antiretroviral treatment program (Joint United Nations Programme on HIV/AIDS 2020). The countries in Africa with the highest number of people living with HIV and on HIV-antiretroviral treatment are shown in Figures 1 and 2. However, most countries provide treatment programs to individuals with an inadequate immune system, which is currently measured as a CD4 count of ≤350/cells mm^{-3} in adults, and thus these statistics may not present the full picture of the number of HIV/AIDS patients in those countries (Van Damme et al. 2006; World Health Organization 2019). Based on this information, there have been enormous governmental and nongovernmental efforts toward implementing a wider coverage of antiretroviral treatment programs (Table 1).

Antiretroviral drugs (ARVDs) are therapeutic agents for the treatment of retroviral infections such as HIV-1, also popularly called the HIV disease. The HIV-1 virus infects the CD4 T cells responsible for the body's immunity. Antiretroviral treatment against HIV-1 does not eliminate the virus but rather prevents its rapid replication (Ncube et al. 2018). The ARVDs as well as

* Address correspondence to patricia.forbes@up.ac.za
Published online 25 May 2021 in Wiley Online Library (wileyonlinelibrary.com).
DOI: 10.1002/etc.5127

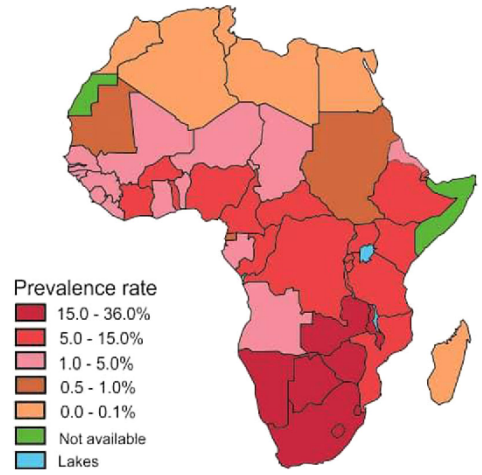

FIGURE 1: Countries in Africa with a fast-growing number of people on antiretroviral drug treatment (Dwyer-Lindgren et al. 2019; Joint United Nations Programme on HIV/AIDS 2020).

other pharmaceuticals are emerging contaminants that are ultimately discharged into water bodies. Approximately 90% of orally administered drugs are passed out as fecal waste into sewage systems, either unaltered or in partially metabolized forms (Halling-Sørensen et al. 1998; Tambosi et al. 2010). Unused drugs and expired drugs are often disposed of indiscriminately and therefore get into drainage systems and ultimately reach waterbodies (Abafe et al. 2018). Potential hotspot reservoirs of ARVDs include wastewaters, on-site sanitation systems, leachates from nonengineered landfills, shallow groundwater systems, and surface waters. There are growing environmental concerns about the pollution potential of ARVDs as a result of the increasing number of people on treatment programs (Table 1).

Antiviral drugs are classified into 2 broad groups, namely, ARVDs, and non-ARVDs (Tyring 2004). Antiretroviral drugs are used to treat retroviruses, which are different from other viruses based on the mode of replication within their host, which involves RNA genetic materials and not DNA materials like other viruses. Over half of the antiviral drugs are antiretroviral, and ARVDs are further classified based on their mode of action, such as nucleoside reverse transcriptase inhibitors (NRTIs), non-nucleoside reverse transcriptase inhibitors (NNRTIs), protease inhibitors, fusion inhibitors, postattachment inhibitors, integrase inhibitors, pharmacokinetic enhancers, and so on. The US Food and Drug Administration has approved >20 ARVDs, and many more are in clinical trials (Swati et al. 2011; Jain et al. 2013; Chahal et al. 2017). Non-ARVDs used for the treatment of virus infections include nucleoside analogs like acyclovir, famciclovir, ganciclovir, valacyclovir, penciclovir, ribavirin, and valganciclovir (Tyring 2004). Other ARVDs widely used in HIV treatment therapy in Africa include nevirapine and efavirenz; their structures are shown in Figure 3.

Emerging chemical pollutants are substances that are yet to be classified as priority pollutants, and thus they are not routinely monitored (Geissen et al. 2015). However, due to their toxicity, persistence, and/or detection in various environmental compartments, they are chemical pollutants of emerging concern and will potentially attract future legislation against illicit or indiscriminate disposal. The ARVDs fall into this category, and although the risk assessment with respect to adverse effects and permissible level/threshold of nontarget exposure to these compounds have not been fully defined, there is growing scientific, public, and regulatory concern because these chemicals have been detected in surface water (Al-Rajab et al. 2010). The environmental hazard of a substance is described by its persistence, bioaccumulation in an organism's tissue, and toxicity. Therefore, before risk assessment of ARVDs

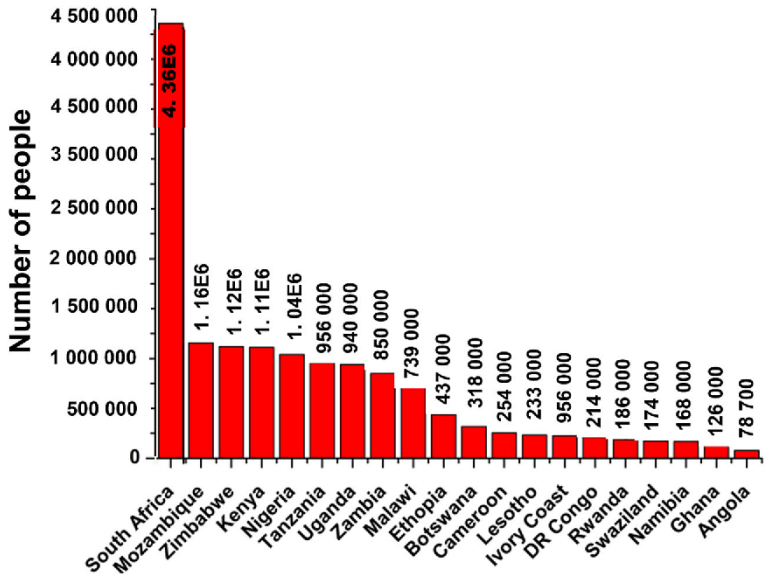

FIGURE 2: Top 20 countries in Africa with the highest number of people on HIV antiretroviral treatment therapy (World Health Organization 2019).

TABLE 1: Antiretroviral therapy coverage and data for the Southern African Development Community[a]

S/N	Country	Estimated antiretroviral therapy coverage (%)	Estimated no. of people receiving antiretroviral therapy	Estimated no. of people living with HIV
1.	Angola	23–33	93 310	290 000–410 000
2.	Botswana	74–89	313 850	340 000–410 000
3.	Comoros	32–100	77	<100–<500
4.	DR Congo	43–65	277 592	420 000–640 000
5.	Eswatini	88–100	191 782	190 000–220 000
6.	Lesotho	61–70	220 828	320 000–360 000
7.	Madagascar	11–17	5166	32 000–49 000
8.	Malawi	71–84	832 908	960 000–1 100 000
9.	Mauritius	22–29	2837	9700–13 000
10.	Mozambique	48–74	1 338 100	1 800 000–2 800 000
11.	Namibia	79–91	177 174	190 000–220 000
12.	Seychelles	No data	No data	No data
13.	South Africa	64–74	5 231 809	6 900 000–8 000 000
14.	Tanzania	67–81	1 277 012	1 500 000–1 800 000
15.	Zambia	80–92	1 064 321	1 200 000–1 300 000
16.	Zimbabwe	74–97	1 149 191	1 200 000–1 600 000

[a]Data from World Health Organization (2019).

can be carried out, there is a need for toxicological profiling based on these intrinsic properties (Escher et al. 2011; Deblonde and Hartemann 2013).

The overall aim of the present review was 1) to provide an African-based status report on the reported extent of ARVD–related water contamination, as a result of the increase in HIV infection and therapy on the African continent; 2) to explore the possible direct/indirect implications of such drug pollution on aquatic fauna and humans; and 3) to describe methods of analysis and a plausible adsorption mechanism of selected waterborne ARVDs onto carbon-based materials, as a possible remediation approach.

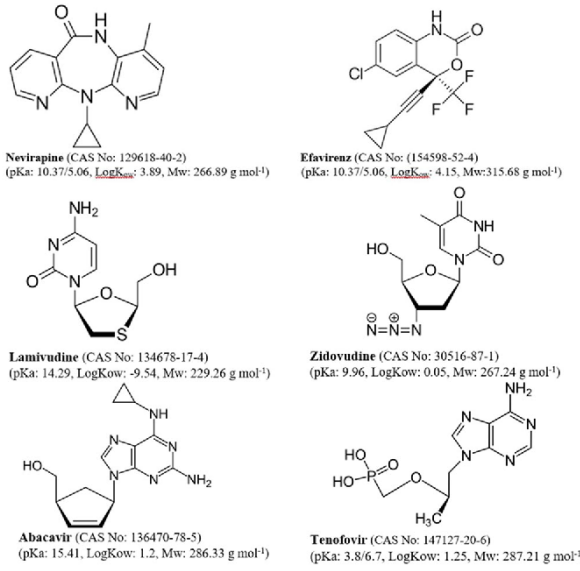

FIGURE 3: Structure of selected antiretroviral drugs with their physicochemical properties (from PubChem 2021). *p*Ka = dissociation constant; log K_{OW} = octanol–water partition coefficient; Mw = molecular weight.

SOURCES AND FATE OF ARVD POLLUTION

The African continent is one the largest consumers of ARVDs, so it is rational to expect potentially higher environmental pollution by ARVDs as a result of poor waste management (Monteiro and Boxall 2010; Ferronato and Torretta 2019; Joint United Nations Programme on HIV/AIDS 2020). Sources of contamination by ARVDs include leaking septic tanks, underground sewage pipes, and runoff after rainfall on landfills (Wooding et al. 2017; Patel et al. 2019). Improper domestic and sewage waste disposal, drug manufacture, hospital waste disposal, and agro-products containing metabolized and untransformed parent compounds are also important sources of ARVD contamination (Fick et al. 2009; Schoeman et al. 2015, 2017; Wood et al. 2016). Aside from ingestion of pharmaceuticals via prescription (or self-medication, which should be discouraged), human exposure to pharmaceuticals also occurs via the food chain, such as drinking contaminated water and eating food sources like crops, vegetables, fish, and dairy products (Ebele et al. 2017). The level of biotransformation that a drug compound undergoes in the body depends on its mechanism of action and physicochemical properties (Bound and Voulvoulis 2005). Some antiviral agents remain unchanged when consumed and are excreted as such (e.g., acyclovir), whereas others undergo extensive biotransformation before excretion from the body (e.g., lamivudine; Galasso et al. 2002; Razonable 2011).

The rate of consumption of ARVDs, based on epidemiological statistics for different countries in Africa, is uncertain, which means that it is difficult to ascertain the amount excreted into the environment. The number of people on ARVD treatment in Africa as of 2016 is presented in Figure 2. In South Africa, >20 tons of the drug combination of efavirenz, lamivudine, and disoproxil fumarate (brand name Symfi, for example) are consumed each day due to the widespread antiretroviral therapy program and HIV status awareness (Abers

et al. 2014; Ncube et al. 2018). Other countries estimated to have consumed >1 ton of HIV antiretroviral medication/d are Kenya, Mozambique, Zimbabwe, Nigeria, and Uganda (Ncube et al. 2018).

The study by Ncube et al. (2018) indicates that >3.9 million people in South Africa are on antiretroviral therapy. Assuming that 3.9 million people are placed on antiretroviral therapy with a daily dose of a combination of ARVDs (mean of 991 mg/d/person, range 590–1996 mg/d/person), as reported by Schoeman et al. (2015), an average total of 1 411 554 kg of ARVD drug compounds are ingested per annum. Antiretroviral drugs such as tipranavir are excreted at 80% and nevirapine at 2.7% via urine; this value varies depending on the type of drug consumed (Schoeman et al. 2017). Assuming a mean of 30% of the drugs are excreted into sewage via urine and feces, then approximately 423 466 kg of ARVDs would reach the water bodies in South Africa each year. The excretion of ARVDs in urine and/or solid waste varies between 2.7 and 94% depending on the nature of the compound, but reports suggest that nevirapine and darunavir have the lowest and highest excretion percentages, respectively (Riska et al. 1999; Vermeir et al. 2009).

Other sources of ARVD contamination include leachate from landfills, effluents from hospitals, inadequate disposal of expired drugs, and waste dumped by research institutions and pharmaceutical companies. Disposal of out-of-date or unwanted medicines, which may occur via the sink/toilet or municipal landfill sites, means they may also eventually leach into groundwater. Prescription practices leading to some unfinished prescriptions contribute to the illicit disposal of unused drugs, thus compounding environmental pollution concerns regarding pharmaceutical products (Bound and Voulvoulis 2005; Orias and Perrodin 2013).

Amid very scarce information on the fate and ecotoxicity of ARVDs, there are reports that tenofovir (a type of ARVD) does not undergo microbial degradation in soils, because no transformation products have been detected, suggesting that ARVDs could be very persistent and stable in soil (Al-Rajab et al. 2010). Another study (Aminot et al. 2018) indicated that hot climatic and aerobic conditions promote the partitioning of ritonavir into solid natural organic matter, resulting in between 5 and 40% adsorption by suspended solids in a river system. The same authors also reported that nevirapine and zidovudine are stable under wastewater treatment plant (WWTP) processes, whereas abacavir, lamivudine, ritonavir, and saquinavir had half-lives of <5 d under biochemical conditions for both wastewater and surface water samples tested (Aminot et al. 2018).

Laboratory-scale studies suggest that ARVDs undergo both photo- and biotransformation in water under environmental conditions, which means that longer holding times for effluents might provide cost-effective treatment solutions in developing countries (Prasse et al. 2010). Slightly >50% of zidovudine and nevirapine were eliminated from urine before application as fertilizer, during a hygienization process at 20 °C for 6 mo (Jaatinen et al. 2016). Chlorination disinfection of wastewater was reported to enhance the persistence of nevirapine and efavirenz due to the deconjugation of their hydroxylated metabolites, and reduction in binding ability of the compounds (K'Oreje et al. 2016; Wood et al. 2016). Unfortunately, none of these studies have been able to attribute the recalcitrance, stability, and persistence of ARVDs to their octanol–water partition coefficient (K_{OW}), logarithmic acid dissociation constant (p*K*a), and/or water solubility.

Although the environmental fate and impact of ARVDs on the environment have not been fully elucidated and understood, it has been established that unintentional and long-term intake of ARVDs from polluted potable water may lead to resistance to the drugs (Ncube et al. 2018; Mtolo et al. 2019). Therefore, there is an urgent need for a comprehensive environmental fate and impact assessment of ARVDs, and extensive monitoring of their concentrations in water bodies such as wastewater and surface water.

ARVD REMOVAL BY CONVENTIONAL WWTPs

Table 2 gives a summary of the levels of 2 major ARVDs in influents and effluents in WWTPs in African countries where studies have been carried out; these levels are compared with what has been reported in other parts of the world. Higher effluent treatment efficiencies were recorded with the advanced wastewater treatment methods adopted by Germany and Belgium, than with the conventional wastewater treatment procedures used in South Africa and Kenya. In addition, nevirapine and efavirenz were present at higher concentrations in influents studied in South Africa, requiring removal and suggesting the high rate of therapeutic application of these ARVDs (Abafe et al. 2018; Moslah et al. 2018). Table 2 also suggests that nevirapine is more recalcitrant to WWTP treatment methods than efavirenz when the influent–effluent ratios are considered. This can be attributed to the difference in physicochemical properties of the drug compounds.

The concentrations of efavirenz and nevirapine in treatment plants in eThekwini Municipality in KwaZulu-Natal, South Africa, ranged from 2100 to 34 000 ng L^{-1} (influent) and 1900 to 34 000 ng L^{-1} (effluent) in a decentralized wastewater treatment facility; from 670 to 24 000 ng L^{-1} (influent) and 540 to 33 000 ng L^{-1} (effluent) in Northern WWTP; and from 2800 to 34 000 ng L^{-1} (influent) and 1400 to 20 000 ng L^{-1} (effluent) in Phoenix WWTP (Abafe et al. 2018). The treatment plants recorded almost 90% removal efficiency for abacavir, lamivudine, and zidovudine from the effluents, but atazanavir, efavirenz, lopinavir, and nevirapine persisted in the effluents (Abafe et al. 2018, Madikizela et al. 2020); thus there is a need to study the ecotoxicological impact of the discharge of the persistent ARVDs into surface water.

Figure 4 shows a significant difference in the removal efficiency of WWTPs from one antiretroviral compound to another, even within the same treatment plant and under similar conditions (Mascolo et al. 2010; Prasse et al. 2010; Ngumba et al. 2016a, 2016b; Abafe et al. 2018). This can be attributed to the difference in physicochemical characteristics and behavior of

TABLE 2: Levels of nevirapine and efavirenz reported in influents and effluents of wastewater treatment plants situated in some African countries compared with Europe

ARVD	Name of WWTP	Country	Concentration in influents (ng L^{-1})	Concentration in effluents (ng L^{-1})	Reference
Nevirapine	Jyväskylä	Finland	13–19	8–10	Ngumba et al. 2016a
	Cantinolle	France	—	<LOD–7.7	Aminot et al. 2015
	Ruhr	Germany	32	22	Prasse et al. 2010
	Decentralized	South Africa	2100	1900	Abafe et al. 2018
	Phoenix	South Africa	2800	1400	Abafe et al. 2018
	Northern	South Africa	670	540	Abafe et al. 2018
	Dandora	Kenya	850	1030	K'Oreje et al. 2016
	Nyalenda	Kenya	3300	2110	K'Oreje et al. 2016
	Kisat	Kenya	2080	2030	K'Oreje et al. 2016
Efavirenz	Gauteng	South Africa	17 400	7100	Schoeman 2015
	Decentralized	South Africa	34 000	34 000	Abafe et al. 2018
	Phoenix	South Africa	34 000	20 000	Abafe et al. 2018
	Northern	South Africa	24 000	33 000	Abafe et al. 2018
	Dandora	Kenya	780	110	K'Oreje et al. 2016
	Nyalenda	Kenya	460	100	K'Oreje et al. 2016
	Kisat	Kenya	1020	110	K'Oreje et al. 2016

WWTP = wastewater treatment plant; ARVD = antiretroviral drug; LOD = limit of detection.

the ARVDs, which makes them both recalcitrant and persistent to varying extents. Abafe et al. (2018) reported that conventional treatment plants in the study areas in South Africa and Kenya proved efficient for the removal of zidovudine, with a removal efficiency ≥99%, However, there are poorer results with the other types of ARVDs, which may lead to bioconcentration, bioaccumulation, and pollution of water bodies with adverse effects on living organisms.

Inefficient removal of ARVDs during the treatment of wastewater released from domestic and municipal sources is one of the major reasons why this class of organic micropollutants is detected in surface and drinking water. Treatment conditions play important roles in the efficiency of conventional WWTPs and membrane bioreactor treatment plants. Some of the factors affecting the optimum performance of treatment plants include sludge retention time, biomass/pollutant concentration, temperature, solution pH, and p*K*a of micropollutants, as well as membrane fouling (Cirja et al. 2008; Adeola and Forbes 2021a).

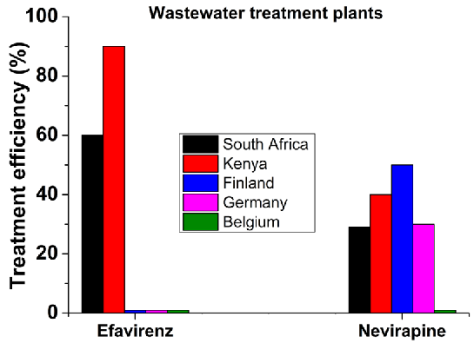

FIGURE 4: Antiretroviral drug removal efficiency of wastewater treatment plants (Mascolo et al. 2010; Prasse et al. 2010; Ngumba et al. 2016a, 2016b; Abafe et al. 2018).

DETECTION AND QUANTITATIVE ANALYSIS OF ARVDS

The indiscriminate discharge of ARVDs into the environment could have catastrophic effects on the biota of aquatic ecosystems (Mascolo et al. 2010). Some pharmaceuticals are nonbiodegradable and recalcitrant to environmental transformation processes (Daouk et al. 2015). Due to the possible bioaccumulation of metabolites or transformation products and parent compounds, the concentrations of these micropollutants in water bodies may increase over time. Thus, analytical methodologies have been developed for detecting and quantifying antiretroviral compounds at low levels in water bodies (in the ppb to ppt range; Mompelat et al. 2009).

Liquid chromatography coupled with tandem mass spectrometry (LC–MS/MS) has been reported for the detection of 13 ARVDs (Abafe et al. 2018). That study was carried out on samples collected from 3 WWTPs in the eThekwini Municipality in KwaZulu-Natal. The method was validated, and the detection limits fell within a range of 2 to 20 ng L^{-1}. The recovery of ARVDs was >50%, with acceptable relative standard deviations. Lamivudine, a dideoxynucleoside reverse transcriptase inhibitor, potent for the treatment of HIV, was also analyzed by LC–MS, and the fragmentation pattern of the drug was elucidated by carrying out MS^n (up to MS^3) and MS/time-of-flight (TOF) studies in positive electrospray ionization (+ve ESI) mode (Bedse et al. 2009).

The 2-stage method involved concentration and clean-up by solid-phase extraction followed by identification and quantification by LC–ESI–MS/MS. The use of matrix-matched calibration curves constructed by spiking surface water was evaluated and compared with the internal standard method using isotopically labeled compounds (Ngumba et al. 2016b; Mosekiemang et al. 2019). It was revealed that the use of stable isotopically labeled standards provided a more accurate quantification of ARVDs and offered an easy solution to ionization problems. The slope obtained from responses

generated by the mass spectrometer, for the internal standard versus analyte concentration does not depend on matrix composition, thus eliminating the need for matrix-matching and yielding more accurate results (Hewavitharana 2011; Ngumba et al. 2016b).

Ultra-high-pressure liquid chromatography-tandem mass spectrometry (UHPLC–MS/MS) is a relatively new method that has been used in South Africa for the quantification of 12 antiretroviral compounds in surface water employing the standard addition method. Water samples were concentrated by a generic automated solid-phase extraction method and analyzed by UHPLC–MS/MS. The concentration of ARVDs reported ranged between 26.5 and 430 ng L^{-1} (Wood et al. 2015). Matrix interference/effects were a challenge during sample analysis, and an average limit of detection of 90.4 ng L^{-1} was reported.

A combination of comprehensive gas chromatography (GCxGC–TOFMS) and UHPLC–quadrupole (Q)TOF–MS/MS) for the determination of ARVDs by multiresidue analysis of surface water in South Africa has been reported (Schoeman et al. 2015; Wooding et al. 2017). An in-house developed polydimethylsiloxane sampler was used, and samples were analyzed with the aid of direct thermal desorption into the inlet of a GCxGC–TOFMS device. The large volume injection method was used during the UHPLC–MS/MS analysis for determination of ARVDs in surface water at ultratrace levels (Wooding et al. 2017).

A comparison between GC–TOFMS and quadrupole GC–MS using drug standards was carried out, which showed lower limits of detection (LODs) with GC–TOFMS similar to GC–electron capture detection. Furthermore, GC–TOFMS has the merits of high-quality full-scan mass spectra and high resolution (Aebi et al. 2002; Bergknut et al. 2006). A similar semiquantitative method was used for the determination of efavirenz and nevirapine in primary settling tank sludges from a WWTP using sonication extraction and GC–TOFMS analysis of samples collected in Gauteng, South Africa. Adequate method LODs and limits of quantitation (LOQs) of 3.9 and 12.9 mg kg^{-1}, respectively (for efavirenz). and 3.4 and 11.4 mg kg^{-1}, respectively (for nevirapine), were determined. The results were reproducible with high precision and accuracy. This affirms that the developed method can be adopted for the analysis of ARVDs, and it has proved to be efficient (Schoeman et al. 2017). However, the development of analytical methods that are easy, efficient, and ecofriendly continues to pose challenges, and more research and innovation are required (Forbes 2021).

Generally, the analysis of water for ARVDs involves sampling, transport, storage, preservation, sample preparation, analyte separation from matrix, detection, and quantification. There is a need for quality assurance because the target pollutants are present at trace levels, and therefore replicate analysis and spiking of samples should be performed as well as analysis of internal standards, surrogate standards, and certified reference materials. Most spectrophotometric methods have certain drawbacks such as low sensitivity, high limits of detection, and tedious experimental procedures. On the other hand, techniques based on LC–MS/MS and GC–TOFMS are relatively expensive while having advantages over other methods such as rapid analysis and a higher degree of resolution (Parastar et al. 2013). Thus, most researchers make them the first choice for precise and accurate qualitative and quantitative analysis of pharmaceuticals. Furthermore, scarce resources, lack of equipment, and the high cost of maintenance of analytical instrumentation are major setbacks to the accurate detection and quantification of ARVDs in most countries in Africa.

CONCENTRATIONS OF ARVDS IN AFRICAN SURFACE WATER

The presence of ARVDs has been reported in surface waters (rivers and man-made lakes [dams]), as well as wastewater influents and effluents in Africa (Wood et al. 2015; Ngumba et al. 2016b, 2020; Abafe et al. 2018; Nibamureke et al. 2019). Surface waters around the globe have scarcely been studied for the presence of ARVDs; however, ARVDs have been detected in rivers and lakes in South Africa, Kenya, Zambia, and other parts of the world (Aminot et al. 2015; Funke et al. 2016; K'Oreje et al. 2016; Wooding et al. 2017, Mosekiemang et al. 2019; Madikizela et al. 2020; Ngumba et al. 2020).

The presence of ARVDs has been detected in surface water and wastewater in South Africa (Wooding et al. 2017), which is of concern because many rural dwellers and inhabitants of informal settlements in Africa collect untreated water from rivers and man-made lakes for personal use, due to limited access to treated water. A study was carried out that aimed to monitor the concentrations of nevirapine and efavirenz in the influent and effluent of a WWTP in Gauteng. Treated wastewater, before and after chlorination, was also examined to determine whether the target ARVDs were removed by chlorination (Schoeman et al. 2015; Wood et al. 2015). The concentrations of nevirapine and efavirenz in wastewater influent and surface water were found to be relatively high, within a range of 2100 to 17 400 ng L^{-1} and <LOD to 1480 ng L^{-1}, respectively, with a treatment efficiency of approximately 50%, which accounts for effluent concentrations of nevirapine and efavirenz within the range of 350 to 7 100 ng L^{-1}, respectively (Wood et al. 2015; Schoeman et al. 2017). These values are among the highest recorded in the literature for the analysis of water obtained from WWTPs, and chlorination did not improve the efficiency of the WWTPs beyond the 50% removal efficiency recorded without its inclusion.

The presence of ARVDs in various aqueous systems in Africa, such as raw WWTP effluents, surface water, groundwater, and even drinking water has been investigated (Ternes et al. 2002; Buchberger 2007; Kummerer 2008). Nevirapine (0.3–6.7 ng L^{-1}), efavirenz (0.3–3.5 ng L^{-1}), and didanosine (0.4–3.3 ng L^{-1}) have been detected in drinking water in South Africa (Swanepoel et al. 2015). The most prevalent ARVD detected in South African aquatic environments has been efavirenz with a concentration as high as 140 µg L^{-1} (Durban WWTP influent sample), whereas lower concentrations ranging from 0.002 to 2.45 µg L^{-1} have been detected in surface water

samples (Rimayi et al. 2018; Mtolo et al. 2019; Ngqwala and Muchesa 2020).

A study was carried out to analyze water quality parameters and concentrations of 24 pharmaceutical compounds, which included antibiotic, antiretroviral, analgesic, anti-inflammatory, and psychiatric drugs in 3 WWTPs, 3 rivers, and 3 groundwater wells in Nairobi and Kisumu, Kenya. The spatial distribution of these emerging pollutants in water bodies was reported (K'Oreje et al. 2016; Ngumba et al. 2016a). Lamivudine (300–167 100 ng L^{-1}), zidovudine (40–17 410 ng L^{-1}), efavirenz (20–560 ng L^{-1}), and nevirapine (330–5620 ng L^{-1}) were detected in 14 river samples collected in Nairobi and Kisumu. It was discovered that shallow wells with proximity to latrines contained the recalcitrant antiretroviral, nevirapine at concentrations as high as 1000 to 2000 ng L^{-1}, which may likely be due to underground seepage and groundwater movement; unfortunately, this untreated well serves as a drinking water source. Similarly, a high concentration range of nevirapine (1.1–228 μg L^{-1}) was detected in grab samples from a river in Machakos Town, Kenya, and ARVDs were more prevalent than antibiotics (Kairigo et al. 2020).

In Zambia, high concentrations of ARVDs were reported in surface water in the peri-urban area of Chunga in Lusaka (Ngumba et al. 2020). The ARVD concentrations ranged from <LOQ to 49 700 ng L^{-1} in surface water, and from 680 to 118,970 ng L^{-1} and 1720 to 55 760 ng L^{-1} in WWTP influent and effluent, respectively. The concentration of lamivudine (10 010 μg L^{-1}) in source-separated urine was higher than values recorded in wastewater in the Zambian study area. Similarly, nevirapine, ritonavir, emtricitabine, atazanavir, and darunavir were detected in the range of <1 to 920 μg L^{-1} in urine collection tanks at the University of KwaZulu-Natal (Bischel et al. 2015). Elevated concentrations detected in human urine suggest the need for precautionary measures in the application of urine as fertilizer. Furthermore, there is a need for treatment of urine before disposal, due to the high concentration of excreted ARVDs, to minimize potential environmental pollution (Udert et al. 2016).

The Orange River is the longest river in South Africa and the seventh longest river in Africa, stretching through South Africa, Botswana, Lesotho, and Namibia. The Orange River forms the southwestern boundary of the Free State Province of South Africa. It flows into the Gariep Dam (the largest in the country) and the Vanderkloof Dam (Figure 5). The Orange River meets with its main tributary, the Vaal River, and then flows further to the southern part of Northern Cape Province to meet with Namibia. The Orange River is highly susceptible to pollution by ARVDs, and varying concentrations of these toxic pharmaceuticals have been reported in the river (Madikizela et al. 2017). Several industrial, agricultural, and domestic activities are carried out along the river channels, which makes them vulnerable to pollution (Earle et al. 2005; Ramollo 2011; Wood et al. 2015). Figure 5 shows that the Gauteng Province is a major hotspot in South Africa, with most of the sampling and detection of ARVDs being found in and around Gauteng Province (Wood et al. 2015; Wooding et al. 2017), which may be attributed to the population density of the province.

A survey carried out by Wood et al. (2015) revealed that nevirapine, lopinavir, and zidovudine were frequently found throughout the selected rivers, man-made lakes, and WWTPs that were sampled. The drugs were present in the ppb (ng L^{-1}) range, with stavudine, nevirapine, and zidovudine having relatively higher concentrations. The Roodeplaat Dam system was included in the sampling because 2 WWTPs discharge effluents into the man-made lakes (the Zeekogat and Baviaanspoort WWTPs). Varying concentrations of pollutants were found in water samples of the 2 WWTPs. Samples from the Vaal River, the Orange River, and the confluence of these (taken within 100 m of each other), differed significantly (Figure 5), which highlights the need for comprehensive monitoring programs.

The Roodeplaat system study (Wood et al. 2015) revealed that ARVD concentrations were lower at the outflow point than at any other sampling point within the man-made lake. Points of higher concentration reported within the dam were possibly due to the depth and homogenization of the water in the area. The monitoring of this man-made lake was prioritized because it is used for recreation (fishing and water sport) and serves as a source of potable water (Wood et al. 2015). Nevirapine was above the LOD in all the surface water samples but could only be quantified at 9 of the 24 sampling locations. In influent samples collected in Kenya, the most frequently detected ARVDs were efavirenz, lamivudine, and nevirapine (K'Oreje et al. 2016; Mtolo et al. 2019, Kairigo et al. 2020), whereas efavirenz is typically most prominent in South Africa. There is vast variation in the concentration reported in the literature. However, whereas the highest concentration of efavirenz in WWTP influents reported in Kenya was 12.4 μg L^{-1}, concentrations as high as 119 and 140 μg L^{-1} have been reported in Zambia and South Africa, respectively (Madikizela et al. 2020). The concentration of efavirenz detected in surface water is highest in Kenya (228 μg L^{-1}) and lower in South Africa (2.45 μg L^{-1}; Mtolo et al. 2019, Kairigo et al. 2020), possibly as a result of differences in waste management and WWTP efficiencies. The prevalence of this compound can be attributed to both its dominant therapeutic application and its persistence in the environment (Rimayi et al. 2018).

POTENTIAL EFFECTS ON HUMANS AND AQUATIC SPECIES

The therapeutic dose of efavirenz is 600 mg (once daily) and that of nevirapine is 200 mg (once daily for 14 d, followed by 200 mg twice daily) in adolescents and adults (Rosenbach et al. 2002). This regime was able to reduce the viral load to below the LOD after 48 wk, with 73% of 40 subjects displaying mild central nervous system effects, 33% diarrhea, and 10% rashes (Molina et al. 2000). The once-daily treatment regime for the management of HIV infection was adopted for convenience, improved adherence, and sustained virologic response. The potential for excretion of unmetabolized drugs into nontarget environments becomes worrisome given the daily dose and consistent usage for several weeks (Schoeman et al. 2015, 2017).

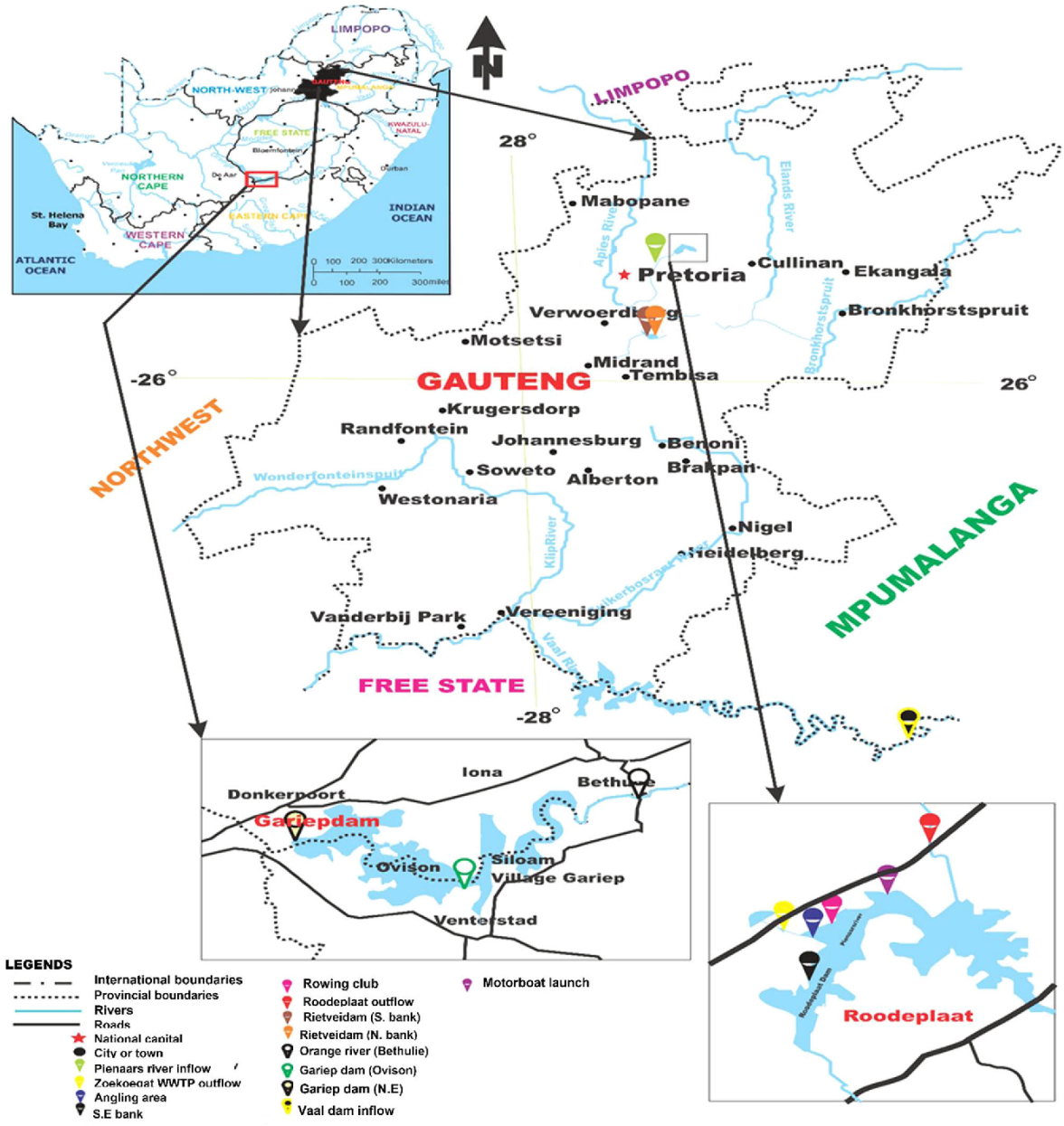

FIGURE 5: Location map of South Africa showing provinces and water bodies where antiretroviral drugs have been detected (Wood et al. 2015; Wooding et al. 2017). WWTP = wastewater treatment plant.

Antiretroviral drugs may cause adverse effects on the central and peripheral nervous systems (Abers et al. 2014). The rate and extent of neuropsychiatric adverse effects varies with different classes of ARVDs and among each drug in their class. Neurotoxicity induced by NRTI occurs due to the inhibition of mitochondrial DNA polymerase. This mechanism of action is also the reason for the mitochondrial myopathy and lactic acidosis that occurs with the use of zidovudine (Anderson and Rower 2010). Zidovudine and abacavir often cause central nervous system disturbances, such as mania and psychosis (Calmy et al. 2009). Efavirenz, which is an NNRTI, is predominantly associated with antiretroviral-related central nervous system toxicity, leading to insomnia, irritability, and vivid dreams (Abers et al. 2014). Three cases of renal toxicity (nephrotoxicity) have been reported in a study carried out in Paris, France (Legendre et al. 2003). The kidney problem was associated with the use of the antiretroviral agent tenofovir. Renal failure, proximal tubular dysfunction, and nephrogenic diabetes insipidus were diagnosed in one of the patients, and a diagnostic test called renal biopsy revealed chronic tubular necrosis with changes in the cells (nuclear changes) in the other 2 patients. Patients placed on tenofovir therapy should be

closely monitored for symptoms of tubulopathy (glycosuria, acidosis, mild increase in plasma creatinine level, and proteinuria). A similar case of nephrotoxicity in a patient was reported with characteristic signs and symptoms of acute renal failure, Fanconi syndrome, and diabetes insipidus as a result of HIV-antiretroviral treatment using tenofovir (Verhelst et al. 2002).

Toxic epidermal necrolysis, or Lyell's syndrome, is a rare idiosyncratic life-threatening side effect of nevirapine administered to infants diagnosed with HIV infection (Tchetnya et al. 2018). Toxic epidermal necrolysis is characterized by severe cutaneous adverse reaction characterized by extensive detachment of the epidermis and mucous membranes, which could potentially lead to blindness in children (Thammakumpee and Yongsiri 2013). However, the World Health Organization recommends efavirenz and nevirapine as highly active antiretroviral therapy (HAART) for low-income countries due to their low cost, efficacy, and easy accessibility (Tchetnya et al. 2018). Studies carried out in Cameroon, Malawi, and Thailand revealed that the earliest symptoms of toxic epidermal necrolysis developed after 8 d and potentially within the first 6 wk of the HAART regime using nevirapine (100 mg once daily for 2 wk and twice daily afterward for 2 wk, with cotrimoxazole antibiotics as prophylaxis against opportunistic infections; Manosuthi et al. 2006; Kiertiburanakul et al. 2009; Joseph et al. 2012). However, efavirenz has been reported to have a relatively lower risk (8–25%) of causing acute and chronic dermatological problems (Tchetnya et al. 2018).

Furthermore, nevirapine, a first-line ARVD, has been associated with chronic liver toxicity in humans after 200 mg was administered once daily for 14 d, followed by 200 mg twice daily (Gozalo et al. 2011). Adverse human health effects caused by ARVD exposures include cough, dizziness, fever, diarrhea, nausea, headache, rash, hepatotoxicity, hypersensitivity, psychosis, insomnia, fatigue, vivid dreams, idiosyncratic myalgia, dyslipidemia, pancreatitis, lactic acidosis, hepatic steatosis, and heart disease (Calmy et al. 2009; Hawkins 2010; Ncube et al. 2018). However, these adverse effects will only occur after exposure to elevated concentrations, drug abuse, overdose, and/or bioaccumulation of ARVDs over a long period and may not be relevant to exposure to low levels in the environment.

Degradation products of nevirapine cause skin rash and liver toxicity and there are growing concerns regarding exposure of nontarget aquatic organisms such as fish to highly specialized compounds such as ARVDs (Kolpin et al. 2002, Nibamureke et al. 2019). Research has shown that a concentration (1480 ng L^{-1}) of nevirapine detected in South African waters did not have significant detrimental effects on *Oreochromis mossambicus* (Mozambique tilapia fish) juvenile growth in terms of length and body mass initially, but a reduction in growth rate after 1 to 2 mo of exposure was observed (Nibamureke et al. 2019).

Antiviral drugs are believed to be one of the most hazardous therapeutic classes due to their toxicological profile with respect to daphnids, fish, and algae, with a maximum effective concentration (EC50) value of 57 mg L^{-1} but are regarded as less toxic to organisms such as crustaceans and diatoms, with EC50 values >100 mg L^{-1} (Sanderson et al. 2004; Minguez et al. 2016). Several antiviral drugs (efavirenz, nevirapine, etc.) and their metabolites (such as 8,14-dihydroxy efavirenz and 12-hydroxy-nevirapine) are nonbiodegradable, leading to their persistence in the environment (Accinelli et al. 2010; Mosekiemang et al. 2019; Madikizela et al. 2020). In this regard, there is a need for proactive advancement of existing sewage treatment plants and wastewater treatment facilities for optimal removal efficiencies.

Madikizela et al. (2017) have shown that current remediation or wastewater treatment methods only partially remove pharmaceutical pollutants from water, including ARVDs. Therefore, it is rational to expect that Africa, as the largest consumer of HIV ARVDs worldwide, would have more antiretroviral waste discharged into surface water. Careful consideration of the water cycle suggests that indiscriminate discharge of pollutants into water bodies or the environment inevitably puts humans at risk, either indirectly through the food chain, or directly through the drinking of untreated water. The lack of ARVD monitoring in drinking water, coupled with overdependence on untreated drinking water by rural dwellers, increases vulnerability and health risks in Africa and other developing countries of the world (Ngumba et al. 2016a; Gwenzi and Chaukura 2018).

Adaramoye et al. (2012) published a study on the ecotoxicity of nevirapine (Viramune®) on specific organs of Wistar rats (liver, kidney, and testis). The rats were exposed to 18 and 36 mg kg^{-1} nevirapine according to body weight. There was no significant ($p > 0.05$) change in body weight or organs of interest for the 18 mg kg^{-1} exposure, nor were there clinical signs of toxicity. However, the higher dose (36 mg kg^{-1}) significantly ($p < 0.05$) increased the weight of the liver, serum total bilirubin level, and activities of γ-glutamyl transferase, alanine, and aspartate aminotransferases. A dose-dependent elevation of 107, 80, and 163% of malondialdehyde in the liver, kidney, and testis of the rats was recorded, respectively. This led to a decrease in hepatic, renal, and testicular functions. There was a 43% decrease in spermatozoa motility, 32% decline in sperm count, and 94% increase in sperm abnormalities. Histopathological findings revealed seminiferous tubule degeneration in the testis, severe liver necrosis, and elevated oxidative stress in rats exposed to elevated concentrations of nevirapine (Adaramoye et al. 2011).

In a study involving the administration of 1.2 mg of raltegravir and darunavir to adult mice, a mean concentration of approximately 15 000 ng mL^{-1} was found in liver serum and 27 000 ng g^{-1} in tissue after 1 h of administration, and the average concentration in the brain ranged from 150 to 200 ng g^{-1} of brain tissue. At 4 h post administration, the concentration was reduced to 300 ng mL^{-1} in serum and 1200 ng g^{-1} in tissue, with only traces in the brain (Asahchop et al. 2017). That study pointed out the role of exposure duration and variation in drug distribution in the biological host, as well as the fact that neuroinflammatory response was evident in brain tissues even at low concentrations. It will be informative to carry out ARVD toxicological studies on biota with due consideration given to human therapeutic dose and environmental concentrations, to establish a relevant correlation among dose-related response (median inhibitory

concentration [IC50]/EC50), environmental exposure, and biological effects.

PROSPECTS AND POSSIBLE REMEDIATION TECHNOLOGIES

The remediation strategies developed over the years for pharmaceuticals, personal care products, and other organic contaminants in aqueous systems include chemical precipitation, ion exchange, membrane filtration, coagulation, photocatalytic degradation, and adsorption (Ahluwalia and Goyal 2007; Demirbas 2008; Fu and Wang 2011; Inyang et al. 2012; Zhang et al. 2014; Wang and Chen 2015; Uddin 2017; Wan et al. 2018).

Although it is acknowledged that mechanisms to prevent contamination of water sources are preferable to end-of-pipe treatment, poor sanitation and infrastructure may consequently lead to ARVD pollution of water. In this case, there are 4 approaches to water remediation: improve the efficiency of existing technology used in the operation of WWTPs, upgrade WWTPs with new remediation tools and technology, control the indiscriminate disposal of micropollutants, and isolate the source (Escher et al. 2011). The focus often includes end-of-pipe measures, such as effluent ozonation, or the application of activated carbon as an advanced tertiary treatment procedure. Ozonoation as a significantly efficient removal has been reported for pharmaceuticals (Hollender et al. 2009; Reungoat et al. 2010). The operational cost involved in the generation of radicals required for the oxidation process raises concerns, especially with the increase in the concentrations of target pollutants and large volumes of polluted water.

Photocatalytic degradation has been used for the breakdown of an ARVD (lamivudine) in water using titanium dioxide (TiO_2) as a catalyst (An et al. 2011). Three process variables, namely, TiO_2 dosage, pH, and lamivudine concentration, were selected to evaluate the efficiency of lamivudine degradation under varying conditions. The results obtained from modeling the surface response indicated that the extent of degradation of lamivudine was highly influenced by the TiO_2 dosage and initial concentration of the ARVDs. The optimum degradation efficiency was achieved at a suitable amount of TiO_2 catalyst and with a minimum concentration of lamivudine. Photocatalysis is an advanced oxidation technology that can be effective for antiretroviral decontamination of water and wastewater and should be explored. However, catalysts often possess limited reusability, due to the loss of catalytic activity with time, as a result of aggregation, fouling, deactivation, or side reactions, which are associated limitations (Sievers et al. 2016; Adeola and Forbes 2021a).

Irradiation by direct sunlight leading to direct and indirect photolysis has been reported for the degradation of ARVDs in water (Zhou et al. 2015). This further supports the fact that photodegradation is an important remediation process for many pollutants in surface waters. Three ARVDs (acyclovir, zidovudine, and lamivudine) were investigated in treated water, freshwater, and seawater under the irradiation from sunlight. The results obtained revealed that zidovudine was easily degraded via direct photolysis, whereas acyclovir and lamivudine were mainly transformed via indirect photolysis. The presence of certain chemical agents such as nitrates, bicarbonates, chloride ions, bromide ions, and dissolved organic matter, naturally occurring or induced, can also influence the rate and extent of transformation via photodegradation (Zhou et al. 2015).

Aerobic biodegradation proved to be efficient for the elimination of acyclovir in wastewater (Peng et al. 2014). Lamivudine can be subjected to forced decomposition by a hydrolytic method (under neutral, acidic, and alkaline conditions), oxidation, photolysis, and thermal stress. The drug is unstable in acid and alkaline conditions but remained stable under neutral pH. It was also degraded extensively in an oxidative environment into several possible degradation products that may be less harmful to the environment; however, this requires further study (Bedse et al. 2009). Another method that can be exploited for the removal of antiretrovirals is an integrated approach involving biodegradation and subsequent ozonolysis, which has proved to be an efficient method for the removal of transformation products of antivirals (carboxy-transformation products; Prasse et al. 2012; Knopp et al. 2016). The formation of carboxy-transformation products via oxidation of the hydroxyl moiety at the 5′ position results in loss of antiviral activity by decreasing the phosphorylation in infected cells. The hypothesis that induced loss of antiretroviral activity of ARVDs could potentially reduce hazards to humans and biota during nontarget exposure is subject to further research. Furthermore, whether there are stable forms of oxidized antiretrovirals is also unknown (Funke et al. 2016). Some antiviral compounds are nonbiodegradable, whereas others are degradable under certain environmental conditions, leading to potentially dangerous metabolites/degradation products. Thus, there is also a need to develop analytical methods that delineate between parent compounds and transformation products with accuracy and precision.

Furthermore, nonpoint source/diffuse source contamination of surface water by ARVDs is among the major contributors to water pollution in Africa. Remedial protocols for surface water pollution can be carried out via in situ water treatment, as already described in this section, or via source control (Anawar and Chowdhury 2020). These methods are categorized into physical, chemical, biological, ecological, and engineering methods (Bai et al. 2020); however, for heavily polluted sites, single methods are often not effective, so the integration of 2 or more methods (integrated systems/hybrid techniques) is required (Adeola and Forbes 2021b). In the physical–engineering approach, aeration is an efficient and widely used technique for enhancing the growth and activity of microbes that could potentially degrade organic pollutants such as ARVDs that are present in wastewater, sewage, and landfills (Capodaglio and Olsson 2019). Similarly, ecological floating beds, wetlands, and biofilm reactors are techniques that adopt microorganism- and plant-based solutions for the remediation of organic chemicals from surface water or diffuse sources of pollution; these can be explored for effects against

ARVD pollution (Anawar and Chowdhury 2020). Other engineering solutions include riverbank filtration, stormwater diversion, hydraulic structures, and dredging, all of which facilitate sedimentation, aeration, sunlight irradiation, and anoxic reactions, but they are very expensive.

A standardized hospital waste management system is vital to environmental safety with regard to the prevalence of ARVDs in surface water in Africa. The need for efficient sorting, collection, packaging, storage, and/or disposal of hospital and municipal waste cannot be overemphasized. Currently, negligence, ineffective collection, and transportation are responsible for poor hospital waste management in Africa (Faure and Rizzo Padoin 2003; Tsakona et al. 2007; Schoeman et al. 2017).

Adsorption of ARVDs using carbon-based adsorbents: A potentially viable water treatment method

The use of carbon-based adsorbents remains the most cost-effective method of remediation of pollutants in environmental matrices (Cao et al. 2009; Hua et al. 2012; Wang et al. 2015; Wan et al. 2015; Inyang et al. 2016; Adeola and Forbes 2021a). In practice, carbon-based adsorbents (including biochar derived from agricultural products/waste and carbonization of wood, graphene-based materials and carbon nanotubes, and granular activated carbon/powdered activated carbon) have been used in the adsorption of several environmental contaminants (Inyang et al. 2014; Ribeiro et al. 2015; Creamer and Gao 2016; Rajapaksha et al. 2016; Fang et al. 2017, 2018; Wang et al. 2017; Zhang et al. 2017; Zou et al. 2019; Adeola and Forbes 2020). Relative to other adsorbents, activated carbon represents a low-cost and environmentally friendly choice (Cai et al. 2019; Zhang et al. 2019). The enhanced adsorption affinity of graphene-based materials for several classes of emerging chemical pollutants has attracted scientific attention (Shen et al. 2015; Pérez-Ramírez et al. 2016; Xiao et al. 2016; Fraga et al. 2019; Adeola and Forbes 2021b), and holds promise for ARVDs.

Generally, organic pollutants such as efavirenz and nevirapine have low water solubility and are nonpolar, so hydrophobic interactions occur during adsorption onto hydrophobic surfaces of the carbon-based adsorbent. Rather than distributing within aqueous systems, ARVDs and other hydrophobic pollutants aggregate, thus creating surface tension and minimal contact with water in the process. Hence the selective adsorption of hydrophobic compounds in an aqueous medium by carbon-based adsorbents is enhanced by partitioning of sorbates and hydrophobic interactions with the sorbent (Adeola and Forbes 2020; Wang et al. 2020). The presence of benzene rings and other reactive functional groups such as –COOH, –OH, $–NH_2$, and so on. in carbon-based adsorbents and composites is important in their chemical modification (Yu et al. 2009, Yang et al. 2019). Possible mechanisms of interaction with ARVDs may include the formation of both covalent and noncovalent binding interactions, as well as hydrogen bonds between the –NH and –N group in nevirapine and efavirenz and carbon-based adsorbents. The aromatic rings of most carbonaceous adsorbents and composites, and the pyridinic/aromatic rings of ARVDs, may also provide a basis for possible hydrophobic interactions/bonding (Figure 6).

Research on the adsorptive removal of ARVDs from surface waters and wastewater under variable environmental conditions (pH, temperature, and salinity) and the role of natural organic matter has not been reported to date. Hence there is an urgent need to investigate the optimum conditions

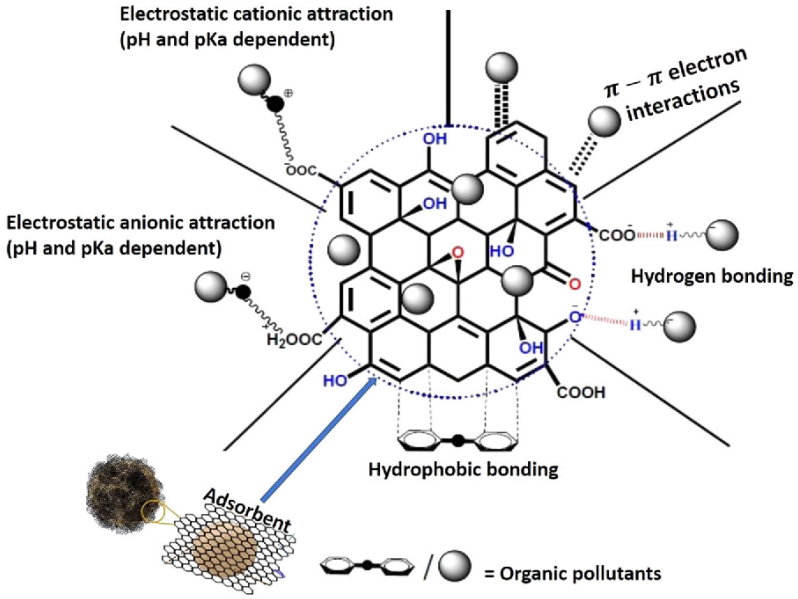

FIGURE 6: Different interactions between carbon-based adsorbents and organic pollutants. (Reproduced from Zhang et al. 2020 with permission from The Royal Society of Chemistry). pKa = dissociation constant.

for the removal of antivirals/ARVDs from wastewater and surface water.

CONCLUSIONS AND RECOMMENDATIONS

The release of ARVDs into the aquatic environment via wastewater, if they are not biodegraded or removed in WWTPs, may lead to environmental pollution and hazards resulting from bioaccumulation and nontarget exposures. Several publications have reported that ARVDs are present in wastewater, rivers, lakes, and in some cases drinking water in Africa. It is important to determine the total bioavailable ARVD compounds in surface water and effluents because this indicates the amount of the compounds that can potentially be taken up by biota in water. Future research should concentrate on the risk assessment of ARVD hotspots; the fate, environmental behavior, and ecotoxicology of ARVDs; and cost-effective interventions to minimize the associated health risks.

Furthermore, we recommend the following considerations going forward.

Pollution potential

Healthcare workers and drug manufacturers need to consider the pollution potential of industrial waste, overprescription, and hospital wastes.

Dose-related responses

Data/information are scarce in terms of relevant ecotoxicological endpoints with respect to human and biota lethal dose/exposure; therefore future studies should consider both the human therapeutic dose and the environmental concentrations, to establish a relevant correlation among dose-related response (IC50/EC50), total bioavailable fraction, environmental exposure, and biological effects.

Setting permissible levels

Africa currently does not have extensive environmental monitoring programs and legislative guidelines for ARVD-related waste management, which implies that there are no maximum permissible levels for the antiretroviral class of compounds in various environmental compartments. Therefore, there is a need for a synergistic effort between international and regional regulatory bodies, in conjunction with experts, to carry out a comprehensive risk assessment of ARVDs in water bodies and to set a permissible level for ARVD concentrations in effluents discharged into water bodies.

Better water treatment methods

There is a need for the development of better and more efficient wastewater, sewage, and drinking water treatment methods in Africa, to minimize the risk of exposure and its consequences. More compact, cost-effective, versatile, and efficient treatment methods such as membrane technology, adsorption, and integrated systems should be given closer attention because they have the advantage of purifying wastewater, without the extensive use of chemicals.

Upgrading of WWTPs

Due to the increasing demand for clean and safe water, there is an urgent need to ensure reusability; thus WWTPs should be well maintained and upgraded to handle the fast-growing environmental and economic demands for clean and safe water, as described by the United Nations Sustainable Development Goals (United Nations 2015).

Research collaboration and adequate funding

In conclusion, the lack of advanced analytical facilities in most African countries and other developing regions of the world will continue to constrain research and monitoring efforts. Therefore, there is a need for public–private partnerships among government agencies, healthcare providers, and pharmaceutical companies, in areas of research funding and development, to ensure that the prevalence of emerging pollutants in water bodies does not destroy our ecosystems.

Acknowledgment—The authors acknowledge the University of Pretoria Commonwealth Doctoral Scholarship (to A. Adeola) and Rand Water for providing research funding.

Author Contributions Statement—A. Adeola: conceptualization, investigation, formal analysis, and writing of original draft; and P. Forbes: formal analysis, writing review and editing, fund acquisition, and supervision.

Data Availability Statement—Data, associated metadata, and calculation tools are available from the corresponding author (patricia.forbes@up.ac.za).

REFERENCES

Abafe OA, Späth J, Fick J, Jansson S, Buckley C, Stark A, Pietruschka B, Martincigh BS. 2018. LC-MS/MS determination of antiretroviral drugs in influents and effluents from wastewater treatment plants in KwaZulu-Natal, South Africa. *Chemosphere* 200:660–670.

Abers MS, Shandera WX, Kass JS. 2014. Neurological and psychiatric adverse effects of antiretroviral drugs. *CNS Drugs* 28:131–145.

Accinelli C, Saccà ML, Batisson I, Fick J, Mencarelli M, Grabic R. 2010. Removal of oseltamivir (Tamiflu) and other selected pharmaceuticals from wastewater using a granular bioplastic formulation entrapping propagules of *Phanerochaete chrysosporium*. *Chemosphere* 81:436–443.

Adaramoye O, Adesanoye O, Adewumi O, Akanni O. 2012. Studies on the toxicological effect of nevirapine, an antiretroviral drug, on the liver, kidney and testis of male Wistar rats. *Hum Exp Toxicol* 31: 676–685.

Adeola AO, Forbes PBC. 2020. Assessment of reusable graphene wool adsorbent for the simultaneous removal of selected 2-6 ringed polycyclic aromatic hydrocarbons from aqueous solution. *Environ Technol*. https://doi.org/10.1080/09593330.2020.1824024

Adeola AO, Forbes PBC. 2021a. Advances in water treatment technologies for removal of polycyclic aromatic hydrocarbons: Existing concepts, emerging trends, and future prospects. *Water Environ Res* 93:1–17.

Adeola AO, Forbes PBC. 2021b. Influence of natural organic matter fractions on PAH sorption by stream sediments and a synthetic graphene wool adsorbent. *Environ Technol Innovat* 21:101202.

Aebi B, Sturny-Jungo R, Bernhard W, Blanke R, Hirsch R. 2002. Quantitation using GC–TOF-MS: Example of bromazepam. *Forensic Sci Int* 128:84–89.

Ahluwalia SS, Goyal D. 2007. Microbial and plant-derived biomass for removal of heavy metals from wastewater. *Bioresour Technol* 98:2243–2257.

Al-Rajab AJ, Sabourin L, Chapman R, Lapen DR, Topp E. 2010. Fate of the antiretroviral drug tenofovir in agricultural soil. *Sci Total Environ* 408:5559–5564.

Aminot Y, Litrico X, Chambolle M, Arnaud C, Pardon P, Budzindki H. 2015. Development and application of a multi-residue method for the determination of 53 pharmaceuticals in water, sediment, and suspended solids using liquid chromatography-tandem mass spectrometry. *Anal Bioanal Chem* 407:8585–8604.

Aminot Y, Fuster L, Pardon P, Le Menach K, Budzinski H. 2018. Suspended solids moderate the degradation and sorption of wastewater-derived pharmaceuticals in estuarine waters. *Sci Total Environ* 612:39–48.

An T, An J, Yang H, Li G, Feng H, Nie X. 2011. Photocatalytic degradation kinetics and mechanism of antivirus drug-lamivudine in TiO_2 dispersion. *J Hazard Mater* 197:229–236.

Anawar H, Chowdhury R. 2020. Remediation of polluted river water by biological, chemical, ecological and engineering processes. *Sustainability* 12:7017.

Anderson PL, Rower JE. 2010. Zidovudine and lamivudine for HIV infection. *Clin Med Rev Ther* 2:a2004.

Asahchop EL, Meziane O, Mamik MK, Chan WF, Branton WG, Resch L, Gill MJ, Haddad E, Guimond JV, Wainberg MA, Baker GB, Cohen EA, Power C. 2017. Reduced antiretroviral drug efficacy and concentration in HIV-infected microglia contributes to viral persistence in brain. *Retrovirology* 14:47.

Bai XY, Zhu XF, Jiang HB, Wang ZQ, He CG, Sheng LX, Zhuang J. 2020. Purification effect of sequential constructed wetland for the polluted water in urban river. *Water* 12:1054.

Bedse G, Kumar V, Singh S. 2009. Study of forced decomposition behavior of lamivudine using LC, LC-MS/TOF and MS^n. *J Pharm Biomed* 49:55–63.

Bergknut M, Frech K, Andersson PL, Haglund P, Tysklind M. 2006. Characterization and classification of complex PAH samples using GC-MS and GC-TOFMS. *Chemosphere* 65:2208–2215.

Bischel HN, Özel Duygan BD, Strande L, McArdell CS, Udert KM, Kohn T. 2015. Pathogens and pharmaceuticals in source-separated urine in eThekwini, South Africa. *Water Res* 85:57–65.

Bound JP, Voulvoulis N. 2005. Household disposal of pharmaceuticals as a pathway for aquatic contamination in the United Kingdom. *Environ Health Perspect* 113:1705–1711.

Buchberger WW. 2007. Novel analytical procedures for screening of drug residues in water, wastewater, sediment and sludge. *Anal Chim Acta* 593:129–139.

Buvé A, Bishikwabo-Nsarhaza K, Mutangadura G. 2002. The spread and effect of HIV-1 infection in sub-Saharan Africa. *Lancet* 359:2011–2017.

Cai Y, Liu L, Tian H, Yang Z, Luo X. 2019. Adsorption and desorption performance and mechanism of tetracycline hydrochloride by activated carbon-based adsorbents derived from sugar cane bagasse activated with $ZnCl_2$. *Molecules* 24:4534.

Calmy A, Hirschel B, Cooper DA, Carr A. 2009. A new era of antiretroviral drug toxicity. *Antivir Ther* 14(16):5–179.

Cao X, Ma L, Gao B, Harris W. 2009. Dairy-manure derived biochar effectively sorbs lead and atrazine. *Environ Sci Technol* 43:3285–3291.

Capodaglio A, Olsson G. 2019. Energy issues in sustainable urban wastewater management: Use, demand reduction and recovery in the urban water cycle. *Sustainability* 12:266.

Chahal HS, Murray JS, Shimer M, Capella P, Presto R, Valdez ML, Lurie PG. 2017. The US Food and Drug Administration's tentative approval process and the global fight against HIV. *J Int AIDS Soc* 20:e25019.

Cirja M, Ivashechkin P, Schäffer A, Corvini PFX. 2008. Factors affecting the removal of organic micropollutants from wastewater in conventional treatment plants (CTP) and membrane bioreactors (MBR). *Rev Environ Sci Biol* 7:61–78.

Creamer AE, Gao B. 2016. Carbon-based adsorbents for post-combustion CO_2 capture: A critical review. *Environ Sci Technol* 50:7276–7289.

Daouk S, Chèvre N, Vernaz N, Bonnabry P, Dayer P, Daali Y, Fleury-Souverain S. 2015. Prioritization methodology for the monitoring of active pharmaceutical ingredients in hospital effluents. *J Environ Manage* 160:324–332.

Deblonde T, Hartemann P. 2013. Environmental impact of medical prescriptions: Assessing the risks and hazards of persistence, bioaccumulation and toxicity of pharmaceuticals. *Public Health* 127:312–317.

Demirbas A. 2008. Heavy metal adsorption onto agro-based waste materials: A review. *J Hazard Mater* 157:220–229.

Dwyer-Lindgren L, Cork MA, Sligar A, Steuben KM, Wilson KF, Provost NR, Mayala BK, VenderHeide JD, Collison ML, Hall JB, Biehl MH, Carter A, Frank T, Douwes-Schultz D, Butsetin R, Casey DC, Deshpanae A, Earl L, Bcheraoui CE, Farag TH, Henry NJ, Kinyoki D, Marczak LB, Nixon MR, Osgood-Zimmerman A, Pigott D, Reiner RC Jr, Ross JM, Schaeffer LE, Smith DL, Weaver ND, Wiens KF. 2019. Mapping HIV prevalence in sub-Saharan Africa between 2000 and 2017. *Nature* 570:189–193.

Earle A, Malzbender D, Turton A, Manzungu E. 2005. A preliminary basin profile of the Orange/Senqu River. African Centre for, Water Research, Johannesburg, South Africa, pp 1–49.

Ebele AJ, Abou-Elwafa Abdallah M, Harrad S. 2017. Pharmaceuticals and personal care products (PPCPs) in the freshwater aquatic environment. *Emerg Contam* 3:1–16.

Escher BI, Baumgartner R, Koller M, Treyer K, Lienert J, McArdell CS. 2011. Environmental toxicology and risk assessment of pharmaceuticals from hospital wastewater. *Water Res* 45:75–92.

Fang J, Gao B, Mosa A, Zhan L. 2017. Chemical activation of hickory and peanut hull hydrochars for removal of lead and methylene blue from aqueous solutions. *Chem Speciat Bioavailab* 29:197–204.

Fang J, Zhan L, Ok YS, Gao B. 2018. Minireview of potential applications of hydrochar derived from hydrothermal carbonization of biomass. *J Ind Eng Chem* 57:15–21.

Faure P, Rizzo Padoin N. 2003. Hôpital et environnement: L'élimination des déchets [Hospital and environment: Waste disposal]. *Ann Pharmaceut Fr* 61:373–377.

Ferronato N, Torretta V. 2019. Waste mismanagement in developing countries: A review of global issues. *Int J Environ Res Public Health* 16:1060.

Fick J, Soderstrom H, Lindberg RH, Phan C, Tysklind M, Larsson JDG. 2009. Contamination of surface, ground, and drinking water from pharmaceutical production. *Environ Toxicol Chem* 28:2522–2527.

Forbes P. 2021. Green sample preparation methods in the environmental monitoring of aquatic organic pollutants. *Curr Opin Green Sustain Chem* 31:100500.

Fraga TJM, Carvalho MN, Ghislandi MG, Sobrinho MA. 2019. Functionalized graphene-based materials as innovative adsorbents of organic pollutants: A concise overview. *Braz J Chem Eng* 36:1–31.

Fu F, Wang Q. 2011. Removal of heavy metal ions from wastewaters: A review. *J Environ Manage* 92:407–418.

Funke J, Prasse C, Ternes TA. 2016. Identification of transformation products of antiviral drugs formed during biological wastewater treatment and their occurrence in the urban water cycle. *Water Res* 98:75–83.

Galasso GJ, Boucher CAB, Cooper DA, Katzenstein DA. 2002. *Practical Guidelines in Antiviral Therapy*, 1st ed. Elsevier, Amsterdam, The Netherlands.

Geissen V, Mol H, Klumpp E, Umlauf G, Nadal M, van der Ploeg M, van de Zee SEATM, Ritsema CJ. 2015. Emerging pollutants in the environment: A challenge for water resource management. *Int Soil Water Conserv Res* 3:57–65.

Gozalo C, Gerard L, Loiseau P, Morand-Joubert L, Peytavin G, Molina JM, Dellamonica P, Becquemont L, Aboulker JP, Launay O, Verstuyft C, Group AS. 2011. Pharmacogenetics of toxicity, plasma trough concentration and treatment outcome with nevirapine-containing regimen in anti-retroviral-naive HIV-infected adults: An exploratory study of the TRIANON ANRS 081 trial. *Basic Clin Pharmacol Toxicol* 109:513–520.

Gwenzi W, Chaukura N. 2018. Organic contaminants in African aquatic systems: Current knowledge, health risks, and future research directions. *Sci Total Environ* 619–620:1493–1514.

Halling-Sørensen B, Nors Nielsen S, Lanzky PF, Ingerslev F, Holten Lützhøft HC, Jørgensen SE. 1998. Occurrence, fate and effects of pharmaceutical substances in the environment—A review. *Chemosphere* 36:357–393.

Hawkins T. 2010. Understanding and managing the adverse effects of antiretroviral therapy. *Antiviral Res* 85:201–209.

Hewavitharana AK. 2011. Matrix matching in liquid chromatography–mass spectrometry with stable isotope labelled internal standards—Is it necessary? *J Chromatogr A* 1218:359–361.

Hollender J, Zimmermann SG, Koepke S, Krauss M, McArdell CS, Ort C, Singer H, von Gunten U, Siegrist H. 2009. Elimination of organic micropollutants in a municipal wastewater treatment plant upgraded with a full-scale post-ozonation followed by sand filtration. *Environ Sci Technol* 43:7862–7869.

Hua M, Zhang S, Pan B, Zhang W, Lv L, Zhang Q. 2012. Heavy metal removal from water/wastewater by nanosized metal oxides: A review. *J Hazard Mater* 211:317–331.

Inyang MI, Gao B, Yao Y, Xue YW, Zimmerman A, Mosa A, Pullammanappallil P, Ok YS, Cao XD. 2016. A review of biochar as a low-cost adsorbent for aqueous heavy metal removal. *Crit Rev Environ Sci Technol* 46:406–433.

Inyang M, Gao B, Yao Y, Xue Y, Zimmerman AR, Pullammanappallil P, Cao X. 2012. Removal of heavy metals from aqueous solution by biochars derived from anaerobically digested biomass. *Bioresour Technol* 110:50–56.

Inyang M, Gao B, Zimmerman A, Zhang M, Chen H. 2014. Synthesis, characterization, and dye sorption ability of carbon nanotube–biochar nanocomposites. *Chem Eng J* 236:39–46.

Jaatinen ST, Palmroth MRT, Rintala JA, Tuhkanen TA. 2016. The effect of urine storage on antiviral and antibiotic compounds in the liquid phase of source-separated urine. *Environ Technol* 37: 2189–2198.

Jain S, Kumar P, Vyas RK, Pandit P, Dalai AK. 2013. Occurrence and removal of antiviral drugs in environment: A review. *Water Air Soil Pollut* 224:1410.

Joint United Nations Programme on HIV/AIDS. 2020. Global HIV & AIDS statistics—2020 fact sheet. Geneva, Switzerland. [cited 2021 April 26]. Available from: https://www.unaids.org/en/resources/fact-sheet

Joseph MN, Laura HS, Lynn FD. 2012. Severe antiretroviral therapy-induced toxic epidermal necrolysis in a child. *Case Rep Dermatol* 4:31–36.

Kairigo P, Ngumba E, Sundberg L-R, Gachanja A, Tuhkanen T. 2020. Contamination of surface water and river sediments by antibiotic and antiretroviral drug cocktails in low and middle-income countries: Occurrence, risk and mitigation strategies. *Water* 12:1376.

Kiertiburanakul S, Malathum K, Watcharananan S. 2009. Predicting factors for unsuccessful switching from nevirapine to efavirenz in HIV-infected patients who developed Nevirapine-associated skin rash. *Int J STD AIDS* 20:176–179.

Knopp G, Prasse C, Ternes TA, Cornel P. 2016. Elimination of micropollutants and transformation products from a wastewater treatment plant effluent through pilot-scale ozonation followed by various activated carbon and biological filters. *Water Res* 100:580–592.

Kolpin DW, Furlong ET, Meyer MT, Thurman EM, Zaugg SD, Barber LB, Buxton HT. 2002. Pharmaceuticals, hormones, and other organic wastewater contaminants in U.S. streams 1999–2000: A national reconnaissance. *Environ Sci Technol* 36:1202–1211.

K'Oreje KO, Vergeynst L, Ombaka D, De Wispelaere P, Okoth M, Van Langenhove H, Demeestere K. 2016. Occurrence patterns of pharmaceutical residues in wastewater, surface water and groundwater of Nairobi and Kisumu city, Kenya. *Chemosphere* 149:238–244.

Kummerer KE. 2008. *Pharmaceuticals in the Environment: Sources, Fate, Effects and Risks*, 3rd ed. SpringerVerlag, Berlin, Germany.

Legendre C, Martinez F, Molina J-M, Karras A, Furco A, Lafaurie M, Droz D, Bourgarit A, Sereni D. 2003. Tenofovir-related nephrotoxicity in human immunodeficiency virus-infected patients: Three cases of renal failure, fanconi syndrome, and nephrogenic diabetes insipidus. *Clin Infect Dis* 36:1070–1073.

Madikizela LM, Tavengwa NT, Chimuka L. 2017. Status of pharmaceuticals in African water bodies: Occurrence, removal and analytical methods. *J Environ Manage* 193:211–220.

Madikizela LM, Ncube S, Chimuka L. 2020. Analysis, occurrence and removal of pharmaceuticals in African water resources: A current status. *J Environ Manage* 253:109741.

Manosuthi W, Thongyen S, Chumpathat N. 2006. Incidence and risk factors of rash associated with efavirenz in HIV-infected patients with preceding nevirapine-associated rash. *HIV Med* 7:378–382.

Mascolo G, Balest L, Cassano D, Laera G, Lopez A, Pollice A, Salerno C. 2010. Biodegradability of pharmaceutical industrial wastewater and formation of recalcitrant organic compounds during aerobic biological treatment. *Bioresour Technol* 101:2585–2591.

Minguez L, Pedelucq J, Farcy E, Ballandonne C, Budzinski H, Halm-Lemeille M-P. 2016. Toxicities of 48 pharmaceuticals and their freshwater and marine environmental assessment in northwestern France. *Environ Sci Pollut Res* 23:4992–5001.

Molina JM, Ferchal F, Rancinan C, Raffi F, Rozenbaum W, Sereni D, Morlat P, Journot V, Decazes JM, Chêne G. 2000. Once-daily combination therapy with emtricitabine, didanosine, and efavirenz in human immunodeficiency virus-infected patients. *J Infect Dis* 182:599–602.

Mompelat S, Le Bot B, Thomas O. 2009. Occurrence and fate of pharmaceutical products and by-products, from resource to drinking water. *Environ Int* 35:803–814.

Monteiro SC, Boxall A. 2010. Occurrence and fate of human pharmaceuticals in the environment. *Rev Environ Contam Toxicol* 202:53–154.

Mosekiemang TT, Stander MA, de Villiers A. 2019. Simultaneous quantification of commonly prescribed antiretroviral drugs and their selected metabolites in aqueous environmental samples by direct injection and solid phase extraction liquid chromatography-tandem mass spectrometry. *Chemosphere* 220:983–992.

Moslah B, Hapeshi E, Jrad A, Fatta-kassinos D. 2018. Pharmaceuticals and illicit drugs in wastewater samples in north-eastern Tunisia. *Environ Sci Pollut Res* 25:18226–18241.

Mtolo SP, Mahlambi PN, Madikizela LM. 2019. Synthesis and application of a molecularly imprinted polymer in selective solid-phase extraction of efavirenz from water. *Water Sci Technol* 79:356–365.

Ncube S, Madikizela LM, Chimuka L, Nindi MM. 2018. Environmental fate and ecotoxicological effects of antiretrovirals: A current global status and future perspectives. *Water Res* 145:231–247.

Ngqwala NP, Muchesa P. 2020. Occurrence of pharmaceuticals in aquatic environments: A review and potential impacts in South Africa. *S Afr J Sci* 116(7/8).

Ngumba E, Gachanja A, Tuhkanen T. 2016a. Occurrence of selected antibiotics and antiretroviral drugs in Nairobi River Basin, Kenya. *Sci Total Environ* 539:206–213.

Ngumba E, Kosunen P, Gachanja A, Tuhkanen T. 2016b. A multiresidue analytical method for trace level determination of antibiotics and antiretroviral drugs in wastewater and surface water using SPE-LC-MS/MS and matrix-matched standards. *Anal Methods* 8:6720–6729.

Ngumba E, Gachanja A, Nyirenda J, Maldonado J, Tuhkanen T. 2020. Occurrence of antibiotics and antiretroviral drugs in source-separated urine, groundwater, surface water, and wastewater in the peri-urban area of Chunga in Lusaka, Zambia. *Water SA* 46:278–284.

Nibamureke UMC, Barnhoorn IEJ, Wagenaa GM. 2019. Assessing the potential effects of nevirapine in South African surface water on fish growth: A chronic exposure of *Oreochromis mossambicus*. *S Afr J Sci* 115:5516.

Orias F, Perrodin Y. 2013. Characterisation of the ecotoxicity of hospital effluents: A review. *Sci Total Environ* 454–455:250–276.

Patel M, Kumar R, Kishor K, Mlsna T, Pittman CU, Mohan D. 2019. Pharmaceuticals of emerging concern in aquatic systems: Chemistry, occurrence, effects, and removal methods. *Chem Rev* 119:3510–3673.

Parastar H, Radović JR, Bayona JM, Tauler R. 2013. Solving chromatographic challenges in comprehensive two-dimensional gas chromatography-time-of-flight mass spectrometry using multivariate curve resolution-alternating least squares. *Anal Bioanal Chem* 405:6235–6249.

Peng X, Wang C, Zhang K, Wang Z, Huang Q, Yu Y, Ou W. 2014. Profile and behavior of antiviral drugs in aquatic environments of the Pearl River Delta, China. *Sci Total Environ* 466–467:755–761.

Pérez-Ramírez EF, Luz-Asunción MDL, Martínez-Hernández AL, Velasco-Santos C. 2016. Graphene materials to remove organic pollutants and heavy metals from water: Photocatalysis and adsorption. Semiconductor photocatalysis—Materials, mechanisms and applications. *IntechOpen*. https://doi.org/10.5772/62777

Prasse C, Schlüsener MP, Schulz R, Ternes TA. 2010. Antiviral drugs in wastewater and surface waters: A new pharmaceutical class of environmental relevance? *Environ Sci Technol* 44:1728–1735.

Prasse C, Wagner M, Schulz R, Ternes TA. 2012. Oxidation of the antiviral drug acyclovir and its biodegradation product carboxy-acyclovir with ozone: Kinetics and identification of oxidation products. *Environ Sci Technol* 46:2169–2178.

PubChem. 2021. Explore Chemistry. National Library of Medicine, Washington, DC. [cited 2021 May 12]. Available from: https://pubchem.ncbi.nlm.nih.gov/#query=

Rajapaksha AU, Chen SS, Tsang DCW, Zhang M, Vithanage M, Mandal S, Gao B, Bolan NS, Ok YS. 2016. Engineered/designer biochar for contaminant removal/immobilization from soil and water: Potential and implication of biochar modification. *Chemosphere* 148:276–291.

Ramollo PP. 2011. Freshwater fish abundance and distribution in the Orange River. *South Africa. J Fish Int* 6:13–17.

Razonable RR. 2011. Antiviral drugs for viruses other than human immunodeficiency virus. *Mayo Clin Proc* 86:1009–1026.

Reungoat J, Macova M, Escher BI, Carswell S, Mueller JF, Keller J. 2010. Removal of micropollutants and reduction of biological activity in a full-scale reclamation plant using ozonation and activated carbon filtration. *Water Res* 44:625–637.

Ribeiro RF, Soares VC, Costa LM, Nascentes CC. 2015. Production of activated carbon from biodiesel solid residues: An alternative for hazardous metal sorption from aqueous solution. *J Environ Manage* 162:123–131.

Rimayi C, Odusanya D, Weiss JM, de Boer J, Chimuka L. 2018. Contaminants of emerging concern in the Hartbeespoort Dam catchment and the uMngeni River estuary 2016 pollution incident, South Africa. *Sci Total Environ* 627:1008–1017.

Riska P, Lamson M, Macgregor T, Sabo J, Hattox S, Pav J, Keirns J. 1999. Disposition and biotransformation of the antiretroviral drug nevirapine in humans. *Drug Metab Dispos* 27:895–901.

Rosenbach KA, Allison R, Nadler JP. 2002. Daily dosing of highly active antiretroviral therapy. *Clin Infect Dis* 34:686–692.

Sanderson H, Johnson DJ, Reitsma T, Brain RA, Wilson CJ, Solomon KR. 2004. Ranking and prioritization of environmental risks of pharmaceuticals in surface waters. *Regul Toxicol Pharmacol* 39:158–183.

Schoeman CMM, Dlamini M, Okonkwo OJ. 2015. Quantification of selected antiretroviral drugs in a wastewater treatment works in South Africa using GC-TOFMS. *J Chromatogr Sep Tech* 6:272.

Schoeman C, Dlamini M, Okonkwo OJ. 2017. The impact of a Wastewater Treatment Works in Southern Gauteng, South Africa on efavirenz and nevirapine discharges into the aquatic environment. *Emerg Contam* 3:95–106.

Shen Y, Fang Q, Chen B. 2015. Environmental applications of three-dimensional graphene-based macrostructures: Adsorption, transformation, and detection. *Environ Sci Technol* 49:67–84.

Sievers C, Noda Y, Qi L, Albuquerque EM, Rioux RM, Scott SL. 2016. Phenomena affecting catalytic reactions at solid–liquid interfaces. *ACS Catalysis* 6:8286–8307.

Swanepoel CBH, Pieters R, Bezuidenhout C. 2015. Presence, concentrations and potential implications of HIV-antiretrovirals in selected water resources in South Africa. Water Research Commission, Gezina, South Africa, pp 1–39.

Swati JV, Vjas RK, Prabhat P, Sangeeta V. 2011. A review on fate of antiviral drugs in environment and detection techniques. *Int J Environ Sci* 1:1526–1541.

Tambosi JL, de Sena RF, Favier M, Gebhardt W, José HJ, Schröder HF. 2010. Removal of pharmaceutical compounds in membrane bioreactors (MBR) applying submerged membranes. *Desalination* 261: 148–156.

Tchetnya X, Ngwasiri CA, Munge T, Aminde LN. 2018. Severe eye complications from toxic epidermal necrolysis following initiation of Nevirapine based HAART regimen in a child with HIV infection: A case from Cameroon. *BMC Pediatr* 18:108.

Ternes TA, Meisenheimer M, McDowell D, Sacher F, Brauch HJ, HaistGulde B, Preuss G, Wilme U, ZuleiSeiberts N. 2002. Removal of pharmaceuticals during drinking water treatment. *Environ Sci Technol* 36: 3855–3863.

Thammakumpee J, Yongsiri S. 2013. Characteristics of toxic epidermal necrolysis and Steven Johnson syndrome: A 5-year retrospective study. *J Med Assoc Thail* 96:399–406.

Tsakona M, Anagnostopoulou E, Gidarakos E. 2007. Hospital waste management and toxicity evaluation: A case study. *Waste Manage* 27:912–920.

Tyring SK. 2004. Antiviral Agents, Vaccines, and Immunotherapies, CRC, Boca Raton, FL, USA.

Udert KM, Etter B, Gouden T. 2016. Promoting sanitation in South Africa through nutrient recovery from urine. *GAIA Ecol Perspect Sci Soc* 25:194–196.

Uddin MK. 2017. A review on the adsorption of heavy metals by clay minerals, with special focus on the past decade. *Chem Eng J* 308:438–462.

United Nations. 2015. United Nations Sustainable Development Goals. Geneva, Switzerland.

Van Damme W, Kober K, Laga M. 2006. The real challenges for scaling up ART in sub-Saharan Africa. *AIDS* 20:653–656.

Verhelst D, Monge M, Meynard JL, Fouqueray B, Mougenot B, Girard P-M, Ronco P, Rossert J. 2002. Fanconi syndrome and renal failure induced by tenofovir: A first case report. *Am J Kidney Dis* 40:1331–1333.

Vermeir M, Lachau-Durand S, Mannens G, Cuyckens F, van Hoof B, Raoof A. 2009. Absorption, metabolism, and excretion of darunavir, a new protease inhibitor, administered alone and with low-dose ritonavir in healthy subjects. *Drug Metab Dispos* 37:809.

Wan S, Qu N, He F, Wang M, Liu G, He H. 2015. Tea waste-supported hydrated manganese dioxide (HMO) for enhanced removal of typical toxic metal ions from water. *RSC Adv* 5:88900–88907.

Wan S, Wu J, Zhou S, Wang R, Gao B, He F. 2018. Enhanced lead and cadmium removal using biochar-supported hydrated manganese oxide (HMO) nanoparticles: Behavior and mechanism. *Sci Total Environ* 616:1298–1306.

Wang B, Gao B, Fang J. 2017. Recent advances in engineered biochar productions and applications. *Crit Rev Environ Sci Technol* 47: 2158–2207.

Wang J, Chen B. 2015. Adsorption and coadsorption of organic pollutants and a heavy metal by graphene oxide and reduced graphene materials. *Chem Eng J* 281:379–388.

Wang L, Shi C, Wang L, Pan L, Zhang X, Zou J. 2020. Rational design, synthesis, adsorption principles and applications of metal oxide adsorbents: A review. *Nanoscale*. https://doi.org/10.1039/C9NR09274A

Wang S, Gao B, Zimmerman AR, Li Y, Ma L, Harris WG, Migliaccio KW. 2015. Removal of arsenic by magnetic biochar prepared from pinewood and natural hematite. *Bioresour Technol* 175:391–395.

Wood TP, Duvenage CSJ, Rohwer E. 2015. The occurrence of anti-retroviral compounds used for HIV treatment in South African surface water. *Environ Pollut* 199:235–243.

Wood TP, Basson AE, Duvenage C, Rohwer ER. 2016. The chlorination behaviour and environmental fate of the antiretroviral drug nevirapine in South African surface water. *Water Res* 104:349–360.

Wooding M, Rohwer ER, Naudé Y. 2017. Determination of endocrine disrupting chemicals and antiretroviral compounds in surface water: A disposable sorptive sampler with comprehensive gas chromatography–time-of-flight mass spectrometry and large volume injection with ultra-high-performance liquid chromatography–tandem mass spectrometry. *J Chromatogr A* 1496:122–132.

World Health Organization 2019. Antiretroviral therapy coverage data and estimates by country. Global Health Observatory Data Repository. Geneva, Switzerland. [cited 2020 September 22]. Available from: https://apps.who.int/gho/data/view.main.23300?lang=en

Xiao J, Lv W, Xie Z, Tan Y, Song Y, Zheng Q. 2016. A flyweight and superelastic graphene aerogel as a high-capacity adsorbent and highly sensitive pressure sensor. *J Mater Chem A* 4:12126–12135.

Yang X, Wan Y, Zheng Y, He F, Yu Z, Huang J, Wang H, Ok YS, Jiang Y, Gao B. 2019. Surface functional groups of carbon-based adsorbents and their roles in the removal of heavy metals from aqueous solutions: A critical review. *Chem Eng J* 366:608–621.

Yu Z, Peldszus S, Huck PM. 2009. Adsorption of selected pharmaceuticals and an endocrine disrupting compound by granular activated carbon. 2. *Model prediction*. *Environ Sci Technol* 43:1474–1479.

Zhang M, Tao S, Wang X. 2020. Interactions between organic pollutants and carbon nanomaterials and the associated impact on microbial availability and degradation in soil: A review. *Environ Sci Nano* 7: 2486–2508.

Zhang W, Lu Y, Sun H, Zhang Y, Zhou M, Song Q, Gao Y. 2019. Effects of multi−walled carbon nanotubes on pyrene adsorption and

desorption in soils: The role of soil constituents. *Chemosphere* 221:203–211.

Zhang XY, Gao B, Creamer AE, Cao CC, Li YC. 2017. Adsorption of VOCs onto engineered carbon materials: A review. *J Hazard Mater* 338:102–123.

Zhang Y, Shen Z, Dai C, Zhou X. 2014. Removal of selected pharmaceuticals from aqueous solution using magnetic chitosan: Sorption behavior and mechanism. *Environ Sci Pollut Res* 21:12780–12789.

Zhou C, Chen J, Xie Q, Wei X, Zhang Y-N, Fu Z. 2015. Photolysis of three antiviral drugs acyclovir, zidovudine and lamivudine in surface freshwater and seawater. *Chemosphere* 138:792–797.

Zou W, Gao B, Ok YS, Dong L. 2019. Integrated adsorption and photocatalytic degradation of volatile organic compounds (VOCs) using carbon-based nanocomposites: A critical review. *Chemosphere* 218: 845–859.

Chapter 4 Single-solute batch adsorption of phenanthrene and pyrene using synthesized graphene wool adsorbent

This chapter deals with the establishment of optimum process conditions for the sorption of selected PAHs using graphene wool (wool) in single-solute batch experiments, and the efficiency of GW was compared with different adsorbents used for PHEN and/or PYR adsorption in literature. The reusability of the novel adsorbent was also examined via several cycles of regeneration and reuse. The format is as published in Water Science and Technology.

Article

Adeola, A.O., Forbes, P.B.C. (2019). Optimization of sorption of selected polycyclic aromatic hydrocarbons by regenerable graphene wool. Water Science and Technology, 80(10): 1931-1943.

DOI: https://doi.org/10.2166/wst.2020.011

Optimization of the sorption of selected polycyclic aromatic hydrocarbons by regenerable graphene wool

Adedapo O. Adeola and Patricia B. C. Forbes

ABSTRACT

A novel graphene wool (GW) material was used as adsorbent for the removal of phenanthrene (PHEN) and pyrene (PYR) from aqueous solution. Adsorption kinetics, adsorption isotherms, thermodynamics of adsorption and effect of pH, ionic strength, and temperature on the adsorption of PHEN and PYR onto GW were comprehensively investigated. Isothermal and kinetic experimental data were fitted to Langmuir, Freundlich, Temkin, Sips and Dubinin–Radushkevich models, as well as pseudo-first-order and pseudo-second-order kinetic models. The adsorption kinetic data best fit the pseudo-second-order kinetic model for PHEN and PYR sorption with R^2 value >0.999, whilst the Sips model best fit isotherm data. Kinetic data revealed that 24 hr of contact between adsorbent and polycyclic aromatic hydrocarbons (PAHs) was sufficient for maximum adsorption, where the Langmuir maximum adsorption capacity of GW for PHEN and PYR was 5 and 20 mg g^{-1} and the optimum removal efficiency was 99.9% and 99.1%, respectively. Thermodynamic experiments revealed that adsorption processes were endothermic and spontaneous. Desorption experiments indicated that irreversible sorption occurred with a hysteresis index greater that zero for both PAHs. The high adsorption capacity and potential reusability of GW makes it a very attractive material for removal of hydrophobic organic micro-pollutants from water.

Key words | adsorption, graphene wool, phenanthrene, pyrene, water treatment

Adedapo O. Adeola
Patricia B. C. Forbes (corresponding author)
Department of Chemistry, Faculty of Natural and Agricultural Sciences,
University of Pretoria,
Lynnwood Road, Hatfield, Pretoria 0002,
South Africa
E-mail: *patricia.forbes@up.ac.za*

INTRODUCTION

Polycyclic aromatic hydrocarbons (PAHs) such as phenanthrene and pyrene are semi-volatile and hydrophobic organic pollutants, found ubiquitously in the environment. PAHs are directly released into the environment via effluent discharge from petroleum and petrochemical industries, subsurface fuel pipeline leakages, and continuous leakage of gasoline from underground storage tanks (Torabian *et al.* 2010; Abdel-Shafy & Kamel 2016). In addition, PAH contamination also arises from tobacco smoking, improper waste disposal and burning of biomass and organic substances (IARC 2010). Some PAHs are difficult to degrade, and are carcinogenic or mutagenic and 16 PAHs are classified as priority pollutants by the United States Environmental Protection Agency (Cai *et al.* 2009). Upon human exposure, they permeate the cell membrane and are absorbed easily because they are carbon-rich and hydrophobic in nature (Yakout & Daifullah 2013).

The adsorption process has been identified as a suitable, simple and effective remediation approach for the removal of several pollutants from water without chemical transformation. Carbonaceous or carbon-based materials have been reported to be effective for the removal of PAHs; however, most of the adsorbents present several challenges including difficulties regarding regeneration and reusability of spent adsorbent (Wang *et al.* 2006; Yang & Xing 2007; Zhao *et al.* 2011; Yang *et al.* 2013; Yang *et al.* 2015; Hassan *et al.* 2018). The presence of carbonaceous materials in water bodies may influence the mobility and fate of organic pollutants, thereby influencing their environmental impact or risks (Liu *et al.* 2016). The adsorption of PAHs has been reported to have higher binding strength onto porous carbon than onto soils, suspended organic matter, and sediments (Ukalska-Jaruga *et al.* 2019). Therefore, a comprehensive understanding of the adsorption mechanism of organic contaminants onto graphene-based materials will assist in shedding light on the fate and distribution of PAHs in aquatic environments, and may provide the possibility of developing a novel adsorbent

doi: 10.2166/wst.2020.011

for water treatment applications. The graphene wool used in this study is a novel material synthesized via the chemical vapor deposition (CVD) method onto a quartz wool substrate under optimized flow rates of hydrogen, argon and methane gas precursors (Schoonraad *et al.* 2020). This wool-like graphene material has not been applied to the removal of any class of pollutants in water to date. Despite several reports on adsorption of PAHs by different graphene-based materials, information on the role of certain environmental variables such as total dissolved solids/salinity/ionic strength as well as thermodynamics of adsorption is unavailable or scanty. This study evaluates adsorption data for a wide range of PAH concentrations (part-per-million and part-per-trillion), which has never been done for any adsorbent, bearing in mind that PAH concentrations in surface waters may differ for different geographical locations.

The overall goal of this work was to apply a novel, regenerable graphene wool material for the removal of phenanthrene and pyrene from water. The role of environmental or process variables such as pH, temperature, ionic strength/total dissolved solids (TDS) of the solution and initial concentration of PAHs on the sorptive removal of the compounds was studied to establish the optimum conditions for effective use of graphene wool for water treatment applications.

EXPERIMENTAL METHODS

Synthesis of graphene wool

The procedure as reported in (Schoonraad *et al.* 2020) was used to prepare the graphene wool (GW). Briefly, quartz wool (Arcos Organics, New Jersey, USA) was placed in the middle of a horizontal quartz tube (50 mm o.d., 44 mm i.d., × 1,000 mm length) in an OTF-1200X-50-5 L high-temperature furnace (MTI Corporation, California, USA). A mixture of 500 sccm argon and hydrogen (both 99.999%, Afrox, South Africa) was introduced into the system, after which the temperature was ramped to 1,200 °C. The substrate was annealed under these conditions for 10 min, after which methane (99.95%, Afrox, South Africa) was introduced for graphene growth. After the growth period had elapsed, the system was cooled under Ar and H_2. Thermal reduction of the hydrocarbon precursor and graphene deposition on silicon substrate is a bottom-up or 'growth' synthesis approach; therefore, it was not necessary to remove the substrate, and thus the term 'graphene wool (GW)' in this study refers to graphene coated on quartz wool.

Characterization of graphene wool adsorbent

The morphology and structure of graphene wool was characterized by a combination of techniques including Raman spectroscopy (WITec alpha300 RAS$^+$ confocal Raman microscope, WiTec, Germany) using a 532 nm excitation laser at low power (5 mW). X-ray photoelectron spectroscopy (XPS) analysis was also previously conducted to characterize the sample composition, and the binding energies were referenced to the C 1s line at 284.8 eV, as detailed in Schoonraad *et al.* (2020). Scanning electron microscopy (SEM) images were also taken using a Zeiss Ultra-Plus 55 field emission scanning electron microscope, operated at 2.0 kV, Zeiss, Germany. High resolution transmission electron microscopy (TEM) images of graphene wool were taken using a JEOL JEM 2100F (JOEL Ltd, Tokyo, Japan) operated at 200 kV (Schoonraad *et al.* 2020). The specific surface area (SSA) of GW was carried out using modified Sears' method (Sears 1956).

Adsorption kinetics and isotherm experiments

Batch adsorption experiments of PAHs onto GW were performed in 40 mL polytetrafluoroethylene screw cap amber vials (Stargate Scientific, South Africa) sealed with aluminum foil at 25 ± 1 °C. Background solution (pH = 7.0) contained 0.01 mol L^{-1} $CaCl_2$ (ACE, South Africa) in deionized water with 200 mg L^{-1} NaN_3 (Sigma-Aldrich, Germany) as a biocide. The sorption kinetic studies were conducted for 48 hours with initial pyrene (PYR) and phenanthrene (PHEN) concentrations of 50 ng L^{-1} (neat standards were purchased from Supelco, USA), and the solid-to-water ratio for graphene wool was 50 mg per 100 mL. Afterwards, the isotherm experiment was conducted with initial concentrations of the PAH solutions ranging from 300 ng L^{-1} to 800 ng L^{-1} and 1 mg L^{-1} to 5 mg L^{-1} respectively. Adsorption isotherms of PHEN and PYR were also determined at varying temperatures of 35, 45 and 55 °C using a thermostated shaking water bath (Wisebath, Celsius Scientific, South Africa) to determine whether the adsorption process is exothermic or endothermic. The role of ionic strength on adsorption of PHEN and PYR onto GW was studied. The sorbates were prepared in 0.01, 0.1 and 1 M $NaCl_2$ (Merck, South Africa) and isotherms were determined. The solution pH was adjusted with 0.1 M HCl (Merck, South Africa) or NaOH (ACE, South Africa) over the pH range from 2 to 12, to study the influence of pH on the removal of PHEN and PYR from aqueous solutions. All the solutions were prepared using

ultra-pure water obtained from a Milli-Q water purification system (Millipore, Bedford, MA, USA).

Quantification

After equilibration, the vials were centrifuged at 3,000 rpm for 5 min to obtain a clear supernatant. The PAH concentrations in the supernatants were analyzed in triplicate ($n = 3$) by fluorescence spectroscopy (Horiba Jobin Yvon Fluoromax-4 spectrofluorometer; excitation wavelength was 290 nm for PHEN and 300 nm for PYR). The regression coefficients (R^2) of matrix-matched calibration curves were obtained from stock solutions of each PAH. The working solutions were in the range of 50–1,000 ng L^{-1} and 1–5 mg L^{-1} for PHEN and PYR respectively. The equation of the curve was used to deduce the equilibrium concentration C_e. The amount of each solute adsorbed (q_e, mg g^{-1}) was calculated using the following mass-balance equation:

$$q_e = \frac{(C_0 - C_e)V_0}{S_m} \quad (1)$$

where C_0 (mg L^{-1}) is the initial concentration, C_e (mg L^{-1}) is the equilibrium solute concentration, V_0 is the initial volume (L) and S_m is the mass (g) of the adsorbent.

$$\text{Removal efficiency (\%)} = \frac{(C_0 - C_e)}{C_0} \times 100 \quad (2)$$

Regeneration of the adsorbent and reusability tests were carried out by solid-phase extraction using 10 mL hexane (≥97% HPLC grade, Sigma-Aldrich, Germany) and placed on the thermostatic shaker for 2 hours at room temperature. PAHs desorbed were quantified using gas chromatography mass spectrometry (GC-MS) due to the expected low concentration (refer to Supplementary Information for details). Afterwards, the GW was dried in a muffle furnace (Labotec, South Africa) at a temperature of 70 °C for 4 hours and was allowed to cool before reuse.

RESULTS AND DISCUSSION

Characterization of graphene wool

The pH of GW was found to be 6.1 and 7.1 in $CaCl_{2(aq)}$ solution and deionized water, respectively. The surface area of GW as determined using Sears' method is 279 $m^2 g^{-1}$, lower than the theoretical surface area of graphene (2,630 $m^2 g^{-1}$), due to coverage over the quartz wool which ultimately defines the surface area (Stoller *et al.* 2008; Wang *et al.* 2014). Raman spectroscopy indicated a crystallite grain size of an average value of 24 nm with three prominent peaks at 1,349, 1,582 and 2,630 cm^{-1} (Figure S1 in the Supplementary Information), which correspond to D, G and 2D bands caused by stretching vibrations of sp3 and sp2 carbon atoms, respectively (Wang *et al.* 2014; Ndiaye *et al.* 2018). XPS analysis of the GW revealed the strongest peak of C=C at 284.4 eV which represents graphene and suggests that the D peak in the Raman spectrum is due to thermal disintegration of the sp2 carbon network into nano-sized oxidized domains which occurred during CVD synthesis (Chen *et al.* 2008; Schoonraad *et al.* 2020). SEM and TEM images of the GW (Figure S1) showed varying translucence as a result of multiple layer staking of the graphene flake-like sheets. The presence of interstitial spaces was also confirmed within the GW aggregates (Figure S1). This suggests that adsorption of PHEN and PYR may occur via multilayer or monolayer coverage of the adsorbent, and/or pore filling mechanisms due to the layered morphology of GW. The interstitial spaces within GW may also be available for adsorption of PAHs.

Adsorption kinetics

The pseudo-first-order and pseudo-second-order kinetic models were investigated and compared in order to study the mechanism of the adsorption process (Zhao *et al.* 2011). The kinetic parameters and correlation coefficients obtained from different models are summarized in Table 1. The kinetic model plots are shown in Figure 1.

Table 1 | Coefficients of sorption kinetics for phenanthrene and pyrene removal by graphene wool adsorbent and their correlation coefficients (R^2) (experimental conditions: $C_0 = 50$ ng L^{-1}; dosage = 50 mg per 100 mL; mixing rate = 200 rpm; T = 25 ± 1 °C; pH = 6.8 ± 0.2 for phenanthrene and pH = 6.7 ± 0.2 for pyrene)

		PAH	
Adsorption kinetics	**Parameters**	**Phenanthrene**	**Pyrene**
First order	Calculated q_e (mg g^{-1})	6.02	10.83
	Experiment q_e (mg g^{-1})	28.60	41.87
	k_1 (hr^{-1})	0.0617	0.0774
	R^2	0.4227	0.5772
Second order	Calculated q_e (mg g^{-1})	28.33	41.84
	Experiment q_e (mg g^{-1})	28.60	41.87
	k_2 (mg g^{-1} hr^{-1})	0.0859	0.0410
	h (mg g^{-1} hr^{-1})	68.94	71.77
	R^2	0.9998	0.9995

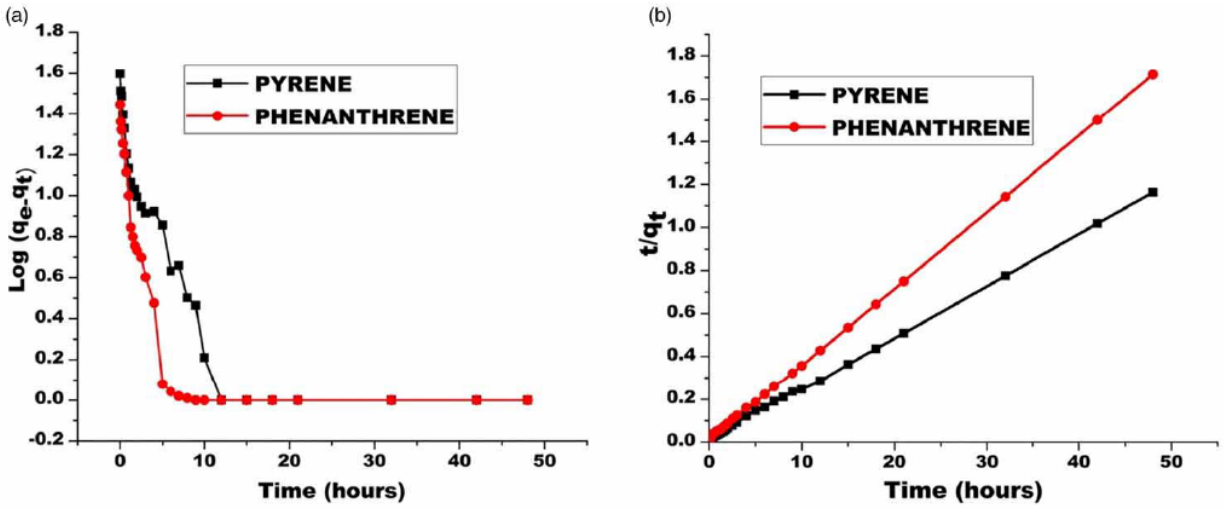

Figure 1 | Lagergren pseudo-first-order and pseudo-second-order kinetics sorption for pyrene and phenanthrene onto graphene wool (experimental conditions: $C_0 = 50$ ng L^{-1}; dosage = 50 mg per 100 mL, mixing rate = 200 rpm, T = 25 ± 1 °C; pH (PYR) = 6.7 ± 0.2 and pH (PHEN) = 6.8 ± 0.2).

The kinetic experimental data were a far better fit with the pseudo-second-order equation with a correlation coefficient (R^2) >0.999, compared with the first-order model (Table 1). The steepness observed in the first 6 hr of phenanthrene sorption and 10 hr of pyrene sorption is attributed to fast initial sorption, due to easily accessible GW sorption sites available to the respective PAH, before a period of slower adsorption (Figure 1). On the basis of correlation coefficients (Zhao *et al.* 2011), the adsorption of PHEN and PYR by GW follows a second-order reaction pathway. The kinetic pathway established for the adsorption of PHEN and PYR onto GW is in agreement with kinetic studies previously reported for reduced graphene oxide adsorption of bisphenol-A, which followed second-order adsorption kinetics (Xu *et al.* 2012). This further confirms that graphene-based materials are efficient adsorbents of hydrophobic organic pollutants, with high adsorption capacity. The experimental adsorption capacity q_e for GW adsorption of PHEN and PYR is 28.60 ng g^{-1} and 41.87 ng g^{-1}, which is similar to that which was predicted using the pseudo-second-order kinetic equation (28.33 and 41.84 ng g^{-1} respectively), which suggests that the adsorption process involves chemisorption (Yu *et al.* 2015).

PHEN and PYR do not contain functional groups which would undergo chemical reactions with GW, but rather chemical interaction involving electron sharing and/or exchange between these PAHs and GW can be expected (Martínez *et al.* 2006). The adsorption rate constant k_2 for adsorption of phenanthrene and pyrene by GW is 0.0859 ng g^{-1} hr^{-1} and 0.0410 ng g^{-1} hr^{-1}, and given that the second-order pathway best describes the sorption process, it can be inferred that the smaller phenanthrene molecule is adsorbed at a faster rate than pyrene.

Sorption isotherm experiments

Effect of initial concentrations

Adsorption isotherm models are used to elucidate the sorbent–sorbate interactions when the adsorption process reaches equilibrium (Zhang *et al.* 2014). The adsorption isotherms of pyrene and phenanthrene on graphene wool are shown in Figure 3. The role of two different ranges of concentrations (with difference in magnitude of 10^{-6} g L^{-1} solute concentration) was used to explain the interaction between PAHs and GW and how concentration could affect the nature of adsorption. The isotherm regression plots and parameters for Freundlich, Langmuir, Temkin, Sips and Dubinin–Radushkevich (D-R) models are presented in Table 2 and Figure 2 for concentrations in the part-per-million (mg L^{-1}) range and Table S2 and Figure S2 (Supplementary Information) for concentrations in the part-per-trillion (ng L^{-1}) range. The correlation coefficient revealed that the isotherm models fitted better with equilibrium data in the high concentration (mg L^{-1}) range, with R^2 values ranging from 0.9414 to 0.9984, than at lower concentration range (ng L^{-1}) with R^2 ranging from 0.7441 to 0.9928 (Table 2 and Table S2).

The Sips isotherm model best fit the data for PHEN and PYR sorption onto GW at high concentration range with R^2 and N values of (0.9956, 0.46) and (0.9984, 0.54) respectively,

Table 2 | Coefficients obtained for four different sorption isotherm models for phenanthrene and pyrene adsorption by graphene wool and their correlation coefficients (R^2) in the part-per-million PAH concentration ranges (experimental conditions: dosage = 20 mg per 30 mL; mixing rate = 220 rpm; T = 25 ± 1 °C; initial conc.: 1–5 mg L^{-1}; contact time = 24 hours; pH = 6.8 ± 0.2 for phenanthrene and pH = 6.7± 0.2 for pyrene)

		PAH	
Isotherm model	**Parameter**	**Phenanthrene**	**Pyrene**
Dubinin–Radushkevich	Q_D (mol g^{-1})	1.0053	1.0008
	B_D (kJ mol^{-1} K^{-1})	6.05×10^{-8}	1.01×10^{-8}
	E (kJ mol^{-1})	2.87	7.04
	R^2	0.9812	0.9920
Freundlich	N	0.6218	0.9665
	K_f ($mg^{1-1/n}$ $L^{1/n}$ g^{-1})	16.2	114.4
	R^2	0.9906	0.9685
Langmuir	q_{max} (mg g^{-1})	5.0	20.0
	K_L (L mg^{-1})	181.8	6.85
	R_L	0.0055	0.127
	R^2	0.9793	0.9635
Sips	q_{max} (mg g^{-1})	5×10^{7}	1.43×10^{8}
(Freundlich–Langmuir)	K_s (L mg^{-1})	7.7×10^{-8}	1.1×10^{-7}
	N	0.46	0.54
	R^2	0.9956	0.9984
Temkin	b_T (kJ mol^{-1})	15.4	22.3
	K_T (L mg^{-1})	6.87×10^{18}	1.51×10^{15}
	R^2	0.9414	0.9872

which suggests that a multilayer adsorption pattern on a heterogeneous surface is likely to define the sorption process of PHEN rather than the monolayer adsorption mechanism postulated by Langmuir (Allen *et al.* 2004). Comparatively, the equilibrium data for the low concentration range (ng L^{-1}) fit best the Temkin isotherm model with an R^2 value of 0.9443 for PHEN and 0.9928 for PYR sorption, which explains that the decline in heat of sorption with increase in adsorption coverage area is linear rather than logarithmic, as the Freundlich equation implies (Vidal *et al.* 2011). The mean sorption energy (E) for PHEN and PYR in the D-R model and high values of the Temkin isotherm constant b_T suggests that interactions exist between GW and the PAHs, which is characteristic of electron transfer and/or sharing leading to π-π interactions (Wang *et al.* 2014).

The Freundlich and Sips constant N indicates the heterogeneity index of the surface of the adsorbent and adsorption intensity due to the formation of new adsorption sites and increase in the adsorption capacity. This explains why the Langmuir maximum adsorption capacity is higher for PYR (20 mg g^{-1}) with N value of 0.9665 and 0.54 for Freundlich and Sips respectively, when compared with values obtained for PHEN (5 mg g^{-1}) (Table 2). This can be attributed to the physicochemical properties of compounds (Table S1, Supplementary Information) such as hydrophobicity (Log K_{ow}), relative solubility (PYR: 0.135 mg L^{-1}, PHEN: 1.18 mg L^{-1} @ 25 °C) and the stronger π-π interactions as a result of the higher number of delocalized electrons, which are all possible explanations as to why PYR has greater maximum adsorption capacity onto GW than PHEN (Zhang *et al.* 2014).

Pyrene and phenanthrene, as well as other PAHs, possess high octanol–water partition coefficients Log K_{ow} (PYR 5.18 and PHEN 4.57) (Yakout & Daifullah 2013) and are very likely to be adsorbed onto hydrophobic surfaces (Khan *et al.* 2007). The maximum adsorption capacity q_{max} for Langmuir and Sips at lower concentration deviated from what was found for PAHs at high concentration (Table 2 and Table S2). At lower concentrations, the lower molecular weight compound (PHEN 178 g mol^{-1}) was better adsorbed onto GW than the higher molecular weight compound (PYR 202.25 g mol^{-1}) via a pore-filling mechanism on porous materials as described by the D-R model with equally strong correlation values of 0.9684 and 0.8770 for PYR and PHEN sorption (Table S2). This is in accordance with Wang *et al.* (2006), in that the molecular size of compounds in relation to pore size of adsorbent is one of the important factors that may influence sorption. The Langmuir dimensionless constant R_L, which indicates how favorable adsorption is, was less than 1 (Table 2 and Table S2), which indicates favorable adsorption of the selected PAHs onto GW at both mg L^{-1} and ng L^{-1} concentration ranges (Rahman & Islam 2009). The linear relationship between Log K_{ow} and adsorption capacity was also reported by Khan *et al.* (2007) for PAH adsorption by different adsorbents. However, it is worth mentioning that GW has a much higher adsorption capacity within the same concentration range for PHEN sorption with a K_f value of 16.2 $mg^{1-1/n}$ $L^{1/n}$ g^{-1}, higher than polyester fiber, kapok and cattail adsorbents used in the respective studies, with K_f values of 2.15, 1.95 and 5.14 $mg^{1-1/n}$ $L^{1/n}$ g^{-1} respectively (Khan *et al.* 2007).

In summary, adsorption of phenanthrene and pyrene increased with increase in initial PAH concentration, and the positive correlation of high initial PAH concentrations with adsorption capacity of GW can be attributed to the larger number of PAH molecules available for interaction with active sites of the GW.

Effect of contact time

Figure S3 shows the typical percentage removal curves as a result of PHEN and PYR adsorption from aqueous solution. With increasing shaking time, the removal efficiency

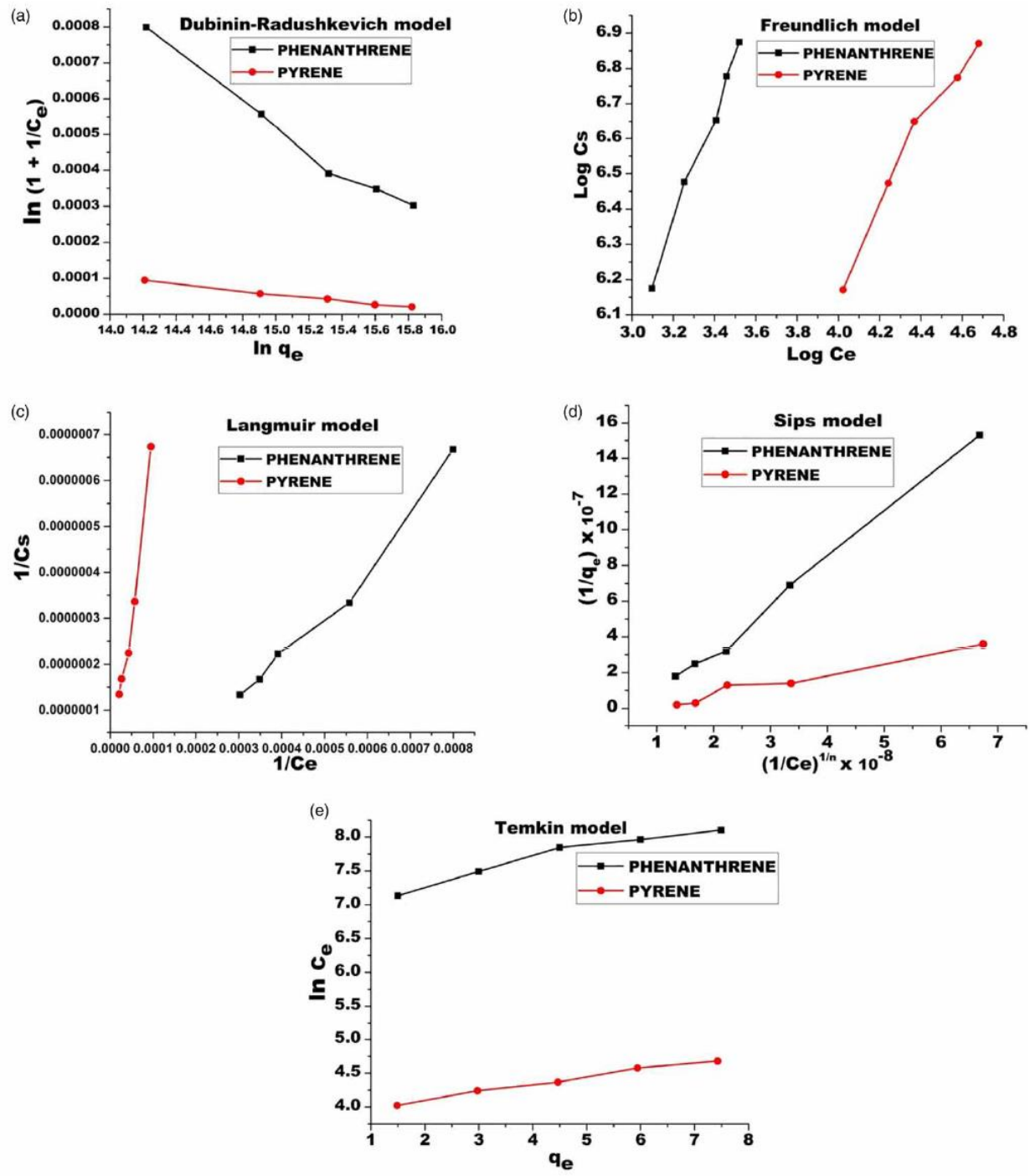

Figure 2 | Plots of isotherm models fitted to experimental data for phenanthrene and pyrene adsorption onto graphene wool.

increased. The initial removal was rapid as shown in the rate curve, followed by a relatively slow sorption process, and finally equilibrium was attained. Furthermore, it can be noted that the sorption rates were fast and more than 60% of total sorption occurred within the first 60 min for PHEN and PYR, while a relatively slow adsorption phase

was apparent after 600 min for pyrene and 240 min for phenanthrene, respectively.

This trend in adsorption is as a result of availability of adsorption or binding sites on the surface of the adsorbent during initial contact; however, the surface active sites get occupied as the adsorption proceeds thus decreasing the sorption rate, due to adsorption to less accessible embedded sites. Fast adsorption is an interesting property of an adsorbent which increases its potential for vast applications (Sepehr *et al.* 2017). The equilibration time was 600 min (15 hours) for PHEN and 1,260 min (21 hours) for PYR and extending the shaking time up to 2,880 min (48 hours) did not further increase the amount of PAHs adsorbed. This informed the decision to use 24 hours as equilibration time for subsequent experiments.

Effect of initial pH on PAH adsorption

Solution pH plays an important role in the adsorption of hydrophobic organic compounds, because it can affect the net charge of the adsorbent and adsorbate. However, the influence of pH is more significant if the compound possesses hydroxyl (-OH) or carboxylic (-COOH) groups because they may easily deprotonate under variable pH conditions. Although such groups are not present in PAHs, they are present in GW (Figure S1). Therefore, the effect of pH on the adsorption of PHEN and PYR on GW was investigated in the pH range of 2–12 due to the fact that the pH of different surfaces and waste water can differ.

It can be clearly seen that the removal efficiency of PHEN and PYR is not significantly influenced by varying pH conditions with a standard deviation of 0.46% for PHEN and 0.08% for PYR. It has been reported in literature that pH has no influence on the adsorption of phenanthrene on active silica gel while others have reported that sorption of phenanthrene on kaolinite, quartz, and goethite were affected by solution pH (Huang *et al.* 1996). The results obtained in this study revealed that the optimum pH conditions for the removal of PHEN and PYR were pH below 7. A weak electrostatic repulsion cannot be ruled out between the electron-rich π systems of PHEN and PYR and the negatively charged surface of the adsorbent at basic pH, causing a decrease in the adsorption, which is more noticeable for PHEN (Figure 3). However, the influence of pH on the overall adsorption efficiency of PHEN and PYR onto GW is negligible.

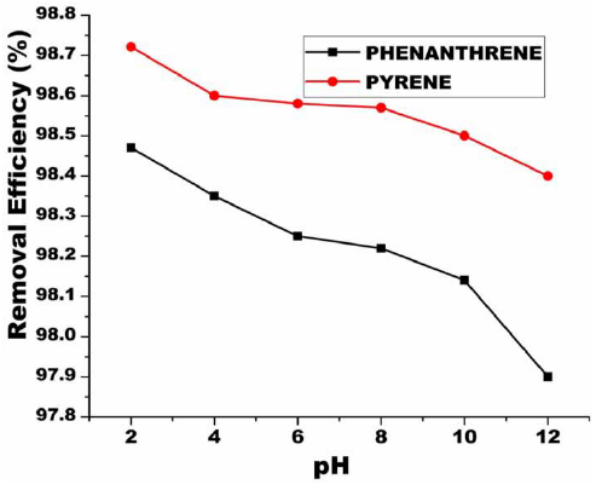

Figure 3 | Effect of pH on pyrene and phenanthrene adsorption onto graphene wool (experimental conditions: $C_0 = 1$ mg L^{-1}; dosage = 20 mg per 30 mL, mixing rate = 200 rpm, T = 25 ± 1 °C, contact time: 24 hours).

Effect of ionic strength/TDS

TDS and ionic strength play vital roles in water quality (Abdel-Shafy *et al.* 2016). Several reports suggest that salinity levels may increase or decrease the adsorption capacity of different carbonaceous materials (Xu *et al.* 2012; Zhang *et al.* 2014). Therefore, the effect of ionic strength on the adsorption of PYR and PHEN onto GW was investigated. Experimental data obtained from the study were fitted to a linear isotherm equation to evaluate adsorption capacities at varying ionic strength/salinity/TDS according to Equation (3):

$$C_s = K_d C_e \tag{3}$$

where C_s (mg g^{-1}) is the amount of PAHs adsorbed, C_e is the equilibrium concentration of PAHs and K_d (L g^{-1}) is the adsorption capacity.

Figure 4 and Table S3 illustrate that increasing the concentration of NaCl caused a significant increase in the adsorption capacities (K_d) of pyrene and phenanthrene with pyrene having the higher adsorption capacity on GW, similar to what was reported in Table 2 for K_f and q_{max} respectively. It has been previously reported that ions such as Ca^{2+}, K^+, Na^+, SO_4^{2-} and Cl^- strongly bind water molecules into hydration shells, thereby reducing the solubility of PAHs in water (Lamichhane *et al.* 2016). Therefore, the cavity volume that accommodates organic solutes pulls the PAH molecules onto the hydrophobic surface of GW as a

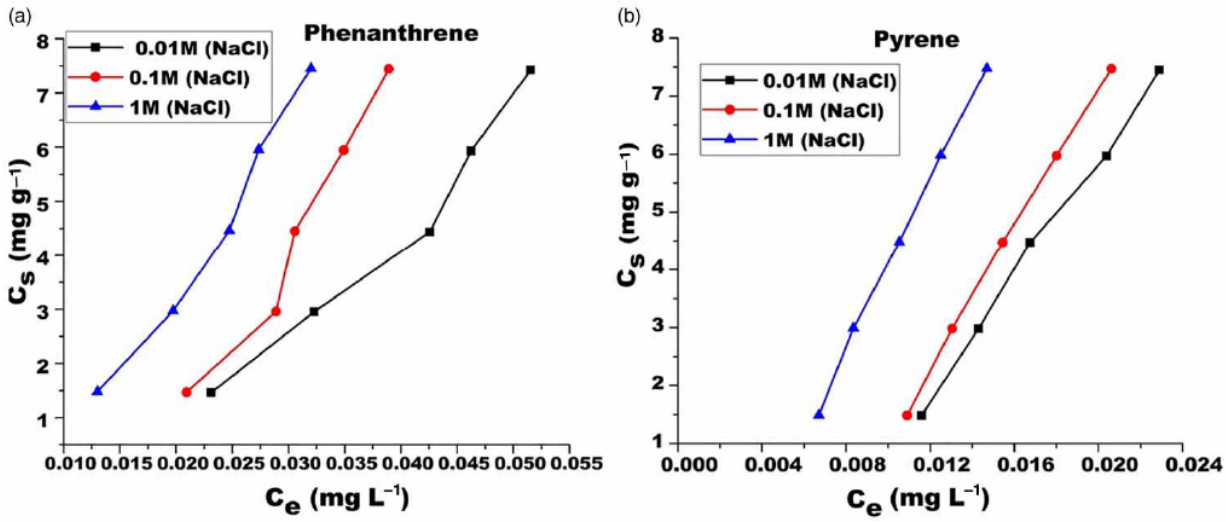

Figure 4 | Effect of ionic strength on adsorption of the selected PAHs from solution (experimental conditions: NaCl conc. = 0.01–1 M; PAH conc. = 1–5 mg L^{-1}; dosage = 20 mg per 30 mL, mixing rate = 200 rpm, T = 25 ± 1 °C).

result of increased polarity of the liquid phase by increased salinity levels. The reduction in available water molecules for PAH dissolution as a result of the strong affinity between the ionic salts and surrounding water molecules is called the 'salting-out effect' (Lamichhane *et al.* 2016). This phenomenon is responsible for the enhanced adsorption and linearity (considering R^2 and K_d values) which indicates improved partition distribution of the solutes between the solid–liquid interphase.

Effect of temperature and thermodynamic studies

Temperature plays a significant role in many chemical and physical processes. Some processes are feasible at ambient temperature while others require additional heat energy to raise the temperature within reaction vessels in order to initiate a physical or chemical change. The effect of temperature on the adsorption of phenanthrene (PHEN) and pyrene (PYR) onto GW was studied at 35, 45 and 55 °C, respectively. The adsorption data were fitted to a linear isotherm model (Equation (3)), and it was observed that the equilibrium concentration of the selected PAHs reduced (Figure S4) and adsorption capacity increased (Table S4) with increase in temperature. Thermodynamic parameters such as free energy change, enthalpy change and entropy change were calculated using the van 't Hoff equations (Equations (4) and (5)) derived from van 't Hoff plots (Figure S5), in order to elucidate the nature of adsorption of PHEN and PYR onto GW as a function of temperature (Yakout & Daifullah 2013).

$$\ln K_d = \frac{\Delta S^\circ}{R} - \frac{\Delta H^\circ}{RT} \tag{4}$$

$$\Delta G^\circ = \Delta H^\circ - T\Delta S^\circ \tag{5}$$

where ΔG° is the change in the Gibbs free energy (cal mol^{-1}); ΔH° is the change in enthalpy (cal mol^{-1}), and ΔS° is the change in entropy (cal mol^{-1} K^{-1}), R = gas constant (1.98 cal mol^{-1} K^{-1}), T = thermodynamic temperature (K) and K_d is adsorption capacity determined from the linear isotherm model.

The thermodynamic parameters calculated using Equations (4) and (5) are listed in Table 3. The calculated ΔH° of the PHEN-GW and PYR-GW system is ~12 and ~28 kcal mol^{-1} respectively. The positive values of ΔH° and ΔS° indicate that the adsorption process is endothermic with an increase in the randomness between the solid-solution interface as temperature increased (Ahmed & Gasser 2012). The negative value of ΔG° indicates spontaneity of the adsorption process and, as the temperature increased, the free energy became more negative indicating that the adsorption of PHEN and PYR became more favorable at higher temperature (Table S4 and Figure S4).

The experimental results reported in this work are in agreement with that reported for the adsorption of naphthalene on GO/FeO•Fe_2O_3 (GO: graphene oxide) and MWCNTs/FeO•Fe_2O_3 (MWCNTs: multi-walled carbon

Table 3 | Thermodynamic parameters for adsorption of phenanthrene (PHEN) and pyrene (PYR) onto graphene wool

	PHEN			PYR		
Temperature (K)	ΔG° (cal mol^{-1})	ΔH° (cal mol^{-1})	ΔS° (cal mol^{-1} K^{-1})	ΔG° (cal mol^{-1})	ΔH° (cal mol^{-1})	ΔS° (cal mol^{-1} K^{-1})
308	−2,752.78			−6,810.76		
318	−3,226.58	11,865.7	47.46	−7,941.66	28,020.9	113.09
328	−3,701.18			−9,072.56		

nanotubes) (Yang *et al.* 2013). Similarly, results reported for adsorption of 1-naphthol onto sulfonated graphene and 1-naphthylamine onto MWCNTs/iron oxides/β-cyclodextrin reveal similar trends, as both reports indicate that the values of ΔH° and ΔS° are both positive and ΔG° is negative (Zhao *et al.* 2011). However, it is worth noting that the ΔH° (enthalpy of adsorption) values found in this study are far higher than those reported in literature, in agreement with what was predicted by the Temkin (b_T) and D-R (E) models (Table 2), suggesting the involvement of strong binding energy between GW and PHEN and between GW and PYR.

Desorption isotherms and hysteresis

Desorption studies aid in predicting the release potential and risk of environmental contamination associated with adsorbed organic pollutants. Therefore, evaluating the sorbed fraction that can return to solution by reaching a new equilibrium is expedient. The $K_{f.des}$ and $1/N_{des}$ values, which represent the desorption capacity and desorption intensity respectively for GW-PHEN and GW-PYR interactions, were obtained by fitting the desorption experimental data to Freundlich isotherms (Cornelissen *et al.* 2005). It is evident from the information presented in Table 4, that the calculated H values for both sorbates were greater than zero ($1/N_{ads} \gg 1/N_{des}$), which suggests that sorption–desorption hysteresis occurred (Ololade *et al.* 2018). The calculated hysteresis index was greater in GW-PYR with lower desorption capacity ($K_{f.des}$) and intensity ($1/N_{des}$) than GW-PHEN, revealing that irreversible entrapment or slow rate of desorption (or both) of sorbed molecules was more in the heavier PAH compound, possessing a higher binding strength than PHEN (Table 2).

Table 4 | Sorption–desorption parameters and hysteresis index (H) derived from Freundlich isotherm model

	Freundlich isotherm				
Sorbate	$K_{f\text{-}des}$	$1/N_{ads}$	$1/N_{des}$	R^2	[a]H
Phenanthrene	6.89	1.6082	1.4707	0.9750	1.0935
Pyrene	2.55	1.0347	0.5747	0.9147	1.8004

[a]H: Sorption–desorption hysteresis index, $H = N_{ads}/N_{des}$.

Irreversible pore deformation of adsorbent and hydrophobicity of chemicals have been reported as possible reasons for hysteretic behavior in sorption processes, which may be due to sorbate-induced alteration of the sorbent from its native thermodynamic state via build-up in unrelaxed free volume (Lu & Pignatello 2002). The pore-deformation mechanism has been hypothesized as the main cause of the irreversible sorption of organic compounds sorbed onto carbonaceous materials and several articles have been published in support of this postulate (Nguyen *et al.* 2004).

Regeneration experiment

GW was regenerated with n-hexane (99.9% purity) by solid-phase solvent extraction and reused in eight successive cycles of adsorption experiments. The adsorption efficiency of the GW for PHEN and PYR in the adsorption–regeneration cycles are shown in Figure 5. This regeneration and reusability experiment revealed that GW can potentially be used for the remediation of water contaminated with PAHs for at least eight cycles without significant loss in removal efficiency. The removal efficiency recorded after subsequent regeneration processes showed that solid-phase extraction at ambient temperature and thermal regeneration at 70 °C was sufficient for the regeneration of GW.

The decision to use hexane was due to its suitable polarity, volatility, and ease of recovery and disposal, and because it is relatively environmentally safe. Furthermore, it works very well for GC-MS applications (Berset *et al.* 1999), which is useful for analytical verification of removal efficiencies. It is equally noteworthy that only about 10% weight loss of the GW due to experimental artifacts was recorded over the eight adsorption–regeneration cycles,

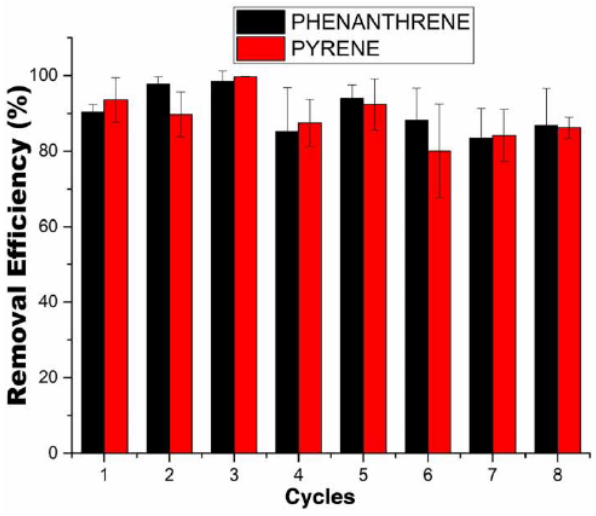

Figure 5 | Removal efficiency of GW after regeneration (experimental conditions: 25 °C; GW: 20 mg; PAH conc.: 300–800 ng L^{-1}, hexane vol.: 10 mL, $n = 3$).

suggesting that graphene wool is very stable and robust and can withstand a considerable amount of physical stress associated with the regeneration process.

Comparison with previous studies

Table 5 reveals that GW competes favorably with adsorbents that have been reported in literature for the removal of PHEN and/or PYR, as a removal efficiency >99% was achieved in this study. The maximum adsorption capacity deduced from the Langmuir isotherm model (q_{max}) and PHEN removal efficiency by GW is higher than that for graphene coated materials and activated carbon (Yang *et al.* 2015; Liu *et al.* 2016). The removal efficiency and adsorption capacity of GW for PYR sorption was found to be higher than that of coke, iron oxide nanoparticles, powdered mesoporous organosilica, biochar, powdered activated carbon, leonardite and graphene oxide (Table 5). The higher adsorption capacity observed for graphene nano-shells (GNS) and activated carbon functionalized with titanate nanotubes (TNT@AC), is likely due to the larger surface area (471.6 $m^2 g^{-1}$ for TNT@AC, 392 $m^2 g^{-1}$ for GNS as compared to 279 $m^2 g^{-1}$ for GW) and hydrophobicity, which promotes higher adsorption capacity than the GW used in our study. However, the role of certain experimental variables such as ionic strength and temperature, which have

Table 5 | Comparison of different materials used for removal of phenanthrene (PHEN) and pyrene (PYR) from aqueous solutions

Adsorbent	Dosage (g L^{-1})	Contact time	Removal efficiency (%)	Adsorption capacity (mg g^{-1})	Reference
Iron oxide nanoparticles	0.09	2.5 hours	98	2.8 (PYR)	Hassan *et al.* (2018)
Coke derived from porous carbon	1.00	7 hours	99	6.2 (PHEN) 5.0 (PYR)	Yuan *et al.* (2010)
Wood char	0.005	9 days	≥ 60	–	Wang *et al.* (2006)
Leonardite (immature coal)	1.00	24 hours	95 (PYR)	–	Zeledón-Toruño *et al.* (2007)
Wood ash obtained at 800 °C	10	24 hours	100 (PYR)	–	Pérez-Gregorio *et al.* (2010)
Biochar obtained at 800 °C	2	–	>95 (PYR & PHEN)	–	Li *et al.* (2014)
Powdered activated carbon (anthracite and coconut shell based)	1.25	30 days	98 (PYR)	–	Amstaetter *et al.* (2012)
Periodic mesoporous organosilica	1.00	24 hours	70	2.6 (PYR)	Vidal *et al.* (2011)
Activated carbon	0.5	10 hours	74.9	1.3 (PHEN)	Liu *et al.* (2016)
Composite of activated carbon and titanate nanotubes	0.5	3 hours	96.8	12.1 (PHEN)	Liu *et al.* (2016)
Graphene nanosheets	0.5	90 hours	–	116 (PHEN) 123 (PYR)	Wang *et al.* (2014)
Graphene oxide	0.5	90 hours	–	5.9 (PHEN) 6.12 (PYR)	Wang *et al.* (2014)
Graphene coated materials	0.5	36 hours	80	1.74 (PHEN)	Yang *et al.* (2015)
Graphene wool	*0.67*	*24 hours*	*98.5–99.9*	*5 (PHEN)* *20 (PYR)*	*This work*

environmental significance with respect to removal of organic pollutants in aqueous medium, was not reported for TNT@AC and GNS (Wang *et al.* 2014; Liu *et al.* 2016). This makes it difficult to ascertain the efficiency of the adsorbents at variable process conditions, whilst these variables were comprehensively evaluated for GW in this study.

The choice of adsorbent for water treatment applications depends on several factors such as efficiency, non-toxicity, availability of material, flexibility, and reusability. Graphene wool shows great potential for water treatment applications considering that it has a removal efficiency >99%. GW has a very high volume-to-mass ratio (low density) and is highly porous, which makes it a suitable packing material and polishing tool in water treatment applications, because it allows for easy flow of water.

CONCLUSION

These results are of great importance for potential environmental and industrial applications of GW for the removal of aromatic compounds from large volumes of aqueous solutions. Thermodynamic, kinetic, and isotherm studies showed that the adsorption process of pyrene and phenanthrene onto graphene wool is endothermic and spontaneous in nature. A detailed analysis of isotherm, kinetic and thermodynamic parameters validates the occurrence of strong interaction between GW and the selected PAHs, indicating chemisorption. The q_{max} of GW for PHEN and PYR obtained from the Langmuir isotherms was 5 and 20 mg g^{-1} respectively, which was among the highest values for PHEN and PYR adsorption reported in the literature. The isotherm and kinetic data fit well to the Sips model and second-order kinetic models and PAH concentration played a significant role in determining which isotherm model best fit experimental data. The dominant causes of the sorbate–sorbent affinities are π-π interactions between GW and the conjugated benzene rings of the selected PAHs, together with other complementary sorption mechanisms such as pore filling and hydrophobic effects.

The result of the effect of ionic strength on PHEN and PYR sorption onto GW indicates that the salting-out effect was likely to overcome the influence of competitive sorption, resulting in higher adsorption capacities and removal efficiencies at higher TDS/salinity levels. The optimum pH for the efficient adsorption of the selected PAHs onto GW was determined to be acidic. Furthermore, the experimental results revealed that spent GW can be regenerated and reutilized via facile solvent extraction and thermal regeneration procedures. Thus, both fresh and regenerated GW adsorbents are economically viable for adsorption of organic pollutants, specifically PAHs.

This comprehensive study revealed that the removal efficiency of PAHs from artificial contaminated water is 98.5 and 99.9% for pyrene and phenanthrene, respectively, under optimum process conditions and adsorption increased with increase in the selected PAH concentration. This suggests that removal of PAHs from contaminated or polluted water can be successfully achieved using GW and that this material may be employed in water treatment plants as a polishing tool.

ACKNOWLEDGEMENTS

Authors acknowledge the University of Pretoria Commonwealth Doctoral Scholarship funding (AA) and the Departments of Chemistry and Physics at the University of Pretoria, especially Prof. Ncholu Manyala, Dr Liezel Van der Merwe and Genna-Leigh Schoonraad for assistance.

CONFLICT OF INTEREST

The authors declare that there is no conflict of interest regarding the publication of this article.

SUPPLEMENTARY MATERIAL

The Supplementary Material for this paper is available online at https://dx.doi.org/10.2166/wst.2020.011.

REFERENCES

Abdel-Shafy, H. I. & Kamel, A. H. 2016 Groundwater in Egypt issue: resources, location, amount, contamination, protection, renewal, future overview. *Egyptian Journal of Chemistry* **59**, 321–362.

Abdel-Shafy, H. I., Salem, M. A., Mansour, M. S. M., El-Khateeb, M. A. & Abdel-Shafy, S. H. 2016 Drinking water issue in North-West Sinai: the problem and solution in a case study. *Egyptian Journal of Chemistry* **59**, 229–240.

Ahmed, I. M. & Gasser, M. S. 2012 Adsorption study of anionic reactive dye from aqueous solution to Mg-Fe-CO_3 layered double hydroxide (LDH). *Applied Surface Science* **259**, 650–656.

Allen, S. J., McKay, G. & Porter, J. F. 2004 Adsorption isotherm models for basic dye adsorption by peat in single and binary

component systems. *Journal of Colloid and Interface Science* **2**, 322–333.

Amstaetter, K., Eek, E. & Cornelissen, G. 2012 Sorption of PAHs and PCBs to activated carbon: coal versus biomass-based quality. *Chemosphere* **87** (5), 573–578.

Berset, J. D., Ejem, M., Holzer, R. & Lischer, P. 1999 Comparison of different drying, extraction and detection techniques for the determination of priority polycyclic aromatic hydrocarbons in background contaminated soil samples. *Analytica Chimica Acta* **383** (2), 263–275.

Cai, S.-S., Syage, J. A., Hanold, K. A. & Balogh, M. P. 2009 Ultraperformance liquid chromatography – atmospheric pressure photoionization-tandem mass spectrometry for high-sensitivity and high-throughput analysis of U.S. Environmental Protection Agency 16 priority pollutants polynuclear aromatic hydrocarbons. *Analytical Chemistry* **81** (6), 2123–2128.

Chen, J., Chen, W. & Zhu, D. 2008 Adsorption of nonionic aromatic compounds to single-walled carbon nanotubes: effects of aqueous solution chemistry. *Environmental Science and Technology* **42** (19), 7225–7230.

Cornelissen, G., Gustafsson, Ö., Bucheli, T. D., Jonker, M. T. O., Koelmans, A. A. & van Noort, P. C. M. 2005 Extensive sorption of organic compounds to black carbon, coal, and kerogen in sediments and soils: mechanisms and consequences for distribution, bioaccumulation, and biodegradation. *Environmental Science and Technology* **39** (18), 6881–6895.

Hassan, S. S. M., Abdel-Shafy, H. I. & Mansour, M. S. M. 2018 Removal of pyrene and benzo(a)pyrene micropollutant from water via adsorption by green synthesized iron oxide nanoparticles. *Advances in Natural Sciences: Nanoscience and Nanotechnology* **9** (1), 015006.

Huang, W., Schlautman, M. A. & Weber, W. J. 1996 A distributed reactivity model for sorption by soils and sediments: the influence of near-surface characteristics in mineral domains. *Environmental Science and Technology* **30** (10), 2993–3000.

IARC (International Agency for Research on Cancer) 2010 *IARC Monographs on the Evaluation of Carcinogenic Risks to Humans*, Vol. 92. World Health Organization, Lyon, France, pp. 1–853.

Khan, E., Khaodhir, S. & Rotwiron, P. 2007 Polycyclic aromatic hydrocarbon removal from water by natural fiber sorption. *Water Environment Research* **79** (8), 901–911.

Lamichhane, S., Bal Krishna, K. C. & Sarukkalige, R. 2016 Polycyclic aromatic hydrocarbons (PAHs) removal by sorption: a review. *Chemosphere* **148**, 336–353.

Li, H., Qu, R., Li, C., Guo, W., Han, X., He, F., Ma, Y. & Xing, B. 2014 Selective removal of polycyclic aromatic hydrocarbons (PAHs) from soil washing effluents using biochars produced at different pyrolytic temperatures. *Bioresource Technology* **163**, 193–198.

Liu, W., Cai, Z., Zhao, X., Wang, T., Li, F. & Zhao, D. 2016 High-capacity and photoregenerable composite material for efficient adsorption and degradation of phenanthrene in water. *Environmental Science and Technology* **50** (20), 11174–11183.

Lu, Y. & Pignatello, J. J. 2002 Demonstration of the 'conditioning effect' in soil organic matter in support of a pore deformation mechanism for sorption hysteresis. *Environmental Science and Technology* **36** (21), 4553–4561.

Martínez, M., Miralles, N., Hidalgo, S., Fiol, N., Villaescusa, I. & Poch, J. 2006 Removal of lead(II) and cadmium(II) from aqueous solutions using grape stalk waste. *Journal of Hazardous Materials* **133** (1), 203–211.

Ndiaye, N. M., Ngom, B. D., Sylla, N. F., Masikhwa, T. M., Madito, M. J., Momodu, D., Ntsoane, T. & Manyala, N. 2018 Three dimensional vanadium pentoxide/graphene foam composite as positive electrode for high performance asymmetric electrochemical supercapacitor. *Journal of Colloid and Interface Science* **532**, 395–406.

Nguyen, T. H., Sabbah, I. & Ball, W. P. 2004 Sorption nonlinearity for organic contaminants with diesel soot: method development and isotherm interpretation. *Environmental Science and Technology* **38** (13), 3595–3603.

Ololade, I. A., Adeola, A. O., Oladoja, N. A., Ololade, O. O., Nwaolisa, S. U., Alabi, A. B. & Ogungbe, I. V. 2018 In-situ modification of soil organic matter towards adsorption and desorption of phenol and its chlorinated derivatives. *Journal of Environmental Chemical Engineering* **6** (2), 3485–3494.

Pérez-Gregorio, M. R., García-Falcón, M. S., Martínez-Carballo, E. & Simal-Gándara, J. 2010 Removal of polycyclic aromatic hydrocarbons from organic solvents by ashes wastes. *Journal of Hazardous Materials* **178** (1), 273–281.

Rahman, M. S. & Islam, M. R. 2009 Effects of pH on isotherms modeling for Cu(II) ions adsorption using maple wood sawdust. *Chemical Engineering Journal* **149**, 273–280.

Schoonraad, G.-L., Madito, M. J., Manyala, N. & Forbes, P. 2020 Synthesis and optimisation of a novel graphene wool material by atmospheric pressure chemical vapour deposition. *Journal of Materials Science* **55**, 545–564.

Sears, G. W. 1956 Determination of specific surface area of colloidal silica by titration with sodium hydroxide. *Analytical Chemistry* **28** (12), 1981–1983.

Sepehr, M. N., Al-Musawi, T. J., Ghahramani, E., Kazemian, H. & Zarrabi, M. 2017 Adsorption performance of magnesium/aluminum layered double hydroxide nanoparticles for metronidazole from aqueous solution. *Arabian Journal of Chemistry* **10** (5), 611–623.

Stoller, M. D., Park, S., Zhu, Y., An, J. & Ruoff, R. S. 2008 Graphene-based ultracapacitors. *Nano Letters* **8** (10), 3498–3502.

Torabian, A., Kazemian, H., Seifi, L., Bidhendi, G. N., Azimi, A. A. & Ghadiri, S. K. 2010 Removal of petroleum aromatic hydrocarbons by surfactant-modified natural zeolite: the effect of surfactant. *CLEAN – Soil, Air, Water* **38** (1), 77–83.

Ukalska-Jaruga, A., Smreczak, B. & Klimkowicz-Pawlas, A. 2019 Soil organic matter composition as a factor affecting the accumulation of polycyclic aromatic hydrocarbons. *Journal of Soils and Sediments* **19** (4), 1890–1900.

Vidal, C. B., Barros, A. L., Moura, C. P., de Lima, A. C. A., Dias, F. S., Vasconcellos, L. C. G., Fechine, P. B. A. & Nascimento, R. F. 2011 Adsorption of polycyclic aromatic hydrocarbons

from aqueous solutions by modified periodic mesoporous organosilica. *Journal of Colloid and Interface Science* **357** (2), 466–473.

Wang, X., Sato, T. & Xing, B. 2006 Competitive sorption of pyrene on wood chars. *Environmental Science and Technology* **40** (10), 3267–3272.

Wang, J., Chen, Z. & Chen, B. 2014 Adsorption of polycyclic aromatic hydrocarbons by graphene and graphene oxide nanosheets. *Environmental Science and Technology* **48** (9), 4817–4825.

Xu, J., Wang, L. & Zhu, Y. 2012 Decontamination of bisphenol-a from aqueous solution by graphene adsorption. *Langmuir* **28** (22), 8418–8425.

Yakout, S. M. & Daifullah, A. A. M. 2013 Removal of selected polycyclic aromatic hydrocarbons from aqueous solution onto various adsorbent materials. *Desalination and Water Treatment* **51** (34–36), 6711–6718.

Yang, K. & Xing, B. 2007 Desorption of polycyclic aromatic hydrocarbons from carbon nanomaterials in water. *Environmental Pollution* **145** (2), 529–537.

Yang, X., Li, J., Ren, X., Huang, Y. & Wang, X. 2013 Adsorption of naphthalene and its derivatives on magnetic graphene composites and the mechanism investigation. *Colloids and Surfaces A* **422**, 118–125.

Yang, K., Chen, B. & Zhu, L. 2015 Graphene-coated materials using silica particles as a framework for highly efficient removal of aromatic pollutants in water. *Scientific Reports* **5**, 11641.

Yu, F., Ma, J. & Bi, D. 2015 Enhanced adsorptive removal of selected pharmaceutical antibiotics from aqueous solution by activated graphene. *Environmental Science and Pollution Research* **22** (6), 4715–4724.

Yuan, M., Tong, S., Zhao, S. & Jia, C. Q. 2010 Adsorption of polycyclic aromatic hydrocarbons from water using petroleum coke-derived porous carbon. *Journal of Hazardous Materials* **181** (1–3), 1115–1120.

Zeledón-Toruño, Z. C., Lao-Luque, C., de las Heras, F. X. C. & Sole-Sardans, M. 2007 Removal of PAHs from water using an immature coal (leonardite). *Chemosphere* **67** (3), 505–512.

Zhang, Y.-L., Liu, Y.-J., Dai, C.-M., Zhou, X.-F. & Liu, S.-G. 2014 Adsorption of clofibric acid from aqueous solution by graphene oxide and the effect of environmental factors. *Water, Air, & Soil Pollution* **225** (8), 2064–2074.

Zhao, G. X., Li, J. X. & Wang, X. K. 2011 Kinetic and thermodynamic study of 1-naphthol adsorption from aqueous solution to sulfonated graphene nanosheets. *Chemical Engineering Journal* **173**, 185–190.

First received 31 October 2019; accepted in revised form 9 January 2020. Available online 20 January 2020

SUPPLEMENTARY INFORMATION

GC-MS ANALYSIS

PAH analysis was carried out with the aid of a gas chromatograph (GC, Agilent 6890) coupled with a mass spectrometer (MSD, Agilent 5975C) in electron impact ionization mode. The analytes (1 µL splitless injection) were separated on a Restek Rxi-PAH column with the following dimensions: 60 m long, 0.25 mm internal diameter and 0.10 µm film thickness. Helium gas of purity > 99 % (Afrox, Gauteng) was used as carrier gas in constant flow mode of 1 mL min^{-1}. The inlet temperature was at 275 ºC and the GC oven temperature was held at 80 ºC for 1 min, then ramped at 30 ºC min^{-1} to 180 ºC, then subsequently to 320 ºC at 5 ºC min^{-1}. The run-time for each injection was 35 min. The ionization potential was 70 eV, the source temperature was 230 ºC and the quadrupole was at 150 ºC. A mass range of m/z 40–350 was recorded in full scan mode. For better sensitivity, the selective ion monitoring mode was employed to detect and quantify the analytes (Munyeza *et al.* 2018). Pure individual standards of pyrene and phenanthrene which had been dissolved in hexane were injected to determine the retention times and mass spectra thereof. Quantification of the selected PAHs was carried out using a six-point calibration with concentrations ranging from 16 to 1600 µg L^{-1} for PHEN and 19 to 1800 µg L^{-1} for PYR. The calibration was derived from the plot of the target analyte peak area versus the concentration of the analyte.

ISOTHERM AND KINETIC DATA ANALYSIS

Adsorption Isotherm

Four different isotherm models were used to fit the adsorption experimental data. These models included the Freundlich, Langmuir, Temkin and D-R isotherm models.

Freundlich Isotherm Model

The Freundlich model, which is used commonly for quantifying hydrophobic organic compounds sorption equilibria has the following form:

$$Non\text{-}linear\ form: : q_e = K_f C_e^N \qquad (1)$$

where q_e is the solid-phase concentration (ng g^{-1}) and C_e is the liquid-phase equilibrium concentration (mg L^{-1}). K_f is the sorption capacity-related parameter and N is the isotherm non-linearity index, an indicator of site energy heterogeneity determined by linear regression of log-transformed data as shown below:

$$Linear\ form:\ Log\ q_e = Log\ K_f + \frac{1}{n} Log\ C_e \qquad (2)$$

The Freundlich isotherm constants K_f and $1/n$ are evaluated from the intercept and the slope respectively, of the linear plot of log q_e versus log C_e (Rahman & Islam 2009).

Langmuir Isotherm Model

The Langmuir mode describing site-limiting sorption equilibrium has the following form:

$$Langmuir: q_e = \frac{q_m K_L Ce}{1 + K_L Ce} \qquad (3)$$

where q_{max} is the maximal sorption capacity and K_L is a solute–surface interaction energy-related parameter. The Langmuir equation can be rearranged to a linear form for the convenience of plotting and determination of the Langmuir constant (K_L). The values of q_{max} and K_L can be determined from the linear plot of $1/q_e$ versus $1/C_e$:

$$Linear\ form:\ \frac{1}{q_e} = \frac{1}{K_L q_{max} C_e} + \frac{1}{q_{max}} \qquad (4)$$

The essential characteristics of the Langmuir isotherm parameters can be used to predict the affinity between the sorbate and the sorbent using the separation factor or dimensionless equilibrium parameter 'R_L', expressed as in the following equation:

$$R_L = \frac{1}{1 + K_L C_0} \qquad (5)$$

where K_L is the Langmuir constant and C_0 is the initial concentration of the PAHs. The value of the separation factor R_L provides important information about the nature of adsorption. The value of R_L is between 0 and 1 for favorable adsorption, while $R_L > 1$ represents unfavorable adsorption and R_L = 1 represents linear adsorption. The adsorption process is irreversible if R_L = 0 (Huang *et al.* 2003; Rahman & Islam 2009).

Dubinin–Radushkevich Isotherm Model

The D-R model was also used to fit experimental adsorption data using equations below:

$$Non\text{-}linear\ form:\ q_e = Q_D\ exp\ (-k_{ad} \cdot \varepsilon^2) \qquad (6)$$

$$Linear\ form:\ lnq_e = lnQ_D - 2B_D RTln(1 + 1/C_e) \qquad (7)$$

where Q_D is the theoretical maximum capacity (mol g^{-1}), B_D is the D-R model constant (kJ mol^{-1} K^{-1}), T is the absolute temperature (K) and R is the gas constant (kJ mol^{-1}). The mean energy of sorption, E (kJ mol^{-1}), is calculated from the relation:

$$E = 1/\sqrt{2B_D} \quad (8)$$

Q_D and B_D can be estimated from the intercept and slope of the plot of ln (q_e) versus ln (1 + $1/C_e$) (Igwe & Augustine 2007).

Temkin Isotherm Model

The non-linear and linearized forms are expressed by the following equations:

$$\textit{Non-linear: } q_e = \frac{RT}{b_T} lnK_T \,.\, C_e \quad (9)$$

$$\textit{Linear form: } q_e = \frac{RT}{b_T} lnK_T + \frac{RT}{b_T} lnC_e \quad (10)$$

where K_T (L g^{-1}) is the Temkin isotherm constant, b_T (J mol^{-1}) is a constant related to the heat of sorption and R (8.314 J mol^{-1} K^{-1}) is the gas constant. A plot of q_e versus ln (C_e) gives a straight-line equation from which K_T and b_T can be evaluated from the slope and the intercept (Mahamadi & Nharingo 2010).

Sips Isotherm Model

The Sips isotherm is used to describe localized adsorption without adsorbate–adsorbate interactions. The Sips model can effectively reduce to the Freundlich model or Langmuir model depending on the value of the equilibrium concentration (C_e). The Sips equation is given as:

$$\textit{Non-linear form: } q_e = \frac{K_s \,.Ce^{\beta s}}{1+ \alpha_s \,.Ce^{\beta s}} \quad (11)$$

$$\textit{Linear form: } \frac{1}{q_e} = \frac{1}{q_{max}K_s}\left(\frac{1}{C_e}\right)^{1/N} + \frac{1}{q_{max}} \quad (12)$$

where K_s (L mg^{-1}) and q_{max} (mg g^{-1}) are the Sips equilibrium constant and maximum adsorption capacity values. The Sips isotherm equation includes the dimensionless heterogeneity factor, n, which describes the system's heterogeneity when its value is between 0 and 1. When n = 1, the Sips equation implies a homogeneous adsorption process (Langmuir) (Allen *et al.* 2004).

Adsorption Kinetics

Pseudo-First-Order Kinetic Model

It is given by equation below:

$$\textit{Non-linear form: } \frac{dq_t}{dt} = k_1(q_e - q_t) \qquad (13)$$

$$\textit{Linear form: } log(q_e - q_t) = log q_e - \frac{k_1}{2.303} \qquad (14)$$

where q_t and q_e are the amount of solute sorbed per mass of sorbent (mg g^{-1}) at any time and at equilibrium, respectively, and k_1 is the rate constant of first-order sorption (min^{-1}). The straight-line plot of log ($q_e - q_t$) against t gives log (q_e) as slope and intercept equal to $k_1/2.303$. Hence the amount of solute sorbed per gram of sorbent at equilibrium (q_e) and the first-order sorption rate constant (k_1) can be evaluated from the slope and the intercept (Lagergren 1898; Kowanga *et al.* 2016).

Pseudo-Second-Order Kinetic Model

The model is represented as follows:

$$\textit{Non-linear form: } \frac{dq_t}{dt} = K_1(q_e - q_t)^2 \qquad (15)$$

$$\textit{Linear form: } \frac{t}{q_t} = \frac{1}{k_2 q_{e^2}} + \left(\frac{1}{q_e}\right) \qquad (16)$$

The kinetic parameters can be evaluated with a straight-line plot of t/q_t against t; q_e and k_2 can be deduced from the slope and intercept respectively. The initial sorption rate is defined by the following equation:

$$h = k_2 q_{e^2} \qquad (17)$$

where k_2 is the rate constant, and q_t is the PAHs uptake capacity at any time t (Kalavathy *et al.* 2005).

FIGURES AND TABLES

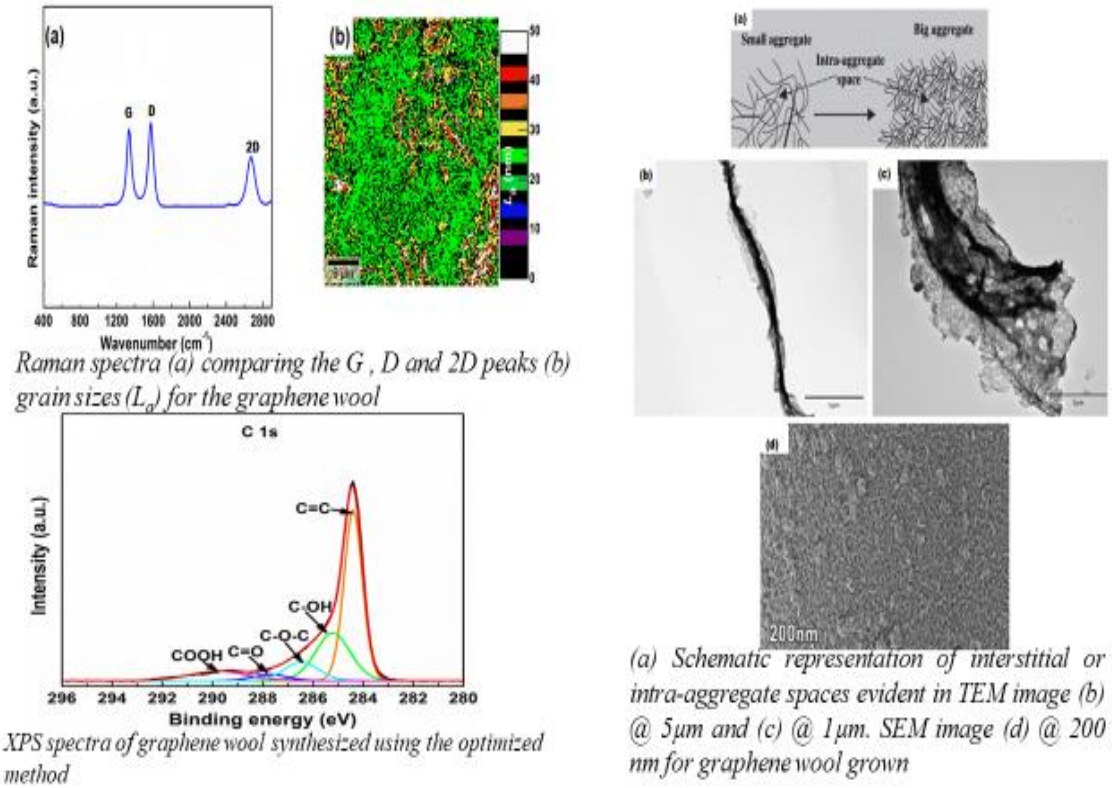

Figure S1: Raman spectroscopy (top-left), X-ray photoelectron spectroscopy (bottom-left), scanning electron microscopy and transmission electron microscopy analysis of graphene wool (right). Adapted from Schoonraad *et al*. (2020) with slight modifications.

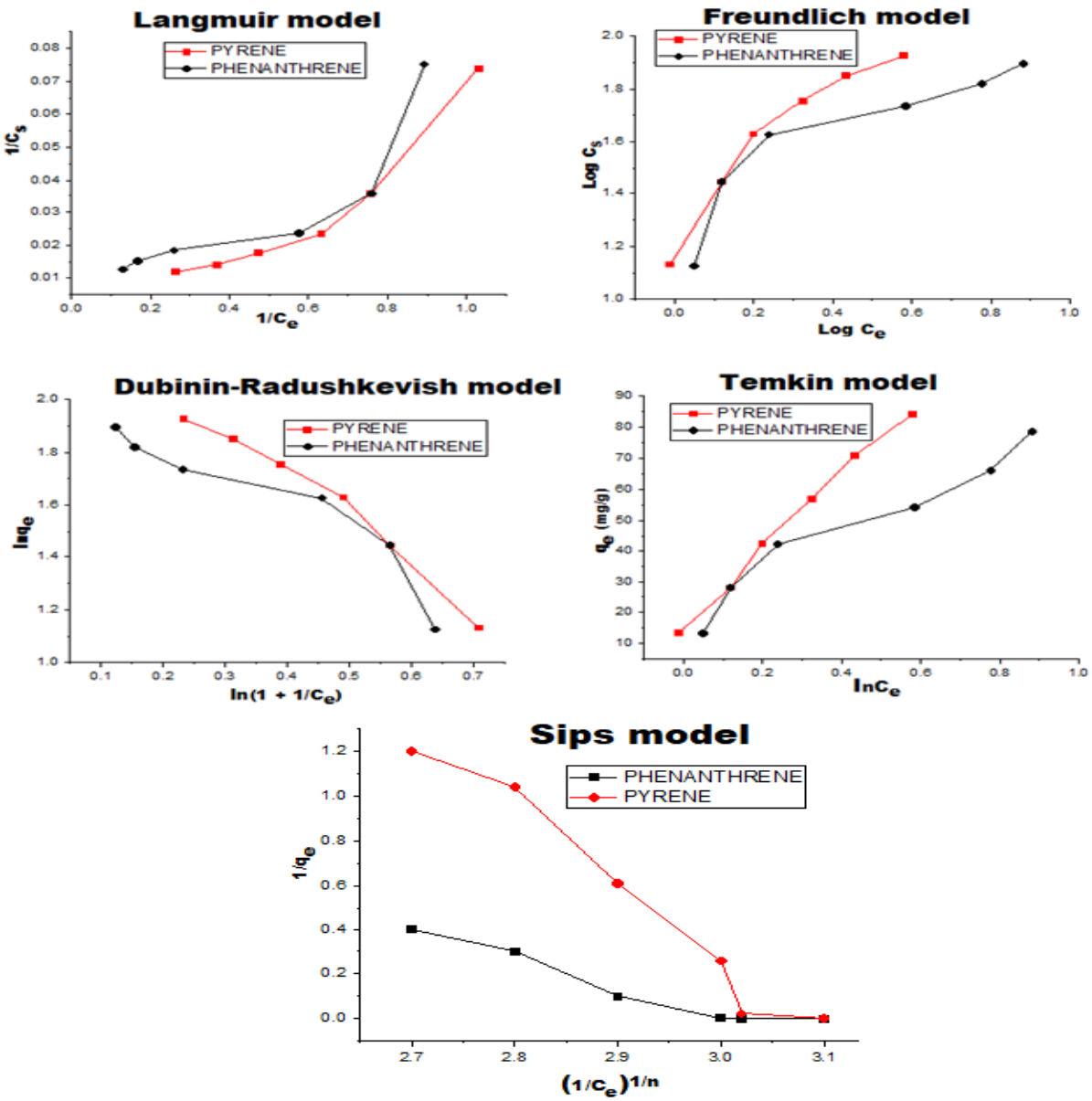

Figure S2: Adsorption isotherm models for phenanthrene and pyrene onto graphene wool in part-per-trillion concentrations (300–800 ng L^{-1}) (experimental conditions: dosage = 20 mg per 30 mL; mixing rate = 220 rpm; T = 25 ± 1 °C; contact time = 24 hours; pH (PYR) = 6.7 ± 0.2 and pH (PHEN)= 6.8 ± 0.2).

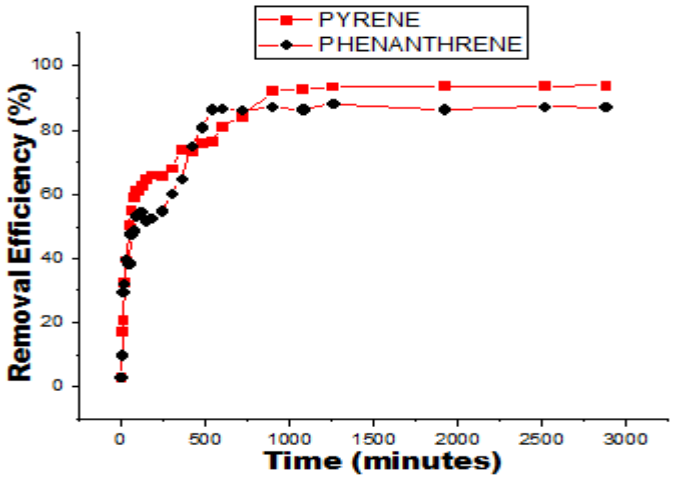

Figure S3: Profile of time–concentration pyrene and phenanthrene adsorption onto graphene wool (experimental conditions: C_o = 50 ng L^{-1}; dosage = 50 mg per 100 mL; mixing rate = 200 rpm; T = 25 ± 1 °C; pH (PYR) = 6.7 ± 0.2 and pH (PHEN)= 6.8 ± 0.2).

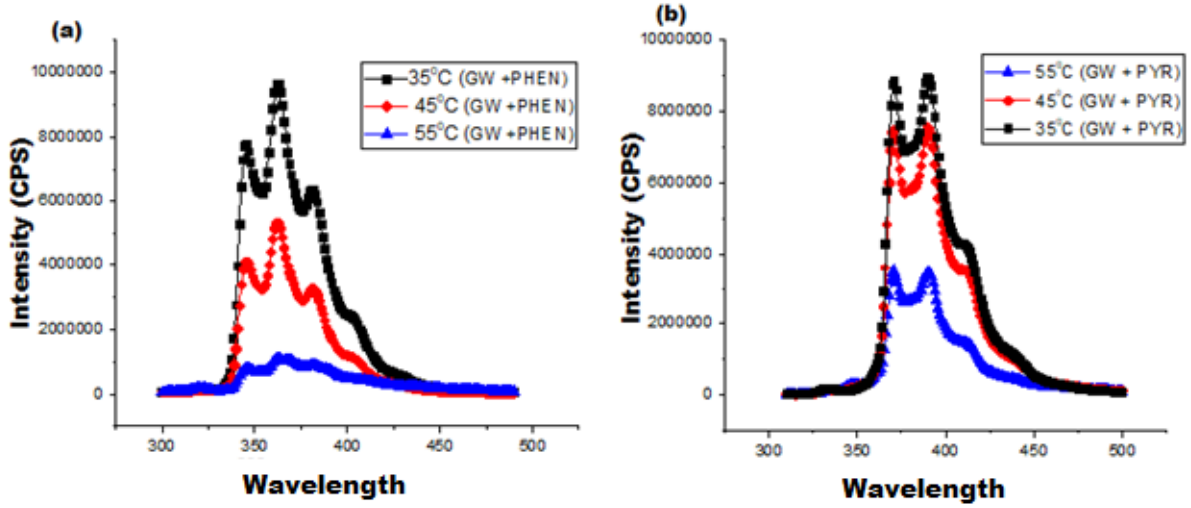

Figure S4: Fluorescence spectra of (a) phenanthrene excited at 290 nm, (b) pyrene excited at 300 nm; after interaction with GW at different temperatures (experimental conditions: mass of GW: 0.02 g; initial conc. of PAHs: 1 ppm; equilibration time: 24 h).

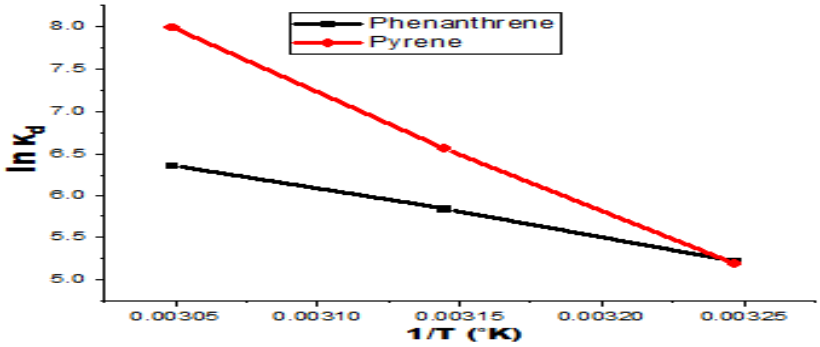

Figure S5: Van 't Hoff equation for phenanthrene and pyrene adsorption onto GW from solution.

Table S1: Selected physicochemical properties of the sorbates

PAH	Molecular structure	Molecular formula	[a]Log K_{ow}	[a]S_w	[a]M_w	[b]B_p	[c]M_D (Å×× Å)
Phenanthrene	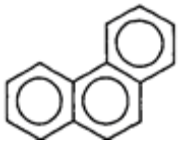	$C_{14}H_{10}$	4.46	1.18	178.2	340	11.7×8.0×3.9
Pyrene	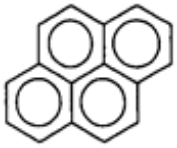	$C_{16}H_{10}$	5.13	0.135	202.3	404	11.7×9.3×3.9

Log K_{ow}: octanol–water partition coefficient, S_w: water solubility (mg L^{-1}), M_w: molecular weight (g $cmol^{-1}$), B_p: boiling points (ºC). M_D: molecular dimension. Cited from [a](Sun *et al.* 2013), [b](Yakout & Daifullah 2013), [c](Potin *et al.* 2004).

Table S1: Coefficients of four different sorption isotherm models for phenanthrene and pyrene adsorption by graphene wool and their correlation coefficients (R^2) in part-per-trillion PAH concentrations (experimental conditions: dosage = 20 mg per 30 mL; mixing rate = 20 rpm; T = 25 ± 1 °C; initial conc.: 300–800 ng L^{-1}; contact time = 24 hours; pH = 6.8 ± 0.2 for PHEN and 6.9 + 0.2 for PYR)

Adsorption isotherm model	Parameter	PAH	
		Phenanthrene	Pyrene
Dubinin–Radushkevich	Q_D (mol g^{-1})	4.62	4.02
	B_D (kJ mol^{-1} K^{-1})	1.47×10^{-4}	1.16×10^{-4}
	E (kJ mol^{-1})	58.14	65.36
	R^2	0.8770	0.9684
Freundlich	n	1.3797	0.7699
	K_f ($ng^{1-1/n}$ $L^{1/n}$ g^{-1})	18.4178	19.5140
	R^2	0.8139	0.9086
Langmuir	q_{max} (ng g^{-1})	1000	59.88
	K_L	0.016	0.2128
	R_L	0.510	0.072
	R^2	0.7441	0.8895
Sips	q_{max} (ng g^{-1})	3.39	0.83
	K_s (L mg^{-1})	9.6×10^{-4}	8.9×10^{-4}
	N	0.22	0.33
	R^2	0.9285	0.9893
Temkin	b_T (kJ mol^{-1})	174.48	305.87
	K_T (L g^{-1})	1.12×10^{-7}	1.67×10^{-7}
	R^2	0.9443	0.9928

Table S3: Effect of ionic strength on phenanthrene and pyrene removal by GW from aqueous solution

Ionic strength	Parameters	Phenanthrene	Pyrene
0.01 mol L^{-1} [NaCl]	R^2	0.9246	0.9043
	K_d	166.24	506.57
	% Removal	98.61	99.37
0.1 mol L^{-1} [NaCl]	R^2	0.9586	0.9985
	K_d	319.97	612.87
	% Removal	98.76	99.38
1 mol L^{-1} [NaCl]	R^2	0.9770	0.9979
	K_d	340.85	742.34
	% Removal	99.11	99.59

Table S4: Effect of temperature on phenanthrene and pyrene removal from aqueous solution

Temperature (°C)	Parameters	Phenanthrene	Pyrene
35	R^2	0.8702	0.9885
	K_d	184.69	242.99
	% Removal	98.5	98.7
45	R^2	0.9780	0.8894
	K_d	342.24	763.06
	% Removal	99.3	99.4
55	R^2	0.9466	0.9769
	K_d	578.8	2169.7
	% Removal	99.7	99.5

References

Allen S. J., Mckay G. & Porter J. F. (2004) Adsorption isotherm models for basic dye adsorption by peat in single and binary component systems. *Journal of Colloid and Interface Science* (2), 322–333.

Huang W. L., Peng P. A. & Yu Z. Q. (2003) Effects of organic matter heterogeneity on sorption and desorption of organic contaminants by soils and sediments. *Applied Geochemistry* 18, 955–972.

Igwe J. C. & Augustine A. A. (2007) Equilibrium sorption isotherm studies of Cd(II), Pb(II) and Zn(II) ions detoxification from waste water using unmodified and EDTA-modified maize husk. *Electronic Journal of Chemistry* 10(4), 535–548.

Kalavathy M. H., Karthikeyan T., Rajgopal S. & Miranda L. R. (2005) Kinetic and isotherm studies of Cu(II) adsorption onto H_3PO_4-activated rubber wood sawdust. *Journal of Colloid and Interface Science* 292(2), 354–362.

Kowanga K. D., Gatebe E., Mauti G. O. & Mauti E. M. (2016) Kinetic, sorption isotherms, pseudo-first-order model and pseudo-second-order model studies of Cu(II) and Pb(II) using defatted *Moringa oleifera* seed powder. *Journal of Phytopharmacology* 5(2), 71–78.

Lagergren S. (1898) About the theory of so-called adsorption of soluble substances. *Kungliga Svenska Veteskapsakademiens Handlingar, Band* 24, 1–29.

Mahamadi C. & Nharingo T. (2010) Utilization of water hyacinth weed (*Eichhornia crassipes*) *f*or the removal of Pb(II), Cd(II) and Zn(II) from aquatic environments: an adsorption isotherm study. *Environmental Technology* 31(11), 1221–1228.

Munyeza C. F., Dikale O., Rohwer E. R. & Forbes P. B. C. (2018) Development and optimization of a plunger assisted solvent extraction method for polycyclic aromatic hydrocarbons sampled onto multi-channel silicone rubber traps. *Journal of Chromatography A* 1555, 20–29.

Potin O., Veignie E. & Rafin C. (2004) Biodegradation of polycyclic aromatic hydrocarbons (PAHs) by *Cladosporium sphaerospermum* isolated from an aged PAH contaminated soil. *FEMS Microbiology Ecology* 51(1), 71–78.

Rahman M. S. & Islam M. R. (2009) Effects of pH on isotherms modeling for Cu(II) ions adsorption using maple wood sawdust. *Chemical Engineering Journal* 149, 273–280.

Schoonraad G.-L., Madito M. J., Manyala N. & Forbes P. (2020) Synthesis and optimisation of a novel graphene wool material by atmospheric pressure chemical vapour deposition. *Journal of Materials Science* 55, 545–564.

Sun Y., Yang S., Zhao G., Wang Q. & Wang X. (2013) Adsorption of polycyclic aromatic hydrocarbons on graphene oxides and reduced graphene oxides. *Chemistry – An Asian Journal* 8(11), 2755–2761.

Yakout S. M. & Daifullah A. A. M. (2013) Removal of selected polycyclic aromatic hydrocarbons from aqueous solution onto various adsorbent materials. *Desalination and Water Treatment* 51(34–36), 6711–6718.

Chapter 5 Competitive adsorption of fifteen polycyclic aromatic hydrocarbons using reusable graphene wool

This chapter evaluates multi-solute adsorption of selected 2-6 ringed PAHs in comparison with single-solute sorption experiments. The role of hydrophobicity of PAHs and adsorbent dosage in the sorbate-sorbent interactions was assessed. The format is as published in Environmental Technology.

Article

Adeola, A.O., Forbes, P.B.C. (2020). Assessment of reusable graphene wool adsorbent for the simultaneous removal of selected 2-6 ringed polycyclic aromatic hydrocarbons from aqueous solution. Environmental Technology. DOI: 10.1080/09593330.2020.1824024

ENVIRONMENTAL TECHNOLOGY
https://doi.org/10.1080/09593330.2020.1824024

Assessment of reusable graphene wool adsorbent for the simultaneous removal of selected 2–6 ringed polycyclic aromatic hydrocarbons from aqueous solution

Adedapo O. Adeola and Patricia B.C. Forbes

Faculty of Natural and Agricultural Sciences, Department of Chemistry, University of Pretoria, Pretoria, South Africa

ABSTRACT

The United States Environmental Protection Agency categorized polycyclic aromatic hydrocarbons (PAHs) as hazardous to humans upon acute and/or chronic exposure. This study investigated the simultaneous adsorption of several PAHs onto graphene wool (GW), thereby providing holistic insights into the competitive adsorption of PAHs onto graphene-based materials. SEM, TEM and FTIR provided evidence for the adsorption of PAHs and successful regeneration of the adsorbent accompanied by distinct morphological changes. Isotherm experiments revealed that adsorption of PAHs was significantly influenced by hydrophobic interactions between the sorbate and hydrophobic surface of GW. The Freundlich multilayer isotherm model best fit the experimental data obtained for both multi-component PAH and single-solute experiments as indicated by the Error Sum of Squares (SSE) obtained from nonlinear regression analysis. Experiments revealed that competitive adsorption had a limiting effect on the overall adsorption capacity as q_{max} and K_d were higher in single-solute than multi-component PAH experiments. The results suggest that partition distribution coefficients (K_d) between the solid–liquid interphase played a significant role in the overall adsorption and a positive correlation between K_d and LogK_{ow} of PAHs was established in single-solute experiments. Sorption-desorption experiments revealed that PAHs were adsorbed with a maximum removal efficiency of 100% at an optimum GW dosage of 2 g/L. Adsorption thermodynamics revealed that PAH adsorption onto GW is spontaneous and endothermic. The adsorbent was regenerated and reused for up to six times and its efficiency remained fairly constant.

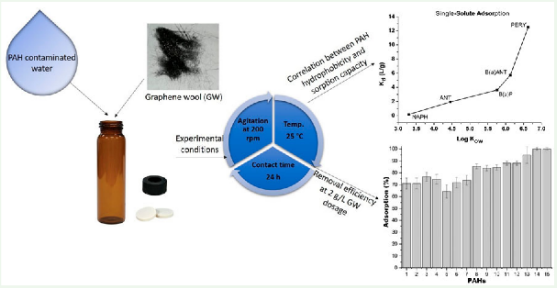

ARTICLE HISTORY
Received 30 April 2020
Accepted 1 September 2020

KEYWORDS
Polycyclic aromatic hydrocarbons; graphene wool; competitive sorption; decontamination; aqueous solution

1. Introduction

Polycyclic aromatic hydrocarbons (PAHs) are a ubiquitous and toxic class of xenobiotic organic contaminants composed of carbon and hydrogen; with proven carcinogenicity such as skin, lung and bladder cancer [1]. They are released into the environment via incomplete combustion, forest fires, burning of fuels, oil spills, urban run-off and other anthropogenic activities [2,3]. PAHs are inadvertently found in food, air, soil, sediment, drinking water and other water bodies [4,5]. Thus the need for a sustainable, efficient and cost-effective remediation approach cannot be over-emphasized.

Graphene has attracted immense global attention from researchers due its structural tunability, thermodynamic stability and well-defined physicochemical properties [6]. Recent developments arising from studies related to graphene has brought about promising applications, ranging from biomedicine, nano-sensors, supercapacitors, pollution monitoring, control and remediation [7–14]. In the field of environmental science, graphene-based materials have been harnessed as efficient next-generation sorbents for water purification applications because their surfaces are largely hydrophobic, porous, and they possess high adsorption

CONTACT Patricia B.C. Forbes patricia.forbes@up.ac.za; Faculty of Natural and Agricultural Sciences, Department of Chemistry, University of Pretoria, Lynnwood Road, Hatfield, Pretoria 0002, South Africa https://www.researchgate.net/profile/

affinities for a vast number of organic contaminants (OCs) [15].

The graphene wool (GW) used in this study was synthesized via a chemical deposition method using quartz wool as a substrate, under optimized flow rates of hydrogen, argon and methane gas as precursors [16]. The adsorption and desorption of phenanthrene and pyrene onto this wool-like graphene adsorbent have been reported based on single-solute, batch sorption experiments [13]. The sorption kinetics were found to follow a pseudo-second-order reaction pathway and 24 h was suitable for optimum adsorption. Furthermore, because single-solute experiments were conducted, several sorption models were easily fitted to isotherm data and a multilayer adsorption mechanism was described via Freundlich and Sips models with $R^2 > 0.99$, and removal efficiencies for individual PAH was > 98%.

However, PAHs are a large class of organic compounds which are rarely found as single solutes in real-life polluted samples [17,18]. Therefore, to establish the actual robustness and efficiency of this novel graphene wool in the decontamination of field water samples, it is necessary to carry out multi-solute, competitive adsorption experiments and account for optimum adsorbent dosage under multi-solute contamination conditions. Furthermore, information regarding the adsorption of 15 co-existing PAHs onto any absorbent is not available in literature, which makes it almost impossible to fully understand the adsorptive behaviour of the PAH class of pollutants in a multi-solute environment.

Therefore, the aim of this study was to evaluate the sorption mechanism controlling the interaction between graphene wool and selected polycyclic aromatic hydrocarbons in aqueous solution via single-solute and multi-component (PAH mix) batch experiments. Furthermore, effects of temperature (adsorption thermodynamics) and adsorbent dosage were determined, as well as removal efficiency from graphene wool (GW) wherein several cycles of regeneration and re-use were evaluated.

2.0. Materials and method

2.1. Materials

9–30 µm coarse quartz wool (Arcos Organics, New Jersey, USA), argon and hydrogen (99.999%, Afrox, South Africa), calcium chloride, sodium azide, hexane and acetone (98% purity, Sigma-Aldrich, Germany) were purchased. A QTM PAH mix and internal standard (Sigma-Aldrich, USA), were used for PAH mix adsorption experiments. The mixed standard contained 2000mg/L of 15 EPA priority polycyclic aromatic hydrocarbons [19], prepared in dichloromethane (naphthalene, acenaphthene, acenaphthylene, fluorene, phenanthrene, anthracene, fluoranthene, pyrene, benzo(a)anthracene, chrysene, benzo (b)fluoranthene, benzo(a)pyrene, indeno (1,2,3-cd)pyrene, dibenz(a,h)anthracene and benzo(g,h,i) perylene); and the internal standard used was mixture of d8-naphthalene, d10-phenathrene, d10-pyrene and d12-chrysene. Neat standards of naphthalene, anthracene, benzo(a)anthracene, benzo(a)pyrene and benzo(ghi)perylene respectively (99% purity) were purchased from Supelco (USA) for use in single-solute batch experiments. Polytetrafluoroethylene (PTFE) membrane syringe filters (0.22 and 0.45 µm) were purchased from Stargate Scientific (South Africa). Reversed-phase C_{18} solid-phase extraction (SPE) cartridges were purchased from CNW Technologies (Shanghai, China). All the solutions were prepared with ultra-pure water obtained from a Milli-Q water (9.2 µS/cm^3) purification system (Millipore, Bedford, MA, USA).

2.2. Adsorbent

Graphene wool was synthesized by a chemical vapour deposition (CVD) method using the optimum established procedure [16]. The quartz wool was placed in a horizontal quartz tube, with the prescribed flow rate of argon, hydrogen and methane gas released at specified time intervals and at an elevated temperature of 1200°C. The graphene wool was characterized by high resolution transmission electron microscopy (TEM) using a JEOL JEM 2100F (JOEL Ltd, Tokyo, Japan) operated at 200 kV; scanning electron microscopy was also carried out with the aid of Zeiss Ultra Plus 55 field emission scanning electron microscope (FE-SEM), operated at 2.0 kV (Zeiss, Germany); Fourier transformed infrared spectroscopy (FTIR) was carried out using a Bruker Alpha-T spectrometer (Bruker Optik GmbH, Ettlingen, Germany), whilst the specific surface area was determined using Sear's method. Refer to [13,16] for a detailed description of the GW synthesis and characterization thereof by various means including high-resolution X-ray photoelectron spectroscopy (XPS) and Raman spectroscopy.

2.3. Sorption isotherm experiments

Batch adsorption experiments of the PAH mixture and single-solute/single PAHs by graphene wool (GW) were performed in 40 mL PTFE screw-capped amber vials (Stargate Scientific, South Africa) sealed with aluminium foil at 25 ± 1°C. Background solution (pH = 7.0) contained 0.01 mol/L $CaCl_2$ (ACE, South Africa) in deionized water with 200 mg/L NaN_3 (Sigma-Aldrich, Germany) as a biocide. Table 1 provides a list of the PAHs used as sorbates in

Table 1. Physicochemical properties of the 15 target polycyclic aromatic hydrocarbons.

PAHs	Molecular formula[a]	Boiling point (°C)[ab]	Log K_{ow}^{ac}	S_w (mg/L)[a]	M_w (g/mol)[a]
Naphthalene	$C_{10}H_8$	217.9	3.30	31.00	128.17
Acenaphthene	$C_{12}H_{10}$	279.0	3.92	3.90	154.21
Acenaphthylene	$C_{12}H_8$	280.0	3.94	9.00	152.19
Fluorene	$C_{13}H_{10}$	294.0	4.18	1.69	166.22
Phenanthrene	$C_{14}H_{10}$	338.4	4.46	1.10	178.23
Anthracene	$C_{14}H_{10}$	341.3	4.45	1.29	178.23
Fluoranthene	$C_{16}H_{10}$	384.0	5.16	0.26	202.25
Pyrene	$C_{16}H_{10}$	394.0	4.88	0.14	202.25
Benzo(a)anthracene	$C_{18}H_{12}$	437.6	5.76	9.4e-3	228.30
Chrysene	$C_{18}H_{12}$	448.0	5.81	2.0e-3	228.30
Benzo(b)fluoranthene	$C_{20}H_{12}$	481.0	6.12	1.5e-3	252.30
Benzo(a)pyrene	$C_{20}H_{12}$	496.0	6.13	1.62e-3	252.30
Indeno(1,2,3-cd)pyrene	$C_{22}H_{12}$	536.0	6.58	6.9e-4	276.30
Dibenz(a,h)anthracene	$C_{22}H_{14}$	524.0	6.50	5e-4	278.30
Benzo(g,h,i)perylene	$C_{22}H_{12}$	550.0	6.63	2.6e-4	276.30

B_p: boiling point (°C)[b] [25,26], Log K_{ow}: octanol–water partition coefficient[c] [27], S_w: water solubility (mg/L), M_w: molecular weight (g/mol)[a] [28].

this study and their properties. The isotherm experiment was conducted with initial concentrations of the PAH mix and single PAH solutions, ranging from 2 µg/20 mL to 10 µg/20 mL obtained by serial dilution with deionized water and 1% methanol to ensure solubilization of PAHs in aqueous medium [20]. The adsorption of the PAH mix and individual PAHs onto graphene wool was carried out in batch experiments using a thermostated shaking water bath (Wisebath, Celsius Scientific, South Africa). To investigate the effect of initial concentration of the solution, 20 mg of GW was introduced into 5 vials containing 2, 4, 6, 8 and 10 µg /20 mL of PAH mixture and individual PAHs, respectively. Each concentration was tested in triplicate. Desorption experiments were carried out as previously described [21]; immediately after the adsorption studies, the supernatant was completely removed and 20 mL of 0.01 mol/L $CaCl_2$ containing 200 mg/L of sodium azide was added to the solid residue. The amount of PAH recovered in solution was determined after equilibration for 24 h and at 25°C. To determine the effect of adsorbent dosage, adsorption experiments were carried out using varying adsorbent masses (20, 25, 30 and 50 mg), for PAH mix concentrations of both 400 and 500 µg/L, in order to determine the average removal efficiencies per dosage. For all the batch experiments, suspensions were agitated at 200 rpm in a shaking water bath for 24 h at 25°C, based on previous reports [13,22], and subsequently centrifuged at 9860×g for 20 min to recover a clear supernatant solution.

2.4. Quantification

Prior to determination of the equilibrium concentration (C_e) for single-solute sorption experiments, the vials were centrifuged at 9860×g for 20 min and 2 mL aliquots of the supernatants were filtered through 0.45 µm syringe filters. Equilibrium concentrations of naphthalene (NAPH), anthracene (ANT), benzo(a)anthracene (B(a)ANT), benzo(a)pyrene (B(a)p) and benzo(ghi)-perylene (PERY) were determined using a Horiba Jobin Yvon Fluoromax-4 spectrofluorometer (Horiba instruments Inc., Edison, NJ, USA) at excitation wavelengths of 280, 300, 320, 330 and 420 nm respectively, with calibration equations derived from 0.2 µg/20 mL to 10 µg/20 mL concentrations of individual PAHs [13].

Solid-phase extraction (SPE) was carried out with the aid of preconditioned C_{18} SPE cartridges (CNW Technologies, China) for multi-solute adsorption experiments, prior to GC-MS analysis [23]. The supernatant was loaded on the cartridge and washed with 5 mL of methanol/deionized water (50:50). The analytes were eluted with 6 mL hexane using the SPE vacuum pump at a flow rate of 0.5 $mLmin^{-1}$. The eluate recovered was concentrated by reducing its volume to 1 mL under nitrogen flow. A matrix-matched calibration was obtained by spiking 20 mL blank deionized water with 2, 4, 6, 8 and 10 µg/20 mL of PAH mix and carrying out the same SPE extraction explained above (equivalent to 2, 4, 6, 8 and 10 ng of PAH mix injected into the GC column in triplicate) and the resulting calibration line equation was used to calculate the equilibrium concentration (C_e). The concentration of PAHs not adsorbed after agitating the solution for 24 h with GW was determined using gas chromatography (GC, Agilent 6890) hyphenated with mass spectrometry (MSD, Agilent 5975C). The amount of PAHs adsorbed (C_s) was determined by the difference between the initial and equilibrium liquid-phase concentrations (C_e) (Equations (1) and (2)). Each experiment was repeated three times.

$$C_s = \frac{(C_0 - C_e)V_0}{S_m} \quad (1)$$

$$\text{Removal efficiency (\%)} = \frac{(C_0 - C_e)}{C_0} \times 100 \quad (2)$$

where C_o (mg/L) is the initial concentration, C_e (mg/L) is the equilibrium solute concentration, V_o is the initial volume (L) and S_m is the mass (g) of the adsorbent.

Graphene wool was regenerated by rinsing with 10 mL hexane and a mixture of acetone-water (50:50) respectively using a thermostated shaker for 2 hr successively at room temperature. Afterwards, the GW was dried in a muffle furnace (Labotec, South Africa) at a temperature of 70°C for 4 hr and was allowed to cool before re-use.

2.5. GC-MS instrumentation

PAH analysis for multi-solute adsorption experiments was carried out with the aid of a gas chromatograph (GC, Agilent 6890) hyphenated to a mass spectrometer (MSD, Agilent 5975C) in electron impact ionization mode. The analytes (1 µL splitless injection) were separated on a Restek Rxi-PAH column with the following dimensions: 60 m long, 0.25 mm internal diameter and 0.10 µm film thickness. Helium gas of purity > 99% (Afrox, Gauteng) was used as carrier gas in constant flow mode at 1 mL/min. The inlet temperature was at 275°C and the GC oven temperature was held at 80°C for 1 min, then ramped at 30°C/min to 180°C, and subsequently to 320°C at 5°C/min. The run-time for each injection was 75 min. The ionization potential was 70 eV, the source temperature was 230°C and the quadrupole was at 150°C. A mass range of m/z 40–350 was recorded in full scan mode. For better sensitivity, the selective ion monitoring mode was employed to detect and quantify the PAH analytes [24]. The 0.5 ng/µL pure PAH mix standard (Sigma-Aldrich, USA) which had been dissolved in hexane was injected to determine the retention time and mass spectrum of each PAH (Figure 1). The internal standard used was a mixture of d8-naphthalene, d10-phenathrene, d10-pyrene and d12-chrysene (0.5 ng/µL). Quantification of the selected PAHs was carried out using five-point calibration curves with concentrations ranging from 2 µg/20 mL to 10 µg/20 mL for all PAHs used in this study. The calibration was derived from the plot of the target analyte peak area divided by the peak area of the internal standard versus the concentration of analyte.

3.0. Results and discussion

3.1. Sorbent characterization

Comprehensive information regarding the characterization of this novel material is available in the literature [13,16]. In addition, the pH of GW was found to be 6.1 and 7.1 in $CaCl_{2(aq)}$ solution and deionized water respectively. The specific surface area of GW, as determined using Sear's method, is 279 m^2/g, which is lower than the theoretical specific surface area of graphene (2630 m^2/g) due to coverage over the quartz wool which ultimately defines the specific surface area [29,30]. The morphology of the adsorbent in its pristine state, after adsorption of PAHs and regeneration were

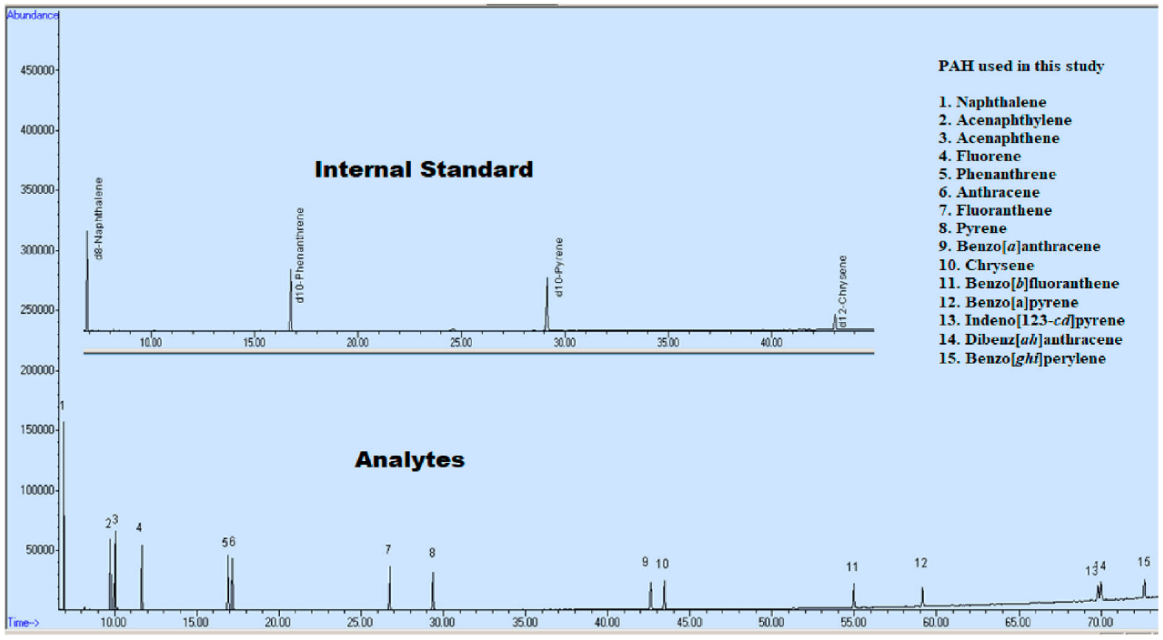

Figure 1. Representative GC-MS SIM chromatogram of the PAH standard mixture after SPE extraction of 10 µg/20 mL PAH aqueous solution. The IS mixture contained d8-naphthalene, d10-phenanthrene, d10-pyrene, d12-chrysene in hexane.

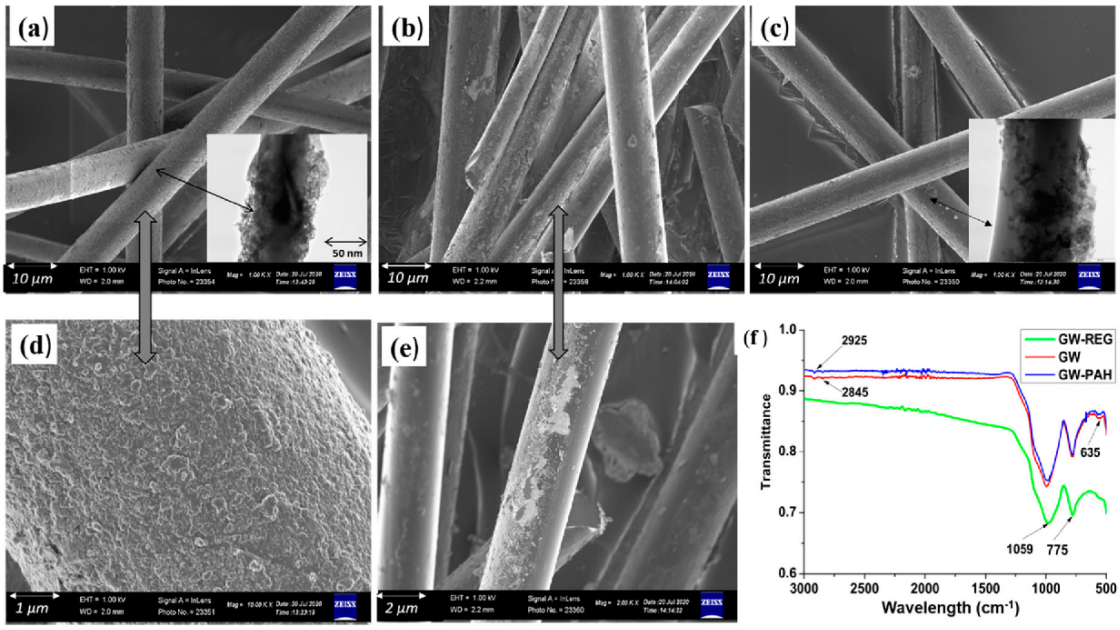

Figure 2. (a) SEM image of pristine graphene wool (1000×) {Inset: TEM image of pristine GW}; (b) SEM image of graphene wool after PAH mix adsorption (1000x); (c) SEM image of regenerated graphene wool (1000×) {Inset: TEM image of regenerated graphene wool}; (d) SEM image of pristine graphene wool (10,000x); (e) SEM image of GW post-adsorption (2000x); (f) FTIR of pristine GW, GW after PAH adsorption (GW-PAH) and regeneration (GW-REG).

examined using scanning electron microscopy and transmission electron microscopy (SEM & TEM) (Figure 2). The high-resolution microscopic analysis revealed that the diameter of each strand of graphene wool is between 6 - 8 microns. Figure 2(a,d) revealed extensive coverage of quartz wool by graphene with a heterogenous and rough surface structure, while Figure 2(b,c,e) revealed obvious morphological changes as a result of the adsorption and regeneration processes. Furthermore, Fourier transformed infrared spectroscopy (Figure 2(f)) revealed two prominent peaks; one peak associated with the sp^2 hybridized C = C backbone of graphene at 775 cm^{-1}, and a broad peak at 1059 cm^{-1} associated with Si-O–C arising from the functionalized quartz wool (SiO_2) coated with graphene [31]. The doublet peak at 2925 and 2845 cm^{-1} is attributed to symmetric and asymmetric sp^2 and sp^3 C–H stretching bands, whilst the peak at 675 cm^{-1} is attributed to C–H out-of-plane bending vibrations of aromatic rings [32]

3.2. Adsorption isotherm

Adsorption isotherm studies provide vital information on the interaction between sorbates and sorbents, especially the amount of analyte adsorbed, and the amount left in solution after equilibrium is reached [33]. Linear regression (Equation (5)) and nonlinear isotherm models such as Freundlich (Equation (3)) and Langmuir models (Equation (4)) were used to fit adsorption experimental data. The Error Sum of Squares (SSE) (Equation (7)) was used to test models used in this study.

$$q_e = K_f\, C_e^N \tag{3}$$

$$q_e = \frac{q_{\max} K_L C_e}{1 + K_L C_e} \tag{4}$$

$$q_e = K_d C_e \tag{5}$$

$$R_L = \frac{1}{1 + K_L q_{\max} C_0} \tag{6}$$

$$\sum_{i=1}^{n} (q_{e,\mathrm{cal}} - q_{e,\,\mathrm{exp}})_i^2 \tag{7}$$

where K_f ((µg/g) (L/µg)^N) and N (dimensionless) are the Freundlich constant and intensity parameter, an indicator of site energy heterogeneity; q_{max} (µg/g) and K_L (L/µg) are the Langmuir maximum adsorption capacity and Langmuir constant associated with solute–surface interaction energy, respectively; q_e is the solid-phase concentration (µg/g), C_e is the liquid phase equilibrium concentration (µg/L), and K_d (L/g) is the sorption distribution coefficient [22,34]. The value of the separation factor R_L (Equation (6)) provides important information about the nature of adsorption. The value of R_L is between 0 and 1 for favourable adsorption, while $R_L > 1$ represents unfavourable adsorption and $R_L = 1$

Table 2. Sorption isotherm parameters for multi-component PAH adsorption by graphene wool (GW) and Error Sum of Squares (SSE) of non-linear regression analysis (Experimental conditions: GW dosage = 20 mg per 20 mL; mixing rate = 200 rpm; T = 25 ± 1 °C; Initial conc.: 2 µg/20 mL – 10 µg/20 mL; contact time = 24 h).

PAHs	Freundlich			Langmuir				Linear		Amount adsorbed
	K_f	SSE	N	q_{max} (µg/g)	SSE	K_L (L/ µg)	R_L	K_d (L/g)	SSE	(µg/g)
Naphthalene	2.5e-5	2.36	2.85	1.63e3	2.37	2.0e-4	9.10e-1	0.22	2.67	155
Acenaphthene	1.2e-1	4.98	0.66	4.47e2	4.99	6.7e-5	9.90e-1	0.03	4.98	156
Acenaphthylene	3.6e-1	4.00	5.40	7.90e-1	4.42	7.2e3	2.76e-7	−0.07	4.44	185
Fluorene	3.4e-1	4.00	5.40	9.40e-1	4.71	5.7e1	3.52e-5	−0.08	4.73	176
Phenanthrene	2.8e-5	4.12	2.69	1.27e3	4.23	1.2e-4	9.43e-1	0.15	4.23	126
Anthracene	1.7e-5	1.03	3.19	1.81e3	1.20	4.5e-4	8.17e-1	−0.02	4.99	164
Fluoranthene	1.5e-5	0.76	3.32	3.71e3	1.00	2.8e-4	8.78e-1	−0.08	4.78	175
Pyrene	1.6e-5	0.64	3.29	3.16e3	0.95	3.3e-4	8.59e-1	−0.08	4.79	173
Benzo(a)anthracene	2.2e-5	1.19	3.13	1.01e2	1.30	6.1e-1	3.27e-3	−0.03	4.98	166
Chrysene	4.0e-5	0.78	3.05	2.96e2	1.00	2.9e-4	8.69e-1	0.03	4.99	161
Benzo(b)fluoranthene	3.6e-3	0.59	2.14	5.65e2	0.78	1.7e-4	9.23e-1	−0.07	4.82	161
Benzo(a)pyrene	1.6e-1	0.71	1.24	6.45e2	0.74	1.4e-4	9.37e-1	−0.06	4.88	152
Indeno(1,2,3-cd)pyrene	1.1e-4	1.85	2.77	8.87e1	1.89	6.2e-1	3.23e-3	−0.04	3.97	192
Dibenz(a,h)anthracene	7.8e-5	1.81	2.86	9.09e1	1.87	6.0e-1	3.30e-3	−0.04	3.96	193
Benzo(g,h,i)perylene	3.2e-5	2.02	3.27	4.91e3	2.13	3.8e-4	8.39e-1	−0.13	3.31	225

represents linear adsorption. The adsorption process is irreversible if $R_L = 0$ [35,36].

The isotherm parameters obtained for the PAH mix (multi-solute) adsorption by GW revealed that the Freundlich isotherm model, which reflects a multilayer adsorption mechanism, best fit experimental data compared to the uniform site energy and monolayer sorption mechanism described by the Langmuir model. This was validated by values of SSE presented in Table 2 [34]. The Langmuir model only fit at lower equilibrium concentrations, but as the concentration increased, the adsorption pattern deviated as a result of site saturation towards a multilayer adsorption pattern. The R_L values for all the PAHs were greater than zero and less than 1, which depicts favourable adsorption [34,37]. The core adsorption mechanism for the interaction between mixtures of PAHs and GW is mainly controlled by $\pi - \pi$ non-covalent bonding and hydrophobic interactions, however, other adsorption mechanisms centred around molecular conformation of the adsorbent and adsorbate also play a role in the multi-solute adsorption of PAHs [30]. The SEM images in Figure 2 confirm that mass transfer occurred between the boundary layer of PAH contaminated water and GW, leading to adsorption of the sorbate onto the active sites (pore walls and holes) of GW. The largely rough and heterogeneous surface of the wool-like material aided the adsorption of the PAHs by increasing the available surface area. The irregular pattern in the values obtained and reported in Table 2 is mainly as a result of the highly competitive nature of the adsorption processes, due to the number of PAH molecules competing for available sites simultaneously.

3.3. Single-solute adsorption isotherms of selected PAHs

Sorption of naphthalene (NAPH), anthracene (ANT), benzo(a)anthracene (B(a)ANT), benzo(a)pyrene (B(a)P) and benzo(g,h,i)perylene (PERY) onto graphene wool (GW) were studied individually in batch isotherm experiments. Similar process variables as the PAH mixture/multi-solute adsorption experiment were maintained for better comparison {viz. adsorbent dosage (1 g/L); individual PAH initial concentration (C_o = 2–10 µg/20 mL); time (24 hr); pH (7); temperature (25 °C); and rpm (200)}.

The Freundlich multilayer adsorption mechanism best described the sorption experimental data for the selected 2–6 ringed PAHs, as this model provided the

Table 3. Freundlich, Langmuir and linear sorption parameters for single-solute adsorption of selected 2–6 ringed PAHs onto GW.

Sorption model	Parameter	NAPH	ANT	B(a)ANT	B(a)P	PERY
	K_f	9.35	9.88e-3	5.61	54.47	5.51e-4
Freundlich	N	0.27	2.34	0.58	1.05	6.03
	SSE	0.39	0.88	0.12	1.43	0.68
Langmuir	q_{max} (µg/g)	4.89e1	1.22e4	2.35e3	1.52e3	1.60e4
	K_L (L/µg)	2.52e-2	1.56e-4	5.94e-3	8.73e3	7.87e-4
	SSE	0.44	1.52	0.13	1.47	1.36
Linear	K_d (g/L)	0.17	1.92	3.62	5.73	12.50
	Predicted q_e (µg/g)	66.63	189.53	202.39	336.25	432.00
	SSE	0.77	1.51	0.48	1.43	1.36

Freundlich model: $q_e = K_f C^N e$; Langmuir model, $q_e = q_{max} Ce/(K_L + C_e)$; Linear model: $q_e = K_d C_e$; Exp. q_e: Predicted amount adsorbed; SSE: Error Sum of Squares.

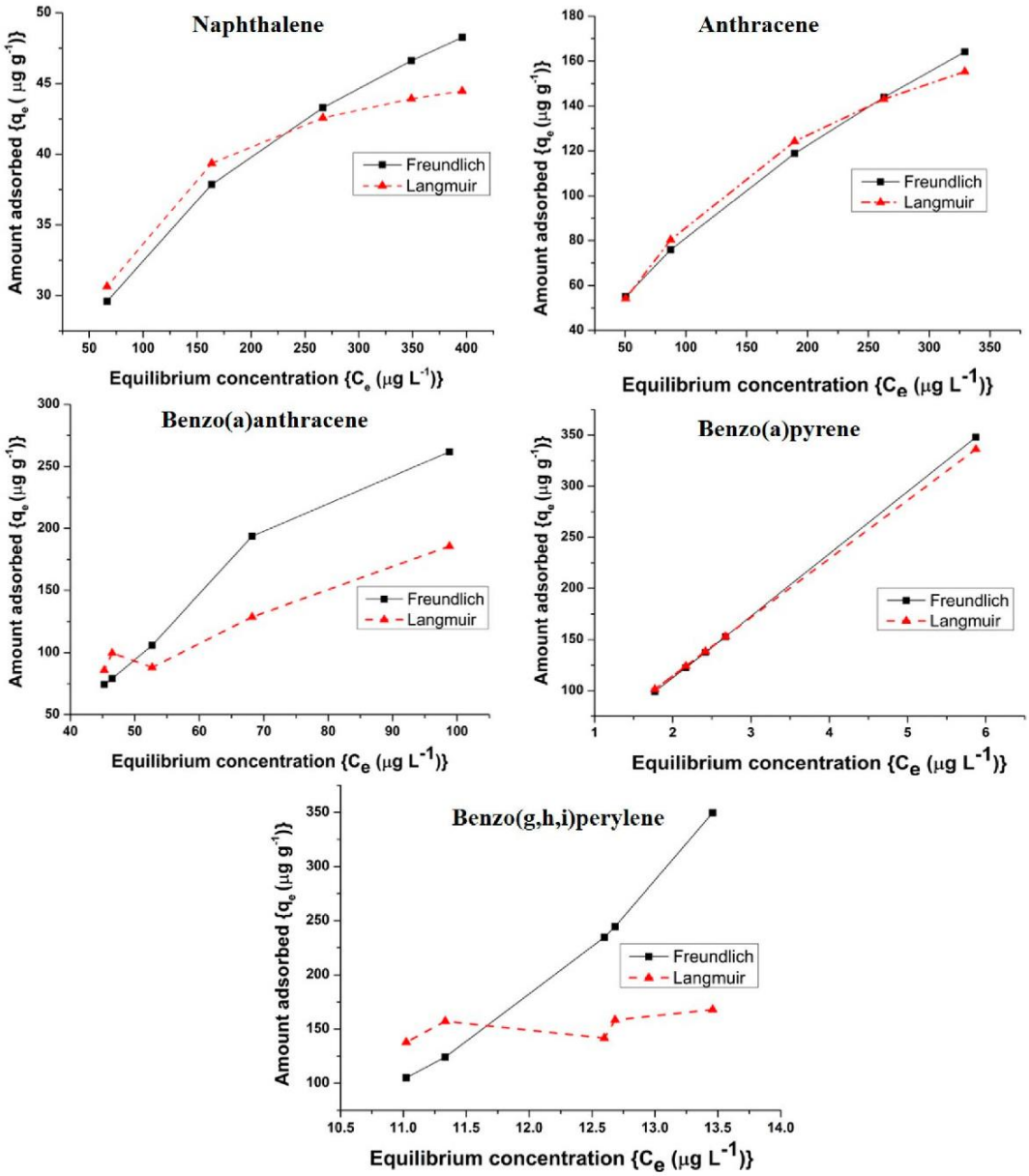

Figure 3. Representation of the Freundlich and Langmuir isotherm models for adsorption of selected individual 2–6 ringed PAHs onto graphene wool using nonlinear regression analysis.

lowest Error Sum of Squares (SSE) (Table 3). The adsorption capacity (K_d) and predicted amount adsorbed (q_e) were higher for higher molecular weight (HMW) PAHs than for lower molecular weight (LMW) PAHs (Table 3, Figure 3). This suggests that adsorption of PAHs onto GW is influenced by the hydrophobicity of the compounds (Figure 4). However, the maximum holding or adsorption capacity (q_{max}), Freundlich adsorption capacity (K_f) and adsorption capacity (K_d) were significantly higher for the selected 2–6 ringed PAHs than those reported in Table 2. This affirms that competitive adsorption in a multi-solute aqueous medium had a limiting effect on the overall sorption of the PAHs by graphene wool.

3.4. Influence of hydrophobicity on competitive adsorption of PAHs

The trend in adsorption of the PAH mixture onto GW can also be elucidated by the effect of hydrophobicity of the PAHs in solution, which can be determined from the logarithm of the octanol/water partition coefficient (LogK_{ow}) [38,39]. There is positive trend in the molecular mass of the compounds and the octanol/water partition

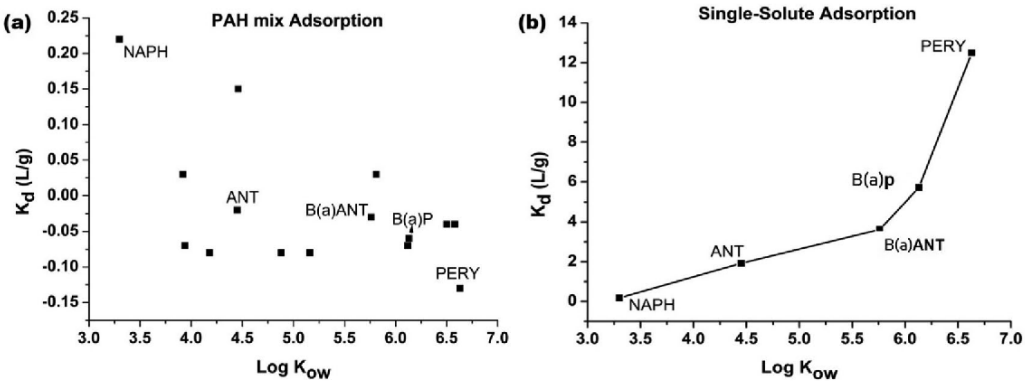

Figure 4. Correlation between hydrophobicity (LogKow) and adsorption capacity (K_d) of PAH interactions with graphene wool at 25°C, (a) adsorption of PAH mixture (unlabelled data points represent other PAHs present in the mix) (b) single-solute adsorption of selected PAHs.

coefficients, however, there are PAHs with the same molecular mass but with a slight difference in the value of Log$K_{ow,}$ which is as a result of their molecular conformation or structure [40,41].

Table 3 and Figure 4 reveal that K_d increased with increase in the LogK_{ow} of the PAHs adsorbed by GW in single-solute experiments, similar to what was previously reported by Lamichhanne *et al.* [42] for acenaphthene, fluorene, phenanthrene, fluoranthene, and pyrene adsorption by different organic carbon fractions. The correlation between sorption capacity and LogK_{ow} is due to the fact that water molecules surround the hydrophobic compounds to form a cage-like structure which stabilizes the less soluble or more hydrophobic PAHs in aqueous solution [43]. The binding mechanism for the PAH molecules onto GW is believed to be dominated by van der Waals-type interactions, also known as hydrophobic bonding [37]. Therefore, the PAH molecules that are more hydrophobic with higher values of LogK_{ow}, favourably interact with GW with stronger hydrophobic interactions and adsorption capacity (K_{ads}) than the less hydrophobic PAHs. This is similar to what was reported by Li *et al.* [44] via DFT simulations of graphene interaction with PAHs, and interaction of a mesoporous silica-based adsorbent with benzo(b)fluoranthene, benzo(a)pyrene, and benzo(g,h,i)perylene [45].

However, there is an obvious deviation from the trend shown in the adsorption of a multi-component PAH mixture, as the correlation between Log K_{ow} and K_d decreased due to the expected complex chemistry of the solution. It is also noteworthy that competitive interaction led to a significant decrease in the adsorption capacity of GW for the respective PAHs (Figure 4). Hydrophobicity and $\pi - \pi$ electron interactions should have favoured sorption of high molecular weight (HMW) and more hydrophobic PAHs in the multi-solute experiment, however, Figure 4 reveals otherwise. This suggests that other factors such as size of the molecules, molecular dynamics/conformations and surface structure of the adsorbent (pore volume & size) may have enhanced adsorption of low molecular weight (LMW) PAHs in the competitive adsorption process.

3.5. Effect of adsorbent dosage

The adsorbent dose of 20, 25, 30 and 40 mg was added to 20 mL solutions containing 8 µg/20 mL and 10 µg/20 mL of PAHs, to determine the average removal efficiency with varying sorbent mass, while other parameters viz. time (24 hr), pH (7), temperature (25 °C) and rpm (200) were constant. With increase in the dosage, PAH removal efficiency increased. The average removal efficiency ranged from 52.2–72.6% at 20 mg, 55.1–80% at 25 mg, 65.3–85.1% at 30 mg and 80–100% at 40 mg dosage, respectively (Figure 5). The results also revealed that competitive adsorption of higher molecular weight (HMW) PAHs were favoured over lower molecular weight (LMW) PAHs, and the improvement in the removal efficiency can be attributed to the availability of vacant sites as dosage increased. Further increase in the adsorbent dosage would potentially yield improvement in removal of LMW PAHs, as HMW PAH removal efficiency already reached its optimum at 40 mg/20 mL (2 g/L) for both 8 µg/20 mL and 10 µg/20 mL PAH concentrations.

3.6. Desorption experiment and hysteresis

The Freundlich constant '*N*' which is regarded as the heterogeneity index and *H*-index which represents the hysteresis index (reversibility of the sorption process) [36] are presented in Table 4. The *N* value for adsorption

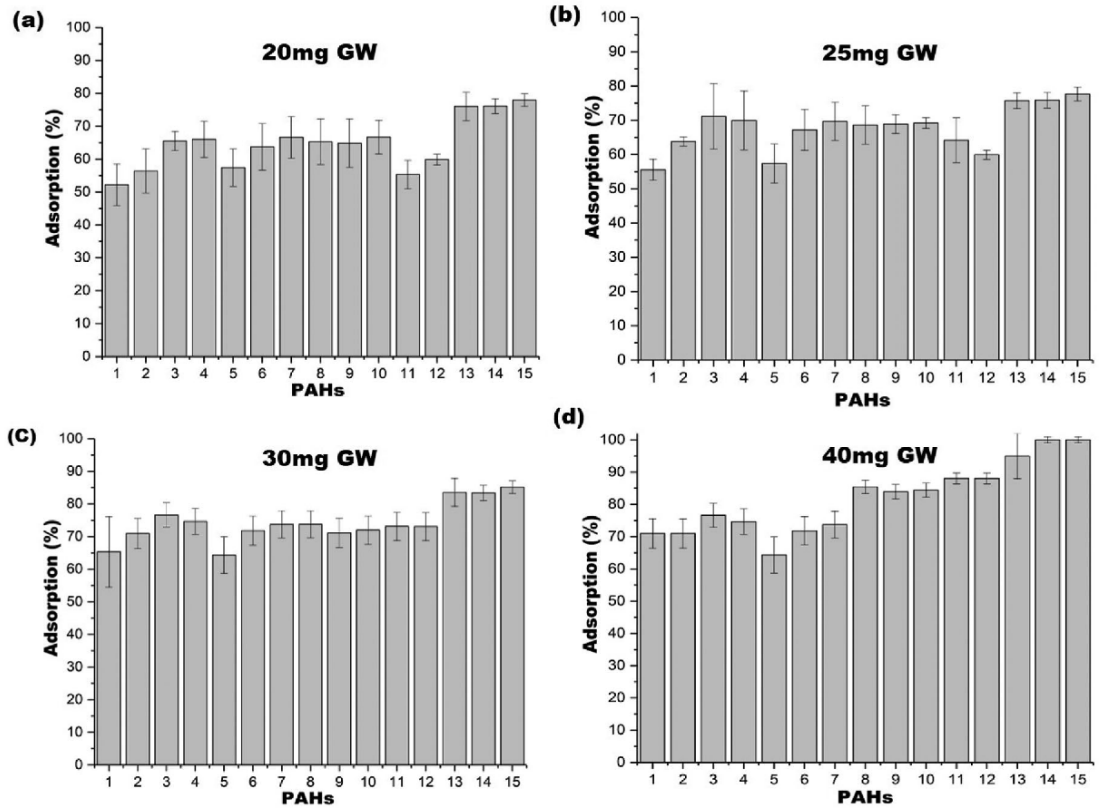

Figure 5. Effect of increasing dose of graphene wool (GW) in 20 mL of 400 and 500 µg/L PAH solution (a) 20 mg GW (b) 25 mg GW (c) 30 mg GW (d) 40 mg GW; (Experimental conditions: 25°C, 200 rpm mixing rate, n = 3). PAHs are; 1= Naphthalene, 2= Acenaphthene, 3= Acenaphthylene, 3= Fluorene, 4= Phenanthrene, 4= Anthracene, 5= Fluoranthene, 6= Pyrene, 7= Benzo(a)anthracene, 8= Chrysene, 9= Benzo(b)fluoranthene, 10= Benzo(a)pyrene, 11= Indeno(1,2,3-cd)pyrene, 12= Dibenz(a,h)anthracene, 13= Benzo(g,h,i)perylene, 14= Dibenz(a,h)anthracene, 15= Benzo(g,h,i)perylene.

(N_{ads}) and *H*-indices were generally higher in multi-solute sorption than for single-solute experiments. The trend in heterogeneity presented is expected due to the number of solutes interacting simultaneously with GW, thus resulting in a more heterogenous sorption-desorption process. Figure 6 revealed that a significant amount of PAHs adsorbed were desorbed with % desorption ranging 45–75% for PAH mix experiments, while the reverse is the case for the single-solute experiments as desorption was found to decrease, ranging from 5.5–56.4%. Furthermore, the trend observed in single-solute desorption in Figure 6 suggests stronger binding interactions between HMW PAHs and GW, supported by the adsorption capacities (K_d) obtained (Table 3); leading to significant sorption irreversibility. It has been reported that lower ring PAHs are preferentially bound to sorbent active sites at lower concentrations and partitioning favours adsorption of higher ring PAHs as concentration increases in a multi-solute, competitive environment [37,39]. Generally, given the high percentage of adsorbed species that were desorbed into aqueous solution in the PAH mix adsorption, it can be

Table 4. Comparison of sorption-desorption parameters and hysteresis index (H) of selected PAHs in multi-solute (M) and single-solute (S) interactions with graphene wool (GW).

PAH	$K_{f\ (des)\ (M)}$	$K_{f\ (des)\ (S)}$	$N_{\ (ads)\ (M)}$	$N_{\ (ads)\ (S)}$	$N_{(des)\ (M)}$	$N_{\ (des)\ (S)}$	$H_{\ (M)}$	$H_{\ (S)}$
Naphthalene	2.28	271.58	2.85	0.27	0.80	0.96	**3.56**	**0.28**
Anthracene	2.23	7.25	3.19	2.34	0.30	4.37	**10.63**	**0.54**
Benzo(a)anthracene	1.73	314.60	3.13	0.58	0.29	1.05	**10.79**	**0.55**
Benzo(a)pyrene	1.91	134.75	1.34	1.05	0.17	0.70	**7.88**	**1.50**
Benzo(g,h,i)perylene	1.75	1.35	3.27	6.03	0.30	1.75	**10.9**	**3.45**

$N_{(ads)}$: Freundlich adsorption intensity; $N_{(des)}$: Freundlich desorption intensity; H: Sorption–desorption hysteresis index; $H = N_{ads}/N_{des}$; M: PAH mixture; S: Single-solute.

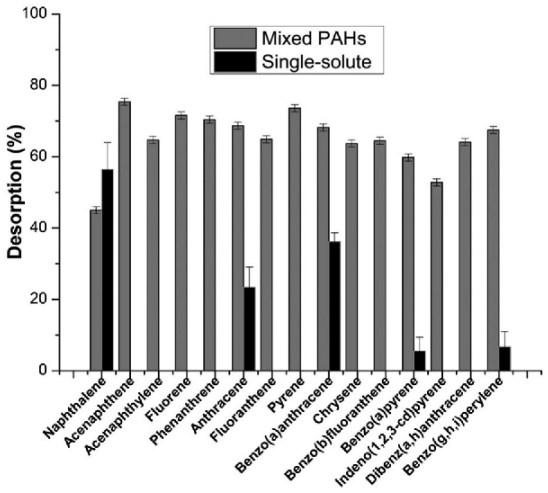

Figure 6. Average desorption rate (%) of PAHs recovered in aqueous solution (Experimental conditions: 20 mL of de-ionized water; temperature: 25°C). Error bars show ± standard deviation, n = 3.

inferred that a significant amount of PAHs were loosely held by weak van der Waal forces and π–π interactions [46], due to significant competition for sorption sites and saturation thereof, and Table 2 also reported lower binding capacity for the PAH mix.

Furthermore, reports revealed that the percent desorption of PAHs in single solute environments are somewhat different from what is obtained for a multi-component systems using geosorbents rich in carbon, and it was suggested that the presence of less hydrophobic PAHs improved the solubility of more hydrophobic solutes, thus increasing their percentage desorption [21]. However, such an effect was absent in the single-solute experiments. Evaluation of Table 4 reveals that higher molecular weight compounds displayed more hysteretic sorption behaviour with higher *H*-indices. This is expected as stronger $\pi - \pi$ interaction with GW is expected between higher ring PAHs than lower ring PAHs due to the number of π electrons, thus making irreversible entrapment or slow desorption more evident with higher ring PAHs. This result correlates with hydrophobicity of the PAHs, the higher the value of LogK_{ow}, the more recalcitrant the PAHs are towards desorbing into aqueous medium [47,48]. Pore-deformation of adsorbents may occur during the sorption process leading to entrapment of PAHs and/or slow desorption rates, which is more likely in multi-solute sorption-desorption processes, leading to higher *H*-indices [49].

3.7. Regeneration and reusability experiment

Graphene wool (GW) was regenerated with n-hexane. Six successive cycles of adsorption experiments were carried out with a PAH concentration range of 2 µg/20 mL to 10 µg/20 mL. The removal efficiency of the PAHs from the GW after each regeneration cycle is shown in Figure 7. The regeneration procedure proved efficient as the removal efficiency of the material was relatively constant, suggesting multiple reusability of the material for remediation of water contaminated with several PAHs simultaneously. However, there is indication that small fragments of the GW were lost during the regeneration cycles, as around 9.6% loss in total mass of the adsorbent was recorded over the entire cycle of six regeneration steps. Morphological changes as a result of the regeneration process after 6 cycles were examined with the aid of TEM, SEM and FTIR, and it revealed that layers of adsorbed solute, appearing as patches on the surface of the adsorbent, were desorbed or removed to a large extent by the regeneration process (Figure 2(c,d)). However, TEM revealed some degree of loss of coverage (Inset: Figure 2(a,c)) and FTIR showed a decline in peak intensities (Figure 2(f)). This loss was potentially responsible for the slight decline in removal efficiency observed for the higher molecular weight PAHs. On the contrary, the removal efficiency of the lower mass PAHs seemed to improve, which suggests that the surface of material may have undergone a slight deformation which may have favoured smaller sized molecules [47,48].

3.8. Adsorption thermodynamics of selected 2 - 6 ringed PAHs

Adsorption is temperature-dependent whereby some processes are feasible at ambient temperature while others require an additional supply of heat energy to overcome an energy barrier or initiate a reaction. The effect of temperature on the adsorption of NAPH, ANT, B(a)ANT, B(a)P and PERY onto graphene wool (GW) was studied at 298, 308 and 318 K, respectively. The adsorption data were fit to a linear isotherm model (Equation (5)), and it was observed that the equilibrium concentration of the selected PAHs reduced and adsorption capacity (K_d) increased with increase in temperature, except for NAPH which is likely due to volatilization losses (Table 5). Thermodynamic parameters such as Gibbs free energy change (ΔG°), enthalpy (ΔH°) and entropy (ΔS°) were calculated using the Van't Hoff equations (Equations (8) and (9)), in order to elucidate the nature of adsorption of NAPH, ANT, B(a)ANT, B(a)P and PERY onto GW as a function of temperature [13,50].

$$\ln K_d = \frac{\Delta S^\circ}{R} - \frac{\Delta H^\circ}{RT} \quad (8)$$

$$\Delta G^\circ = -RT\ln \cdot K_d \quad (9)$$

where ΔG is the change in the Gibbs free energy (kJ/

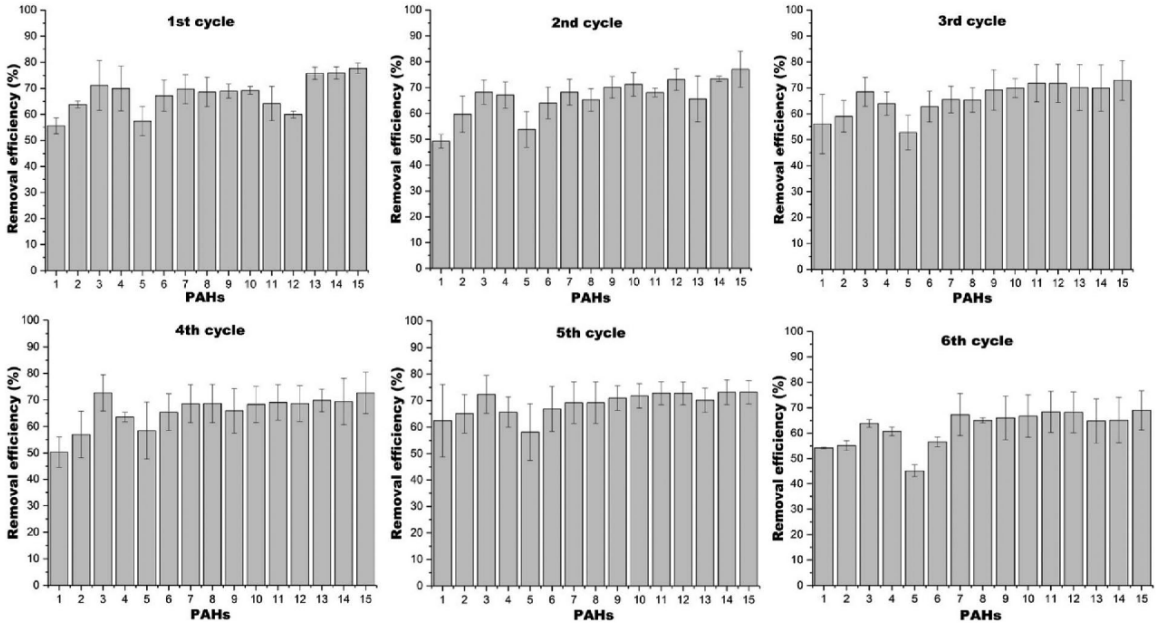

Figure 7. Percentage adsorption of the PAHs used in this study by GW (Experimental conditions – mass of adsorbent: 20 mg; volume of solution: 20 mL; temperature: 25°C, concentration of PAHs: 2 µg/20 mL to 10 µg/20 mL). Error bars show ± standard deviation, $n = 3$. PAHs are; 1= Naphthalene, 2= Acenaphthene, 3= Acenaphthylene, 3= Fluorene, 4= Phenanthrene, 4= Anthracene, 5= Fluoranthene, 6= Pyrene, 7= Benzo(a)anthracene, 8= Chrysene, 9= Benzo(b)fluoranthene, 10= Benzo(a)pyrene, 11= Indeno(1,2,3-cd)pyrene, 12= Dibenz(a,h)anthracene, 13= Benzo(g,h,i)perylene, 14= Dibenz(a,h)anthracene, 15= Benzo(g,h,i)perylene.

mol); ΔH is the change in enthalpy (kJ/mol), and ΔS is the change in entropy (kJ/mol), R = gas constant (8.314 J/mol K), T = thermodynamic temperature (K), and K_d = adsorption capacity (L/g).

Table 5 revealed that adsorption of selected PAHs onto GW involved a spontaneous endothermic reaction, with positive and negative values of ΔH and ΔG respectively, except for NAPH. Furthermore, an increase in temperature improved the sorption feasibility of ANT, B(a)ANT, B(a)P and PERY, considering the trend in ΔG values. The low enthalpy values (ΔH) suggest that PAH interaction with GW is mainly physisorption and not chemisorption [50]. Several reports have shown that the thermodynamic behaviour of PAHs differ with respect to interactions with different adsorbents [13,42,45,50,51]. However, there is a consensus that thermodynamic parameters are mostly influenced by the morphology of the sorbent and physicochemical properties of the sorbate. The information provided in this study reveals the vital role of temperature regimes towards the potential application of GW for removal of PAHs from aqueous solution.

3.9. Comparison with previous studies

Researchers have reported on the competitive adsorption of PAHs onto different adsorbents. Activated

Table 5. Thermodynamic parameters for adsorption of selected 2–6 ringed PAHs onto graphene wool (GW).

PAHs	Temperature (K)	K_d (L/g)	ΔG° (kJ/mol)	ΔH° (kJ/mol)	ΔS° (kJ/mol K)
	308	0.17	4540		
Naphthalene	318	0.15	4858	−8.81e-2	1.41e-2
	328	0.14	5198		
	308	1.92	−1616		
Anthracene	318	1.94	−1657	3.06e-2	4.74e-2
	328	1.99	−1818		
	308	0.65	−1067		
Benzo(a)anthracene	318	1.59	−1188	8.31e-4	2.83e-2
	328	2.20	−2085		
	308	5.73	−6268		
Benzo(a)pyrene	318	6.58	−6587	1.66e-4	2.83e-2
	328	12.07	−6958		
	308	12.50	−10,030		
Benzo(g,h,i)perylene	318	12.70	−10,721	2.49e-5	2.82e-2
	328	13.90	−12,673		

carbon was used to adsorb 15 PAHs from vegetable oil and 68-93% efficiency was achieved with the recalcitrant higher molecular weight PAHs having better removal efficiency [51]. The removal of fluorene, pyrene, benzo (k)fluoranthene, benzo(a)pyrene and benzo(g,h,i)perylene from water using immature coal (leonardite) was studied [52]. The results showed that adsorption increased with increase in LogK_{ow} and an adsorption efficiency of 82% was recorded for B[*a*]P and B[*k*]F.

Competitive adsorption of phenanthrene, pyrene, fluorene, fluoranthene and benzo(a)anthracene onto zeolite and organo-zeolite have been reported [53]. Results showed that adsorption indices were in the range of 50-83% for organo-zeolite and less than 50% for zeolite, with the exception of benzo(a)anthracene which recorded the highest removal efficiency of 75% due to its higher partition coefficient (log K_{ow}). Wang et al. [30] reported that adsorption of selected PAHs on graphene nanosheets and graphene oxide increased with increase in hydrophobicity in the order pyrene > phenanthrene > naphthalene. A more recent report involving zeolite and modified zeolite as adsorbents recorded the following removal efficiencies for PAHs; 47.6 and 43.9% for the zeolite and modified zeolite for benzo(k)fluoranthene, 62.9 and 69.5% for benzo(b)fluoranthene, and 43.8 and 37.2% for benzo(a)pyrene [45]. Most of the values were less than what was recorded for graphene wool, nonetheless, they also reflect the dominant influence of hydrophobicity on the overall uptake of PAHs in a competitive and multi-solute environment.

4.0. Conclusion

This study revealed that a mixture of several polycyclic aromatic hydrocarbons categorized as priority pollutants by the United States Environmental Protection Agency can be effectively removed from water using a novel graphene wool as adsorbent. The robust, flexible and porous nature of this material makes it a suitable adsorbent for the simultaneous adsorption of PAHs. Sorption-desorption studies revealed that higher molecular weight PAHs were better removed by the GW. The release potential into aqueous medium was also evaluated and results indicated the occurrence of hysteresis (some degree of irreversible adsorption). The optimum dosage was 2 g/L (40 mg/20 mL) of GW adsorbent for higher molecular weight PAHs, with concentration as high as 10 µg/20 mL and average removal efficiencies at optimum dosage were between 71–100% with good RSD values (1–5.5%, n = 3). Hydrophobic and $\pi - \pi$ interactions dominated the adsorption process of the PAHs investigated in this study in the single-solute experiments, whilst molecular size/conformation of PAHs, morphology of adsorbent and solution chemistry influenced multi-solute competitive adsorption. Results obtained from the regeneration and reusability experiments showed that GW was reasonably stable and can be reused without significant loss of efficiency. With the right fabrication, this new form of graphene (GW) may be used to make filters and adsorbents for water purification purposes due to its wool-like structure, water permeability and other morphological and physicochemical properties. The material can also be harnessed for the decontamination of water containing other emerging hydrophobic pollutants, as a result of its proven affinity for hydrophobic organic contaminants such as PAHs.

Acknowledgements

Authors are grateful to University of Pretoria Commonwealth Doctoral Scholarship, Rand Water, and the Departments of Chemistry and Physics at the University of Pretoria, especially Prof. Ncholu Manyala, Dr. Liezel Van der Merwe, Genna-Leigh Schoonraad, Chiedza Munyeza and Sifiso Nsibande.

Disclosure statement

No potential conflict of interest was reported by the author(s).

Funding

This work was supported by University of Pretoria Commonwealth Doctoral Scholarship [grant number AA]; Rand Water [grant number PF].

ORCID

Adedapo O. Adeola http://orcid.org/0000-0002-7011-2396
Patricia B.C. Forbes http://orcid.org/0000-0003-3453-9162

References

[1] Cai S-S, Syage JA, Hanold KA, et al. Ultraperformance liquid chromatography–atmospheric pressure photoionization-tandem mass spectrometry for high-sensitivity and high-throughput analysis of U.S. Environmental Protection Agency 16 priority pollutants polynuclear aromatic hydrocarbons. Anal Chem. 2009;81(6):2123–2128. doi:10.1021/ac802275e.

[2] Olivella MA, Ribalta TG, de Febrer AR, et al. Distribution of polycyclic aromatic hydrocarbons in riverine waters after Mediterranean forest fires. Sci Total Environ. 2006;355 (1):156–166. doi:10.1016/j.scitotenv.2005.02.033.

[3] Karyab H, Yunesian M, Nasseri S, et al. Polycyclic aromatic hydrocarbons in drinking water of Tehran, Iran. J Environ Health Sci Eng. 2013;11(1):25–32. doi:10.1186/2052-336X-11-25.

[4] Maliszewska-Kordybach B, Smreczak B, Klimkowicz-Pawlas A. Concentrations, sources, and spatial distribution of individual polycyclic aromatic hydrocarbons (PAHs) in agricultural soils in the Eastern part of the EU: Poland as a case study. Sci Total Environ. 2009;407(12):3746–3753. doi:10.1016/j.scitotenv.2009.01.010.

[5] Martorell I, Perelló G, Martí-Cid R, et al. Polycyclic aromatic hydrocarbons (PAH) in foods and estimated PAH intake by the population of Catalonia, Spain: Temporal trend. Environ Int. 2013;36(5):424–432. doi:10.1016/j.envint.2010.03.003.

[6] Kyzas GZ, Deliyanni EA, Bikiaris DN, et al. Graphene composites as dye adsorbents: Review. Chem Eng Res Des. 2018;129:75–88. doi:10.1016/j.cherd.2017.11.006.

[7] Li X, Wang X, Zhang L, et al. Chemically derived, ultrasmooth graphene nanoribbon semiconductors. Science. 2008b;319(5867):1229–1232. doi:10.1126/science.1150878.

[8] Vermeir M, Lachau-Durand S, Mannens G, et al. Absorption, metabolism, and excretion of darunavir, a new protease inhibitor, administered alone and with low-dose ritonavir in healthy subjects. Drug Metab Dispos. 2009;37(4):809. doi:10.1124/dmd.108.024109.

[9] Mueller T, Xia FN, Avouris P. Graphene photodetectors for high-speed optical communications. Nat Photonics. 2010;4:297–301. doi:10.1038/nphoton.2010.40.

[10] Zhang L, Xia J, Zhao Q, et al. Functional graphene oxide as a nanocarrier for controlled loading and targeted delivery of mixed anticancer drugs. Small. 2010;6(4):537–544. doi:10.1002/smll.200901680.

[11] Hu M, Mi B. Enabling graphene oxide nanosheets as water separation membranes. Environ Sci Technol. 2013;47(8):3715–3723. doi:10.1021/es400571g.

[12] Paixão MM, Vianna MTG, Marques M. Graphene and graphene nanocomposites for the removal of aromatic organic compounds from the water: systematic review. Mater Res Express. 2018;5(1):012002. doi:10.1088/2053-1591/aaa047.

[13] Adeola AO, Forbes PBC. Optimisation of the sorption of selected polycyclic aromatic hydrocarbons by regenerable graphene wool. Water Sci Technol. 2019;80(10):1931–1943. doi:10.2166/wst.2020.011.

[14] Nsibande SA, Forbes PBC. Development of a turn-on graphene quantum dot-based fluorescent probe for sensing of pyrene in water. RSC Adv. 2020;10:12119–12128. doi:10.1039/C9RA10153E.

[15] Ersan G, Apul OG, Perreault F, et al. Adsorption of organic contaminants by graphene nanosheets: A review. Water Res. 2017;126:385–398. doi:10.1016/j.watres.2017.08.010.

[16] Schoonraad G-L, Madito MJ, Manyala N, et al. Synthesis and optimisation of a novel graphene wool material by atmospheric pressure chemical vapour deposition. J Mater Sci. 2020;55:545–564. doi:10.1007/s10853-019-03948-0.

[17] Abdel-Shafy HI, Mansour MSM. A review on polycyclic aromatic hydrocarbons: source, environmental impact, effect on human health and remediation. Egypt J Pet. 2016;25:107–123. doi:10.1016/j.ejpe.2015.03.011.

[18] Mojiri A, Zhou JL, Ohashi A, et al. Comprehensive review of polycyclic aromatic hydrocarbons in water sources, their effects and treatments. Sci Total Environ. 2019;696(133971):1–16. doi:10.1016/j.scitotenv.2019.133971.

[19] USEPA, U.S. Environmental Protection Agency office of the science advisor risk assessment forum. Framew Hum Health Risk Assess Inf Decis Mak. 2014. https://www.epa.gov/sites/production/files/2014-12/documents/hhra-framework-final-2014

[20] Crisafully R, Milhome MA, Cavalcante RM, et al. Removal of some polycyclic aromatic hydrocarbons from petrochemical wastewater using low-cost adsorbents of natural origin. Bioresour Technol. 2008;99(10):4515–4519. doi:10.1016/j.biortech.2007.08.041.

[21] Hussein TA, Ismail ZZ. Desorption of selected PAHs as individuals and as a ternary PAH mixture within a water-soil-nonionic surfactant system. Environ Technol. 2013;34(3):351–361. doi:10.1080/09593330.2012.696718.

[22] Vidal CB, Barros AL, Moura CP, et al. Adsorption of polycyclic aromatic hydrocarbons from aqueous solutions by modified periodic mesoporous organosilica. J Colloid Interface Sci. 2011;357(2):466–473. doi:10.1016/j.jcis.2011.02.013.

[23] Sibiya P, Potgieter M, Cukrowska E, et al. Development and application of solid phase extraction method for polycyclic aromatic hydrocarbons in water samples in Johannesburg area, South Africa. S Afr J Chem. 2012;65:206–213.

[24] Munyeza CF, Dikale O, Rohwer ER, et al. Development and optimization of a plunger assisted solvent extraction method for polycyclic aromatic hydrocarbons sampled onto multi-channel silicone rubber traps. J Chromatogr A. 2018;1555:20–29. doi:10.1016/j.chroma.2018.04.053.

[25] May WE, Wasik SP, Freeman DH. Determination of the solubility behavior of some polycyclic aromatic hydrocarbons in water. Anal Chem. 1978;50(7):997–1000. doi:10.1021/ac50029a042.

[26] Haynes WM. CRC Handbook of chemistry and Physics, 2009–2010, 90th ed. J Am Chem Soc. 2009;131:12862–12862. doi:10.1021/ja906434c.

[27] Hansch C, Leo A, Hoekman D. Exploring QSAR - hydrophobic, electronic, and steric constants. Washington (DC): American Chemical Society; 1996; 39, 1189-1190. https://doi.org/10.1021/jm950902o.

[28] Kim S, Chen J, Cheng T, et al. Pubchem 2019 update: improved access to chemical data. Nucleic Acids Res. 2018;47(D1):D1102–D11D9. doi:10.1093%2Fnar%2Fgky1033.

[29] Stoller MD, Park S, Zhu Y, et al. Graphene-based ultracapacitors. Nano Lett. 2018;8(10):3498–3502. doi:10.1021/nl802558y.

[30] Wang J, Chen Z, Chen B. Adsorption of polycyclic aromatic hydrocarbons by graphene and graphene oxide nanosheets. Environ Sci Technol. 2014;48(9):4817–4825. doi:10.1021/es405227u.

[31] Ţucureanu V, Matei A, Avram AM. FTIR spectroscopy for carbon family study. Crit Rev Anal Chem. 2016;46:502–520. doi:10.1080/10408347.2016.1157013.

[32] Yang H, Li F, Shan C, et al. Covalent functionalization of chemically converted graphene sheets via silane and its reinforcement. J Mater Chem. 2009;19:4632–4638. doi:10.1039/B901421G.

[33] Cooney DO. Adsorption Designer for Wasterwater Treatment. London: Lewis Publishers; 1999.

[34] Anthony ET, Ojemaye MO, Okoh AI, et al. Synthesis of CeO_2 as promising adsorbent for the management of free-DNA harboring antibiotic resistance genes from tap-water. Chem Eng J. 2020;401:125562, doi:10.1016/j.cej.2020.125562.
[35] Rahman MS, Islam MR. Effects of pH on isotherms modeling for Cu (II) ions adsorption using maple wood sawdust. Chem Eng J. 2009;149:273–280. doi:10.1016/j.cej.2008.11.029.
[36] Ololade IA, Adeola AO, Oladoja NA, et al. In-situ modification of soil organic matter towards adsorption and desorption of phenol and its chlorinated derivatives. J Environ Chem Eng. 2018;6(2):3485–3494. doi:10.1016/j.jece.2018.05.034.
[37] Wang X, Sato T, Xing B. Competitive sorption of pyrene on wood chars. Environ Sci Technol. 2006;40(10):3267–3272. doi:10.1021/es0521977.
[38] Li L, Xie S, Cai H, et al. Quantitative structure-property relationships for octanol-water partition coefficients of polybrominated diphenyl ethers. Chemosphere. 2008a;72(10):1602–1606. doi:10.1016/j.chemosphere.2008.04.020.
[39] Zou M, Zhang J, Chen J, et al. Simulating adsorption of organic pollutants on finite (8,0) single-walled carbon nanotubes in water. Environ Sci Technol. 2012;46(16):8887–8894. doi:10.1021/es301370f.
[40] Sabljić A, Güsten H, Verhaar H, et al. QSAR modelling of soil sorption. improvements and systematics of log KOC vs. log KOW correlations. Chemosphere. 1995;31(11):4489–4514. doi:10.1016/0045-6535(95)00327-5.
[41] Toropov AA, Toropova AP, Raska I. QSPR modeling of octanol/water partition coefficient for vitamins by optimal descriptors calculated with SMILES. Eur J Med Chem. 2008;43(4):714–740. doi:10.1016/j.ejmech.2007.05.007.
[42] Lamichhane S, Bal Krishna KC, Sarukkalige R. Polycyclic aromatic hydrocarbons (PAHs) removal by sorption: a review. Chemosphere. 2016;148:336–353. doi:10.1016/j.chemosphere.2016.01.036.
[43] Atkins P, Paula J. Physical chemistry for the life Sciences. New York: W. H. Freeman and Company; 2006.
[44] Li B, Ou P, Wei Y, et al. Polycyclic aromatic hydrocarbons adsorption onto graphene: a DFT and AIMD study. Materials (Basel, Switz). 2018;11(5):726. doi:10.3390/ma11050726.
[45] Costa JAS, de Jesus RA, da Silva CMP, et al. Efficient adsorption of a mixture of polycyclic aromatic hydrocarbons (PAHs) by Si–MCM–41 mesoporous molecular sieve. Powder Technol. 2017;308:434–441. doi:10.1016/j.powtec.2016.12.035.
[46] Okoli CP, Adewuyi GO, Zhang Q, et al. Aqueous scavenging of polycyclic aromatic hydrocarbons using epichlorohydrin, 1,6-hexamethylene diisocyanate and 4,4-methylene diphenyl diisocyanate modified starch: pollution remediation approach. Arab J Chem. 2015;12(8):2760–2773. doi:10.1016/j.arabjc.2015.06.004.
[47] Nguyen TH, Sabbah I, Ball WP. Sorption nonlinearity for organic contaminants with diesel soot: method development and isotherm interpretation. Environ Sci Technol. 2004;38(13):3595–3603. doi:10.1021/es0499748.
[48] Sander M, Pignatello JJ. Sorption irreversibility of 1,4-dichlorobenzene in two natural organic matter–rich geosorbents. Environ Toxicol Chem. 2009;28(3):447–457. doi:10.1897/08-128.1.
[49] Jonker MTO, Koelmans AA. Extraction of polycyclic aromatic hydrocarbons from soot and sediment: solvent evaluation and smplications for sorption mechanism. Environ Sci Technol. 2002;36:4107–4113. doi:10.1021/es0103290.
[50] Yakout M, Daifullah AAM. Removal of selected polycyclic aromatic hydrocarbons from aqueous solution onto various adsorbent materials. Desalin Water Treat. 2013;51:6711–6718. doi:10.1080/19443994.2013.769916.
[51] Gong Z, Alef K, Wilke B-M, et al. Activated carbon adsorption of PAHs from vegetable oil used in soil remediation. J Hazard Mater. 2007;143(1):372–378. doi:10.1016/j.jhazmat.2006.09.037.
[52] Zeledón-Toruño C, Lao-Luque C, de las Heras FXC, et al. Removal of PAHs from water using an immature coal (leonardite). Chemosphere. 2007;67(3):505–512. doi:10.1016/j.chemosphere.2006.09.047.
[53] Lemić J, Tomašević-Čanović M, Adamović M, et al. Competitive adsorption of polycyclic aromatic hydrocarbons on organo-zeolites. Microporous Mesoporous Mater. 2007;105(3):317. https://doi.org/10.1016/j.micromeso.2007.04.014.

Chapter 6 Influence of natural organic matter on the adsorption of PAHs by sediments and graphene wool adsorbent

This chapter evaluates the role of different fractions of natural organic matter (NOM) on the adsorption of selected PAHs and provides insight into the influence of NOM on the adsorption capacity of graphene wool. The isolation and characterization of fractions of natural organic matter (NOM) recovered from stream sediment was carried out and the impact of NOM on solution chemistry and the inhibitory influence on the PAH removal efficiency of graphene wool (GW) was reported. The format is as published in Environmental Technology and Innovations.

Article

Adeola, A.O., Forbes, P.B.C. (2021). Influence of natural organic matter fractions on PAH sorption by stream sediments and a synthetic graphene wool adsorbent. Environmental Technology and innovations, 21, 101202.

DOI: https://doi.org/10.1016/j.eti.2020.101202

Influence of natural organic matter fractions on PAH sorption by stream sediments and a synthetic graphene wool adsorbent. Environmental Technology and innovations

Adedapo O. Adeola [a] and Patricia B.C. Forbes [a*]

[a]*Department of Chemistry, Faculty of Natural and Agricultural Sciences, University of Pretoria, Lynnwood Road, Hatfield, Pretoria 0002, South Africa.*

Corresponding author email address: patricia.forbes@up.ac.za

Graphical abstract

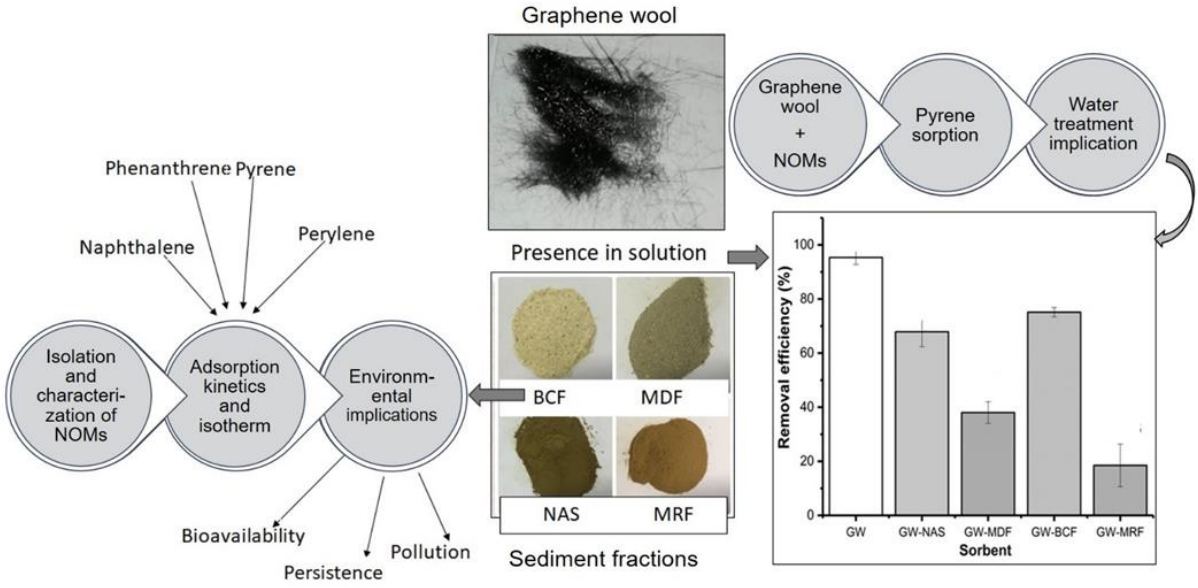

Highlights

- Sequestration of PAHs is controlled by hydrophobic-organophilic interactions.
- Dual and complementary sorption mechanisms described PAH-NOM interactions.
- Mineral-rich NOMs (MRF) exhibit faster sorption rates but lower sorption capacity.
- Carbon-rich fractions (MDF & BCF) of sediments have higher sorption capacities.
- MRF reduced the PAH decontamination efficiency of graphene wool significantly.

Environmental Technology & Innovation 21 (2021) 101202

Contents lists available at ScienceDirect

Environmental Technology & Innovation

journal homepage: www.elsevier.com/locate/eti

Influence of natural organic matter fractions on PAH sorption by stream sediments and a synthetic graphene wool adsorbent

Adedapo O. Adeola, Patricia B.C. Forbes *

Department of Chemistry, Faculty of Natural and Agricultural Sciences, University of Pretoria, Lynnwood Road, Hatfield, Pretoria 0002, South Africa

ARTICLE INFO

Article history:
Received 22 June 2020
Received in revised form 6 October 2020
Accepted 6 October 2020
Available online 8 October 2020

Keywords:
Graphene wool
Isotherm
Kinetics
Natural organic matter (NOM)
Polycyclic aromatic hydrocarbons (PAHs)
Sorption process

ABSTRACT

The sorption of selected PAHs onto sediment components and graphene wool were studied. Different natural organic matter (NOM)- mineral-deficient (MDF), mineral-rich (MRF), and black carbon (BCF) fractions were recovered from natural sediment (NAS) using sequential separation methods. Detailed characterization of sediment components using BET, ICP-OES, SEM–EDS, XRD, and FTIR were carried out and significant changes in the physicochemical properties of sorbents due to the treatment procedure were revealed. Experimental data showed that a pseudo-second-order and Freundlich adsorption model best fit kinetic and isotherm studies, validated by the least values of Error Sum of Squares (SSE). Isotherm data revealed that complementary processes involving both multilayer adsorption and partitioning of PAHs occurred. NAS, BCF, and MDF with higher % OC had higher Freundlich and maximum adsorption capacities (K_f and q_{max}) than MRF for PAHs and an *S*-type sorption curve ($N > 1$) dominated the PAH–NOM interaction, with few exceptions for LMW PAHs. MRF significantly diminished the efficiency of graphene wool in the removal of selected PAHs from aqueous solution, as both adsorption capacity (K_d) and efficiency reduced from 16.9 g L^{-1} and 95.4% to 0.3 g L^{-1} and 18.5% respectively. Sorption of the selected PAHs was slightly favored under acidic pH and higher temperatures. The sorption reaction was endothermic for NAPH & PHEN, and exothermic for PYR & PERY. Furthermore, aromaticity and hydrophobic moieties of the different PAHs and NOM significantly influenced the π-π and hydrophobic–organophilic interactions that may have occurred, which led to some degree of irreversible sorption as shown by *H*-indices. Therefore, the probable impact of each NOM fraction on the mobility and environmental risk management/remediation of PAHs is herewith evaluated.

1. Introduction

Polycyclic aromatic hydrocarbons (PAHs) are a ubiquitous and potentially carcinogenic class of environmental contaminants (ECs), composed of compounds with several aromatic rings (Gupta and Kumar, 2020). In South Africa, the total concentrations of PAHs in Buffalo River were in the range of 14.91–206 μg L^{-1} (in water) and 1107–22,310 μg kg^{-1} (in sediment) (Adeniji et al., 2019), while as high as 8310 μg L^{-1} was detected in wastewater influents (Limpopo Province, South Africa) (Mojiri et al., 2019). Natural organic matter (NOM) is a heterogeneous mixture of organic compounds, which are present in water supplies and at trace levels in treated water (Mahato and Gupta, 2020). NOM is either an amorphous

* Corresponding author.
E-mail address: patricia.forbes@up.ac.za (P.B.C. Forbes).

https://doi.org/10.1016/j.eti.2020.101202
2352-1864/

or condensed phase of carbon, also referred to as hard carbon, soot, black carbon, coal-derived particles, etc., which have been reported in natural sediments either as dissolved organic carbon (DOC) and/or particulate organic carbon (POC) and they have been postulated to be responsible for the desorption resistance and recalcitrance of contaminants in water bodies (Karickhoff et al., 1979; Kraaij et al., 2003; Ran et al., 2007).

In the environment, strong interactions exist between several hydrophobic organic contaminants (HOCs) and natural organic matter (NOM), and this plays a vital role in their fate, mobility, human exposure risk, and toxicity in aquatic environments. Furthermore, the bioavailability, pollution potential, and persistence of sediment-bound hydrophobic organic compounds depend on their physicochemical properties, and partitioning between the solid and aqueous interphase is indicative of potential risk with respect to recontamination of water bodies (Ghosh et al., 2001; Lu and Pignatello, 2002). Thus, there is a need to study the sorption–desorption interactions between different fractions of NOM and PAHs.

The efficiency of treatment strategies for PAH polluted aquatic environment, is influenced by the PAHs bound to sediment, which could potentially partition into the aqueous phase. Thus, to establish the fate and possible remediation strategy suitable for different classes of environmental contaminants in water, including PAHs, the amount of PAH adsorbed onto sediment components/NOMs must be accounted for (Ran et al., 2007; Ololade et al., 2018). In the last decade, graphene has attracted scientific interest in technological development for the remediation of polluted water, either in its pristine condition or as composites (Singh et al., 2018; Adeola and Forbes, 2019; Das et al., 2020). Due to the fact that NOM in untreated water leads to the fouling of pipelines and membrane filters used in water treatment plants (Yu et al., 2018; Mahato and Gupta, 2020); it is imperative to study the influence of different fractions of NOM on the adsorption performance of graphene wool.

This study aims at providing insights into the mechanisms of adsorption of PAHs onto sediment components, and the release potential of adsorbed PAHs into waters bodies and aquifers. Delineation of condensed and amorphous phases of NOM as well as understanding the role of *in-situ* mineral enrichment on the overall adsorption of two-to-five ringed PAHs, are all vital aspects of this study. This investigation will also provide useful information on how the presence of different NOM will potentially influence the efficiency of synthetic graphene-based materials (GBMs) used for water treatment purposes.

2. Materials and methods

2.1. Chemicals

Neat standards (98% purity) of naphthalene (NAPH), phenanthrene (PHEN), pyrene (PYR), and perylene (PERY) were purchased from Supelco (USA). PAHs are hydrophobic compounds; however, their solubility can be ensured using established procedures (Crisafully et al., 2008). The stock solutions were prepared by dissolving a known weight of PAH neat standard in 30% (v/v) methanol in deionized water to promote the dissolution of the respective PAHs.

Sodium azide (NaN_3) was purchased from Sigma-Aldrich (Germany), nitric acid (HNO_3), hydrochloric acid (HCl), sodium chloride (NaCl), sodium hydroxide (NaOH), and calcium chloride ($CaCl_2$) were purchased from Associated Chemical Enterprises (ACE, Johannesburg, South Africa). Sterile syringe filters (33 mm diameter) with a 0.45 μm pore size containing a hydrophilic polyethersulfone (PES) membrane were purchased from Merck (Darmstadt, Germany). All the solutions were prepared with ultra-pure water (9.2 $\mu S/cm^3$) obtained from a Milli-Q water purification system (Millipore, Bedford, MA, USA).

2.2. Equipment and characterization

Fluorescence emission measurements were taken using a Horiba Jobin Yvon Fluoromax-4 spectrofluorometer (Horiba Instruments Inc., Edison, NJ, USA). Elemental analysis was carried out using inductively coupled plasma-optical emission spectrometry (ICP-OES, Spectro Arcos model, Thermo Fisher Scientific, South Africa). Powder X-ray diffraction (XRD) patterns were obtained using a Bruker, D2 Phaser, Cu (Kα) radiation ($\lambda = 1.54184$ Å) (Bruker AXS GmbH, Karlsruhe, Germany). Scanning electron microscopy (SEM) images were taken using a Zeiss Ultra-Plus 55 field emission scanning electron microscope (FE-SEM), operated at 2.0 kV and equipped with an energy dispersive X-ray spectrometer (EDS) (OXFORD Link-ISIS-300 Zeiss, Germany). FTIR spectra were obtained using a Bruker Alpha-T spectrometer (Bruker Optik GmbH, Ettlingen, Germany). The surface area and porous structure of sediment components were determined by N_2 adsorption–desorption isotherms at 77 K, using a NOVA Touch Surface Analyzer system (Anton Paar, South Africa) in a relative pressure (P/P_0) range of 0.01–1.0, following a model of Brunauer–Emmett–Teller (BET) and Barrett–Joyner–Halenda (BJH) techniques. 10 mg of the NOM fractions were weighed into pre-cleaned crucibles and placed in a muffle furnace (Carbolite™, ThermoFisher Scientific, South Africa) at 350 °C for 16 h. After cooling the samples were re-weighed and the weight difference was used to estimate the organic carbon content (%) (Frangipane et al., 2009; Nelson and Sommers, 2018). Point zero net charge (PZNC) was determined using the salt addition method (Mahmood et al., 2011). A shaking water bath was purchased from Celsius Scientific (South Africa). The ionic strength of solutions was monitored using an Orion Star A112 conductivity benchtop meter (Thermo Scientific, South Africa), and pH was measured using a 780-pH meter (Metrohm Herisau, Switzerland).

2.3. Sediment collection and treatment

Stream sediment was collected from the University of Pretoria sports campus, South Africa (latitude E28° 14′ 46″ and longitude S25° 45′ 10″), using a stainless-steel trowel cleaned with methanol, and samples were transported in clean polypropylene zip-lock bags. Each sediment sample was air-dried for 48 h at ambient temperature, ground with a clean agate mortar and pestle, and sieved with a mesh size of 54 μm in the laboratory. The sieved sediment was stored in air-tight glass bottles at ambient temperature before further treatment.

The natural sediment (NAS) in addition to three sorbent fractions; mineral-deficient fraction (MDF), black carbon fraction (BCF), and a mineral-rich fraction (MRF) obtained from the NAS sample, were used in this study to evaluate the influence of NOM fractions on sorption of 2- to 5- membered ring PAHs. Briefly, the bulk sediment sample was split into two portions and from one portion, the first isolate (MDF sample) was recovered via the treatment of NAS with 1 N HCl for 45 min at ambient temperature (Ololade et al., 2018). After rinsing with deionized water, the sample was treated with a mixture of 1 N HCl and 10% HNO_3, three times successively for 12 h at ambient temperature. The solid residue recovered after centrifuging at 3800 g for 30 min and filtration using Whatman filter paper (11 μm pore size), was washed with deionized water and freeze-dried at −4 °C for 24 h (Gelinas et al., 2001). The BCF sample was obtained by thermal oxidation of the MDF sample in a crucible, heated in a tube furnace at 375 °C for 24 h, where the residue obtained is condensed organic matter, composed of cross-linked heterocyclic compounds (Ran et al., 2007; Ololade et al., 2018). *In-situ* enrichment of minerals in the native sediment (NAS) was done by repeatedly adding 30% H_2O_2 with stirring at 40 °C. This was repeated until the solution became clear, indicating that most of the organic matter had been removed (Mikutta et al., 2005), and the residue (MRF) was rinsed with deionized water and freeze-dried before sorption studies.

2.4. Isotherm sorption experiment

Batch sorption experiments were carried out in sealed 40 mL PTFE screw cap amber vials (Stargate Scientific, South Africa) at 25 ± 1 °C. Background solution (pH = 7.0) contained 0.01 mol L^{-1} $CaCl_2$ (ACE, South Africa) in deionized water with 200 mg L^{-1} NaN_3 (Sigma-Aldrich, Germany) as a biocide. The experiments were conducted in triplicate with varying initial NAPH, PHEN, PYR, or PERY concentrations. Sorption kinetic studies were carried out using 100 mL beakers, sealed with aluminum foil. 20 mg of each adsorbent was treated with 50 mL of NAPH, PHEN, PYR, or PERY (500 μg L^{-1}) in a background electrolyte solution (pH = 7 ± 0.1). The vials were equilibrated for 24 h and supernatants were taken for fluorescence spectrometric analysis at different time intervals. For the isotherm study, each of the bulk sediment and isolated components (40 mg) were treated with 20 mL of NAPH, PHEN, PYR, or PERY solution (100, 200, 300, 400, and 500 μg L^{-1}) in a background electrolyte solution (pH = 7 ± 0.1). The vials were shaken in a thermostated shaking water bath at 200 rpm at 25 ± 2 °C for 24 h (Adeola and Forbes, 2019). Subsequently, supernatants from adsorption experiments were decanted for subsequent measurements, while 20 mL of fresh 0.01 mol L^{-1} $CaCl_2$ containing 200 mg L^{-1} of sodium azide was introduced into the vials containing the sorbents with 100 to 500 g L^{-1} initial concentration of NAPH, PHEN, PYR or PERY for desorption experiments as previously described (Wang et al., 2008). Prior to the determination of the equilibrium concentration for both adsorption and desorption experiments, the vials were centrifuged at 3000 g for 20 min and a 2 mL aliquot of the supernatant was filtered through a 0.45 μm syringe filter. Equilibrium concentrations of NAPH, PHEN, PYR, or PERY were determined by fluorescence spectrophotometry at excitation wavelengths of 280, 290, 341, and 410 nm respectively. The amount of each solute adsorbed and desorbed (q_e, μg g^{-1}) was calculated as follows;

$$q_e = \frac{(C_0 - C_e)V_0}{S_m} \tag{1}$$

where C_o (μg L^{-1}) is the initial PAH concentration, C_e(μg L^{-1}) is the equilibrium solute concentration, V_o is the initial volume (L) and S_m is the mass (g) of the adsorbent.

$$\textit{Removal efficiency}\ (\%) = \frac{(C_0 - C_e)}{C_0} \times 100 \tag{2}$$

Furthermore, to investigate the competitive or synergistic influence of NOM derived from stream sediments on the removal efficiency of a synthetic graphene-based material (GBM), 20 mg of graphene wool; synthesized via chemical deposition method as previously described (Adeola and Forbes, 2019; Schoonraad et al., 2020), was weighed into 25 pairs of 40 mL amber vials. 10 mg of NAS, MDF, BCF, or MRF were added separately into 5 vials each and 5 vials with graphene wool only were used as a control. 20 mL of PYR solutions (100–500 μg L^{-1}) in 0.01 M $CaCl_2$ background electrolyte solution (pH = 7 ± 0.1) were added into the five sets of vials and were equilibrated for 24 h. All experiments were carried out in triplicate.

2.5. Effect of initial pH and temperature

In this study, the effects adsorption temperature (25, 35, and 45 °C) and pH (3, 5, 7, 9, and 11) on the adsorption of NAPH, PHEN, PYR, and PERY onto NAS, MDF, BCF, and MRF were investigated. The pH of the solution was adjusted with 0.1 N HCL and 0.1 N NaOH. Adsorption equilibrium experiments and subsequent quantification were carried out as described in Section 2.4, in triplicate.

Table 1
Sorbent fraction characterization.

Sorbent	pH	CEC (M_{eq}/100 mg)	OC (%)	PZNC	S_{BET} (m^2 g^{-1})	V_{tpv} (cc g^{-1})	V_{BET} (nm)
NAS	6.8	27.4	6.8	5.4	15.3	0.073	7.80
MDF	4.5	1.3	9.4	5.1	26.1	0.145	7.80
BCF	5.7	0.6	9.8	4.4	7.2	0.040	10.68
MRF	6.2	8.4	3.4	2.7	390.5	1.049	7.45

CEC = cation exchange capacity (Hendershot and Duquette, 1986).
OC = organic carbon content (Frangipane et al., 2009; Nelson and Sommers, 2018).
PZNC = point of zero net charge (Mahmood et al., 2011).
S_{BET} = specific surface area by multipoint BET method (Gregg and Sing, 1982).
V_{tpv} = total pore volume calculated from the amount of N_2 adsorbed at $P/P_0 = 0.98$ (Haghseresht and Lu, 1998).
V_{BET} = BET average pore diameter.

2.6. Quality control

Experimental procedures were carried out under strict adherence to quality control guidelines. PAH standards were used to quantify the concentrations of the four PAHs, and the calibration curves showed high correlation coefficients ($R^2 > 0.9$). PAHs were not detectable in blank experiments, which indicated that the influence of pre-existing PAHs in the sediment samples on the overall adsorption was negligible. Each series of experiments was repeated in triplicate to establish reproducibility. For each experiment batch, vials without adsorbent were included as controls. These controls showed no significant losses to the walls of glassware or microbial degradation during the equilibration period.

3. Results and discussion

3.1. Characterization of sorbents

The data on sorbent characterization and PAH properties are presented in Table 1 and S1. The specific surface area (SSA), pore volume, and width were derived from the N_2-BET isotherm; cation exchange capacity (CEC) was calculated from Ca, Mg, K, and Al obtained from ICP-OES (Table S2) (Hendershot and Duquette, 1986), and organic carbon content (% OC) was determined using a thermal combustion method as previously described (Section 2.2). The NOM fractions employed in this study had varying physical and chemical characteristics and a relatively wide range of organic carbon (OC) content of 3.4 to 9.8% due to the treatment procedures employed. The point zero net charges shown in Figure S1 revealed that the treatment procedure significantly altered the charge on the surface of the material and PZNC were more acidic (Table 1). The SEM images (Fig. 1) reflect the accessibility of the sorbents, as the surfaces were largely heterogeneous, rough, microporous, and had an irregular grain structure with MRF being less aggregated and having a smaller grain size. The treatment procedures created pores with irregular spheres observed in the MDF and BCF sorbent fractions. Optical images revealed different colorations of the bulk sediment and its derivatives.

The hump nature of the XRD pattern (Fig. 1) for NAS confirms its amorphous state, whilst the sequential modification thereof led to narrow and sharp peaks, confirming improved crystallinity of the isolates. The peak at around 26° is due to the (002) lattice plane arising from the graphite structure of carbon black, which is more prominent for the BCF fraction with the highest % OC. A slight peak shift to the right for treated samples is due to lattice contraction as a result of the treatment process (Shang et al., 2015). FTIR spectra revealed different intensities of the Fe–O stretching mode (737.3 cm^{-1}) for all samples and a doublet O–H stretching mode associated with $Fe(OH)_2$ and $Fe(OH)_3$ at 3727.9 and 3716.7 cm^{-1} for NAS and MRF samples (Wang and Andrews, 2006). The spectra revealed major adsorption peaks at 1020–1200 cm^{-1}, 1110–1080 cm^{-1}, 400–800 cm^{-1}, and 1650 cm^{-1} assigned to C–OH, siloxane or silicone (Si–O–C), C–O, C=H bends, C–N stretching, and carbonyl (C=O). Generally, the spectra revealed distinct similarities in functionality but different band strengths. The trend in peak intensity of the various sorbents was in the order of BCF < MRF < MDF < NAS. EDS and ICP results (Figure S2 and Table S2) confirmed that the treatment processes altered the mineralogy of the samples, considering the relative abundance of the elements.

Fig. 1(c) depicts type-IV N_2 isotherms at standard temperature and pressure (STP), for the sediments and its components derived via the *in-situ* treatment procedure. The plot revealed an H3 hysteresis between the adsorption and desorption isotherms, followed by a steep increase in the amount of N_2-adsorbed at higher relative pressures, previously ascribed to mesoporous adsorbents (Oyedotun et al., 2019), especially the MRF with significantly higher specific surface area (S_{BET}) and pore volume (V_{tpv}) of 390 m^2 g^{-1} and 1.049 cc g^{-1} respectively (Table 1). Fig. 1(c) displays desorption pore size distribution of the sorbents determined via the BJH technique, displaying several peaks which depict that all sorbents possess both microporous (0 – 2 nm) and mesoporous (2 – 8 nm) structures. The SSA and PV were in the order; MRF > MDF > NAS > BCF, interestingly, BCF has the largest pore width of 10.68 nm, which can be attributed to the thermal oxidation (at 375 °C) process that BCF was derived from.

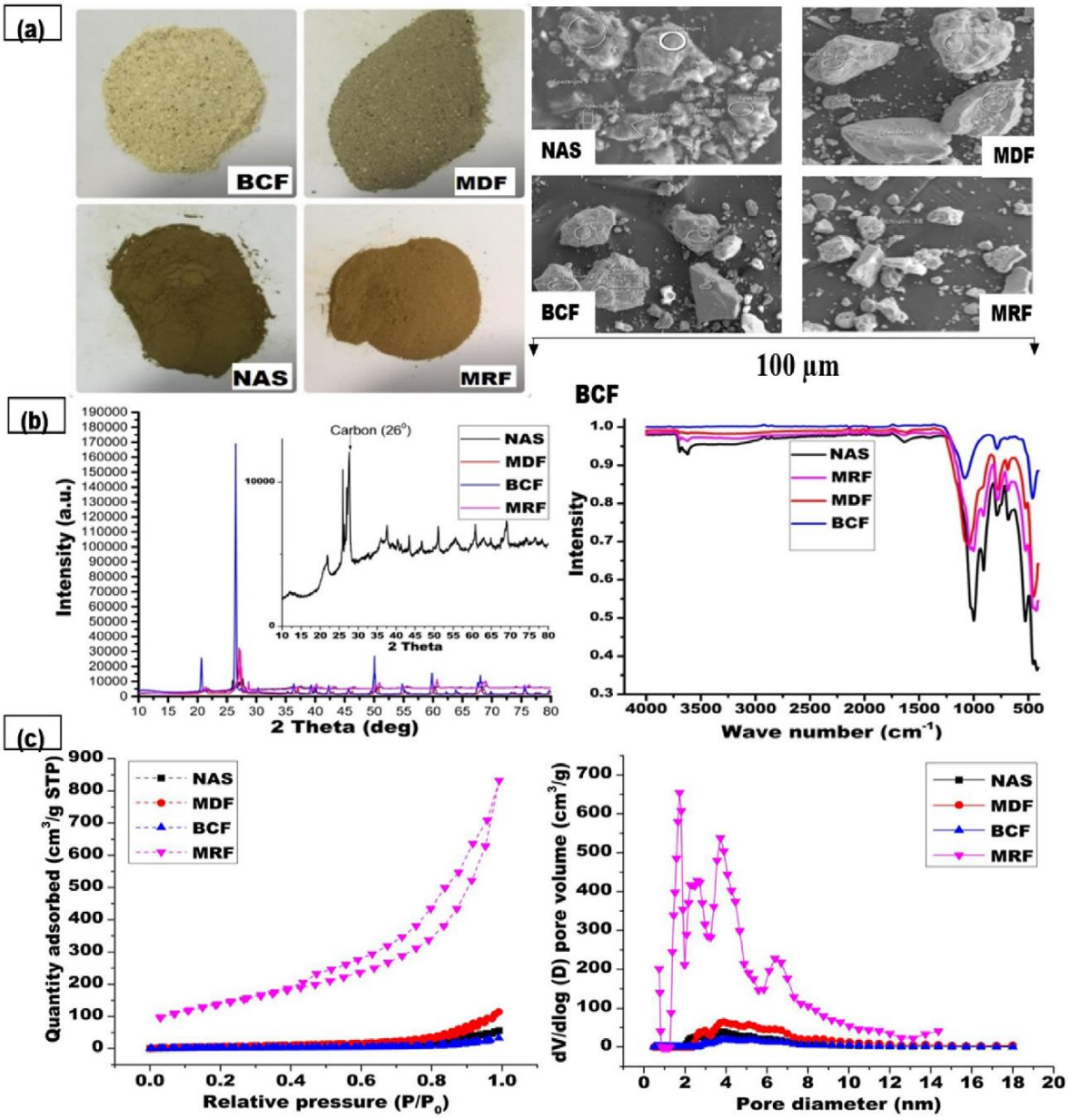

Fig. 1. (a) Optical and SEM images (b) XRD and FTIR spectra (c) N_2 – Isotherm and pore size distribution plots for natural sediment and its components.

3.2. Sorption kinetics

The pseudo-first-order and pseudo-second-order kinetic models were investigated and compared in order to study the mechanism of the adsorption process (Zhao et al., 2011; Adeola and Forbes, 2019). The amount of solute sorbed per gram of sorbent at equilibrium (q_e) and the first-order and second-order sorption rate constants (k_1 and k_2) can be evaluated from the slope and the intercept deduced from a plot of log ($q_e - q_t$) against t for first-order, and a plot of t/q_t against t for second-order kinetic models, respectively (Lagergren, 1898; Younis et al., 2015; Adeola and Forbes, 2019). The kinetic parameters obtained from models employed are summarized in Table 2 and the kinetic plots are displayed in Fig. 2. The second-order equation fit far better with experimental data obtained from this study (Fig. 2 and S5), with correlation coefficients (R^2) ranging from 0.934 to 0.997, compared with the first-order model with R^2 values ranging from 0.601 to 0.896 (Table 2). The experimental adsorption capacity, q_e, for NAPH, PHEN, PYR, and PERY interaction with

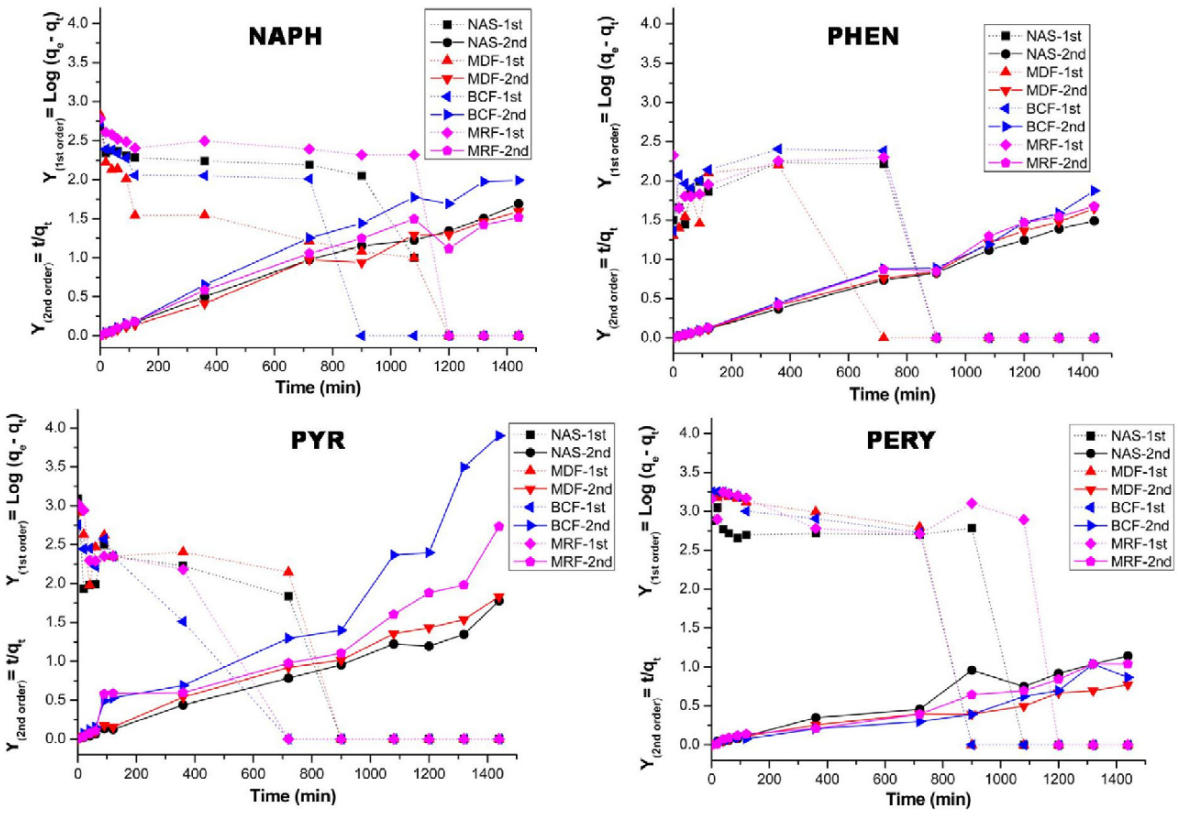

Fig. 2. Lagergren pseudo-first-order and pseudo-second-order kinetics sorption for naphthalene, phenanthrene, pyrene, and perylene onto sediment components.

Table 2
Coefficients of sorption kinetics for adsorption of selected 2- to 5- ringed PAHs by sediment components and the corresponding correlation coefficients (R^2).

PAH	Sorbent	1st order				2nd order			
		Cal. q_e (μg g^{-1})	*Exp.* q_e (μg g^{-1})	K_1 (min^{-1})	R^2	*Cal.* q_e (μg g^{-1})	*Exp.* q_e (μg g^{-1})	$K_{2*}(10^{-4})$ (μg g^{-1} min^{-1})	R^2
NAPH	NAS	0.996	894	6.02	0.864	909	894	0.44	0.996
	MDF	0.997	904	4.52	0.658	909	904	3.90	0.997
	BCF	0.995	668	5.76	0.885	667	668	0.58	0.987
	MRF	0.996	778	6.45	0.698	769	778	0.51	0.965
PHEN	NAS	0.997	1089	4.48	0.601	1000	1089	1.09	0.997
	MDF	0.996	1029	3.59	0.678	909	1029	0.83	0.994
	BCF	0.996	832	4.93	0.698	833	832	0.80	0.988
	MRF	0.997	836	4.67	0.729	833	836	1.30	0.991
PYR	NAS	0.996	1005	5.43	0.842	909	1005	1.20	0.985
	MDF	0.995	969	6.18	0.862	833	969	0.45	0.994
	BCF	0.995	405	5.62	0.896	417	405	1.20	0.939
	MRF	0.995	751	5.99	0.885	667	751	0.25	0.934
PERY	NAS	0.995	1261	7.12	0.754	1250	1261	1.31	0.962
	MDF	0.994	2175	7.15	0.878	2000	2175	0.08	0.980
	BCF	0.994	1745	7.85	0.889	1667	1745	1.10	0.980
	MRF	0.996	1560	7.90	0.649	1429	1560	0.36	0.978

Cal. q_e: Calculated amount adsorbed; Exp. q_e: Experimental amount adsorbed; K_1: First order rate constant; K_2: Second-order rate constant.

different sediment components, is similar to what was calculated or predicted using the second-order kinetic equation, which further confirms that the adsorption process follows the second-order kinetic pathway and this suggests that chemisorption may have occurred either via hydrogen or covalent bonding between the sediment components and the selected PAHs (Yu et al., 2015). The time-concentration profile revealed a fast rate of adsorption occurred in the first 60

min, due to the abundance of sorption sites, before proceeding to equilibrium after different times for the different PAHs and sorbents used in this study (Figure S5).

Table 2 revealed that *in-situ* mineral enrichment (MRF) which involves the release of minerals trapped in the organic carbon framework and reduction of the % OC content in the sediment sample (Table 1 and S2), led to improved rate constants K_1 and K_2 when compared with NAS. The BCF which is regarded as condensed organic matter due to the extensive cross-linkage which largely defines its structural chemistry (Ran et al., 2002; Ololade et al., 2018), has a lower rate constant K_2 than values obtained for MDF, containing amorphous carbon, for lower molecular weight (LMW) PAHs (NAPH and PHEN). However, the reverse was observed for higher molecular weight (HMW) PAHs (PYR and PERY), with BCF possessing a higher sorption rate constant K_2.

3.3. Sorption isotherm

The characterization results of sorbents revealed both chemical and structural differences (Table 1, Figure S2), and the physicochemical properties of the chosen 2- to 5- membered ring PAHs also vary (Table S1). Hence, differences in the sorption behavior of the four PAHs are expected. The detailed isotherm data are presented in Table S2–S4, a summary of the data is provided in Table 3, and isotherm model plots are presented in Figure S3 and S4. Based on the Error Sum of Squares (SSE) values obtained from nonlinear regression analysis of sorption equilibrium data, complimentary sorption mechanisms took place across all sorbents and PAHs. The results indicate that both multilayer adsorption and partitioning occurred during the sorption experiments, similar to what was reported by Wang et al. (2008). However, the layer-on-layer adsorption mechanism described by the Freundlich model best fits the adsorption data and is validated by the least values of SSE obtained.

The maximum adsorption capacities of sediments were mainly found in the order BCF > MDF > NAS > MRF (Table 3), which correlates with % OC as listed in Table 1. The surface of NOM possesses largely hydrophobic sites that promote hydrophobic–organophilic interactions between the hydrophobic moieties of selected PAHs and sediment components. Table 3 reveals higher values of adsorption capacities (K_f and K_d) and maximum adsorption capacity (q_{max}) for the mineral-deficient fraction (MDF) over the mineral-rich fractions of NOM (MRF), thus establishing a positive correlation between overall adsorption capacities and % OC of the respective fractions.

The adsorption capacity/coefficient (K_d) is also regarded as the partition distribution/partitioning coefficient (K_p) and is derived from the same linear model equation (equation S6). The fact that K_d and/or K_p is lower for higher molecular weight PAHs, suggests that heavier PAHs were less available for solid–liquid partitioning, unlike lower molecular weight PAHs. This unusual trend may be due to organic vs mineral content of the native sediments and morphology (i.e. pore size and structure) of the sorbents. Results of ICP-OES and EDS analysis revealed that the sediment used in this study is rich in minerals, which could potentially offset the hydrophobicity of the surface of the sorbent and partitioning of HMW PAHs (Yu et al., 2014). However, the relatively higher adsorption maxima (q_{max}) reported for PERY, compared with PYR and PHEN, can be attributed to the fact that sorption mechanisms were not entirely controlled by partitioning but by the tendency for multilayer adsorption of sorbates (Freundlich model).

Several authors have reported that the N value relates to the heterogeneity index of the adsorbate and energy distribution of hard, glassy, or condensed natural organic matter. It was also postulated that lower N values reflect more heterogeneous adsorption sites and the extent of NOM maturation (Weber et al., 1992; Ran et al., 2002, 2003; Xiao et al., 2004; Ololade et al., 2018). The values of N were mostly greater than unity, which affirms that the chemical and thermal treatment procedure led to maturation (irreversible transformation) of the native sediment, making the isolates (MDF and BCF) more organophilic, thus improving their sorption capacities except for MRF. There is stronger interaction between MDF-PAHs and BCF-PAHs, than the interaction between MRF-PAHs, considering the higher values of Langmuir constants, $K_{L,}$ and q_{max} (Table 3). Furthermore, when $N > 1$, as the case for most of the HMW PAHs and NOM used in this study, it depicts an S-type isotherm curve. The S-type shape indicates that there is weak PAH–NOM interaction at lower concentrations and the sorption process is enhanced at higher PAH concentrations (Ololade et al., 2018). However, complete saturation of the NOM was not achieved in this study (Figure S3) due to the low concentration range (ppb), as the choice of concentration employed was informed by levels of PAHs typically present in the environment.

3.4. Desorption isotherms and hysteresis effects

Desorption experiments were conducted using the adsorbed PAHs on each NOM sample as the total mass of sorbate in the desorption system and the actual amount desorbed was accounted for with the aid of the mass balance equation (Eq. (1)). This was necessary to be able to predict the release potential, binding capacities, and risk of environmental recontamination associated with adsorbed PAHs (Wang et al., 2008).

Table 4 revealed that there was a significant difference between the adsorption intensity (N_{ads}) and desorption intensity (N_{des}). Therefore, the hysteresis indices *(H)* ($H = N_{ads}/N_{des}$), for the PAHs across the different NOM were greater than 1 for HMW PAHs (PYR & PERY), which suggests that sorption–desorption hysteresis took place to a larger extent. However, NAPH and PHEN displayed some degree of reversible adsorption onto different NOMs, with H-indices less than 1. The unique behavior of NAPH and PHEN can be attributed to its physicochemical properties, such as lower molecular weight and hydrophobicity (Log*Kow*) (Table S1). It is worthy to note that the majority of the H-indices for PAHs were in the

Table 3
Summary of Freundlich, Langmuir, and linear sorption parameters for sorption of selected 2- to 5- ringed PAHs onto natural sediment and its component fractions.

Sorption model	Parameter	NAS	MDF	BCF	MRF
Freundlich	K_f	6.2e−3−24.10	9.4e−6−70.60	3.1e−2−12.36	2.4e−3−11.71
	N	0.26−2.45	0.23−3.46	0.04−1.85	0.38−2.39
	SSE	0.002−0.19	0.023−2.01	0.200−2.24	0.014−1.15
Langmuir	q_{max} (μg g^{-1})	94.1−7853.2	54.5−10678	239.6−13212	234.5−5807.4
	K_L (L μg^{-1})	1.9e−4−0.08	2.2e−4−0.3	1.5e−4−15.30	2e-4−0.02
	SSE	0.003−0.90	0.069−2.60	0.54−2.25	0.25−1.28
Linear	K_d	0.50−6.13	0.32−6.05	0.09−2.07	0.27−3.03
	SSE	0.03−1.23	0.19−2.60	0.54−2.53	0.23−1.27
	$Log\ K_{oc}$	0.85−1.34	0.53−1.81	0.04−1.32	0.60−1.93

Freundlich model: $qe = K_f C^N e$; Langmuir model, $q_e = q_{max} Ce/(K_L + C_e)$; Linear model: $q_e = K_d C_e$; K_{oc} is the OC-normalized sorption capacity coefficient with a unit of μg/g-OC/(μg $L^{-1})^n$.

Table 4
Sorption–desorption parameters and hysteresis indices derived from the Freundlich isotherm model.

PAH	Sorbent	$LogK_{f(des)}$	N_{ads}	N_{des}	[a]H	Desorption ± SD (%)
NAPH	NAS	1.82	0.89	2.87	0.31	6.19 ± 5.65
	MDF	1.79	1.19	3.24	0.37	8.23 ± 6.29
	BCF	1.17	1.32	1.69	0.78	12.49 ± 6.57
	MRF	1.62	0.59	2.94	0.20	8.97 ± 6.98
PHEN	NAS	1.33	0.26	2.27	0.12	10.02 ± 3.62
	MDF	0.92	0.31	1.29	0.24	17.92 ± 17.60
	BCF	−0.78	0.04	0.39	0.10	27.72 ± 36.24
	MRF	3.86	1.15	0.54	2.13	35.87 ± 33.74
PYR	NAS	0.82	0.79	0.47	1.68	54.52 ± 16.61
	MDF	2.21	4.24	4.16	1.02	62.67 ± 14.44
	BCF	−0.56	1.46	1.19	1.23	86.38 ± 17.67
	MRF	−12.21	0.38	0.17	2.23	70.18 ± 17.96
PERY	NAS	4.86	2.45	1.22	2.01	53.49 ± 7.96
	MDF	−14.78	2.57	0.15	17.13	67.53 ± 11.84
	BCF	0.55	1.85	0.76	2.43	54.44 ± 6.04
	MRF	3.17	2.39	0.28	8.54	63.17 ± 13.74

[a]H: Sorption–desorption hysteresis index.
$H = N_{ads}/N_{des}$; SD: Standard deviation.

order, PERY > PYR > PHEN > NAPH, which reflect differences in binding strengths, while *in-situ* sediment treatment led to greater desorption of adsorbed PAHs, as % desorption values were higher in modified NOM than untreated sediments, thus revealing that the isolates had a lower capacity to retain PAHs. Table 4 revealed that the native (NAS) sample had the least % desorption across the PAHs investigated, which may be due to its pristine condition and high binding strength (q_{max}). The relatively high % desorption of MRF reflects its inability to retain PAHs, due to its morphology and/or low % OC content. Higher % desorption for larger PAHs (PYR and PERY) as compared to smaller PAHs can be attributed to size-controlled interactions between sorbate molecules and active sites/pores. Smaller PAHs are expected to penetrate deeper into pores via intra-particle diffusion and are thus more difficult to remove (Hall et al., 2009). Adsorption and desorption are complementary processes that take place simultaneously at different rates during batch sorption experiments until the maximum adsorption capacity of the material is reached. Hysteresis, which is regarded as irreversible adsorption, occurs when the intensity (N_{ads}) of adsorption is greater than desorption intensity (N_{des}) (Cornelissen et al., 2005).

For a material designed for remediation, it is preferred that the H index be greater than 1 in an aqueous medium, which reflects higher adsorption intensity and lower desorption intensity. Thus the employment of a suitable organic solvent would be required to force or enhance desorption/regeneration after the adsorption cleanup has been achieved. An H-index greater than unity is also desirous in aquatic environments as adsorbed organic contaminants (OCs) held by sediments will pose a lower tendency to recontaminate surface water. Adsorbent pore deformation (irreversible collapse or disorientation) and hydrophobicity of the sorbates are responsible for hysteretic behavior in sorption dynamics (Lu and Pignatello, 2002). PAH-induced alteration of the sorbent and solution chemistry (Adeola and Forbes, 2019), were potential factors that could lead to the build-up of pressure, pore expansion, pore deformation, and deviation of NOM from the native thermodynamic state.

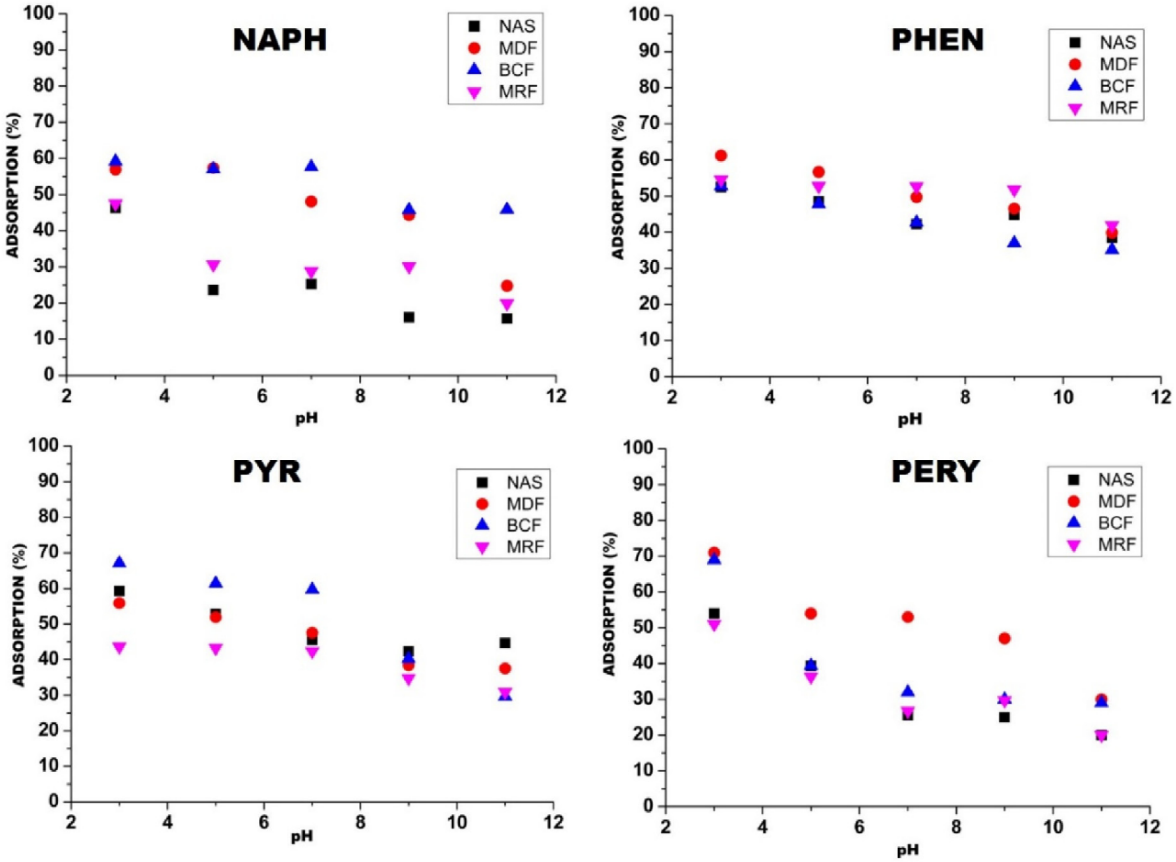

Fig. 3. Effect of solution pH on adsorption of selected PAHs onto sediment components. (Experimental conditions: C_o = 500 μg L^{-1}; dosage = 1 g L^{-1}, mixing rate = 200 rpm, T = 25 ± 1 °C, contact time: 24 h).

3.5. Effect of pH on the sorption of PAHs onto sediment components

Solution pH influences the sorption process of many organic contaminants onto different soils and sediments because it alters the net charge of the adsorbent and sorbate (Ololade et al., 2018; Adeola and Forbes, 2019). Several reports indicate that PAH sorption is not influenced by pH since PAHs do not ionize in water (Guo et al., 2018). However, depending on the nature of the adsorbent, solution pH may influence the sorption process of PAHs (Huang et al., 1996).

Generally, acidic pH appears to favor adsorption of the PAHs slightly more than basic pH across the NOM fractions and the role of pH was more significant for perylene (PERY) adsorption (Fig. 3). The PZNC of the sorbents ranged from 2.7 to 5.4 (Table 1, Figure S1). Thus, the somewhat higher % adsorption of the respective PAHs onto the different sediment components under acidic conditions may be as a result of the positively charged surface of the adsorbent in acidic solution, which may promote the formation of hydrogen bonds and/or electrostatic attraction between the PAHs and sediment components due to the presence of -NH, C-OH and -OH groups in the sediment components. It is noteworthy that the effect of pH on adsorption of any of the 5-ringed PAHs onto any material at all has only been reported once in the literature (Schlautman and Morgan, 1994). Schlautman and Morgan (1994) reported that samples containing minerals such as silicates, as we have in NOM fractions (Table S2), have point zero surface charge at pH ≥ 2.0. Point zero charge (PZC or PZNC) is the point in which the net surface charge of the material is zero, and this could be anywhere on the pH scale for different materials (Bakatula et al., 2018). For the materials described by Schlautman and Morgan (1994), the surface of the material is dominantly negatively charged at pH > 2, leading to electrostatic repulsion and a decline in % adsorption occurs.

3.6. Effect of temperature and thermodynamic studies

Thermodynamic parameters such as Gibb's free energy (ΔG), enthalpy (ΔH), and entropy (ΔS) of the adsorption process for PAH and NOM were estimated from the Vant't Hoff plots (Fig. 4), using the Van't Hoff equations (Eqs. (3)

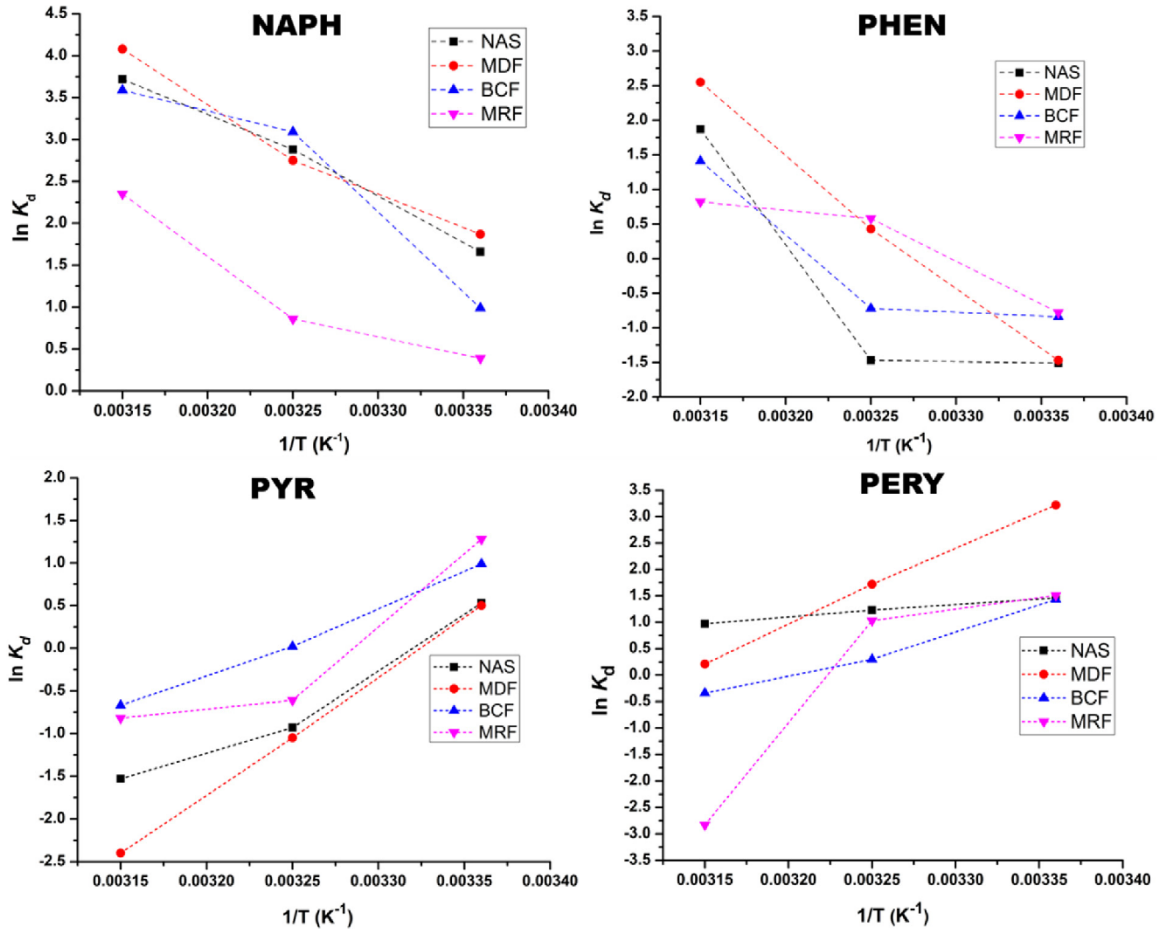

Fig. 4. Plot of Van't Hoff plots for NAPH, PHEN, PYR and PERY adsorption onto sediment components at 298, 308 and 318 K.

and (4)) (Yakout and Daifullah, 2013; Gupta and Singh, 2018; Adeola and Forbes, 2019)

$$\ln K_d = \frac{\Delta S^\circ}{R} - \frac{\Delta H^\circ}{RT} \quad (3)$$

$$\Delta G^\circ = \Delta H^\circ - T\Delta S^\circ \quad (4)$$

Temperature plays a significant role in several chemical and physical processes as some reactions are feasible at room temperature, while others require an additional supply of heat energy to initiate the reaction. Therefore, the role of temperature on the adsorption of NAPH, PHEN, PYR, and PERY onto sediment components was studied at 298, 308, and 318 K, respectively.

The Van't Hoff plot (Fig. 4) revealed that the adsorption capacity of the different NOM fractions, expressed as "$ln\ K_d$", increased with an increase in temperature for the LMW PAHs (NAPH & PHEN), but decreased for HMW PAHs (PYR & PERY). Table S7 also revealed that adsorption of the PAHs onto the stream sediment components involved a spontaneous endothermic reaction for LMW PAHs (NAPH & PHEN), with positive and negative values of ΔH and ΔG respectively. For the HMW PAHs used in this study, heat is generated and emitted to the surroundings, indicating an exothermic process with negative enthalpy values ($-\Delta$H) for PYR and PERY. Furthermore, an increase in temperature improves the sorption feasibility for NAPH and PHEN as ΔG became more negative, whilst for PYR and PERY adsorption was more feasible at room temperature or below, considering the trend in ΔG values. Several reports have shown that the thermodynamic behavior of PAHs differs for different adsorbents (Ghosh et al., 2001; Zhao et al., 2011; Younis et al., 2015; El-shahawi et al., 2017; Gupta and Singh, 2018).

Some sorbate–sorbent interactions are endothermic, such as pyrene adsorption by some carbonaceous adsorbents (Younis et al., 2015; Girardello et al., 2016; Adeola and Forbes, 2019), while pyrene interaction with activated carbon and

Table 5
Freundlich, Langmuir and linear sorption parameters for sorption of pyrene onto GW and GW-NOM hybrids.

Sorption model	Parameter	GW	GW-NAS	GW-MDF	GW-BCF	GW-MRF
Freundlich	$LogK_f$	1.89	−3.87	−0.79	0.46	−0.13
	N	3.2	0.2	0.8	1.1	5.2
	R^2	0.999	0.946	0.993	0.993	0.899
Langmuir	q_{max} (μg g^{-1})	344.8	35.6	212.8	1667.0	23.2
	K_L (L μg^{-1})	0.1	0.009	0.002	0.001	0.002
	R^2	0.996	0.953	0.995	0.997	0.979
Linear	K_d (g L^{-1})	16.9	4.2	0.6	1.8	0.3
	$Exp.q_e$ (μg g^{-1})	230.8	128.2	81.7	138.1	43.2
	R^2	0.940	0.948	0.985	0.985	0.706
	RE (%)	95.8	67.4	38.0	75.1	16.5

Freundlich model: $q_e = K_f C^N e$; Langmuir model, $q_e = q_{max} Ce/(K_L + C_e)$; Linear model: $q_e = K_d C_e$; Exp. q_e: Experimental amount adsorbed. RE (%): percent removal efficiency.

mineral-rich adsorbents has been reported to be exothermic (El-shahawi et al., 2017; Hassan et al., 2018). Furthermore, both positive and negative values of ΔH within the range of −7100 J mol^{-1} and + 3800 J mol^{-1} were reported for NAPH sorption onto silt under different temperature regimes, suggesting that both endothermic and exothermic sorption processes may occur within the same sorbate–sorbent interaction (Wauchope et al., 1983; Unuabonah et al., 2016). This further confirms the complex sorption thermodynamics of PAHs and affirms the importance of temperature regimes in the adsorption process towards its application in the remediation of PAH pollution. Thermodynamic parameters are influenced by the morphology and chemical composition of the NOM fractions, which vary for different geological environments, and thus the sequestration of different PAHs within sediments in an ecological environment cannot be fully understood if the composition of the NOM is not determined.

3.7. Influence of NOM on GW-pyrene interaction

A detailed study on the adsorption kinetics and sorption–desorption isotherm of pyrene interaction with graphene wool (GW) has previously been reported (Adeola and Forbes, 2019). Thus, this section focuses on results obtained from the addition of different NOM fractions into solutions containing graphene wool and pyrene, in order to establish the synergistic or competitive influence of sediment components on the overall removal efficiency of pyrene by graphene wool (GW). Table 5 and Fig. 5 revealed that the presence of the sediment components/NOM in the sorption process played a dominant competitive role and had an inhibitory effect on the overall removal efficiency of pyrene. The presence of NOM altered the sorption mechanism from multilayer adsorption, described by the Freundlich isotherm model for GW-pyrene, to a monolayer adsorption mechanism for GW-NOM-pyrene interactions; considering the R^2 values (Table 1). Furthermore, the influence of bulk sediment and its components differ as removal efficiencies were in the order of GW > GW-BCF > GW-NAS > GW-MDF > GW-MRF (Fig. 5). The high maximum adsorption capacity (q_{max}) of GW-BCF (Table 5), suggests that the presence of condensed organic carbon (BCF) in a PAH contaminated water body would potentially be least detrimental to the removal efficiency of GBMs. MRF significantly impeded the removal of pyrene from aqueous solution as adsorption capacity (K_d), experimental amount adsorbed ($Exp.\ q_e$), and removal efficiency reduced (16.9 to 0.3 g L^{-1}), (230.8 to 43.2 μg g^{-1}) and (95.4 to 16.5%) respectively. This suggests that the presence of NOM containing high amounts of minerals may reduce the adsorption efficiency of graphene wool significantly, as the minerals could be leached into the solution and adversely alter the solution's chemistry (Lamichhane et al., 2016).

There are reports that metals and other minerals bind strongly to graphene-based materials (GBMs) (Xu and Wang, 2017). Therefore, it can be hypothesized that the prominent inhibitory role of MRF may be because some of the minerals listed in Table S2, may have leached into the solution and competitively adsorbed on the sorption sites of GW due to the comparatively larger surface area of MRF (BET-Fig. 1(c) and Table 1), or that NOM rich with minerals will possess a strong affinity for graphene active sites, thus clogging and reducing the number of available sites (resulting in them being less organophilic) for pyrene adsorption onto GW. Cai et al. (2015) reported that NOM is sorbed rapidly by graphene, which diminishes the available sites for PAH adsorption. However, we have been able to further relate that NOM with high OC content, would compete for sites with PAHs, but still allows for some degree of PAH adsorption as compared to NOM rich in minerals.

It is also noteworthy that the conductivity of the solution containing 20 mg GW and pyrene decreased on the addition of 10 mg of different NOM, from 828 μS cm^{-1}(GW) to 815 μS cm^{-1}(GW-NAS), 810 μS cm^{-1} (GW-MDF), 822 μS cm^{-1} (GW-BCF) and 789 μS cm^{-1} (GW-MRF). An increase in pH was also observed: from an acidic pH of 6.48 to a basic pH of 7.23 for GW and GW-MRF in pyrene contaminated solutions, while GW-NAS, GW-MDF, and GW-BCF maintained fairly acidic pHs of 6.85, 6.52, and 6.59 respectively. These changes in solution chemistry may play a vital role in pyrene adsorption by graphene wool and other GBMs, especially regarding ionic strength and pH. An increase in solutions' ionic strength and an acidic pH have been reported to enhance the adsorption of pyrene by GBMs (Lamichhane et al., 2016; Adeola

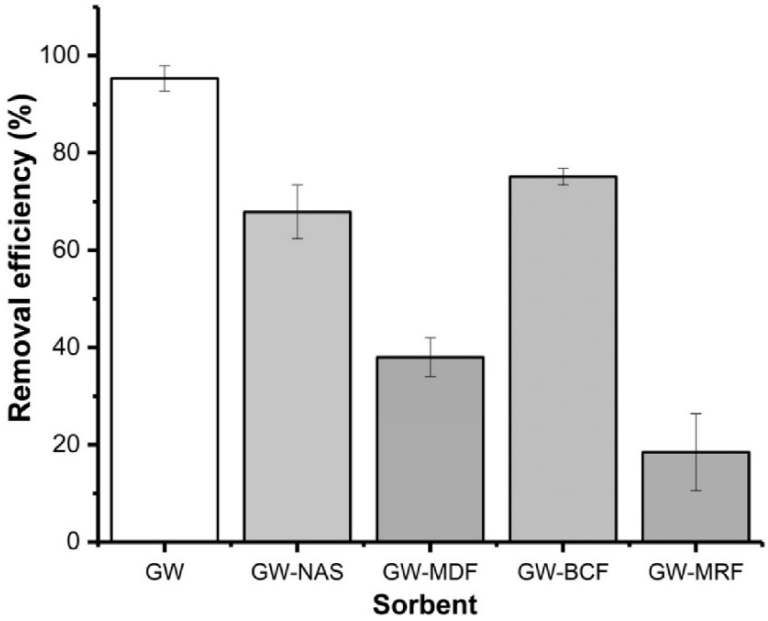

Fig. 5. Removal efficiency and adsorption capacity (K_d) of pyrene by graphene wool (GW) in the presence of different NOM.

and Forbes, 2019). Thus, the inhibitory influence of sediment components can be attributed to the unfavorable conditions created by the NOMs, especially by the presence of mineral-rich NOM fractions which could lead to fouling of graphene wool, if utilized for water treatment application.

3.8. Influence of the number of aromatic rings on sorption capacity

Several reports indicate that PAHs interact with different carbonaceous adsorbents mainly via $\pi - \pi$ interactions (Amstaetter et al., 2012; Wang et al., 2014; Nsibande et al., 2019; Adeola and Forbes, 2019). The number of aromatic rings is directly proportional to the number of π- electrons available for bonding, thus the experimental amount adsorbed of the selected PAHs by sediment components was mainly in the order of PERY > PYR > PHEN > NAPH (Figure S5).

Generally, oxides of metals in high oxidation states, such as Fe^{3+} and Al^{3+}, are Lewis acids that can act as electron-withdrawing species due to their vacant orbitals, which could potentially displace hydrogen from aromatic rings in solution, thereby causing the weakening or deactivation of the aromatic ring (Kuznetsov et al., 2018). Therefore, in the quest to stabilize the aromatic rings, delocalized π-electrons that could have been available for bonding, are held by PAHs to strengthen the rings. The electron-withdrawing nucleophilic atoms present in relatively high concentration in the mineral-rich fraction of the sediment components (Table S2), may be responsible for why MRF has a lower adsorption intensity (K_L) than MDF across most of the PAHs (Table 3), and the significant inhibitory influence played by MRF on sorption efficiency of GW (Fig. 5).

On the contrary, the higher values of % OC for BCF and MDF enhance their hydrophobic nature due to the high degree of aliphatic and aromatic compounds they possess (Ran et al., 2007). Furthermore, aromaticity contributes largely to octanol–water partition coefficients (K_{ow}) of organic contaminants, as K_{ow} is used to describe the extent of hydrophobicity of compounds. Thus, improved sorptive interaction between NOMs (BCF and MDF) and PAHs can be attributed to the relative abundance of hydrophobic aromatic moieties, and hydrophobic interactions between PAHs and hydrophobic moieties of the NOM contributed extensively to the overall hydrophobic–organophilic sorption process.

4. Conclusion

The *in-situ* modification of natural organic matter derived from stream sediment was used to establish the roles of different fractions of NOM on the sequestration of selected PAHs via a sorption process. Delineation of sediment components was achieved via effective chemical and thermal treatment procedures, confirmed by XRD, SEM-EDX, ICP-OES, FTIR, BET as well as other basic characterization to determine % organic carbon (OC), sorbent pH, etc. Results suggest that *in-situ* removal of various NOM components has a significant influence on the adsorption–desorption potential of PAHs. MDF and BCF fractions adsorbed PAHs to a greater extent than mineral-rich fractions. Furthermore, the sorption process of selected PAHs onto all sorbent fractions was dominated by the interaction between hydrophobic moieties and hydrophobic sites at the sediment–water boundary/interface rather than by the surface area of sorbents. The observed

hysteresis revealed the potential impact of each sediment component on the sequestration of PAHs in aquatic systems. With respect to the recontamination of surface water, NOMs with higher % OC would bind PAHs more and would not readily desorb them at the same intensity with which they were adsorbed (hysteresis), thus making PAHs more persistent in sediments and less bioavailable in water.

Graphene-based materials (GBMs) have attracted significant interest for water treatment applications in the last two decades. Therefore, the influence of NOM on the efficiency of these materials in the treatment of PAH-contaminated water provides useful information, as NOM is present in aquatic systems as dissolved organic carbon (DOC) and particulate organic carbon (POC). Results revealed that the presence of NOM diminishes the efficiency of the adsorption of pyrene by graphene wool by altering the solution chemistry, clogging sorption sites, and/or selectively binding to active sites, with the mineral-rich fraction (MRF) of NOM impeding the adsorption of PAHs the most. This study revealed the invaluable role of black carbon (BC) and amorphous carbon, as well as mineral enrichment, in the adsorption and retention of hydrophobic organic compounds (HOCs) within sediment matrices, and the potential impact of each NOM fraction in the environmental risk management (remediation) of PAH contaminated water.

CRediT authorship contribution statement

Adedapo O. Adeola: Conceptualization, Investigation, Formal analysis, Writing - original draft. **Patricia B.C. Forbes:** Formal analysis, Writing - review & editing, Fund acquisition, Supervision.

Declaration of competing interest

The authors declare that they have no known competing financial interests or personal relationships that could have appeared to influence the work reported in this paper.

Acknowledgments

Authors acknowledge the University of Pretoria Commonwealth Doctoral Scholarship, South Africa (AA), Rand Water, and the Departments of Chemistry and Physics at the University of Pretoria, South Africa for their support.

Appendix A. Supplementary data

Supplementary material related to this article can be found online at https://doi.org/10.1016/j.eti.2020.101202.

References

Adeniji, A.O., Okoh, O.O., Okoh, A.I., 2019. Levels of polycyclic aromatic hydrocarbons in the water and sediment of Buffalo River Estuary, South Africa and their health risk assessment. Arch. Environ. Contam. Toxicol. 76, 657–669. http://dx.doi.org/10.1007/s00244-019-00617-w.

Adeola, A.O., Forbes, P.B.C., 2019. Optimisation of the sorption of selected polycyclic aromatic hydrocarbons by regenerable graphene wool. Water Sci. Technol. 80 (10), 1931–1943. http://dx.doi.org/10.2166/wst.2020.011.

Amstaetter, K., Eek, E., Cornelissen, G., 2012. Sorption of PAHs and PCBs to activated carbon: Coal versus biomass-based quality. Chemosphere 87, 573–578. http://dx.doi.org/10.1016/j.chemosphere.2012.01.007.

Bakatula, E.N., Richard, D., Neculita, C.M., Zagury, G.J., 2018. Determination of point of zero charge of natural organic materials. Environ. Sci. Pollut. Res. 25, 7823–7833. http://dx.doi.org/10.1007/s11356-017-1115-7.

Cai, N., Peak, D., Larese-Casanova, P., 2015. Factors influencing natural organic matter sorption onto commercial graphene oxides. Chem. Eng. J 273, 568–579. http://dx.doi.org/10.1016/j.cej.2015.03.108.

Cornelissen, G., Gustafsson, Ö., Bucheli, T.D., Jonker, M.T.O., Koelmans, A.A., van Noort, P.C.M., 2005. Extensive sorption of organic compounds to black carbon, coal, and kerogen in sediments and soils: mechanisms and consequences for distribution, bioaccumulation, and biodegradation. Environ. Sci. Technol. 39, 6881–6895. http://dx.doi.org/10.1021/es050191b.

Crisafully, R., Milhome, M.A., Cavalcante, R.M., Silveira, E.R., De Keukeleire, D., Nascimento, R.F., 2008. Removal of some polycyclic aromatic hydrocarbons from petrochemical wastewater using low-cost adsorbents of natural origin. Bioresour. Technol. 99, 4515–4519. http://dx.doi.org/10.1016/j.biortech.2007.08.041.

Das, L., Das, P., Bhowal, A., Bhattachariee, C., 2020. Synthesis of hybrid hydrogel nano-polymer composite using Graphene oxide, Chitosan and PVA and its application in waste water treatment. Environ. Technol. Innov. 18, 100664. http://dx.doi.org/10.1016/j.eti.2020.100664.

El-shahawi, M., Bashammakh, A.S., Alwael, H., Alsibaai, A.A., Dowaidar, A.M., 2017. Adsorption characteristics of polycyclic aromatic hydrocarbons from non-aqueous media using activated carbon derived from phenol formaldehyde resin: Kinetics and thermodynamic study. Environ. Sci. Pollut. Res. Int. 24 (5), 4228–4240. http://dx.doi.org/10.1007/s11356-015-4936-2.

Frangipane, G., Pistolato, M., Molinaroli, E., Guerzoni, S., Tagliapietra, D., 2009. Comparison of loss on ignition and thermal analysis stepwise methods for determination of sedimentary organic matter. Aquat. Conserv. 19, 24–33. http://dx.doi.org/10.1002/aqc.970.

Gelinas, Y., Prentice, K.M., Baldock, J.A., Hedges, J., 2001. An improved thermal oxidation method for the quantification of soot/graphite carbon in sediments and soils. Environ. Sci. Technol. 21, 3519–3525. http://dx.doi.org/10.1021/es010504c.

Ghosh, U., Talley, J.W., Luthy, R.G., 2001. Particle-scale investigation of PAH desorption kinetics and thermodynamics from sediment. Environ. Sci. Technol. 35, 3468–3475. http://dx.doi.org/10.1021/es0105820.

Girardello, F., Rovani, S., Giovanela, M., Fernandes, A.N., 2016. Removal of pyrene from aqueous solutions by adsorption onto Brazilian peat samples. Adsorpt. Sci. Technol. 34, 538–551. http://dx.doi.org/10.1177/0263617416670168.

Gregg, S., Sing, K., 1982. Adsorption, Surface Area and Porosity, second ed. Academic Press.

Guo, W., Wang, S., Wang, Y., Lu, S., Gao, Y., 2018. Sorptive removal of phenanthrene from aqueous solutions using magnetic and non-magnetic rice husk-derived biochars. R. Soc. Open Sci. 5, 172382. http://dx.doi.org/10.1098/rsos.172382.

Gupta, H., Kumar, R., 2020. Distribution of selected polycyclic aromatic hydrocarbons in urban soils of Delhi, India. Environ. Technol. Innov. 17, 100500. http://dx.doi.org/10.1016/j.eti.2019.100500.
Gupta, H., Singh, S., 2018. Kinetics and thermodynamics of phenanthrene adsorption from water on orange rind activated carbon. Environ. Technol. Innov. 10, 208–214. http://dx.doi.org/10.1016/j.eti.2018.03.001.
Haghseresht, H., Lu, G., 1998. Adsorption characteristics of phenolic compounds onto coal-rejected-derived adsorbents. Energy Fuels 12, 1100–11007. http://dx.doi.org/10.1021/ef9801165.
Hall, S., Tang, R., Baeyens, J., Dewil, R., 2009. Removing polycyclic aromatic hydrocarbons from water by adsorption on silicagel. Polycycl. Aromat. Comp. 29, 160–183. http://dx.doi.org/10.1080/10406630903017534.
Hassan, S.S.M., Abdel-Shafy, H.I., Mansour, M.S.M., 2018. Removal of pyrene and benzo(a)pyrene micropollutant from water via adsorption by green synthesized iron oxide nanoparticles. Adv. Nat. Sci-Nanosci. 9, 015006. http://dx.doi.org/10.1088/2043-6254/aaa6f0.
Hendershot, W.H., Duquette, M., 1986. A simple barium chloride method for determining cation exchange capacity and exchangeable cations. Soil Sci. Soc. 15, 178–191. http://dx.doi.org/10.2136/sssaj1986.03615995005000030013x.
Huang, W., Schlautman, M.A., Weber, W.J., 1996. A distributed reactivity model for sorption by soils and sediments. 5. The influence of near-surface characteristics in mineral domains. Environ. Sci. Technol. 30, 2993–3000. http://dx.doi.org/10.1021/es960029w.
Karickhoff, S.W., Brown, D.S., Scott, T.A., 1979. Sorption of hydrophobic pollutants on natural sediments. Water Res. 13, 241–248. http://dx.doi.org/10.1016/0043-1354(79)90201-X.
Kraaij, R., Mayer, P., Busser, F.J.M., van het Bolscher, M., Seinen, W., Tolls, J., Belfroid, A.C., 2003. Measured pore-water concentrations make equilibrium partitioning work a data analysis. Environ. Sci. Technol. 37, 268–274. http://dx.doi.org/10.1021/es020116q.
Kuznetsov, D.A., Han, B., Yu, Y., Rao, R.R., Hwang, J., Román-Leshkov, Y., Shao-Horn, Y., 2018. Tuning redox transitions via inductive effect in metal oxides and complexes, and implications in oxygen electrocatalysis. Joule 2, 225–244. http://dx.doi.org/10.1016/j.joule.2017.11.014.
Lagergren, S., 1898. About the theory of so-called adsorption of soluble substances. K. Sven. Veteskapsakademiens Handl. Band 24, 1–29.
Lamichhane, S., Bal Krishna, K.C., Sarukkalige, R., 2016. Polycyclic aromatic hydrocarbons (PAHs) removal by sorption: A review. Chemosphere 148, 336–353. http://dx.doi.org/10.1016/j.chemosphere.2016.01.036.
Lu, Y., Pignatello, J.J., 2002. Demonstration of the conditioning effect in soil organic matter in support of a pore deformation mechanism for sorption hysteresis. Environ. Sci. Technol. 36, 4553–4561. http://dx.doi.org/10.1021/es020554x.
Mahato, J.K., Gupta, S.K., 2020. Modification of Bael fruit shell and its application towards natural organic matter removal with special reference to predictive modeling and control of THMs in drinking water supplies. Environ. Technol. Innov. 18, 100666. http://dx.doi.org/10.1016/j.eti.2020.100666.
Mahmood, T., Saddique, M.T., Naeem, A., Westerhoff, P., Mustafa, S., Alum, A., 2011. Comparison of different methods for the point of zero charge determination of NiO. Ind. Eng. Chem. Res. 50, 10017–10023. http://dx.doi.org/10.1021/ie200271d.
Mikutta, R., Kleber, M., Kaiser, K., Jahn, R., 2005. Review: Organic matter removal from soils using hydrogen peroxide, sodium hypochlorite, and disodium peroxodisulfate. Soil Sci. Soc. Am. J. 69, 129–135. http://dx.doi.org/10.2136/sssaj2005.0120.
Mojiri, A., Zhou, J.L., Ohashi, A., Ozaki, N., Kindaichi, T., 2019. Comprehensive review of polycyclic aromatic hydrocarbons in water sources, their effects and treatments. Sci. Total Environ. 696, 133971. http://dx.doi.org/10.1016/j.scitotenv.2019.133971.
Nelson, D.W., Sommers, L.E., 2018. Total carbon, organic carbon, and organic matter. In: Sparks, D., Page, A., Helmke, P., Loeppert, R., Soltanpour, P.N., Tabatabai, M.A., Johnston, C.T., Sumner, M.E. (Eds.), Methods of Soil Analysis. http://dx.doi.org/10.2136/sssabookser5.3.c34.
Nsibande, S.A., Montaseri, H., Forbes, P.B.C., 2019. Advances in the application of nanomaterial-based sensors for detection of polycyclic aromatic hydrocarbons in aquatic systems. TRAC-Trend Anal. Chem. 115, 52–69. http://dx.doi.org/10.1016/j.trac.2019.03.029.
Ololade, I.A., Adeola, A.O., Oladoja, N.A., Ololade, O.O., Nwaolisa, S.U., Alabi, A.B., Ogungbe, I.V., 2018. In-situ modification of soil organic matter towards adsorption and desorption of phenol and its chlorinated derivatives. J. Environ. Chem. Eng. 6, 3485–3494. http://dx.doi.org/10.1016/j.jece.2018.05.034.
Oyedotun, K.O., Masikhwa, T.M., Lindberg, S., Matic, A., Johansson, P., Manyala, N., 2019. Comparison of ionic liquid electrolyte to aqueous electrolytes on carbon nanofibres supercapacitor electrode derived from oxygen-functionalized graphene. Chem. Eng. J. 375, 121906. http://dx.doi.org/10.1016/j.cej.2019.121906.
Ran, Y., Huang, W., Rao, P.S.C., Liu, D., Sheng, G., Fu, J., 2002. The role of condensed organic matter in the nonlinear sorption of hydrophobic organic contaminants by a peat and sediments. J. Environ. Qual. 31, 1953–1962. http://dx.doi.org/10.2134/jeq2002.1953.
Ran, Y., Sun, K., Ma, X., Wang, G.H., Grathwohl, P., Zeng, E.Y., 2007. Effect of condensed organic matters on solvent extraction and aqueous leaching of PAHs based in soils and sediments. J. Environ. Pollut. 43, 111–123. http://dx.doi.org/10.1016/j.envpol.2006.11.028.
Ran, Y., Xiao, B., Huang, W., Peng, P., Liu, D., Fu, J., Sheng, G., 2003. Kerogen in an aquifer and its strong sorption for hydrophobic organic contaminants. J. Environ. Qual. 32 (5), 1701–1709. http://dx.doi.org/10.2134/jeq2003.1701.
Schlautman, M.A., Morgan, J.J., 1994. Sorption of perylene on a nonporous inorganic silica surface: Effects of aqueous chemistry on sorption rates. Environ. Sci. Technol. 28, 2184–2190. http://dx.doi.org/10.1021/es00061a029.
Schoonraad, G.-L., Madito, M.J., Manyala, N., Forbes, P., 2020. Synthesis and optimisation of a novel graphene wool material by atmospheric pressure chemical vapour deposition. J. Mater. Sci. 55, 545–564. http://dx.doi.org/10.1007/s10853-019-03948-0.
Shang, H., Lu, Y., Zhao, F., Chao, C., Zhang, B., Zhang, H., 2015. Preparing high surface area porous carbon from biomass by carbonization in a molten salt medium. RSC Adv. 5, 75728–75734. http://dx.doi.org/10.1039/C5RA12406A.
Singh, N.B., Nagpal, G., Agrawal, S., Rachna, 2018. Water purification by using adsorbents: A review. Environ. Technol. Innov. 11, 187–240. http://dx.doi.org/10.1016/j.eti.2018.05.006.
Unuabonah, E.I., Olu-Owolabi, B.I., Böhm, L., Düring, R.A., 2016. Adsorption of polynuclear aromatic hydrocarbons from aqueous solution: Agrowaste-modified kaolinite vs surfactant modified bentonite. Bull. Chem. Soc. Ethiop. 30 (3), 369–376. http://dx.doi.org/10.4314/bcse.v30i3.5.
Wang, X., Andrews, L., 2006. Infrared spectral of $M(OH)_{1,2,3}$(M= Mn, Fe, Co, Ni) molecules in solid argon and the character of first row transition metal hydroxide bonding. J. Phys. Chem. A 110, 10035–10045. http://dx.doi.org/10.1021/jp0624698.
Wang, J., Chen, Z., Chen, B., 2014. Adsorption of polycyclic aromatic hydrocarbons by graphene and graphene oxide nanosheets. Environ. Sci. Technol. 48, 4817–4825. http://dx.doi.org/10.1021/es405227u.
Wang, L., Niu, J., Yang, Z., Shen, Z., Wang, J., 2008. Effects of carbonate and organic matter on sorption and desorption behavior of polycyclic aromatic hydrocarbons in the sediments from Yangtze River. J. Hazard Mater. 154, 811–817. http://dx.doi.org/10.1016/j.jhazmat.2007.10.096.
Wauchope, R.D., Savage, K.E., Koskinen, W.C., 1983. Adsorption–desorption equilibria of herbicides in soil: naphthalene as a model compound for entropy-enthalpy effects. Weed Sci. 31, 744–751. http://dx.doi.org/10.1017/S0043174500070296.
Weber, W.J., McGinley, P.M., Katz, L.E.A., 1992. Distributed reactivity model for sorption by soils and sediments. conceptual basis and equilibrum assessments. Environ. Sci. Technol. 26, 1955–1962. http://dx.doi.org/10.1021/es00034a012.
Xiao, B., Yu, Z., Huang, W., Song, J., Peng, P., 2004. Black carbon and kerogen in soils and sediments. their roles in equilibrium sorption of less-polar organic pollutants. Environ. Sci. Technol. 38, 5842–5852. http://dx.doi.org/10.1021/es049761i.
Xu, L., Wang, J., 2017. The application of graphene-based materials for the removal of heavy metals and radionuclides from water and wastewater. Crit. Rev. Environ. Sci. Technol. 47, 1042–1105. http://dx.doi.org/10.1080/10643389.2017.1342514.

Yakout, S.M., Daifullah, A.A.M., 2013. Removal of selected polycyclic aromatic hydrocarbons from aqueous solution onto various adsorbent materials. Desalin. Water Treat. 51, 6711–6718. http://dx.doi.org/10.1080/19443994.2013.769916.

Younis, S.A., El-Gendy, N.S., El-Azab, W.I., Moustafa, Y.M., 2015. Kinetic, isotherm, and thermodynamic studies of polycyclic aromatic hydrocarbons biosorption from petroleum refinery wastewater using spent waste biomass. Desalin. Water Treat. 56, 3013–3023. http://dx.doi.org/10.1080/19443994.2014.964331.

Yu, W., Liu, T., Crawshaw, J., Liu, T., Graham, N., 2018. Ultrafiltration and nanofiltration membrane fouling by natural organic matter: Mechanisms and mitigation by pre-ozonation and ph. Water Res. 139, 353–362. http://dx.doi.org/10.1016/j.watres.2018.04.025.

Yu, F., Ma, J., Bi, D., 2015. Enhanced adsorptive removal of selected pharmaceutical antibiotics from aqueous solution by activated graphene. Environ. Sci. Pollut. Res. 22, 4715–4724. http://dx.doi.org/10.1007/s11356-014-3723-9.

Yu, H., Xiao, H., Wang, D., 2014. Effects of soil properties and biosurfactant on the behavior of PAHs in soil-water systems. Environ. Syst. Res. 3, 6. http://dx.doi.org/10.1186/2193-2697-3-6.

Zhao, G.X., Li, J.X., Wang, X.K., 2011. Kinetic and thermodynamic study of 1-naphthol adsorption from aqueous solution to sulfonated graphene nanosheets. Chem. Eng. J. 173, 185–190. http://dx.doi.org/10.1016/j.cej.2011.07.072.

SUPPLEMENTARY INFORMATION (SI)

ADSORPTION MODELS

Kinetic experimental data was fitted to pseudo-first-order (eq. 1) and pseudo-second-order (eq. 2) kinetic models following the equations below:

$$q_t = q_e(1 - e^{-k_1 t}) \qquad (1)$$

$$q_t = \frac{q_e^2 k_2 t}{1 + k_2 q_e t} \qquad (2)$$

Where: q_t and q_e are the amount of solute sorbed per mass of sorbent (μg g^{-1}) at any time (t) and equilibrium, respectively; k_1 (min^{-1}) and k_2 (g μg^{-1} min^{-1}) are rate constants for first-order and second-order adsorption (Lagergren, 1898; Kowanga et al., 2016). The initial sorption rate (h) is defined by equation 3 (Kalavathy et al., 2005).

$$h = k_2 q_e^2 \qquad (3)$$

Furthermore, this study employed three different isotherm models viz: Freundlich (eq. 4), Langmuir (eq.5) and linear (eq.6), to fit the adsorption experimental data and Sum of Square Error (SSE) (eq.7) for validation:

$$q_e = K_f C_e^N \qquad (4)$$

$$q_e = \frac{q_{max} K_L C_e}{1 + K_L C_e} \qquad (5)$$

$$q_e = K_d C_e \qquad (6)$$

$$\sum_{i=1}^{n} (q_{e,cal} - q_{e,exp})_i^2 \qquad (7)$$

where K_f (μg/g) $(L/\mu g)^N$) and N (dimensionless) is Freundlich constant and intensity parameter, an indicator of site energy heterogeneity (He et al., 2006); q_{max} (μg/g) and K_L (L/μg) is the Langmuir maximum adsorption capacity and Langmuir constant associated with solute–surface interaction energy, respectively; q_e is the solid-phase concentration (μg/g), C_e is the liquid phase equilibrium concentration (μg/L), K_d (L/g) is the sorption distribution coefficient, respectively.

The K_d is a valuable parameter in the evaluation of organic pollutants partitioning in the water environment. The K_d was used to estimate the single point organic carbon-normalized distribution coefficients, K_{oc} according to the following:

$$K_{oc} = K_d / f_{oc} \approx q_e / (C_e . f_{oc}) \qquad (8)$$

where f_{oc} is the fraction of organic carbon (Ololade et al., 2018).

FIGURES

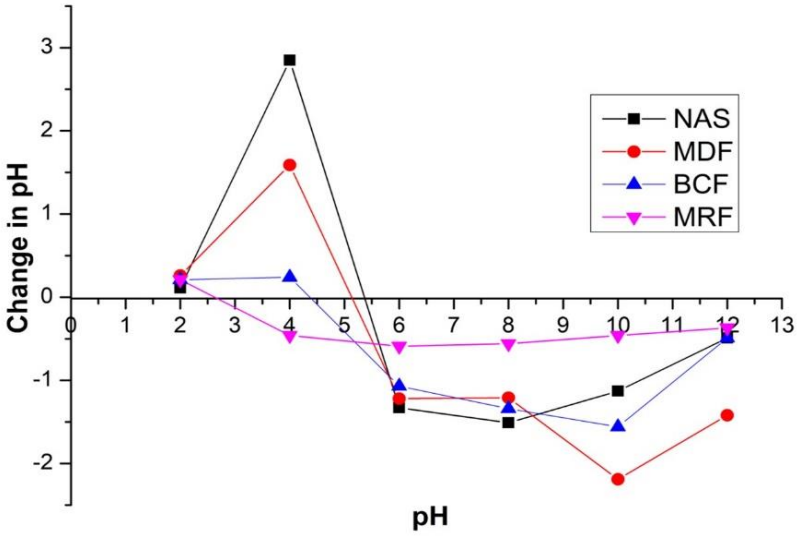

Figure S1: Point of zero net charge of sediment and its components

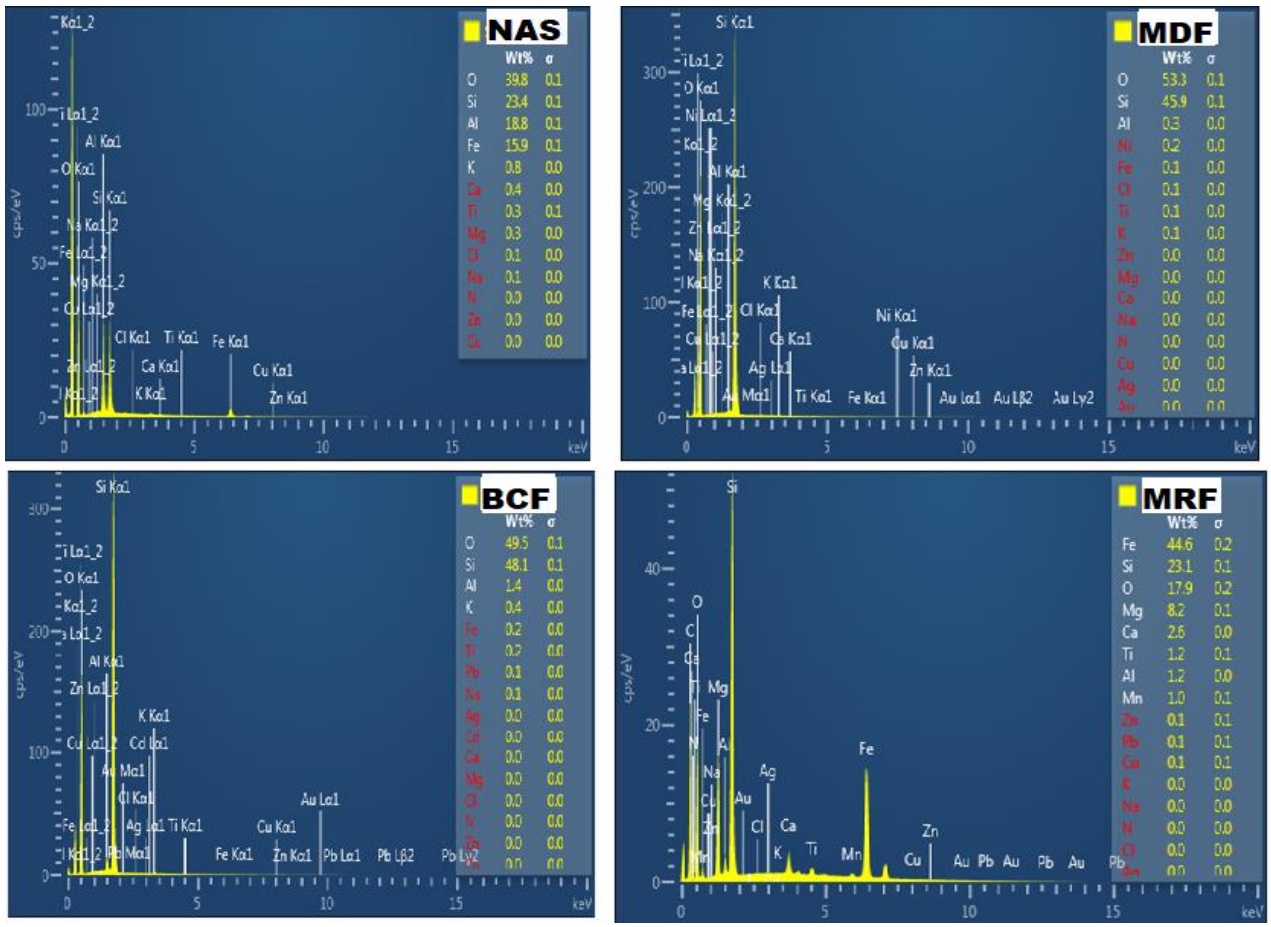

Figure S2: Results of EDS analysis of natural sediment and its components

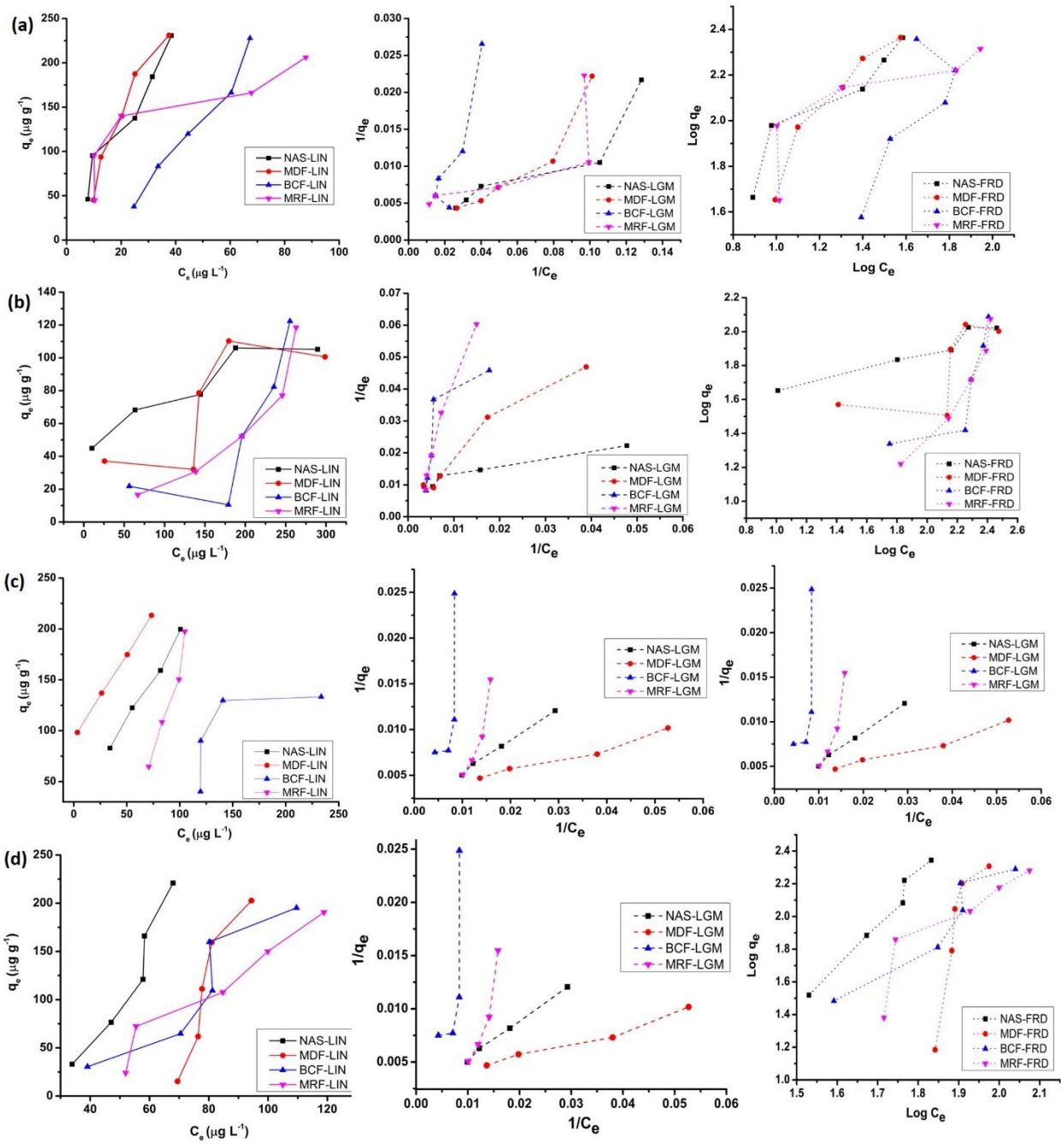

Figure S3: Linear equation isotherm plots for Linear (LIN), Langmuir (LGM), and Freundlich (FRD) sorption models, (a) Naphthalene (b) Phenanthrene (c) Pyrene (d) Perylene, onto natural sediment (NAS), mineral-deficient fraction (MDF), black carbon fraction (BCF) and mineral-rich fraction (MRF).

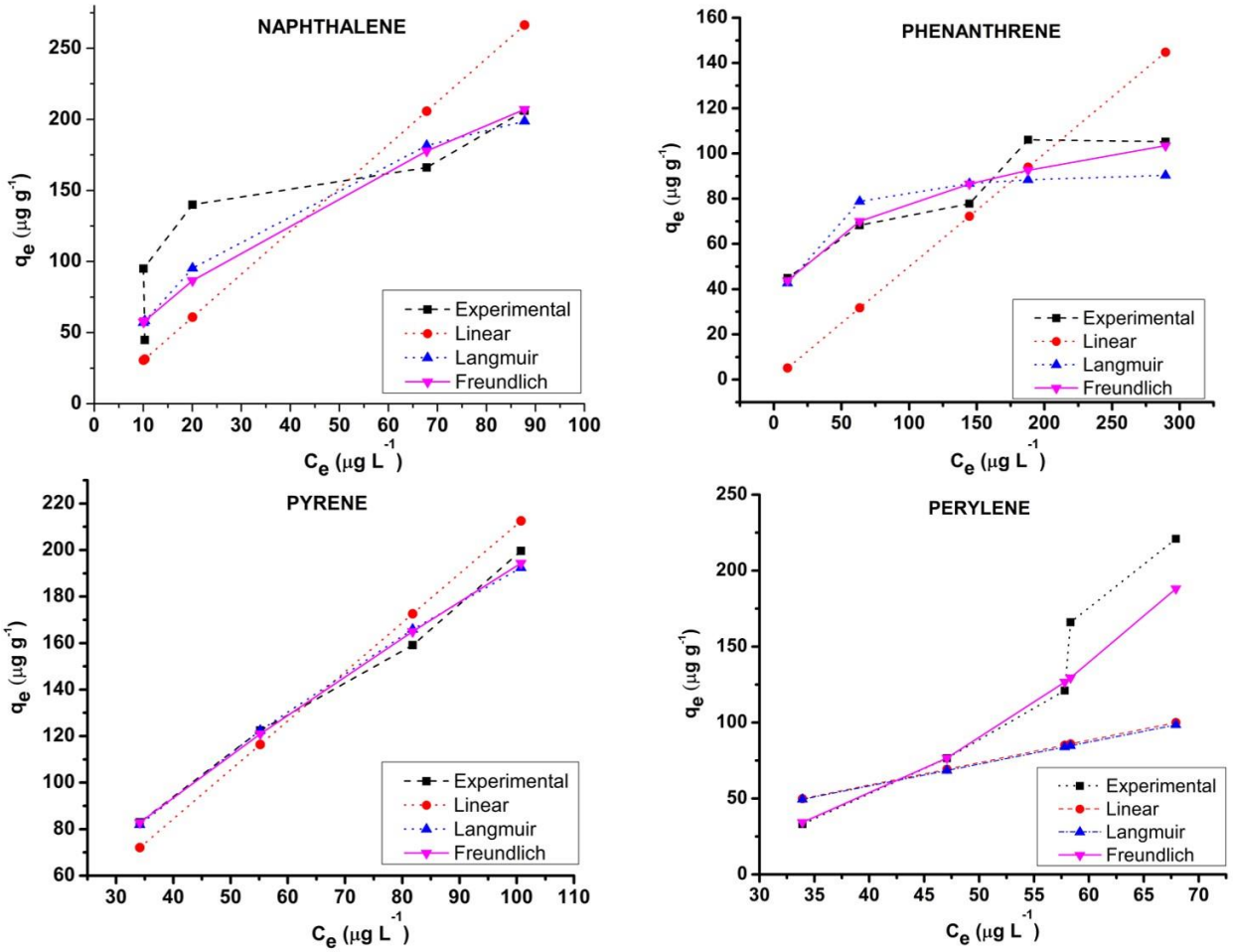

Figure S4: Representative nonlinear equation isotherm model plots for adsorption of selected PAHs onto natural sediments and validated by Error Sum of Squares (SSE).

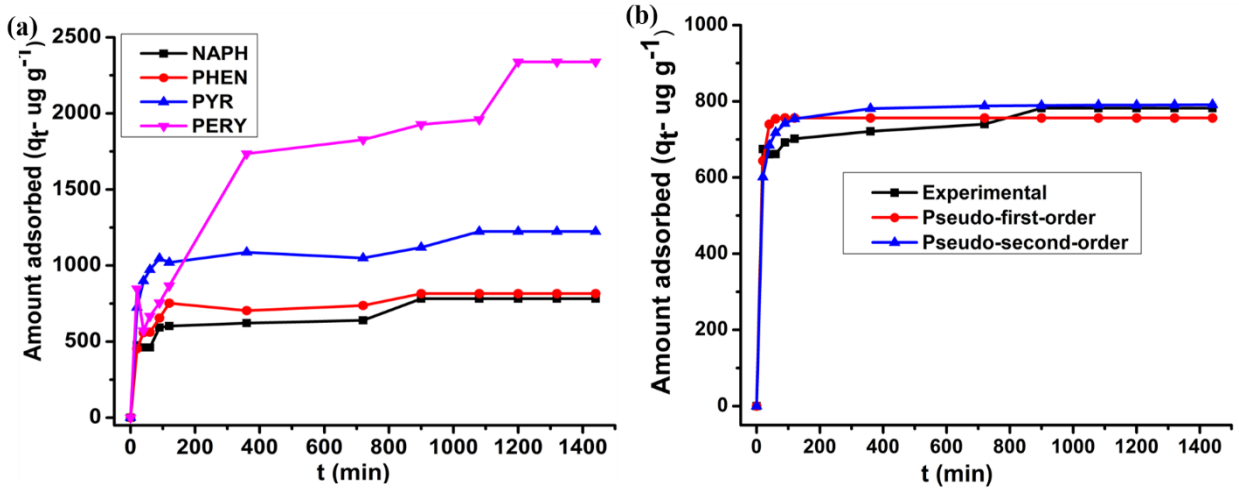

Figure S5: (a) Time-concentration profile of adsorption of NAPH, PHEN, PYR, and PERY onto natural sediment (b) Fitting pseudo-first (PFO) and second (PSO) order kinetic models to adsorption of NAPH on natural sediment {Error Sum of Squared (SSE) are 0.13 (PFO) and 0.08 (PSO)}.

TABLES

Table S1: Physicochemical properties of selected polycyclic aromatic hydrocarbons

PAHs	Molecular formula	[a]Log*Kow*	[c]Sw (mg L^{-1})	[a]Mw (g mol^{-1})	[b]Bp ($^{\circ}$C)
Naphthalene	$C_{10}H_8$	3.30	31.0	128.2	217.9
Phenanthrene	$C_{14}H_{10}$	4.46	1.18	178.2	340.0
Pyrene	$C_{16}H_{10}$	5.13	0.135	202.3	404.0
Perylene	$C_{22}H_{12}$	6.30	4e-4	252.3	467.0

Log K_{ow}:octanol-water partition coefficient, S_w: water solubility (mg L^{-1}), M_w: molecular weight (g cmol^{-1}), B_p: boiling points (^{o}C). Cited from [a](Sun et al., 2013), [b](Yakout and Daifullah, 2013), [c](Potin et al., 2004).

Table S2: ICP-OES elemental analysis of concentration (ppm ± std) major elements present in natural and fractions of stream sediment.

Elements	Natural Sediment (NAS)	Mineral Deficient Fraction (MDF)	Black Carbon Fraction (BCF)	Mineral Rich Fraction (MRF)
Aluminum (Al)	218.55 ± 0.61	9.29 ± 0.37	3.105 ± 0.05	65.50 ± 0.20
Iron (Fe)	692.20 ± 0.60	12.67 ± 0.02	1.63 ± 0.02	298.90 ± 0.69
Phosphorus (P)	16.17 ± 0.07	2.48 ± 0.07	1.03 ± 0.15	15.69 ± 0.24
Silicon (Si)	28.34 ± 0.58	3.49 ± 0.97	1.68 ± 0.17	18.43 ± 0.24
Manganese (Mn)	14.92 ± 0.21	0.06 ± 0.0	0.03 ± 0.001	1.84 ± 0.02
Lead (Pb)	0.71 ± 0.10	< 0.09 ± 0.01	< 0.14 ± 0.014	0.31 ± 0.04
Sodium (Na)	10.54 ± 0.17	2.01 ± 0.05	1.42 ± 0.07	7.01 ± 0.10
Potassium (K)	6.94 ± 0.08	4.81 ± 0.10	4.23 ± 0.06	5.58 ± 0.11
Calcium (Ca)	31.74 ± 0.09	2.64 ± 0.05	1.60 ± 0.02	8.26 ± 0.05
Magnesium (Mg)	16.54 ± 0.15	0.65 ± 0.01	0.30 ± 0.002	6.76 ± 0.01

Table S3: Sorption model parameters for adsorption of NAPH onto natural sediments and its components

Sorption models	Parameters	NAS	MDF	BCF	MRF
	K_f	8.46	3.48	0.63	14.71
Freundlich	N	0.89	1.19	1.32	0.59
	SSE	0.14	0.14	0.44	0.40
Langmuir	$q_{max}\,(\mu g\ g^{-1})$	1049	10678	13212	293
	$K_L\,(L\ \mu g^{-1})$	0.007	0.001	0.0002	0.02
	SSE	0.15	0.20	0.54	0.36
Linear	K_d	6.13	6.05	2.07	3.03
	SSE	0.17	0.19	0.54	1.01
	$LogK_{oc}$	1.95	1.81	1.32	1.93

Table S4: Sorption model parameters for adsorption of PHEN onto natural sediments and its components

Sorption models	Parameters	NAS	MDF	BCF	MRF
	K_f	24.10	10.88	12.36	0.06
Freundlich	N	0.26	0.31	0.04	1.31
	SSE	0.03	0.87	2.24	1.15
Langmuir	$q_{max}\,(\mu g\ g^{-1})$	94	55	240	235
	$K_L\,(L\ \mu g^{-1})$	0.08	0.07	15.30	0.001
	SSE	0.09	0.96	2.23	0.25
Linear	K_d	0.50	0.34	0.09	0.27
	SSE	1.23	1.12	2.53	0.23
	$LogK_{oc}$	0.87	0.56	0.04	0.60

Table S5: Sorption model parameters for adsorption of PYR onto natural sediments and its components

Sorption models	Parameters	NAS	MDF	BCF	MRF
	K_f	5.13	70.60	0.05	1.0e-3
Freundlich	N	0.79	0.23	1.46	0.38
	SSE	0.002	0.023	0.510	0.014
Langmuir	$q_{max}\,(\mu g\ g^{-1})$	624	180	3402	6216
	$K_L\,(L\ \mu g^{-1})$	4e-3	3e-1	1e-4	2e-4
	SSE	0.003	0.069	0.57	0.29
Linear	K_d	2.11	3.59	0.48	1.21
	SSE	0.03	0.92	0.57	0.28
	$LogK_{oc}$	0.85	1.58	0.58	1.26

Table S6: Sorption model parameters for adsorption of PERY onto natural sediments and its components

Sorption models	Parameters	NAS	MDF	BCF	MRF
	K_f	6.2e-3	9.4e-6	3.1e-2	2.4e-3
Freundlich	N	2.45	3.46	1.85	2.39
	SSE	0.19	2.01	0.20	0.36
Langmuir	$q_{max}\,(\mu g\ g^{-1})$	7853	1521	6960	5807
	$K_L\,(L\ \mu g^{-1})$	1.9e-4	2.2e-4	1.5e-4	1.3e-4
	SSE	0.90	2.60	0.59	1.28
Linear	K_d	1.47	0.32	1.06	0.75
	SSE	0.89	2.60	0.58	1.27
	$LogK_{oc}$	1.34	0.53	1.03	1.04

Table S7: Thermodynamic parameters for the adsorption of naphthalene (NAPH), phenanthrene (PHEN), pyrene (PYR) and perylene (PERY) onto sediment components

PAH	Temp. (K)	NAS			MDF			BCF			MRF		
		ΔG ($J\ mol^{-1}K^{-1}$)	ΔH ($J\ mol^{-1}$)	ΔS ($J\ mol^{-1}$)	ΔG ($Jmol^{-1}K^{-1}$)	ΔH ($J\ mol^{-1}$)	ΔS ($k\ Jmol^{-1}$)	ΔG ($J\ mol^{-1}K^{-1}$)	ΔH ($J\ mol^{-1}$)	ΔS ($J\ mol^{-1}$)	ΔG ($J\ mol^{-1}K^{-1}$)	ΔH ($J\ mol^{-1}$)	ΔS ($J\ mol^{-1}$)
NAPH	298	-37.7			-80.2			-45.9			-19.9		
	308	-86.2	1207.4	4.2	-125.2	1260.8	4.5	-99.1	1502.5	5.2	-57.9	1112.5	3.8
	318	-128.2			-170.2			-151.1			-95.9		
PHEN	298	56.9			5.2			40.5			20.9		
	308	-5.1	1904.5	6.2	-11.2	2298.8	7.5	6.6	1269.4	4.1	-10.4	925.9	3.0
	318	-67.1			-86.2			-34.4			-28.1		
PYR	298	-13.2			-15.4			-28.8			-25.1		
	308	14.4	-1186.8	-3.9	32.5	-1661.5	-5.5	2.2	-952.6	-3.1	14.9	-1217.1	-4.0
	318	53.3			87.5			33.2			54.9		
PERY	298	-41.8			-113.4			-34.1			-71.4		
	308	-33.8	-280.2	-0.8	-59.4	-1722.6	-5.4	-1.1	-1017.5	-3.3	-10.8	-2453.2	-8.0
	318	-25.8			-5.4			31.9			90.8		

References

He, Y., Xu, J.M., Wang, H.Z., Ma, Z.H., Chen, J.Q., 2006. Detailed sorption isotherms of pentachlorophenol on soils and its correlation with soil properties. Environ. Res. 101, 362–372. https://doi.org/10.1016/j.envres.2006.01.002

Kalavathy, M.H., Karthikeyan, T., Rajgopal, S., Miranda, L.R., 2005. Kinetic and isotherm studies of Cu(II) adsorption onto H_3PO_4-activated rubber wood sawdust. J. Colloid and Interface Sci. 292, 354-362. https://doi.org/10.1016/j.jcis.2005.05.087

Kowanga, K.D., Gatebe, E., Mauti, G.O., Mauti, E.M., 2016. Kinetic, sorption isotherms, pseudo-first-order model and pseudo-second-order model studies of Cu(II) and Pb(II) using defatted Moringa oleifera seed powder. J. Phytopharmacol. 5, 71-78.

Lagergren, S., 1898. About the theory of so-called adsorption of soluble substances. Kungliga Svenska Veteskapsakademiens Handlingar, Band 24, 1-29.

Ololade, I.A., Adeola, A.O., Oladoja, N.A., Ololade, O.O., Nwaolisa, S.U., Alabi, A.B., Ogungbe, I.V., 2018. In-situ modification of soil organic matter towards adsorption and desorption of phenol and its chlorinated derivatives. J. Environ. Chem. Eng. 6, 3485-3494. https://doi.org/10.1016/j.jece.2018.05.034.

Potin, O., Veignie, E., Rafin, C., 2004. Biodegradation of polycyclic aromatic hydrocarbons (PAHs) by Cladosporium sphaerospermum isolated from an aged PAH contaminated soil. FEMS Microbiol Ecol. 51, 71-78. https://doi.org/10.1016/j.femsec.2004.07.013.

Sun, Y., Yang, S., Zhao, G., Wang, Q., Wang, X., 2013. Adsorption of polycyclic aromatic hydrocarbons on graphene oxides and reduced graphene oxides. Chem. Asian J. 8, 2755-2761. https://doi.org/10.1002/asia.201300496.

Yakout, S.M., Daifullah, A.A.M., 2013. Removal of selected polycyclic aromatic hydrocarbons from aqueous solution onto various adsorbent materials. Desalin. Water Treat. 51, 6711-6718. https://doi.org/10.1080/19443994.2013.769916.

Chapter 7 Remediation of antiretroviral drug contaminants in aqueous solution using graphene wool adsorbent

This chapter presents adsorption as a remedial option for the removal of selected antiretroviral drug contaminants in aqueous systems. The kinetics, isotherm and thermodynamics were studied in order to elucidate sorption mechanisms and capacity. The computational aspect of this study was carried out by a collaborator (Jurgens de Lange). This chapter is presented as it was published in Applied Surface Science Advances (Elsevier).

Article

Adeola, A.O., de Lange, J., Forbes, P.B.C. (2021). Adsorption of antiretroviral drugs, efavirenz and nevirapine from aqueous solution by graphene wool: Kinetic, equilibrium, thermodynamic and computational studies, 6, 100157.

DOI: http://dx.doi.org/10.1016/j.apsadv.2021.100157

Adsorption of antiretroviral drugs, efavirenz and nevirapine from aqueous solution by graphene wool: kinetic, equilibrium, thermodynamic and computational studies

Adedapo O. Adeola [a], Jurgens de Lange [a] and Patricia B.C. Forbes [a*]

[a]*Department of Chemistry, Faculty of Natural and Agricultural Sciences, University of Pretoria, Lynnwood Road, Hatfield, Pretoria 0002, South Africa.*

*Corresponding author email address: patricia.forbes@up.ac.za

Highlights

- Experimental and computational investigation of GW-EFV and GW-NEV interactions
- >80% removal efficiency of antiretroviral drugs by graphene wool was achieved.
- GW-NVP revealed higher sorption capacity and binding energy than for GW-EFV.
- GW-NVP adsorption is a spontaneous endothermic process while GW-EFV is exothermic.
- Computational studies revealed dispersion interactions and H-bonding at specific pH range.

Applied Surface Science Advances 6 (2021) 100157

Contents lists available at ScienceDirect

Applied Surface Science Advances

journal homepage: www.sciencedirect.com/journal/applied-surface-science-advances

Adsorption of antiretroviral drugs, efavirenz and nevirapine from aqueous solution by graphene wool: Kinetic, equilibrium, thermodynamic and computational studies

Adedapo O. Adeola, Jurgens de Lange, Patricia B.C. Forbes *

Department of Chemistry, Faculty of Natural and Agricultural Sciences, University of Pretoria, Lynnwood Road, Hatfield, Pretoria 0002, South Africa

ARTICLE INFO

Keywords:
Antiretroviral drug
Efavirenz
Nevirapine
Emerging contaminant
Graphene wool

ABSTRACT

The increasing concentrations of pharmaceutical and personal care products in water bodies have attracted attention due to the risk of non-target exposures. The application of any graphene-based material for the remediation of antiretroviral drug contamination has not been reported, therefore graphene wool was synthesized by chemical vapour deposition as adsorbent for the removal of efavirenz (EFV) and nevirapine (NVP) from water. Results revealed that adsorption of EFV was best fitted to the intraparticle diffusion model, with multilinearity (multiple adsorption steps). The pseudo-second-order model best describes GW-NVP interaction. Isotherm parameters revealed that Sips and Freundlich model best fit GW-EFV and GW-NVP interactions, with the least value of SSE < 0.04 and 1.27, respectively. GW demonstrated higher adsorption capacity and adsorption maxima for NVP with K_d and q_m values of $\sim$ 2.54 L/g and $\sim$ 48.31 mg/g, compared to $\sim$ 1.48 L/g and $\sim$ 4.41 mg/g obtained for EFV adsorption. Isotherm parameters suggest that GW adsorbed NVP slightly better with stronger binding strength than EFV, with removal efficiencies of 84% (NVP) and 80% (EFV) under optimum conditions. A heterogeneous adsorption mechanism was suggested for GW-EFV sorption, in contrast to a less heterogeneous and multilayer adsorption mechanism for GW-NVP adsorption. NVP adsorption is a spontaneous exothermic process, while GW-EFV interaction is a spontaneous endothermic process. Experimental results were supported by computational studies, which revealed the influence of strong dispersion interactions and H-bonding at specific pH ranges.

1. Introduction

Pharmaceuticals and personal care products (PPCP) are a vast and unique class of emerging chemical pollutants (ECP). They may cause physiological effects and alter systemic processes in humans upon exposure to low concentrations, which makes non-target exposures worrisome [1, 2]. In the last decade, the occurrence of antiviral and antiretroviral drugs as microcontaminants in drinking and surface water has received significant attention in both developing and developed parts of the world [3-6]. The risk assessment and adverse effects of exposure to these chemicals are not fully understood, but there is growing scientific, public, and regulatory concern as these drug compounds have been detected in surface waters [7-9]. The toxicological profile of selected antiviral drugs suggests that they are hazardous to aquatic fauna, with a low maximal effective concentration (EC_{50}) value of 57 mg/L [4]. Several antiviral drugs and their metabolites are nonbiodegradable, hence they persist in the environment [6, 10].

Antiretroviral drugs (ARVDs) are therapeutic agents for the treatment of retroviral infections, primarily the human immunodeficiency virus type 1 (HIV-1). The virus that causes HIV disease attacks the CD4-T cells responsible for body immunity, thus making humans vulnerable or susceptible to infections and diseases [11-12]. Antiretroviral treatment therapy against HIV-1 does not eliminate the virus but inhibits its rapid replication and increases the life expectancy of infected people [13].

This page is inserted as it is not possible to submit just a revised version of the manuscript with changes shown in red. It is mandatory on your system to submit a "Revised manuscript (clean version)", which was done. However we received a request twice thereafter for the same revision to "Please remove the former manuscripts. Please keep only one manuscript, the one that contains the corrections marked in red colour." The former manuscript was removed during the first revision already.

* Corresponding author.
E-mail address: patricia.forbes@up.ac.za (P.B.C. Forbes).

https://doi.org/10.1016/j.apsadv.2021.100157
Received 24 May 2021; Received in revised form 13 August 2021; Accepted 30 August 2021
Available online 8 September 2021

Table 1
Physicochemical properties of target antiretroviral drugs (ARVD).

ARVD (and abbreviation)	Molecular formula	LogK_{ow}	S_w	MM	pKa
Efavirenz (EFV)	$C_{14}H_9ClF_3NO_2$	4.70	0.093	315.68	10.20/ 12.52
Nevirapine (NVP)	$C_{15}H_{14}N_4O$	3.89	0.705	266.30	2.80

Log K_{ow}: octanol–water partition coefficient, S_w: water solubility (mg/L), MM: molar mass (g/mol), pKa:-log of acid-dissociation constant. Cited from pubchem [25, 26].

About 90% of orally administered drugs are removed unaltered or partially metabolized from the body as faecal waste, and they are thus found in sewage waste [14]. Similarly, unused and expired drugs may be disposed indiscriminately resulting in contamination of drainage systems and other water bodies [15].

Efavirenz and nevirapine exert distinct pathways for the inhibition of the proliferation of HIV, and they are classified amongst the most common ARVDs [16]. Adsorption of efavirenz onto biosolids has reportedly enhanced the removal efficiency of ARVDs in conventional wastewater treatment plants (WWTPs) in South Africa, with an efavirenz sludge concentration as high as 43 mg/kg, while 22.5% removal efficiency of nevirapine was also reported [17]. A Kenyan study reported decontamination efficiencies of 11 – 49% (nevirapine) and 83 – 92% (efavirenz) in three WWTPs [18]. Premised on the bioactivities of PCPPs at very low concentrations, non-target exposures via drinking water supplies and improper waste disposal, the inefficient performance of many existing wastewater and sewage treatment plants (WWTPs & STPs), and toxicities of pharmaceutical products; there is a need for more research on sustainable, efficient and ecofriendly remediation approaches (such as adsorption processes, green bioremediation, etc.) for removal of ARVDs from aqueous systems.

Adsorption techniques arising from material science advances have proven useful in mitigating the challenge of emerging chemical pollutants (such as pharmaceuticals) in water [19-21]. The adsorption method for the decontamination of water polluted with organic chemical pollutants has benefits such as simplicity in design and operation, low operational cost, easy adaptability, and minimal tendency of generating secondary pollutants or undesirable by-products [22-24]. Graphene-based materials (GBMs) have been harnessed as efficient next-generation sorbents for water purification applications, because their surface is largely hydrophobic, porous, and possesses high adsorption affinities for a vast number of organic contaminants (OCs) [19, 21, 22]. However, the application of graphene-based materials for the remediation of any antiretroviral drug contamination in water has not been reported previously.

Therefore, the overall aim of this study was to synthesize graphene wool (GW) for the removal of selected ARVDs from an aqueous solution. Sorption isotherm, kinetics, thermodynamic and computational studies were carried out to elucidate and evaluate the sorption mechanism(s) of GW-ARVD interactions, as well as the adsorption capacities and removal efficiency of graphene wool for potential use in the purification of ARVD-contaminated water. **Table 1** provides a summary of the basic physicochemical properties of the target ARVDs chosen for this study. Efavirenz and nevirapine were chosen as target antiretroviral drugs based on their toxicity, prevalence and persistence in surface waters [4].

2. Experimental methods

2.1. Synthesis of graphene wool (GW)

Graphene wool was synthesized using an established bottom-up approach as reported in [27]. Briefly, quartz wool (Arcos Organics, New Jersey, USA) was carefully arranged at the centre of a horizontal quartz tube (50 mm o.d., 44 mm i.d., x 1 m length) in a high-temperature furnace (OTF-1200X-50–5 L, MTI Corporation, California, USA). 500 sccm argon and hydrogen (analytical grade, 99.999%, Afrox, South Africa) were pre-mixed and released into the thermal reactor at 1200 °C. The quartz wool was annealed under this temperature and gas flow for 10 min, thereafter methane gas (analytical grade, 99.95%, Afrox, South Africa) was added for graphene growth. The system was cooled under Ar and H_2 gas after the optimized growth time had elapsed. Thus, the graphene wool (GW) synthesized is a composite of quartz wool coated with graphene.

2.2. Characterisation of graphene wool (GW) adsorbent

Surface morphology was examined using scanning electron microscopy (SEM) with aid of a Zeiss Ultra-Plus 55 field emission scanning electron microscope (FE-SEM), operated at 2.0 kV (OXFORD Link-ISIS-300 Zeiss, Germany); High-resolution transmission electron microscopy (TEM) images were taken using a JEOL JEM 2100F (JOEL Ltd, Tokyo, Japan) operated at 200 kV. The crystal structure of GW was also examined using a Bruker BV 2D Phaser X-ray diffraction (XRD) instrument with reflection geometry at 2θ values (10 – 60°) with a 5.24 s requisition time per step, operated with a Cu $K\alpha_1$ radiation source (λ = 0.15406 nm) at 50 kV and 30 mA. The surface area and porosity of GW were determined by N_2 adsorption-desorption isotherms at 77 K, using a NOVA Touch Surface analyzer system (Anton Paar, South Africa) in a relative pressure (P/P_0) range of 0.01−1.0, following a model of Brunauer−Emmett−Teller (BET) and Barrett−Joyner−Halenda (BJH) techniques

2.3. Adsorption kinetics and isotherm experiments

Batch adsorption experiments of efavirenz (EFV) and nevirapine (EFV) onto GW adsorbent were carried out in 40 mL PTFE screw-capped vials (Stargate Scientific, South Africa) at 25 ± 1 °C. Background electrolyte contained 0.01 mol/L $CaCl_2$ (analytical grade, ACE, South Africa) in deionized water (9.2 μS/cm^3, Millipore, Bedford, MA, USA), and 200 mg/L NaN_3 (analytical grade, Sigma-Aldrich, Germany) to inhibit microbial activity. Kinetic experiments were conducted for 72 h with initial EFV and NVP concentrations of 5 mg/L (99% pure standards, analytical grade were purchased from Sigma-Aldrich, Germany), and the mass per volume ratio was 10 mg of graphene wool per 5 mL solution.

Afterwards, the isotherm experiments were carried out with initial concentrations of ARVD solutions ranging between 1 - 20 mg/L, respectively. Desorption experiments were carried out by adding fresh 5 mL of background electrolyte after the supernatant from the adsorption studies had been decanted. Sorption thermodynamic evaluations were carried out at varying temperatures of 298, 308, and 318 K using a thermostated shaking water bath (Wisebath, Celsius Scientific, South Africa). The role of solution pH was studied over the pH range of 2 - 13, and the pH of the solutions was adjusted using 0.1 M HCl (analytical grade, Merck, South Africa) and/or 0.01 M NaOH (analytical grade, ACE, South Africa). Adsorption performance of GW for the removal of EFV and NVP was also studied at varying contact times (0, 15, 30, 60, 120, 240, 360, 600, 840, 1440, 2160, 2880, 3600, and 4320 mins, respectively). All experiments were carried out in duplicate.

2.4. Quantification

After equilibration for 24 h, the vials were centrifuged at 3000 rpm for 5 min to obtain a clear supernatant, which was then filtered using a 0.22 μm syringe filter (Stargate scientific, South Africa) and collected in 2 mL LC vials for analysis by ultra-performance liquid chromatography coupled with tandem mass spectrometry (UPLC-MS/MS).

2.4.1. UPLC-MS/MS analysis

Analysis of the supernatant was carried out using sensitive and rapid ultra-performance liquid chromatography (UPLC); accompanied by

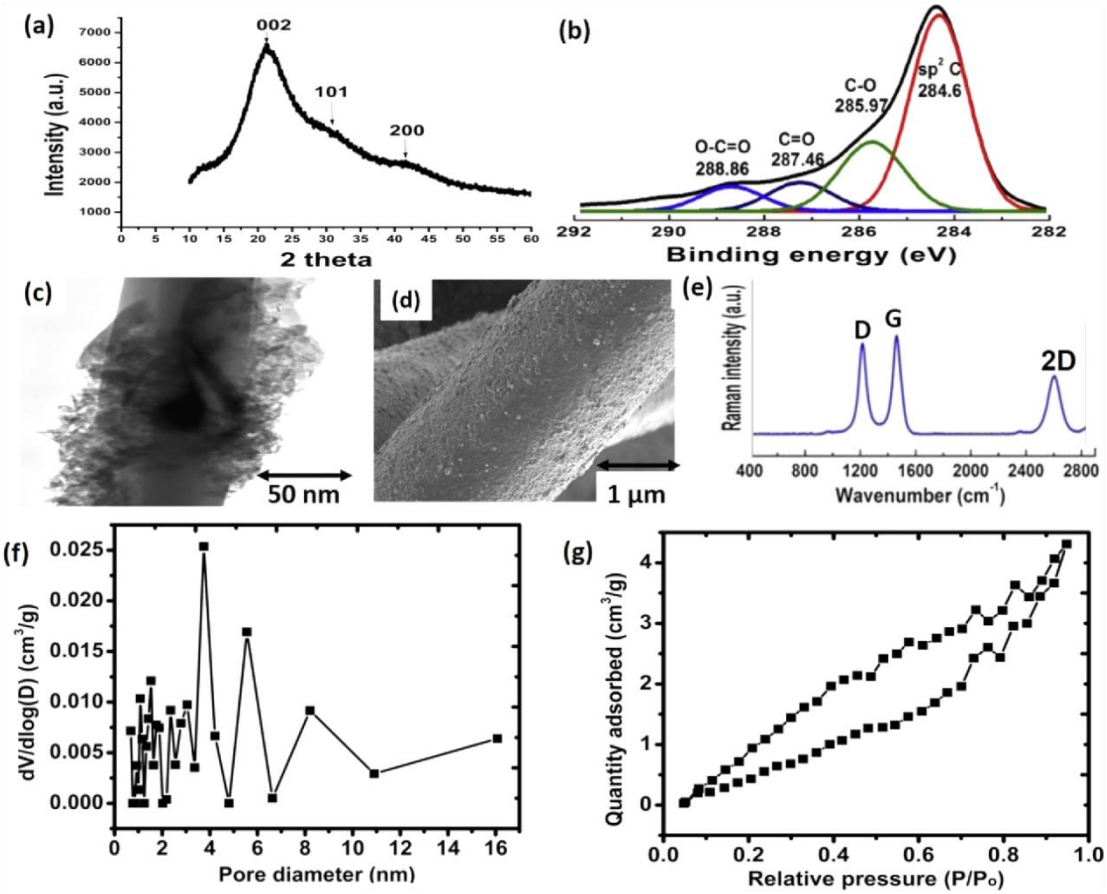

Fig. 1. Characterisation of graphene wool adsorbent, (a) XRD pattern (b) XPS spectrum (c) TEM image (d) SEM image (e) Raman spectrum showing the D, G and 2D peaks unique to multilayer graphene (f) Pore size distribution of GW and (g) N_2-sorption isotherm obtained from BET analysis.

electrospray ionization (ESI) in positive and negative mode (NVP and EFV, respectively) and mass spectrometric (MS) detection with a triple-quadrupole MS/MS system (Waters Inc., Milford, Massachusetts, USA). Chromatographic separation was achieved using an Acquity UPLC® ethylene bridged hybrid (BEH) shield reversed-phase C18 column (1.7 µm particle size, 100 mm length × 2.1 mm internal diameter) equipped with an Acquity UPLC C18 guard column (Waters, Milford, MA). EFV and NVP separation was carried out with 0.1% formic acid (HPLC grade) in water (solvent A) and 0.1% formic acid in acetonitrile (solvent B, HPLC grade), while the temperature of the column was maintained at 40 °C, the flow rate was set at 0.3 mL/min and a gradient run time of 5 min. The LC system was equipped with an autosampler with 5 µL injection volume per analysis, and samples were analysed in duplicate ($n = 2$) and standards in triplicates ($n = 3$). The MS discharge electrode was set at 5 µA for electrospray negative and positive ionization for EFV and NVP, respectively; the gas temperature was set at 250 °C, sheath gas temperature at 300 °C, the gas flow rate was set at 10 L/min, Delta EMV set at 400 V, nebuliser pressure of 35 psi, and capillary voltage was set at 3000 V.

Data acquisition and analysis was carried out using MassLynx™ (version 4.2) software (Waters, Milford, MA) and QuanLynx Method Editor V4.2 was used to prepare the calibration curve and quantification of EFV and NVP. The calibration curves were obtained from stock solutions of each ARVD with regression coefficient (R^2) > 0.98. The working standards were in the range of 0.01 – 5 mg/L for EFV and NVP, respectively. Equilibrium concentrations (C_e) were deduced from the equation of the curve and the amount adsorbed was calculated using the mass-balance equation presented below:

$$q_e = \frac{(C_0 - C_e)V_0}{S_m} \quad (1)$$

Where C_o (mg/L) is the initial concentration, C_e (mg/L) is the equilibrium solute concentration, V_o is the initial volume (L) and S_m is the mass (g) of the adsorbent.

$$\text{Removal efficiency } (\%) = \frac{(C_0 - C_e)}{C_0} \times 100 \quad (2)$$

2.5. Computational study of GW-ARVD interaction

EFV and NVP, in various conformers and tautomers, were optimized with Density Functional Theory (DFT), using B3LYP/6–31G(d) and the conductor-like polarizable continuum solvation model (CPCM) with water. Interactions between EFV, NVP, and various forms of a 5 × 5 graphene sheet (including functionalization with –O and –OH groups) were optimized. All structures are true local energy minima unless otherwise noted. All electronic structure calculations were performed with Gaussian 16, rev. C [28]. Selected wavefunctions were further investigated with the Fragment, Atomic, Localized, Delocalized and Interatomic (FALDI) density decomposition scheme [29, 30] using in-house codes and in conjunction with atomic basins defined by the Quantum Theory of Atoms in Molecules (QTAIM) [31], as implemented

Table 2
Kinetic parameters for efavirenz and nevirapine adsorption by graphene wool (GW) adsorbent and sum of square of errors (SSE) from nonlinear regression analysis.

Adsorption kinetics	Parameter	ARVD Efavirenz (EFV)	Nevirapine (NVP)
First order	*Predicted q_e (mg/g)*	1.193	3.269
	Experimental q_e (mg/g)	1.956	4.717
	K_1 (1/min)	1.017	1.000
	SSE	**1.180**	**1.237**
Second order	*Predicted q_e (mg/g)*	1.494	4.730
	Experimental q_e (mg/g)	1.956	4.717
	K_2 (mg/g.min)	0.040	0.007
	h (mg/g.min)	0.090	0.220
	Half-life ($t_{0.5}$)	16.670	21.140
	SSE	**0.830**	**0.288**
Weber-Morris intraparticle diffusion	*K_{id} (mg/g.min$^{1/2}$)*	0.022	0.051
	C	0.821	2.375
	SSE	**0.306**	**0.441**

in AIMAll v. 19.10.12 [32]. FALDI was used to calculate and visualize inter-fragment delocalization indices (DIs), through the joint overlap of atomic overlap matrices. FALDI delocalization indices (DIs) were performed without the localized-delocalized overlap correction [30] and correspond to orthodox QTAIM-defined DIs. Visualizations of FALDI fields were performed with visual molecular dynamics (VMD) [33].

3. Results and discussion

3.1. Characterisation of graphene wool

Figure (1a) reveals that graphene wool (GW) has an amorphous structure with an intercellular spacing of d_{002} = 3.70 Å, confirmed by the broad diffraction plane C (002) appearing at 2θ = 22.5°. The shift of carbon plane (002) to lower Bragg angle (26.4° to 22.5°) and broad peak confirms the coverage of the wool substrate by several layers of graphene, thus creating an amorphous carbon phase [34]. The hump nature of the diffraction pattern is a result of the presence of amorphous silica substrate with weak peaks at 30° and 42° respectively [35, 36]. The XPS and Raman spectra (Fig. 1**b** & 1**e**) revealed sp^2 $C = C$ structure as the most intense peak at 284.6 eV, which reflects a partially disordered network of the graphene multilayer structure and accounts for the D peak in the Raman spectrum (Fig. 1**e**) [27, 37-39].

The SEM and TEM analysis provided high-resolution microscopic images of GW (Fig. 1**c** & 1**d**). The analysis revealed that the diameter of each strand of GW is between 6 - 8 μm and extensive coverage of the substrate by graphene, with a rough and heterogeneous surface morphology. The BET analysis revealed a H4-isotherm curve associated with complex materials/composites (Fig. 1**f**) and the pore size distribution plot (Fig. 1**g**) showed that GW adsorbent has both micropores (pore diameter > 2 nm) and mesopores (2 nm < pore diameter < 50 nm), but no macropores [39]. The specific surface area (SSA), pore volume, and pore diameter were 29.6 m^2/g, 0.039 cc/g, and 1.37 nm respectively.

3.2. Adsorption kinetics and effect of contact time

The pseudo-first-order (PFO) eq. (3)), pseudo-second-order (PSO) (eq. (4)), and Weber-Morris intraparticle diffusion (eq. (5)) models were used to fit the time-concentration profile of adsorption of efavirenz and nevirapine onto synthesized graphene wool adsorbent (Fig. 1). Reaction pathways in adsorption processes are influenced by contact time. The sorption rate and mechanisms of adsorption can be deduced from time-concentration data derived from sorbate-sorbent interaction prior to equilibrium [41, 42]. The initial adsorption rate and half-life were also calculated (eq. (6) and (7) and the models were validated using the sum of square of errors (SSE) (eq. (8)) [40–42]. The kinetic parameters obtained from the models are presented in **Table 2**.

$$q_t = q_e\left(1 - e^{-K_1 t}\right) \tag{3}$$

$$q_t = \frac{q_e^2 K_2 t}{q_e K_2 t + 1} \tag{4}$$

$$q_t = K_{id} t^{0.5} + C \tag{5}$$

$$h = K_2 q_e^2 \tag{6}$$

$$t_{0.5} = \frac{1}{K_2 q_e} \tag{7}$$

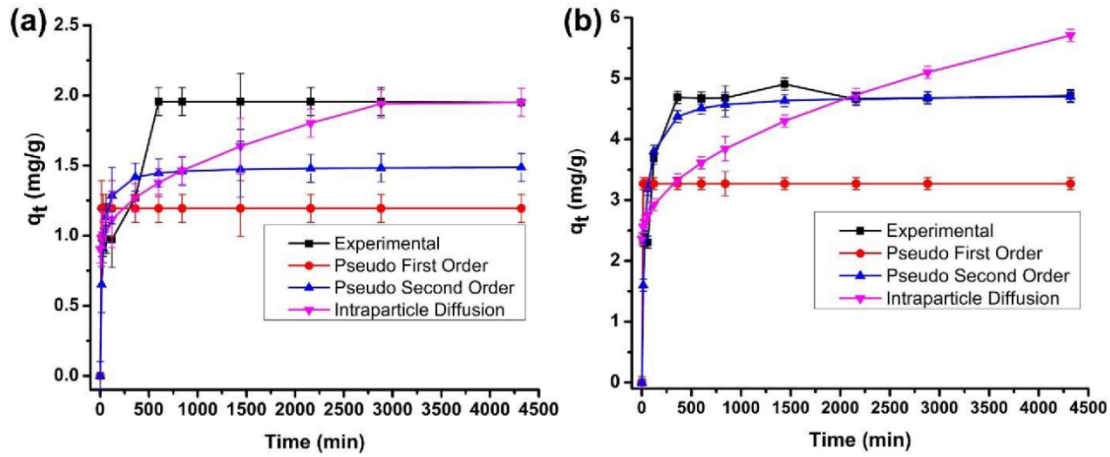

Fig. 2. Lagergren pseudo-first-order, pseudo-second-order and Weber-Morris intraparticle diffusion models of adsorption of (a) efavirenz and (b) nevirapine; onto graphene wool (Experimental conditions: Co = 5 mg/L; dosage = 10 mg per 5 mL, mixing rate = 200 rpm, T = 25 ± 1 °C). Error bars show ± relative standard deviation.

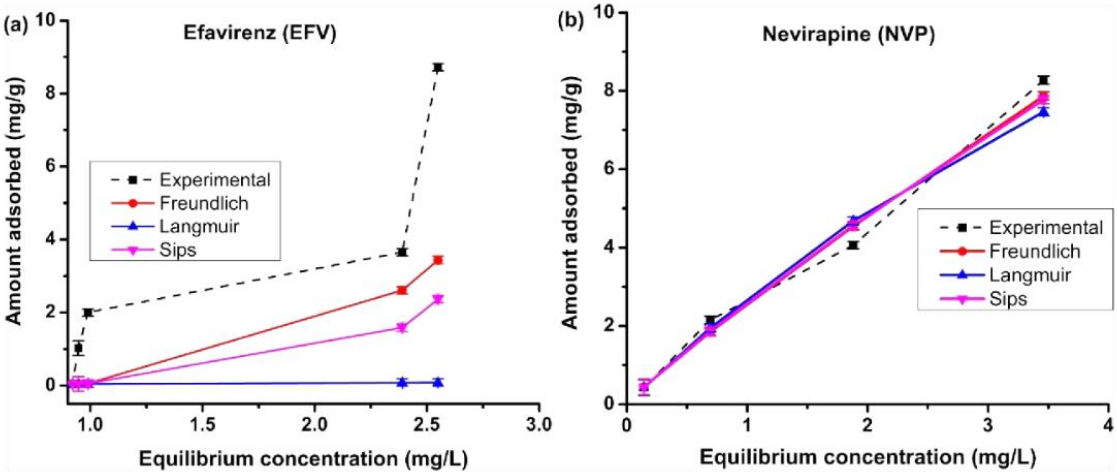

Fig. 3. Plots of sorption isotherm model for (a) efavirenz (EFV) adsorption and (b) nevirapine adsorption onto GW adsorbent (Experimental conditions: C_o = 1 – 20 mg/L; dosage = 10 mg per 5 mL, mixing rate = 200 rpm, T = 25 ± 1 °C). Error bars show ± relative standard deviation.

Table 3
Coefficients obtained for sorption isotherm models for selected antiretroviral drugs adsorption by graphene wool (GW) and sum of square of errors (SSE) (Experimental conditions: dosage = 20 mg per 10 mL; mixing rate = 200 rpm; T = 25 ± 1 °C; initial conc.: 1 - 20 mg/L; contact time = 24 h).

Isotherm model	Parameter	Efavirenz	Nevirapine
Linear	K_d *(L/g)*	1.482	2.544
	SSE	1.368	0.093
Freundlich	N	1.263	0.902
	K_F	1.269	2.569
	SSE	1.295	0.038
Langmuir	q_{max} *(mg/g)*	8.99e2	25.547
	K_L *(L/mg)*	0.002	0.119
	R_L	0.940	0.248
	SSE	1.370	0.042
Sips	*ms*	23.503	0.945
(Freundlich-Langmuir)	K_s *(L/mg)*	1.065	0.058
	q_m *(mg/g)*	4.408	48.313
	SSE	1.263	0.039

$$\sum_{i=1}^{n} \left(q_{e,cal} - q_{e,\ exp}\right)_i^2 \tag{8}$$

Where q_t and q_e are the amount of adsorbate sorbed per mass of adsorbent (mg/g) at a time (t) and equilibrium, respectively; K_1 (1/min) and K_2 (g/mg × min) are pseudo-first-order and pseudo-second-order rate constants, respectively; K_{id} (mg/g × $min^{1/2}$) and C (mg/g) are the intraparticle diffusion rate constant and constant associated with boundary layer thickness, respectively; and h (μg/g × min) and $t_{0.5}$ are the initial adsorption rate and half-life, respectively.

Table 2 revealed that the adsorption of efavirenz and nevirapine are best fitted to intraparticle diffusion and pseudo-second-order (PSO) kinetic models, given the lowest values of SSE. Fig. 2**(a)** revealed that EFV adsorption patterns exhibit multiple linearities, suggesting that several steps governed the GW-EFV interaction. The boundary layer constant (C) is both greater than zero for GW-EFV and GW-NVP which suggests that other mechanisms aside from film diffusion occurred during adsorption of both sorbates [41]. The initial steps include bulk transport and film diffusion between the sorbent-solution boundary layer, followed by adsorption of EFV onto pores of GW [41, 43]. The SSE suggests that even though the intraparticle diffusion model also fit GW-NVP interaction, the pseudo-second-order (PSO) model best describes the adsorption pathway for nevirapine (Fig. 2**b**). This suggests that some degree of chemical adsorption took place and contributed significantly to the adsorption rate and mechanism for NVP uptake. The predicted and experimental amount adsorbed (q_e) for nevirapine are of similar magnitude (47.3 and 47.2), which further confirms that PSO best fits GW-NVP interaction.

The initial steepness observed in Fig. 2 in the first 240 min of contact, reflects fast initial adsorption due to availability of GW sorption sites to the respective ARVDs, before a period of slow adsorption as available sites diminish, and equilibrium is reached after site saturation. The GW-EFV and GW-NVP reached equilibrium after 600 min and 360 min, respectively. The initial rate constant (h) reveals that the rate of adsorption of nevirapine is faster than efavirenz in the first 120 mins (Table 2), which could be attributed to lower molecular weight (size), availability of lone electron pairs, and π-electrons for binding interactions with GW. However, the PSO overall rate constant (K_2) suggests that EFV had a faster diffusion-controlled rate of adsorption, which was faster than the rate of chemisorption governing the adsorption of NVP [42, 44].

3.3. Adsorption isotherm

Adsorption isotherms provide vital information on the nature of the interaction between sorbates and sorbents, especially the amount of analyte adsorbed, and the amount unadsorbed after equilibrium is reached [40]. Linear regression and nonlinear isotherm models such as Linear (eq. (9)), Freundlich (eq. (10)), Langmuir (eq. (11)), and Sips model (eq. (13)) were used to fit adsorption experimental data. The sum of square of errors (SSE) (eq. (8)) was used to test all models used in this study [44, 45].

$$q_e = K_d C_e \tag{9}$$

$$q_e = K_F C_e^N \tag{10}$$

$$q_e = \frac{q_{max} K_L C_e}{1 + K_L C_e} \tag{11}$$

$$R_L = \frac{1}{1 + K_{L q_{max}} C_0} \tag{12}$$

$$q_e = \frac{q_m K_s C_e^{ms}}{1 + K_s . C_e^{ms}} \tag{13}$$

where K_F (mg/g) (L/mg)^N) and N (dimensionless) are the Freundlich constant and intensity parameter, an indicator of site energy

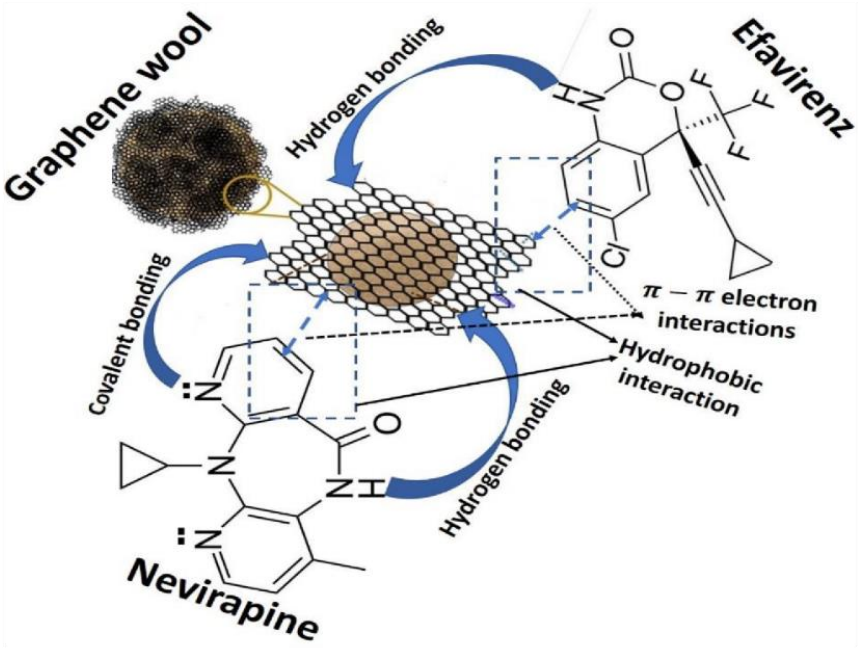

Fig. 4. Probable mechanisms of interaction between graphene wool and selected ARVDs.

Table 4
Sorption-desorption parameters and hysteresis index (*H*) derived from Freundlich isotherm model.

Sorbates	$K_{f,des}$	N_{ads}	N_{des}	SSE	R^2	*H
Efavirenz	0.70	1.26	4.39	1.50	0.992	0.29
Nevirapine	4.29	0.90	1.21	0.17	0.997	0.74

**H*: Sorption–desorption hysteresis index, $H = \equiv N_{ads}/N_{des}$; $\boldsymbol{N_{(ads)}}$: *Freundlich adsorption intensity,* $\boldsymbol{N_{(des)}}$: *Freundlich desorption intensity.*

heterogeneity; q_{max} (mg/g) and K_L (L/mg) are the Langmuir maximum adsorption capacity and Langmuir constant associated with solute–surface interaction energy, respectively; K_s (L/mg) *and* q_{max} (mg/g) are Sips isotherm model constants and maximum adsorption capacity and *ms* is Sips isotherm exponent; q_e is the solid-phase concentration (mg/g), C_e is the liquid phase equilibrium concentration (mg/L), and K_d (L/g) is the sorption distribution coefficient [22, 40]. The value of the separation factor R_L (eq. (12)) provides important information about the nature of adsorption; ($R_L < 1$ = favourable adsorption; $R_L > 1$ = unfavourable adsorption; $R_L = 1$ = linear adsorption; $R_L = 0$ = irreversible) [,][37,38].

The one, two, and three-parameter models used in this study provided useful insight into the nature and mechanism of adsorption of the selected ARVDs by graphene wool; and nonlinear regression analysis of experimental data using equations (9 - 13), have been reported to provide a more accurate fit than linear regression [44, 45]. Isotherm data for EFV was best fitted by Sips isotherm model with least SSE < 1.27, while NVP was best described by a multilayer adsorption mechanism depicted by Freundlich model with SSE < 0.039, respectively (Fig. 3, Table 3).

Sips is a hybrid of the Langmuir and Freundlich model and describes heterogeneous adsorption systems [45]. Thus, given that it best fit EFV adsorption, this implies that the interaction of EFV with GW is complex and highly heterogeneous, which accounts for the comparatively high heterogeneity (*N & ms*) index (Table 3). Basic models such as Freundlich and Langmuir would not completely describe the EFV sorption mechanism, due to limitations caused by increased adsorbate concentration and the nature of solute normally associated with the Freundlich model [45, 46]. Therefore, at low adsorbate concentration, the Sips model could reduce to Freundlich model (multilayer adsorption), and at high concentration of adsorbate, it predicts Langmuir model (monolayer adsorption).

The solute–surface interaction energy (K_L), Sips maximum adsorption capacity (q_m) and adsorption capacities (K_d & K_F) revealed that NVP has stronger binding strength and higher sorption capacity onto GW adsorbents, while GW-EFV interaction is mainly dominated by weak van der Waal's and hydrophobic bonding interactions considering its hydrophobicity (Log*Kow*) and structure (Table 1).

3.3.1. *Plausible sorbent-sorbate mechanism of interaction*

The mechanism of interaction between adsorbents and adsorbates is often influenced by the moieties/functional groups and molecular/electronic conformation of the adsorbents and adsorbates. The bulky molecular nature of organic compounds including pharmaceuticals often leads to several competing interactions. In this study, the Sips model described the adsorption of EFV and NVP onto GW well, which affirms the existence of complex interactions, which can be influenced by concentrations of target compounds, solution's pH, and temperature of the system. The electron pairs on the nitrogen atom in the pyridine aromatic structure present in nevirapine, suggest possible covalent bonding interactions between NVP and electrophiles without disruption of the aromatic ring of NVP. This provided a plausible explanation for the stronger interaction between GW-NVP than GW-EFV as presented by isotherm data (Table 3).

Other non-covalent bonding interactions are probable between GW-EFV and GW-NVP, and they include binding mechanisms such as π-π stacking, hydrogen bonding, van der Waals and hydrophobic bonding (Fig. 4), which have been reported to control the adsorption of several organic pollutants by graphene-based materials [47-49]. Furthermore, the presence of electronegative atoms such as fluorine, chlorine, and nitrogen in the target compounds, as well as the proton-rich structure of graphene; indicate that electrostatic attraction and repulsion in ionic aqueous medium cannot be ruled out, especially under varying pH [50].

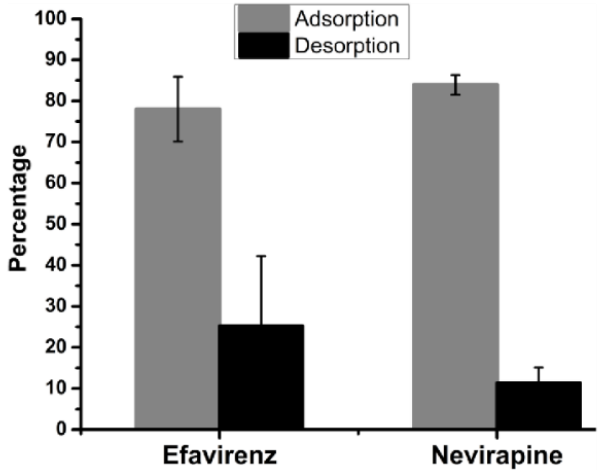

Fig. 5. Percentage adsorption and desorption of efavirenz (EFV) and nevirapine (NVP) by graphene wool (GW). Error bars show ± standard deviation, $n = 5$.

3.4. Desorption isotherm and hysteresis

The release and subsequent recontamination potential of adsorbed compounds are often evaluated by desorption studies. Thus, evaluating the fraction of adsorbed EFV and NVP, that can desorb into an aqueous solution by reaching a new equilibrium is vital for GW industrial application and decontamination processes [41]. Hysteresis index (H), which is a measure of the irreversibility of the sorption process, was calculated for GW-EFV and GW-NVP interactions. Table 4 revealed H-index values for both ARVDs were greater than zero ($1/N_{ads} > > > 1/N_{des}$), which implies that some degree of sorption–desorption hysteresis occurred [51].

The calculated hysteresis index was greater in GW-NVP, which suggests a higher tendency for irreversible sorption (hysteresis) in GW-NVP sorption-desorption interaction (Table 4). This can be attributed to stronger binding strength and possible sorption site defects and entrapment of adsorbed molecules [41, 52]. Experimental data revealed that more of NVP was adsorbed as clearly observed in the isotherm parameters, with significantly higher binding capacity (Table 2 and Fig. 5). On the contrary, GW-EFV displayed higher values of heterogeneity index (N_{ads} and N_{des}) suggesting a heterogeneous interaction, which potentially leads to sorption disequilibrium, weaker binding capacity, and faster rate of desorption of adsorbed molecules. Fig. 5 revealed that the % adsorption and desorption for efavirenz are 80 and 25.3%, and nevirapine are 84 and 11.5%, respectively. Nevirapine displayed weaker desorption potential which suggests stronger binding strength between nevirapine and GW (Fig. 5).

3.5. Effect of pH on adsorption of selected ARVDs

The need to study the influence of pH on the adsorption of organic pollutants including PPCPs, in contaminated aqueous solution is germane towards predicting optimum process conditions. The presence of specific moieties such as -OH, -COOH, -NH groups in many pharmaceutical products ensures protein-binding and transport in blood for pharmacological action and therapeutic effects [53], however, these functionalities make them susceptible to deprotonation under variable pH conditions. Furthermore, pKa values of efavirenz and nevirapine are presented in Table 1, and many notable reports have affirmed that the acid dissociation constant (pKa) largely influences the effect of pH on sorption processes of PCPPs, as pH range determines when the bulky compound is cationic or anionic in aqueous solution [54-56]. Generally, solution pH alters the surface properties of adsorbents and speciation of the compounds in the solution.

Efavirenz becomes anionic at a pH range beyond its dual pKa values of 10.20 and 12.52, which is mainly responsible for the steep decline in

Table 6
Calculated interaction and binding energies of ARVDs onto various forms of graphene sheets.

Adduct	ΔE_{int}	ΔE_{bind}	Inter-molecular delocalized electrons		
	(kJ/mol)	*(kJ/mol)*	*Total*	*Dispersion*	*H-bonds*
NVP					
GW···NVP—H	–117.15	–104.27	0.94	0.94	0.00
GW···NVP^-	–99.66	–93.01	0.91	0.91	0.00
GW–NVP *(covalent)*	–95.10	+113.97			
GW(OH)···NVP-H	–149.49	–127.40	1.17	1.01	0.17
GW(OH)···NVP^-	–149.41	–126.23			
GW(O)···NVP^-	–100.04	–95.81			
EFV					
GW···EFV-H_2	–117.53	–112.30	1.01	1.01	0.00
GW···EFV^{2-}	–105.48	–94.94	0.97	0.97	0.00
GW(OH)···EFV-H_2	–145.39	–139.03			
GW(O)···EFV-H_2	–134.27	–125.69			
GW(O)···EFV^{2-}	–95.23	–89.87	1.19	1.14	0.05

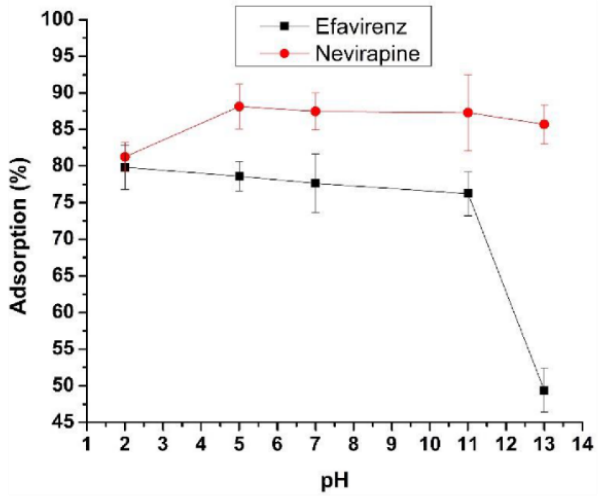

Fig. 6. Effect of pH on efavirenz and nevirapine adsorption onto graphene wool (Experimental conditions: Co = 5 mg/L; dosage = 10 mg per 10 mL solution, mixing rate = 200 rpm, $T = 25 \pm 1$ °C, contact time: 24 h). Error bars show ± relative standard deviation.

Table 5
Thermodynamic parameters for adsorption of efavirenz and nevirapine onto graphene wool (GW).

Temperature (K)	Efavirenz				Nevirapine			
	ln *b*	ΔG (kJ/mol)	ΔH (kJ/mol)	ΔS (kJ/mol.K)	ln *b*	ΔG (kJ/mol)	ΔH (kJ/mol)	ΔS (kJ/mol.K)
298	6.45	−15.98			10.36	−25.67		
308	11.52	−29.50	208.80	0.76	10.34	−26.48	−1.97	0.08
318	11.65	−30.80			10.31	−27.26		

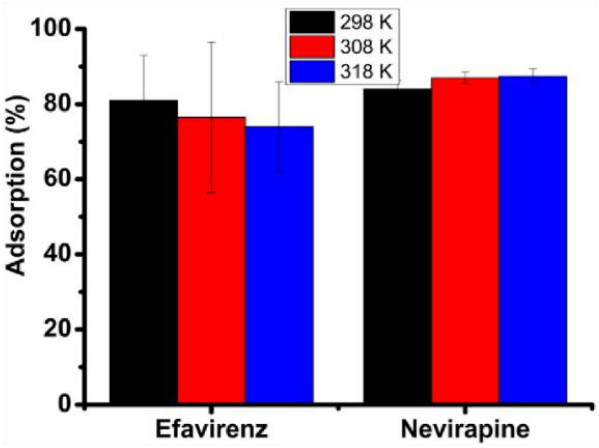

Fig. 7. Effect of temperature on adsorption performance of GW. Error bars show ±standard deviation $n = 5$. (Experimental conditions: $C_o = 1 - 20$ mg/L; dosage = 10 mg per 5 mL, mixing rate = 200 rpm, $T = 25 - 45$ °C).

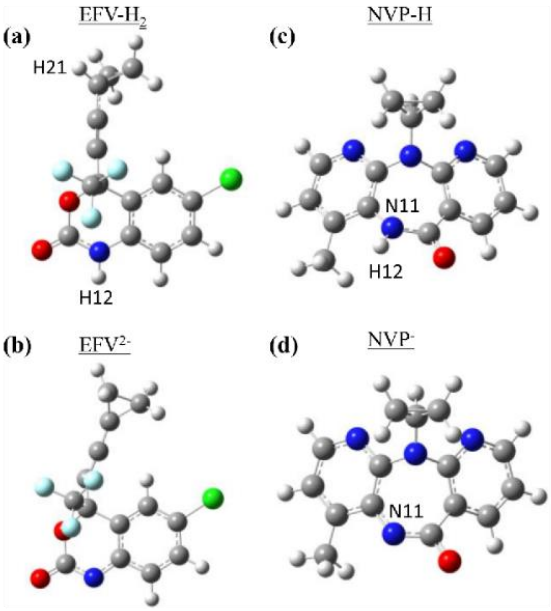

Fig. 8. DFT lowest-energy structures of protonated and deprotonated forms of efavirenz [EFV, (a) and (b)] and nevirapine [NVP, (c) and (d)]. Selected atoms and deprotonation sites are shown.

% adsorption in the basic medium. This is a result of electrostatic repulsion between the anionic EFV and deprotonated GW (negatively charged sorbent). The pKa of NVP is 2.8 and it is mainly anionic at pHs above its pKa value. This explains the slight increase in adsorption at acidic pH above its pKa (optimum at pH 5) because GW is protonated (positively charged) in an acidic medium, thus resulting in an attraction. A slight decline in adsorption at basic pH is due to weak electrostatic repulsion between the anionic NVP and negatively charged sorbent in the basic medium. The weak impact of electrostatic attraction and repulsion on NVP adsorption suggests that its adsorption onto GW is controlled by other mechanism(s) (Fig. 4) and electrostatic/van der Waal's attraction is complementary. A similar trend was reported for the adsorption of PCPPs such as carbamazepine, diclofenac, and clofibric acid by graphene oxide (GO) and chitosan [54, 55]

3.6. Adsorption thermodynamics and effect of temperature

Temperature plays a significant role in many physicochemical and biological processes. Adsorption thermodynamic parameters such as a change in enthalpy (ΔH), change in entropy (ΔS) and Gibbs free energy variation (ΔG), were derived from Van't Hoff equation eq. (14) and (15). The adsorption equilibrium constant (b) was deduced from the isotherm data using Eq. (11), at varying temperatures and used for the Van't Hoff plot (**Fig. 7b**) [50, 57]:

$$\ln b = \frac{\Delta S^{\circ}}{R} - \frac{\Delta H^{\circ}}{RT} \tag{14}$$

$$\Delta G^{\circ} = -RT \ln b \tag{15}$$

where ΔG is the change in the Gibbs free energy (kJ/mol); ΔH is the change in enthalpy (kJ/mol), and ΔS is the change in entropy (J/mol.K), R = gas constant (8.314 J/mol K), T = thermodynamic temperature (K). The value of b is derived from the Langmuir adsorption constant (K_L) by multiplying its value (in L/mg) by 1000 to convert the units to L/g, and then multiplied by the molar mass of the antiretroviral drug as stated in **Table 1**.

EFV adsorption is an endothermic process (ΔH) while NVP is exothermic ($-\Delta H$) (**Table 5**). The negative ΔG and positive ΔS for GW-NVP and GW-EFV interactions confirm a spontaneous adsorption process, with an increase in spontaneity as temperature increases from 25 to 45 °C [21, 50]. The EFV adsorption diminished from 81% at room temperature to 74% at 45 °C, which could be attributed to a higher degree of disorderliness/randomness as temperature increased (Fig. 7). While NVP adsorption slightly improved from 84% at ambient temperature to 87% at 45 °C, which could be due to relatively lower net displacement in the sorbent-solution interphase (considering entropy values) [57]. The values of the adsorption equilibrium constant (ln b) and ΔG reveal that the impact of increasing temperature is more significant in GW-EFV interactions.

3.7. Computational studies of GW-EFV and GW-NVP interactions

Computational modelling using Density Functional Theory (DFT) was performed to assist with the interpretation of experimental results, as well as to further explore the interactions between EFV, NVP, and graphene wool. Optimized structures of protonated and deprotonated forms of EFV (EFV–H_2 and EFV^{2-}, respectively) and NVP (NVP–H and NVP^{-}, respectively) are shown in Fig. 8. The sequence of (de)protonation for each structure was established through the selection of the lowest energy tautomers of all possible ionized states; interestingly, the acidic proton associated with pKa = 10.20 in EFV was found to be –C≡≡C–**C**H$(CH_2)_2$ – H21 in Fig. 8**(a).**

Since the synthesized graphene wool contains C—O functional groups (XPS spectrum, Fig. 1**(b))**, graphene wool was modelled using three different structures: i) a single 5 × 5 graphene sheet, $C_{75}H_{17}$, labelled as GW, ii) a graphene sheet functionalized with a single O atom, labelled as GW(O) and iii) a graphene sheet functionalized with a single OH group, labelled as GW(OH). Constructing adducts of the absorbates and the three different forms of GW allow for a careful investigation of the effects of dispersion, electrostatics, covalent and non-covalent interactions. In particular, the *binding energy*,

$$\Delta E_{\text{bind}} = E(\text{adduct}) - E(\text{adsorbent}) - E(\text{adsorbate}) \tag{16}$$

calculates the adsorption energy relative to the lowest-energy, undeformed graphene sheet and adsorbates. In contrast, the *interaction energy*,

$$\Delta E_{\text{int}} = E(\text{adduct}) - E^{*}(\text{adsorbent}) - E^{*}(\text{adsorbate}) \tag{17}$$

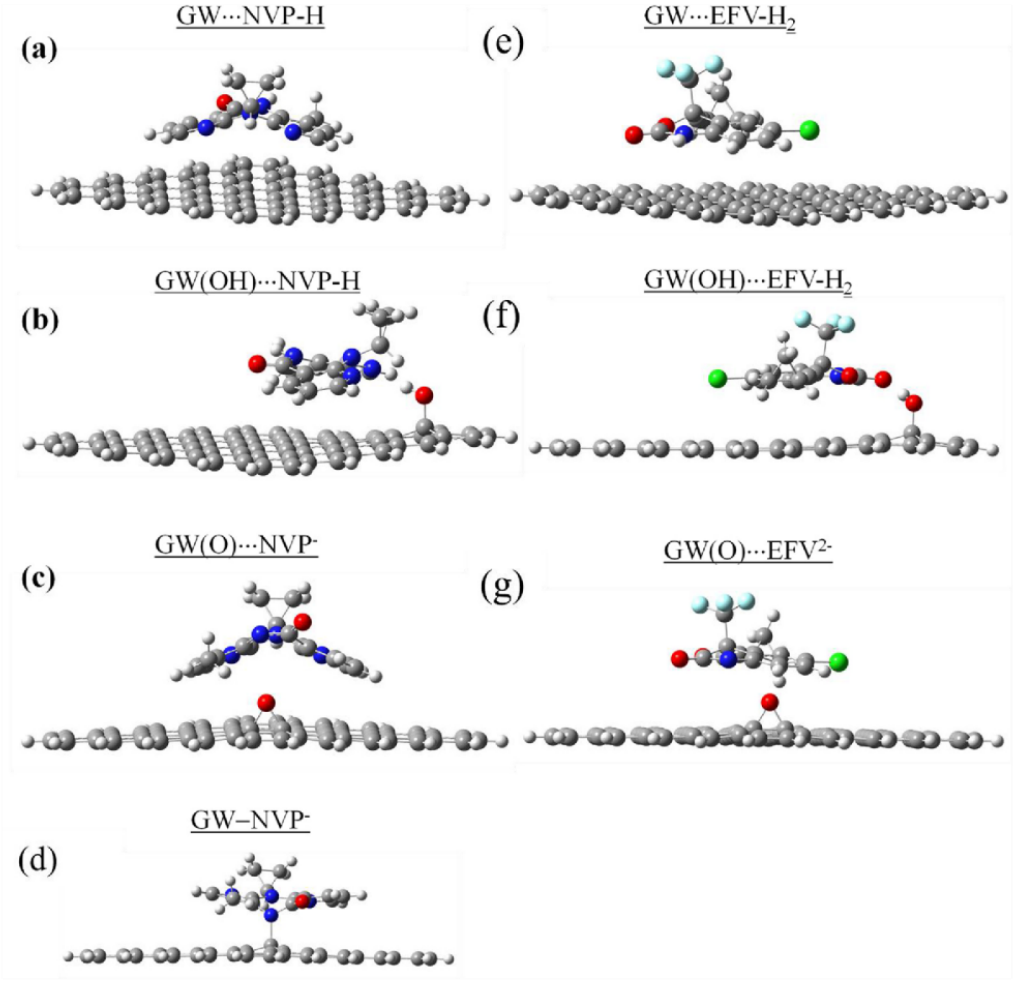

Fig. 9. DFT lowest-energy adducts between reduced graphene oxide (GW, graphene sheet), protonated and deprotonated graphene oxide (GW(OH), GW(O)) as adsorbents and various (de)protonated forms of EFV and NVP.

calculates the adsorption energy relative to the pre-organized, deformed molecules, where E^*(adsorbent) and E^*(adsorbate) are single-point structures in the geometry of the adsorbed adduct. The difference between ΔE_{bind} and ΔE_{int} is therefore the energy required to pre-organize the geometries of both adsorbent and adsorbate from their equilibrium structures to the conformations found in the adsorbed adduct, $\Delta E_{bind} = \Delta E_{int} + \Delta E_{org}(\text{adsorbent}) + \Delta E_{org}(\text{adsorbate})$.

The interactions between the ARVDs and the fully reduced GW are shown in Table 6. Interestingly, the neutral forms of NVP and EFV interact with a graphene sheet (Fig. 9) in a very comparable fashion (ΔE_{int}= –117.15 and –117.53 kJ/mol, respectively) given the parameters of the model: no functional groups present on a monolayer graphene sheet and lack of any cooperative effects. In these conditions, similar interaction energy indicates that the degree of dispersion and electrostatic interaction between GW and adsorbate is very similar for both NVP and EFV. However, NVP needs to deform more than EFV in order to adsorb to the GW surface, resulting in a slightly stronger overall binding energy for the adsorption of EFV (ΔE_{bind}= –104.27 and –112.30 kJ/mol for NVP and EFV, respectively). When both NVP and EFV are deprotonated, binding and interaction energies become less negative and indicate weaker adsorption. For instance, ΔE_{int} = –99.66 kJ/mol in the GW···NVP$^-$ adduct, +17.49 kJ/mol higher than its neutral NVP-H counterpart. This observation therefore fully supports the reported experimental results, suggesting that negative charges on the deprotonated ARVDs leads to larger electrostatic repulsion with the generally electronegative graphene sheet.

It is plausible from the EFV···GW and NVP···GW interaction energies that these ARVDs adsorb to graphene primarily through dispersive interactions. The total number of electrons shared between each ARVD and the graphene sheet was modelled using FALDI and is tabulated in Table 6. NVP-H shares a surprisingly large total of 0.94 e^- (almost a full electron) with GW. However, no single diatomic contact makes a significant contribution – of a total of 3128 inter-molecular diatomic contacts in the GW···NVP-H adduct, the largest diatomic contribution is a fractional 0.023 e^- (3% of the total number of electrons shared), arising from a C···C contact (visualized in Fig. 10). Rather, the remarkable ability of graphene to delocalize electrons results in a strong dispersive interaction resulting from many, cumulative weak diatomic interactions. EFV-H_2 shares slightly more electrons with GW(O) (1.01 e^-) than NVP-H, indicating an even stronger dispersive interaction. On the other hand, the deprotonated forms of both ARVDs share slightly fewer electrons than their protonated counterparts. For instance, EFV^{2-} shares slightly fewer electrons (0.97 e^-) with the monolayer graphene sheet than EFV-H_2.

Low and high pH conditions can be simulated by considering the

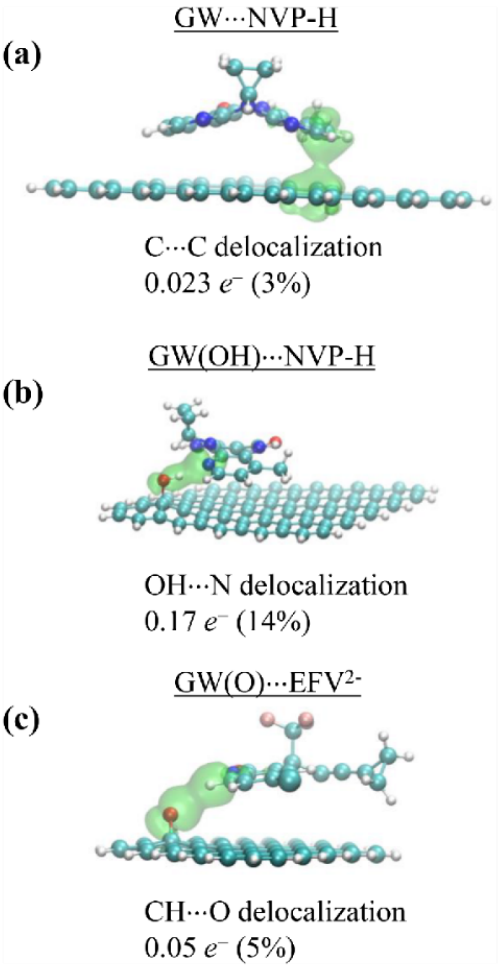

Fig. 10. DFT lowest-energy adducts between reduced graphene oxide (GW, graphene sheet), protonated and deprotonated graphene oxide [GW(OH), GW (O)] as absorbates and various (de)protonated forms of EFV and NVP.

functionalized GW model, either as GW(OH) or GW(O), respectively. When the graphene sheet is functionalized in this manner, results in Table 6 display a slightly different picture. The interaction and binding energies of NVP-H are stabilized when adsorbing to a GW(OH), ΔE_{bind} = –127.40 kJ/mol for GO(OH)···NVP-H, –23.14 kJ/mol lower than for rGO···NVP-H. Very similar values are observed for the deprotonated GW (OH)···NVP^- adduct. The origin of this stabilization in functionalized graphene relative to a reduced GW is clearly an OH···N hydrogen-bond (Fig. 9(b)), which is confirmed with FALDI – an additional 0.17 e^- are shared amongst the relevant O, H, and N atoms (visualized in **Fig. 10 (b)**). At high pH conditions, the GW(OH) sheet is expected to be deprotonated to GW(O). As a result, the GW(O)···NVP^- interaction is destabilized (ΔE_{bind} = −95.81 kJ/mol) relative to GW(OH)···NVP-H and is very similar to the GW···NVP^- adduct, due to a lack of any significant H-bonding. Of particular note, however, is the interaction of EFV with GW(OH) and GW(O). When both absorbent and absorbate are protonated (as expected for low pH conditions), the GW(OH)···EFV-H_2 interaction is the strongest out of all adducts investigated (ΔE_{bind} = –33.23 kJ/mol). However, as the graphene sheet and EFV molecule are deprotonated, the adduct is destabilized: ΔE_{bind} = +13.39 kJ/mol higher in GW(O)···EFV-H_2 and +49.20 kJ/mol higher in the fully protonated GW(O)···EFV^{2-}. This result fully supports the presented experimental findings that the degree of adsorption of EFV decreases at high pH, Fig. 6. It also lends credence that EFV is predominantly adsorbed through dispersion interactions with graphene at neutral and basic pH conditions. A weak CH···O interaction is detected in the GW(O)···EFV^{2-} adduct, but it only contributes 0.05 e^- to the total number of delocalized electrons (**Fig. 10(c)**). Interestingly, the total number of delocalized electrons due to dispersion is the highest in GW(O)···EFV^{2-} of all adducts investigated (1.14 e^-) which, in conjunction with the relatively destabilized binding energy, indicates a significant degree of electrostatic repulsion is present.

Finally, we have only been able to find a single adduct with a *covalent* bond between adsorbate and graphene. Specifically, NVP^- can bind through the deprotonated nitrogen atom (N11, **Fig. 8(c)**) to form the GW–NVP^- covalently bonded complex, **Fig. 9(d)**. The structure is metastable, however, in a very shallow potential energy well. All other candidate covalent adducts, including all forms of EFV and other conformations of NVP with graphene, were disregarded as unlikely due to extremely large binding energies at average covalent bond distances. The GW–NVP^- complex is characterized by moderately negative interaction energy (ΔE_{int} = –95.10 kJ/mol) but positive binding energy (ΔE_{bind} = +113.97 kJ/mol), Table 6. Our modelling therefore suggests that the graphene–NVP^- covalent bond is attractive but requires large deformations in both adsorbate and absorbent in order to form. In addition, as we did not find any other structures which seems to support covalent bonding with graphene, it is highly probable that the observed covalent bond is a feature exclusive to the deprotonated form of NVP^-. It is very likely that a more complex model including e.g., multiple graphene layers, the inclusion of defects or increased graphene functionalization will further stabilize this covalent complex, but such modelling lies outside of the scope of this work.

Conclusion

A comprehensive risk-based assessment of graphene is currently unavailable; however, many researchers believe that the material does not pose a high health risk based on its composition, but it may pose a potential risk as a result of its thin and lightweight nature. Particularly, graphene in the particulate form could prove worrisome regarding inhalation risks. The physical structure of the graphene-based material and the fabrication method is therefore critical. With respect to graphene wool, the quartz wool substrate acts as solid support, assisting with immobilization of the graphene. This study revealed that graphene wool can be used as an effective adsorbent for the removal of antiretroviral drug contaminants, specifically efavirenz and nevirapine from aqueous solution. The Sips, Freundlich, pseudo-second-order, and intraparticle diffusion adsorption models best describe the sorption processes, and experimental variables such as pH and temperature only slightly influence nevirapine adsorption. This suggests that its interaction is majorly controlled by strong electronic interaction between moieties containing lone pairs leading to hydrogen bonding, and π-π stacking between GW and NVP. It could be concluded that GW-EFV interaction is comparably weaker, with less hysteresis and higher desorption potential, and is controlled by hydrophobic and electrostatic interactions. Computational studies suggest that both GW···EFV and GW···NVP interactions are predominantly controlled by dispersive interactions, although specific (de)protonation of functional groups on the graphene layer can lead to significant additional stabilization through hydrogen bonds. This study presents the first experimental and computational investigation of the potential application of a graphene-based material (graphene wool) as an efficient next-generation sorbent for the removal of antiretroviral drug contamination in water. Furthermore, unlike most graphene generated in the form of flakes or powder, graphene wool provides a wool-like form that may be more suitable as a packing material for filters and other water polishing tools. The synthesis of graphene wool is facile and eco-friendly without extensive use of chemicals. Therefore, under appropriate operating conditions, the graphene wool adsorbent can potentially be utilized as a water polishing

tool for the removal of antiretroviral drug contaminants and other organic chemical pollutants.

Conflict of interest

The authors declare that there is no conflict of interest regarding the publication of this article.

Declaration of Competing Interests

The authors declare that they have no known competing financial interests or personal relationships that could have appeared to influence the work reported in this paper.

Acknowledgements

Authors acknowledge the University of Pretoria Commonwealth Doctoral Scholarship (AA) and the Rand Water Professorial Chair program (PF) for providing funding for this research.

References

[1] M. Parolini, A. Pedriali, A. Binelli, Application of a biomarker response index for ranking the toxicity of five pharmaceutical and personal care products (PPCPs) to the bivalve dreissena polymorpha, Arch. Environ. Contam. Toxicol. 64 (2013) 439–447, https://doi.org/10.1007/s00244-012-9847-3.

[2] A.J. Ebele, M. Abou-Elwafa Abdallah, S. Harrad, Pharmaceuticals and personal care products (PPCPs) in the freshwater aquatic environment, Emerg. Contam. 3 (2017) 1–16, https://doi.org/10.1016/j.emcon.2016.12.004.

[3] B. Petrie, R. Barden, B. Kasprzyk-Hordern, A review on emerging contaminants in wastewaters and the environment: current knowledge, understudied areas and recommendations for future monitoring, Water Res 72 (2015) 3–27, https://doi.org/10.1016/j.watres.2014.08.053.

[4] A.O. Adeola, P.B. Forbes, Antiretroviral drugs in african surface waters: prevalence, analysis, and potential remediation, Environ Toxicol Chem (2021), https://doi.org/10.1002/etc.5127.

[5] J. Funke, C. Prasse, T.A. Ternes, Identification of transformation products of antiviral drugs formed during biological wastewater treatment and their occurrence in the urban water cycle, Water Res 98 (2016) 75–83, https://doi.org/10.1016/j.watres.2016.03.045.

[6] C. Prasse, M.P. Schlüsener, R. Schulz, T.A. Ternes, Antiviral drugs in wastewater and surface waters: a new pharmaceutical class of environmental relevance? Environ. Sci. Technol. 44 (2010) 1728–1735, https://doi.org/10.1021/es903216p.

[7] A.J. Al-Rajab, L. Sabourin, R. Chapman, D.R. Lapen, E. Topp, Fate of the antiretroviral drug tenofovir in agricultural soil, Sci. Total Environ. 408 (2010) 5559–5564, https://doi.org/10.1016/j.scitotenv.2010.07.074.

[8] M. Wooding, E.R. Rohwer, Y. Naudé, Determination of endocrine disrupting chemicals and antiretroviral compounds in surface water: a disposable sorptive sampler with comprehensive gas chromatography – time-of-flight mass spectrometry and large volume injection with ultra-high performance liquid chromatography–tandem mass spectrometry, J. Chromatogr. A. 1496 (2017) 122–132, https://doi.org/10.1016/j.chroma.2017.03.057.

[9] C. Schoeman, M.Mashiane C, M. Dlamini, O.J. Okonkwo, Quantification of selected antiretroviral drugs in a wastewater treatment works in South Africa using GC-TOFMS, J. Chromatogr. Sep. Tech. 6 (2015) 272, https://doi.org/10.4172/2157-7064.1000272.

[10] G. Mascolo, L. Balest, D. Cassano, G. Laera, A. Lopez, A. Pollice, C. Salerno, Biodegradability of pharmaceutical industrial wastewater and formation of recalcitrant organic compounds during aerobic biological treatment, Bioresour. Technol. 101 (2010) 2585–2591, https://doi.org/10.1016/j.biortech.2009.10.057.

[11] E. Ngumba, A. Gachanja, T. Tuhkanen, Occurrence of selected antibiotics and antiretroviral drugs in Nairobi River Basin, Kenya, Sci. Total Environ. 539 (2016) 206–213, https://doi.org/10.1016/j.scitotenv.2015.08.139.

[12] D. Gökengin, F. Doroudi, J. Tohme, B. Collins, N. Madani, HIV/AIDS: trends in the Middle East and North Africa region, Int. J. Infect. Dis. 44 (2016) 66–73, https://doi.org/10.1016/j.ijid.2015.11.008.

[13] S. Ncube, L.M. Madikizela, L. Chimuka, M.M. Nindi, Environmental fate and ecotoxicological effects of antiretrovirals: a current global status and future perspectives, Water Res 145 (2018) 231–247, https://doi.org/10.1016/j.watres.2018.08.017.

[14] J.L. Tambosi, L.Y. Yamanaka, H.J. José, R.d.F.P.M. Moreira, H.F. Schröder, Recent research data on the removal of pharmaceuticals from sewage treatment plants (STP), Quím. Nova 33 (2010) 411–420, https://doi.org/10.1590/S0100-40422010000200032.

[15] B. Halling-Sørensen, S. Nors Nielsen, P.F. Lanzky, F. Ingerslev, H.C. Holten Lützhøft, S.E. Jørgensen, Occurrence, fate and effects of pharmaceutical substances in the environment- a review, Chemosphere 36 (1998) 357–393, https://doi.org/10.1016/S0045-6535(97)00354-8.

[16] G. Kumari, R.K. Singh, Highly active antiretroviral therapy for treatment of HIV/AIDS patients: current status and future prospects and the Indian scenario, HIV & AIDS Rev. 11 (2012) 5–14, https://doi.org/10.1016/j.hivar.2012.02.003.

[17] C. Schoeman, M. Dlamini, O.J. Okonkwo, The impact of a wastewater treatment works in southern Gauteng, South Africa on efavirenz and nevirapine discharges into the aquatic environment, Emerg. Contam. 3 (2017) 95–106, https://doi.org/10.1016/j.emcon.2017.09.001.

[18] K.O. K'Oreje, L. Vergeynst, D. Ombaka, P. De Wispelaere, M. Okoth, H. Van Langenhove, K. Demeestere, Occurrence patterns of pharmaceutical residues in wastewater, surface water and groundwater of Nairobi and Kisumu city, Kenya, Chemosphere 149 (2016) 238–244, https://doi.org/10.1016/j.chemosphere.2016.01.095.

[19] S.-J. Zou, Y.-F. Chen, Y. Zhang, X.-F. Wang, N. You, H.-T. Fan, A hybrid sorbent of α-iron oxide/reduced graphene oxide: studies for adsorptive removal of tetracycline antibiotics, J. Alloys Compd. 863 (2021), 158475.

[20] Y.-X. Song, S. Chen, N. You, H.-T. Fan, L.-N. Sun, Nanocomposites of zero-valent iron@activated carbon derived from corn stalk for adsorptive removal of tetracycline antibiotics, Chemosphere 255 (2020), 126917.

[21] S.-J. Zou, B.-H. Ding, Y.-F. Chen, H.-T. Fan, Nanocomposites of graphene and zirconia for adsorption of organic-arsenic drugs: performances comparison and analysis of adsorption behavior, Environ. Res. 195 (2021), 110752.

[22] A.O. Adeola, P.B.C. Forbes, Advances in water treatment technologies for removal of polycyclic aromatic hydrocarbons: existing concepts, emerging trends, and future prospects, Water Environ. Res. 93 (3) (2021) 343–359, https://doi.org/10.1002/wer.1420.

[23] N. You, X.-F. Wang, J.-Y. Li, H.-T. Fan, H. Shen, Q. Zhang, Synergistic removal of arsanilic acid using adsorption and magnetic separation technique based on Fe_3O_4@graphene nanocomposite, J. Indust. Eng. Chem. 70 (2019) 346–354.

[24] D. Balarak, G. McKay, Utilization of MWCNTs/Al2O3 as adsorbent for ciprofloxacin removal: equilibrium, kinetics and thermodynamic studies, J. Environ. Sci. Health A. 56 (3) (2021) 324–333, https://doi.org/10.1080/10934529.2021.1873674.

[25] PubChem, Bethesda (MD): National Library of Medicine (US), National Center For Biotechnology Information, PubChem Compound Summary for CID, 2004, p. 4463. Nevirapine; [cited 2020 Aug. 10]. Available from: https://pubchem.ncbi.nlm.nih.gov/compound/Nevirapine.

[26] PubChem, Bethesda (MD): National Library of Medicine (US), National Center For Biotechnology Information, PubChem Compound Summary for CID, 2004, p. 64139. Efavirenz; [cited 2020 Aug. 10]. Available from: https://pubchem.ncbi.nlm.nih.gov/compound/Efavirenz.

[27] G.-.L. Schoonraad, M.J. Madito, N. Manyala, P. Forbes, Synthesis and optimisation of a novel graphene wool material by atmospheric pressure chemical vapour deposition, J. Mater. Sci. 55 (2020) 545–564, https://doi.org/10.1007/s10853-019-03948-0.

[28] Gaussian 16, Revision C.01, M. J. Frisch, G. W. Trucks, H. B. Schlegel, G. E. Scuseria, M. A. Robb, J. R. Cheeseman, G. Scalmani, V. Barone, G. A. Petersson, H. Nakatsuji, X. Li, M. Caricato, A. V. Marenich, J. Bloino, B. G. Janesko, R. Gomperts, B. Mennucci, H. P. Hratchian, J. V. Ortiz, A. F. Izmaylov, J. L. Sonnenberg, D. Williams-Young, F. Ding, F. Lipparini, F. Egidi, J. Goings, B. Peng, A. Petrone, T. Henderson, D. Ranasinghe, V. G. Zakrzewski, J. Gao, N. Rega, G. Zheng, W. Liang, M. Hada, M. Ehara, K. Toyota, R. Fukuda, J. Hasegawa, M. Ishida, T. Nakajima, Y. Honda, O. Kitao, H. Nakai, T. Vreven, K. Throssell, J. A. Montgomery, Jr., J. E. Peralta, F. Ogliaro, M. J. Bearpark, J. J. Heyd, E. N. Brothers, K. N. Kudin, V. N. Staroverov, T. A. Keith, R. Kobayashi, J. Normand, K. Raghavachari, A. P. Rendell, J. C. Burant, S. S. Iyengar, J. Tomasi, M. Cossi, J. M. Millam, M. Klene, C. Adamo, R. Cammi, J. W. Ochterski, R. L. Martin, K. Morokuma, O. Farkas, J. B. Foresman, and D. J. Fox, Gaussian, Inc., Wallingford CT, 2016.

[29] J.H. de Lange, I. Cukrowski, Toward deformation densities for intramolecular interactions without radical reference states using the fragment, atom, localized, delocalized and interatomic (FALDI) charge density decomposition scheme, J. Comput. Chem. 38 (2017) 981–997, https://doi.org/10.1002/jcc.24772.

[30] J.H. de Lange, I. Cukrowski, Exact and exclusive electron localization indices within QTAIM atomic basins, J. Comput. Chem. 39 (2018) 1517–1530, https://doi.org/10.1002/jcc.25223.

[31] R.F. Bader, Atoms in Molecules, Wiley Online Library, 2020.

[32] AIMAll (Version 19.10.12), Todd A. Keith, TK Gristmill software, Overland Park KS, USA, 2019 (aim.tkgristmill.com).

[33] W. Humphrey, A. Dalke, K. Schulten, VMD: visual molecular dynamics, J. Mol. Graph. 14 (1996) 33–38, https://doi.org/10.1016/0263-7855(96)00018-5.

[34] G.A. Haghighat, M.H. Saghi, I. Anastopoulos, A. Javid, A. Roudbari, S.S. Talebi, S. K. Ghadiri, D.A. Giannakoudakis, M. Shams, Aminated graphitic carbon derived from corn stover biomass as adsorbent against antibiotic tetracycline: optimizing the physicochemical parameters, J. Mol. Liq. 313 (2020), 113523, https://doi.org/10.1016/j.molliq.2020.113523.

[35] F.T. Johra, J.-.W. Lee, W.-.G. Jung, Facile and safe graphene preparation on solution based platform, J. Ind. Eng. Chem. 20 (2014) 2883–2887, https://doi.org/10.1016/j.jiec.2013.11.022.

[36] M.V. Khedkar, S.B. Somvanshi, A.V. Humbe, K.M. Jadhav, Surface modified sodium silicate based superhydrophobic silica aerogels prepared via ambient pressure drying process, J. Non-Cryst. Solids 511 (2019) 140–146, https://doi.org/10.1016/j.jnoncrysol.2019.02.004.

[37] J. Chen, W. Chen, D. Zhu, Adsorption of nonionic aromatic compounds to single-walled carbon nanotubes: effects of aqueous solution chemistry, Environ. Sci. Technol. 42 (2008) 7225–7230, https://doi.org/10.1021/es801412j.

[38] Y. Huang, J. Tang, L. Gai, Y. Gong, H. Guan, R. He, H. Lyu, Different approaches for preparing a novel thiol-functionalized graphene oxide/Fe-Mn and its application

for aqueous methylmercury removal, Chem. Eng. J. 319 (2017) 229–239, https://doi.org/10.1016/j.cej.2017.03.015.
[39] A.A. Mirghni, K.O. Oyedotun, B.A. Mahmoud, A. Bello, S.C. Ray, N. Manyala, Nickel-cobalt phosphate/graphene foam as enhanced electrode for hybrid supercapacitor, Compos. B. Eng. 174 (2019), 106953, https://doi.org/10.1016/j.compositesb.2019.106953.
[40] E.T. Anthony, M.O. Ojemaye, A.I. Okoh, O.O. Okoh, Synthesis of CeO2 as promising adsorbent for the management of free-DNA harboring antibiotic resistance genes from tap-water, Chem. Eng. J. 401 (2020), 125562, https://doi.org/10.1016/j.cej.2020.125562.
[41] A.O. Adeola, P.B.C. Forbes, Optimization of the sorption of selected polycyclic aromatic hydrocarbons by regenerable graphene wool, Water Sci. Technol. 80 (2019) 1931–1943, https://doi.org/10.2166/wst.2020.011.
[42] W.J. Weber, E.H. Smith, Simulation and design models for adsorption processes, Environ. Sci. Technol. 21 (1987) 1040–1050, https://doi.org/10.1021/es00164a002.
[43] F. Yu, J. Ma, D. Bi, Enhanced adsorptive removal of selected pharmaceutical antibiotics from aqueous solution by activated graphene, Environ. Sci. Pollut. Res. 22 (2015) 4715–4724, https://doi.org/10.1007/s11356-014-3723-9.
[44] E.E. Jasper, V.O. Ajibola, J.C. Onwuka, Nonlinear regression analysis of the sorption of crystal violet and methylene blue from aqueous solutions onto an agro-waste derived activated carbon, Appl. Water Sci. 10 (2020) 132, https://doi.org/10.1007/s13201-020-01218-y.
[45] K.Y. Foo, B.H. Hameed, Insights into the modeling of adsorption isotherm systems, Chem. Eng. J. 156 (2010) 2–10, https://doi.org/10.1016/j.cej.2009.09.013.
[46] B. Nagy, C. Mânzatu, A. Măicăneanu, C. Indolean, L. Barbu-Tudoran, C. Majdik, Linear and nonlinear regression analysis for heavy metals removal using Agaricus bisporus macrofungus, Arab. J. Chem. 10 (2017) S3569–S3579, https://doi.org/10.1016/j.arabjc.2014.03.004.
[47] X.-J. Zhao, H. Hou, X.-T. Fan, Y. Wang, Y.-M. Liu, C. Tang, S.-H. Liu, P.-P. Ding, J. Cheng, D.-H. Lin, C. Wang, Y. Yang, Y.-Z. Tan, Molecular bilayer graphene, Nat. Commun. 10 (2019) 3057, https://doi.org/10.1038/s41467-019-11098-9.
[48] V. Georgakilas, J.N. Tiwari, K.C. Kemp, J.A. Perman, A.B. Bourlinos, K.S. Kim, R. Zboril, Noncovalent functionalization of graphene and graphene oxide for energy materials, biosensing, catalytic, and biomedical Applications, Chem. Rev. 116 (2016) 5464–5519, https://doi.org/10.1021/acs.chemrev.5b00620.
[49] D. Hao, Y.-X. Song, Y. Zhang, H.-T. Fan, Nanocomposites of reduced graphene oxide with pure monoclinic-ZrO_2 and pure tetragonal-ZrO_2 for selective adsorptive removal of oxytetracycline, Appl. Surf. Sci. 543 (2021), 148810.
[50] A.R.D. Verliefde, E.R. Cornelissen, S.G.J. Heijman, J.Q.J.C. Verberk, G.L. Amy, B. Van der Bruggen, J.C. van Dijk, The role of electrostatic interactions on the rejection of organic solutes in aqueous solutions with nanofiltration, J. Membr. Sci. 322 (2008) 52–66, https://doi.org/10.1016/j.memsci.2008.05.022.
[51] A.O. Adeola, P.B.C. Forbes, Influence of natural organic matter fractions on PAH sorption by stream sediments and a synthetic graphene wool adsorbent, Environ. Technol. Innovat. 21 (2021), 101202, https://doi.org/10.1016/j.eti.2020.101202.
[52] J. Li, C. Chen, S. Zhang, X. Ren, X. Tan, X. Wang, Critical evaluation of adsorption–desorption hysteresis of heavy metal ions from carbon nanotubes: influence of wall number and surface functionalization, Chem. Asian J. 9 (2014) 1144–1151, https://doi.org/10.1002/asia.201301475.
[53] C. Tesseromatis, A. Alevizou, The role of the protein-binding on the mode of drug action as well the interactions with other drugs, Eur. J. Drug Metab. Ph. 33 (2008) 225–230, https://doi.org/10.1007/BF03190876.
[54] Y. Zhang, Z. Shen, C. Dai, X. Zhou, Removal of selected pharmaceuticals from aqueous solution using magnetic chitosan: sorption behavior and mechanism, Environ. Sci. Pollut. Res. 21 (2014) 12780–12789, https://doi.org/10.1007/s11356-014-3212-1.
[55] T.J. Al-Musawi, A.H. Mahvi, A.D. Khatibi, D. Balarak, Effective adsorption of ciprofloxacin antibiotic using powdered activated carbon magnetized by iron(III) oxide magnetic nanoparticles, J. Porous Mater. 28 (2021) 835–852, https://doi.org/10.1007/s10934-021-01039-7.
[56] Y. Liu, Is the free energy change of adsorption correctly calculated? J. Chem. Eng. Data 54 (2009) 1981–1985.
[57] L. Wang, C. Shi, L. Wang, L. Pan, X. Zhang, J.-J. Zou, Rational design, synthesis, adsorption principles and applications of metal oxide adsorbents: a review, Nanoscale 12 (2020) 4790–4815, https://doi.org/10.1039/C9NR09274A.

Chapter 8 Development of Graphene wool doped with silver nanoparticles for adsorption of selected PAH and antibacterial activity against drug-resistant bacteria

In this chapter, graphene wool was doped with lipopeptide-stabilized silver nanoparticles and characterized. This composite was applied to remove benzo(a)pyrene (often regarded as most carcinogenic PAH) from water. Given the background information on the antimicrobial property of AgNPs, the antibacterial activity of this composite was evaluated against selected Gram-positive and Gram-negative bacteria and optimum dosage was established. Thus, this chapter evaluates the potential for dual application of the composite as an adsorbent and antibacterial agent. This chapter is presented as it was published in Applied Water Science (Springer).

Article

Adeola, A.O., Kubheka, G., Chirwa, E.M.N., Forbes, P.B.C. (2021). Facile synthesis of graphene wool doped with oleylamine-capped silver nanoparticles (GW-αAgNPs) for water treatment applications, 11(11), 172.

DOI: http://dx.doi.org/10.1007/s13201-021-01493-3

Applied Water Science (2021) 11:172
https://doi.org/10.1007/s13201-021-01493-3

ORIGINAL ARTICLE

Facile synthesis of graphene wool doped with oleylamine-capped silver nanoparticles (GW-αAgNPs) for water treatment applications

Adedapo O. Adeola[1] · Gugu Kubheka[1] · Evans M. N. Chirwa[2] · Patricia B. C. Forbes[1]

Received: 27 July 2021 / Accepted: 6 September 2021

Abstract
The facile synthesis of graphene wool doped with oleylamine-capped silver nanoparticles (GW-αAgNP) was achieved in this study. The effect of concentration, pH, temperature and natural organic matter (NOM) on the adsorption of a human carcinogen (benzo(a)pyrene, BaP) was evaluated using the doped graphene wool adsorbent. Furthermore, the antibacterial potential of GW-αAgNP against selected drug-resistant Gram-negative and Gram-positive bacteria strains was evaluated. Isotherm data revealed that adsorption of BaP by GW-αAgNP was best described by a multilayer adsorption mechanism predicted by Freundlich model with least ERRSQ < 0.79. The doping of graphene wool with hydrophobic AgNPs coated with functional moieties significantly increased the maximum adsorption capacity of GW-αAgNP over GW based on the q_{max} and q_m predicted by Langmuir and Sips models. π-π interactions contributed to sorbent-sorbate interaction, due to the presence of delocalized electrons. GW-αAgNP-BaP interaction is a spontaneous exothermic process (negative $\Delta H°$ and ΔG), with better removal efficiency in the absence of natural organic matter (NOM). While GW is more feasible with higher maximum adsorption capacity (q_m) at elevated temperatures, GW-αAgNP adsorption capacity and efficiency is best at ambient temperature, in the absence of natural organic matter (NOM), and preferable in terms of energy demands and process economics. GW-αAgNP significantly inhibited the growth of Gram-negative *Pseudomonas aeruginosa* and Gram-positive *Bacillus subtilis* strains, at 1000 mg/L dosage in preliminary tests, which provides the rationale for future evaluation of this hybrid material as a smart solution to chemical and microbiological water pollution.

Keywords Adsorption · Antimicrobial property · Graphene wool composite · Silver nanoparticles · Water treatment

Introduction

Benzo(a)pyrene (BaP) is regarded as one of the most hazardous environmental pollutants exhibiting both genotoxic and carcinogenic toxicity in humans according to the International Agency for Research on Cancer (IARC) (IARC 2010; Hardonnière et al. 2016). BaP belongs to the group of ubiquitous emerging chemical pollutants (ECPs) known as polycyclic aromatic hydrocarbons (PAHs) (Adeola & Forbes 2020; Munyeza et al. 2020). BaP is persistent in the environment and poses health risk due to its recalcitrance to biodegradation (Yerushalmi et al. 2006). The maximum acceptable concentration (MAC) of PAHs in surface water is 0.01 µg/L; however, several reports suggest that BaP levels detected in South Africa are higher than the MAC value, thus posing a potential health risk (Adeniji et al. 2019).

Furthermore, the adaptive resistance of several bacteria to antibiotics, such as chloramphenicol, penicillin, etc., has led to the interesting discovery that silver nanoparticles can inhibit microbial growth and may be lethal against drug-resistant bacteria (Anthony et al. 2014; McBirney et al. 2016; Huang et al. 2017). Advances in research into a hybrid approach to environmental protection and remediation have brought about the need for the development of "smart" materials/composites with multifunctional capabilities for improved efficiency and process economics (Bezza and Chirwa 2016; Miren et al. 2018; Adeola & Forbes 2021b). Several materials with antimicrobial properties have been developed for the removal of pollutants in aqueous matrices,

✉ Patricia B. C. Forbes
patricia.forbes@up.ac.za

[1] Department of Chemistry, Faculty of Natural and Agricultural Sciences, University of Pretoria, Lynnwood Road, Hatfield, Pretoria 0002, South Africa

[2] Water Utilisation and Environmental Engineering Division, Department of Chemical Engineering, University of Pretoria, Lynnwood Road, Hatfield, Pretoria 0002, South Africa

Published online: 08 October 2021

examples of such materials are polyanilineTi(IV)arsenophosphate (Bushra et al. 2014), iron and manganese coated silica gel (Ahmad et al. 2015), chitosan doped with silver nanoparticles (Ishihara et al. 2015), nano-silver-supported activated carbon (Eltugral et al. 2016), graphene foam/TiO_2 nanosheet hybrids (Wang et al. 2017), iron nanoparticles (Da'na et al. 2018), silk fiber doped with tannic acid (Zhang et al. 2019), antimicrobial polymer (Li et al. 2020) chitosan/nitrogen-doped graphene quantum dots (Amari et al. 2021), etc. The design of composites has reportedly enhanced physicochemical properties of adsorbents such as specific surface area, stability, conductivity, tensile strength, chemical robustness, charge mobility, flexibility, thin-film thickness, and provided a basis for the growing interest in the utilization of composites for water treatment applications (Adeola & Forbes 2021b).

A comprehensive risk-based assessment of graphene-based composites is currently unavailable; however, it is assumed that the composites may not pose a significant health risk based on their composition, but their lightweight nature may pose inhalation risks (Schinwald et al. 2012). Thus, the physical structure of the graphene-based material and the fabrication method is critical. With respect to graphene wool doped with oleylamine-capped silver nanoparticles (GW-αAgNPs), the quartz wool substrate acts as a solid support, assisting with immobilization of the graphene and silver nanoparticles. Furthermore, unlike most composites generated in the form of flakes and powder, GW-αAgNPs presents a wool-like form that may be more suitable as a packing material for filters and other water polishing tools.

The overall aim of this study was to synthesize a composite of graphene wool and silver nanoparticles (GW-αAgNPs) with antibacterial activity, for the removal of a human carcinogen, namely benzo(a)pyrene, from polluted water. The influence of process variables such as pH, temperature, and initial concentration of BaP on the sorption mechanism was established for optimum efficiency of the composite. Furthermore, the antibacterial activity of the composite was tested and is discussed briefly for potential dual application toward water treatment.

Experimental methods

Chemicals

Neat standard (98% purity) of benzo(a)pyrene (BaP) was purchased from Supelco (USA). Sodium azide (NaN_3), silver nitrate ($AgNO_3$, 99.9%), oleic acid (99%), oleylamine (99%), phenyl ether (99%), and Tryptic Soybean Broth (TSB) were purchased from Sigma-Aldrich (Germany). Nitric acid (HNO_3), hydrochloric acid (HCl), sodium chloride (NaCl), sodium hydroxide (NaOH), ethanol (EtOH), hexane, and calcium chloride ($CaCl_2$) were purchased from Associated Chemical Enterprises (ACE, Johannesburg, South Africa). 9–30 µm coarse quartz wool (Arcos Organics, New Jersey, USA), argon, and hydrogen (99.999%, Afrox, South Africa) were purchased for GW synthesis. Sterile syringe filters (33 mm diameter) with a 0.22 µm pore size containing a hydrophilic polyethersulfone (PES) membrane were purchased from Merck (Darmstadt, Germany). The antibacterial tests were carried out using model Gram-negative *Pseudomonas aeruginosa* CB1 and Gram-positive *Bacillus subtilis* CN2 bacterial strains that had been previously isolated and deposited in the GenBank database under the accession numbers KP793922 and KP7939228, respectively (Bezza and Chirwa 2016). All the solutions were prepared with de-ionized water (DI, 9.2 µS/cm^3) obtained from a Milli-Q water purification system (Millipore, Bedford, MA, USA).

Facile synthesis of GW-αAgNPs

Graphene wool was synthesized using the chemical vapor deposition method on a quartz wool substrate whereby an optimized stream of argon, hydrogen, and methane gas was temperature ramped to 1200 °C as previously described (Adeola & Forbes 2019, 2020; Schoonraad et al. 2020). Lipopeptide-coated silver nanoparticles were synthesized in phenyl ether with oleylamine and oleic acid as both reducing agents and capping agents (Liu et al. 2011; Sha et al. 2011; Çınar et al. 2011).

The composite was prepared as follows: Briefly, GW (200 mg) and DI water (100 mL) were added into a sealed bottle (250 mL) and stirred gently for 1 h using a magnetic stirrer, before the addition of the dopant mixture. Ag nanoparticles (300 mg) dispersed in diphenyl ether (100 mL) were added into the GW solution and stirred for 12 h at room temperature under argon, to ensure that AgNPs coordinated with graphene wool at the water/diphenyl ether interface. The GW–αAgNP composite was rinsed with acetone and centrifuged at 6000 rpm for 10 min, three times consecutively. The obtained GW–αAgNP composites were then washed with hexane to remove residual oleylamine. The final GW–αAgNP composite was freeze-dried for 48 h. The facile synthesis is illustrated in Scheme 1.

Characterization of the synthesized adsorbent

The morphology of GW and GW-αAgNPs was examined by a combination of techniques including scanning electron microscopy (SEM), with images obtained from a Zeiss Ultra-Plus 55 field emission scanning electron microscope (FE-SEM), operated at 2.0 kV (Zeiss, Germany). High-resolution transmission electron microscopy (TEM) images of capped-AgNPs and GW-αAgNPs were taken using a JEOL

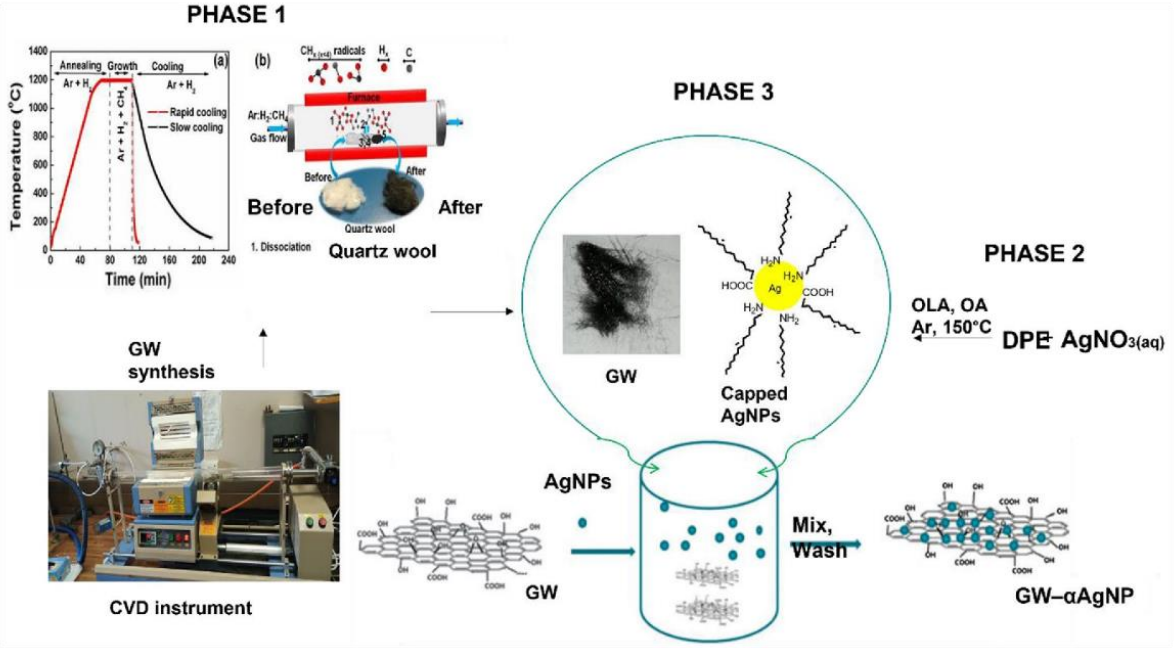

Scheme 1 Illustration of the synthetic route to graphene wool-silver nanoparticles composite

JEM 2100F (JOEL Ltd, Tokyo, Japan) operated at 200 kV and equipped with an energy dispersive X-ray spectrometer (EDS) (OXFORD Link-ISIS-300 Zeiss, Germany). The specific surface area (SSA) of GW was determined using the modified Sears' method (Sears 1956; Adeola & Forbes 2019). FTIR spectra of GW, capped AgNPs and GW-αAgNPs were obtained using a Bruker Alpha-T spectrometer (Bruker Optik GmbH, Ettlingen, Germany). Elemental analysis of natural organic matter (NOM) was examined using inductively coupled plasma-optical emission spectrometry (ICP-OES, Spectro Arcos model, Thermo Fisher Scientific, South Africa). The conductivity of the background electrolyte was confirmed using an Orion Star A112 conductivity benchtop meter (Thermo Scientific, South Africa), and pH was monitored using a 780-pH meter (Metrohm Herisau, Switzerland).

Sorption isotherm experiments

Batch adsorption experiments of BaP onto GW and GW-αAgNPs were carried out in 40 mL PTFE screw cap amber vials (Stargate Scientific, South Africa) at 25 ± 1 °C in a thermostated shaking water bath (Wisebath, Celsius Scientific, South Africa). Background electrolyte (pH = 7.0) contained 0.01 mol/L $CaCl_2$ (ACE, South Africa) in DI water with 200 mg/L of sodium azide (Sigma-Aldrich, Germany) as a biocide. The isotherm experiment was conducted with initial concentrations of the BaP solutions ranging from 100 µg/L to 500 µg/L. The BaP desorption isotherm was examined by the addition of 5 mL fresh electrolyte with equilibration for 24 h, after decanting the adsorption supernatant as previously described (Wang et al. 2008; Adeola & Forbes 2021a). Adsorption isotherms of BaP were also performed at varying temperatures of 25, 35, and 45 °C using a thermostated shaking water bath (Wisebath, Celsius Scientific, South Africa) to determine adsorption thermodynamics. The role of solution pH was evaluated by pH adjustment with 0.1 M HCl (Merck, South Africa) or NaOH (ACE, South Africa) over the pH range from 2 to 12, to elucidate the pH effect on the removal of BaP from aqueous solution.

Quantification

After equilibration, centrifugation of the vials was performed at 6000 rpm for 10 min to recover a clear supernatant. BaP concentrations were analyzed in triplicate (n = 3) by fluorescence spectroscopy (Horiba Jobin Yvon Fluoromax-4 spectrofluorometer). For all fluorescence measurements, the excitation and quantification emission wavelengths were at 330 and 464 nm, while the excitation and emission slit widths were set at 5 nm. The regression coefficient (R^2) of the calibration curve was obtained from working solutions in the range of 100 µg/L to 500 µg/L of BaP and blanks were included for both calibration and sorption

experiments. The equilibrium concentration (C_e, µg/L) was deduced from the calibration equation. The amount of solute adsorbed (q_e, µg/g) was extrapolated using a mass-balance equation (***Eq. 1***) and removal efficiency was estimated using ***Eq. 2***:

$$q_e = \frac{(C_0 - C_e)V_0}{S_m} \quad (1)$$

where C_o (µg/L) is the initial concentration, C_e (µg/L) is the equilibrium solute concentration, V_o is the initial volume (L) and S_m is the mass (g) of the adsorbent.

$$Removal\ efficiency(\%) = \frac{(C_0 - C_e)}{C_0} \times 100 \quad (2)$$

Antibacterial test of GW- αAgNPs

Sterilization of all glassware and media was carried out in an autoclave at 121 °C for 15 min. A facile test was conducted of bacteria inhibition of GW-αAgNP against model Gram-negative and Gram-positive bacteria strains (*Pseudomonas aeruginosa* CB1 and *Bacillus subtilis* CN2) previously isolated in our laboratory (Bezza et al., 2020). The inocula of *P. aeruginosa* and *B. subtilis* were cultured overnight in Tryptic Soybean Broth (TSB) under aerobic conditions at 37 °C. The inhibitory concentration of the composite against visible growth of *P. aeruginosa* and *B. subtilis* after 24 h of incubation at 37 °C was investigated. Concentrations ranging from 0–1000 mg/L of GW-αAgNP were prepared in sterilized conical flasks containing 100 mL TSB. Thereafter each flask was inoculated with 10 µL of the cultured inoculum. Optical density measurements were taken after the incubation period. Experiments were conducted in duplicate and controls containing nutrient broth inoculated with inoculum without the inclusion of GW-αAgNPs. Bacteria concentration was estimated in relation to absorbance/optical density at 600 nm (OD_{600}) using a UV/Vis spectrophotometer (Shimadzu UV-1800, Labotec, South Africa) and corrected by subtracting the background absorbance of the control (Anthony et al. 2014; Bezza et al. 2020).

Results and discussion

Adsorbent characterization

The morphology of the synthesized composite was examined using SEM and TEM (Fig. 1a and b). The high-resolution images revealed a heterogeneous surface structure with extensive coverage of GW with AgNPs. The oleylamine-capped AgNPs were analyzed with TEM prior to conjugation with GW, and spherical particles with a mean diameter of 12.67 ± 3.9 nm were estimated via particle size analysis using the ImageJ software (Fig. 1b and d). Qualitative analysis of GW-αAgNP using EDS confirmed the presence and relative abundance of silver and carbon (Fig. 1c). FTIR (Fig. 1e and f) revealed two prominent peaks associated with the sp^2 hybridized C=C backbone of graphene and a broad peak of Si–O-C of functionalized quartz wool (SiO_2) coated with graphene at 775 and 1059 cm^{-1}, respectively (Adeola & Forbes 2020). Bands at 2921, 2856, 1631, 1450 cm^{-1} regions arising from C–H, C=O, C–N stretching vibrations were observed in GW-αAgNP, respectively (Fig. 1e). Figure 1f revealed that several functional groups enhanced the stability of AgNPs and facilitated coordination with GW (Jyoti et al. 2016). The bands at 3325, 2921, 2856, 1743, 1631, 1450, 1377, 1240, 1043 and 460 cm^{-1} correspond to N–H, C–H, C–C, C=O, C–N, C=N, and Ag–O stretching, respectively, indicating the presence of oleylamine/oleic acid as the capping agent of silver nanoparticles (Mojahed et al. 2011; Prakash et al. 2013; Tran & Jeong 2015).

Sorption isotherm experiments

Adsorption isotherm models are used to investigate the nature of sorbent-sorbate interactions of adsorption (Wang et al. 2018; Zhang et al. 2019; Adeola & Forbes 2021a). Linear regression and nonlinear isotherm models such as Linear (Eq. 3), Freundlich (Eq. 4), Langmuir (Eq. 5), and Sips model (Eq. 6) were used to fit adsorption experimental data. The Error Sum of Squares (ERRSQ) (Eq. 7) was used to test all models used in this study.

$$q_e = K_d C_e \quad (3)$$

$$q_e = K_F C_e^N \quad (4)$$

$$q_e = \frac{q_{max} K_L C_e}{1 + K_L C_e} \quad (5)$$

$$q_e = \frac{q_m K_s C_e^{ms}}{1 + K_s . C_e^{ms}} \quad (6)$$

$$\sum_{i=1}^{n} (q_{e,cal} - q_{e,\,exp})_i^2 \quad (7)$$

where K_F (mg/g) $(L/mg)^N$) and N (dimensionless) is the Freundlich constant and intensity parameter, an indicator of site energy heterogeneity; q_{max} (mg/g) and K_L (L/mg) are the Langmuir maximum adsorption capacity and Langmuir constant associated with solute–surface interaction energy, respectively; K_s (L/mg) and q_{max} (mg/g) are Sips isotherm model constants and maximum adsorption capacity and ms is Sips isotherm exponent; q_e is the solid-phase

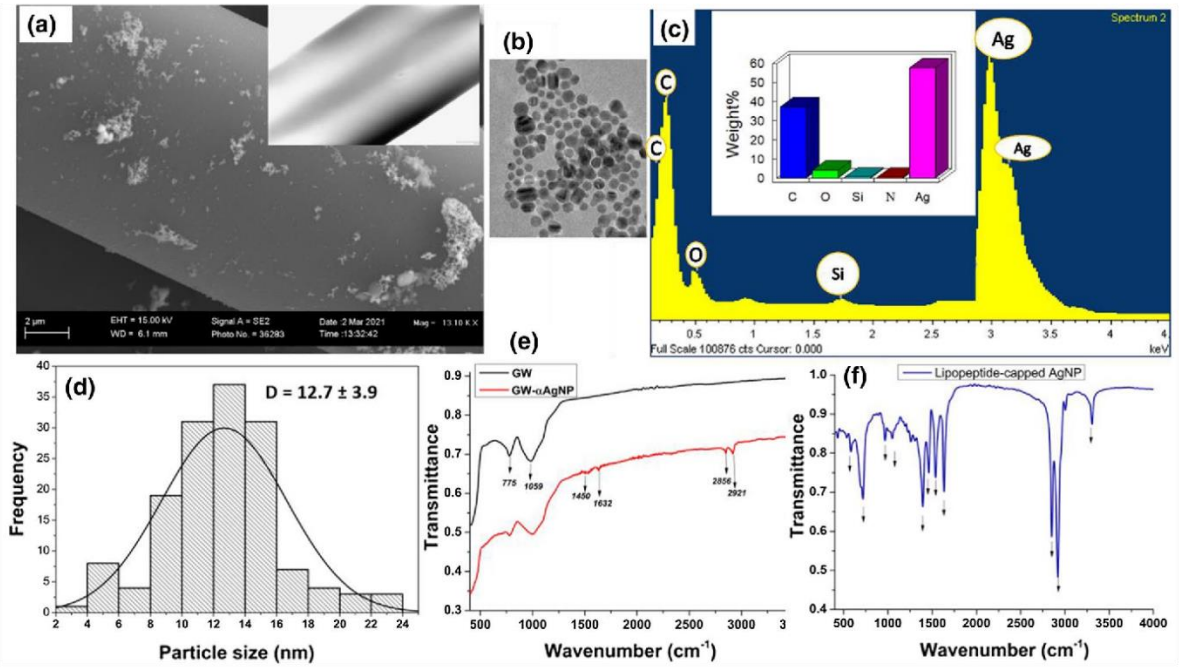

Fig. 1 Characterization of GW-αAgNP composite, **a** SEM image of GW-αAgNP (2 µm scale) (inset: TEM image of GW (200 nm scale)), **b** TEM image of oleylamine-capped AgNPs prior to doping experiment (50 nm scale), **c** EDS spectrum of GW-αAgNP (inset: Relative abundance of constituent element obtained from EDS site mapping), **d** Particle size distribution of capped AgNPs with estimated diameter, **e** and **f** FTIR spectra of GW, GW-αAgNP and oleylamine-capped AgNP

concentration (mg/g), C_e is the liquid phase equilibrium concentration (mg/L), and K_d (L/g) is the sorption distribution coefficient (Ololade et al. 2018; Adeola & Forbes 2019).

The isotherm regression parameters for Freundlich, Langmuir, Linear, and Sips model are presented in Table 1 and Fig. 2. The hysteresis index (H) which is a measure of the irreversibility of the sorption process was calculated for doped graphene wool and pristine graphene wool (Table 1). Isotherm data for GW-αAgNP adsorption of BaP was best described by a multilayer adsorption mechanism predicted by the Freundlich model with least ERRSQ < 0.79, while BaP adsorption onto GW was best fitted to the Sips model

Table 1 Sorption–desorption parameters for adsorption of BaP onto GW-αAgNP and GW (desorption hysteresis index (H) derived from Freundlich isotherm model)

Sorption models	Adsorption parameters			Desorption parameters		
		GW-αAgNP	GW		GW-αAgNP	GW
Freundlich	$K_{f\,(ads)}$	1.12e3	0.60e2	$K_{f\,(des)}$	0.55e2	0.21e2
	$N_{\,(ads)}$	3.13	0.1	$N_{\,(des)}$	0.1	0.01
	SSE	0.78	2.50	*H-index	31.3	10.0
Langmuir	q_{max} (µg/g)	13.67e3	0.59e2			
	K_L (L/µg)	2.01e-4	6.67e4			
	SSE	2.03	1.88			
Linear	K_d	2.75	0.93			
	SSE	1.58	2.45			
Sips	K_s	3.36	2.38			
	q_m (µg/g)	97.62	59.76			
	m_s	9.68	6.05			
	SSE	2.03	1.87			

*H: Sorption–desorption hysteresis index, $H = N_{ads}/N_{des}$

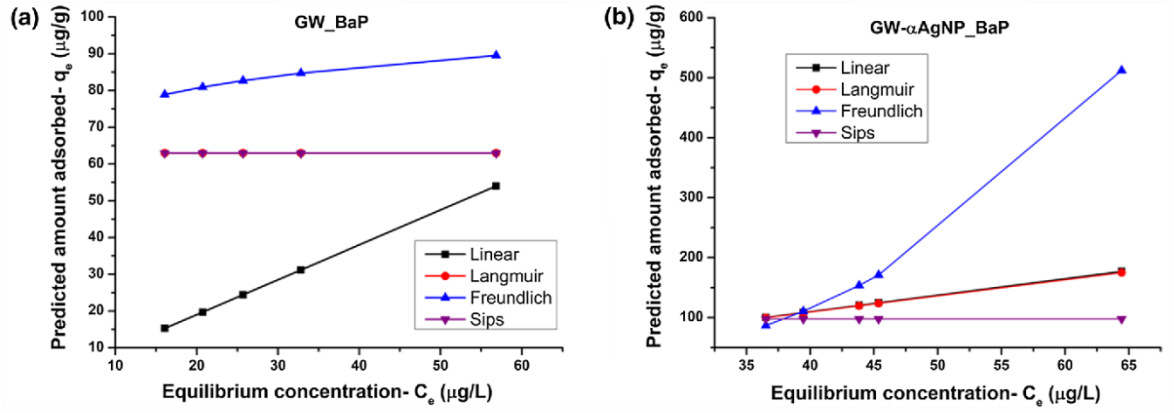

Fig. 2 Adsorption isotherm model plots for the interaction between sorbate and sorbents **a** GW and BaP **b** doped GW-αAgNP and BaP. (Experimental conditions: C_o = 100–500 µg/L; dosage = 5 mg per 5 mL, mixing rate = 200 rpm, T = 25 ± 1 °C, contact time: 24 h)

(Langmuir–Freundlich hybrid) with ERRSQ < 1.88, respectively (Table 1). These findings are consistent with previous results obtained from the adsorption of phenanthrene and pyrene onto pristine graphene wool (Adeola & Forbes 2019). The doping of graphene wool with hydrophobic AgNPs coated with organic functional moieties significantly increased the maximum adsorption capacity of GW-αAgNP over GW based on the q_{max} & q_m predicted by Langmuir and Sips models, respectively (Table 1). BaP is a hydrophobic PAH with a high octanol–water partition coefficient logK_{ow} of 6.13 (Adeola & Forbes 2020), and several reports suggest a strong affinity between PAHs and hydrophobic surfaces of adsorbents (Khan et al. 2007; Lamichhane et al. 2016; Yakout & Daifullah 2013; Yuan et al. 2018). π-π interactions between the graphene wool composite and the aromatic structure of BaP, due to the presence of delocalized electrons, also contributes to the adsorption process (Zhao et al. 2011; Zhang et al. 2013; Yang et al. 2015; Adeola & Forbes 2019).

Furthermore, oleylamine and oleic acid used as capping agents as well as the linker between GW and AgNP are large hydrophobic organic molecules that may have improved the surface hydrophobicity of the composite. Thus, this may in turn enhance partitioning (mass transfer) of hydrophobic BaP onto the surface of the composite, leading to enhanced adsorption capacity (K_d and q_{max}). The doping of graphene with oleylamine-capped AgNPs accounts for the comparatively high surface and adsorption heterogeneity (N & m_s) index (Table 1). It is evident that adsorption–desorption interactions between sorbate and sorbents displayed a significant degree of hysteresis, as calculated *H-index* values for both sorbates were greater than 1 ($N_{ads} > > > N_{des}$) (Table 1) (Ololade et al. 2018; Adeola & Forbes 2021a). However, irreversible entrapment and/or slow rate of desorption of sorbed BaP was three-fold higher in GW-αAgNP than pristine GW, further confirming higher binding strength with BaP. Pore deformation and alteration of the surface structure of sorbents via build-up in unrelaxed pore volume also cause hysteretic behavior in sorption processes (Nguyen et al. 2004; Cornelissen et al. 2005). Therefore, the high hysteretic behavior of GW-αAgNP, which exemplifies better retention of BaP against recontamination of treated water, maybe due to entrapment of solutes by the collapse of the GW- αAgNP composite structure due to the adsorption process conditions and agitation.

Comparison of adsorbents reported for benzo(a)pyrene removal

Table 2 reveals that graphene wool (GW) and doped graphene wool (GW-αAgNP) competes favorably with other adsorbents reported in the literature for the removal of benzo(a)pyrene from aqueous solutions, with efficiency >94%. The maximum adsorption capacity deduced from the Langmuir isotherm model (q_{max}) for GW is lower than some of the adsorbents, however, the adsorption capacity of GW-αAgNPs is higher than activated carbon (AC), biochar and granular activated carbon (GAC) for BaP adsorption based on available literature. The higher adsorption capacity of GW-αAgNP may be due to surface modification associated with the doping experiment; creation of binding sites/pores and enhanced hydrophobic sorbate-sorbent interactions. Oleylamine and oleic acid used as capping agents as well as the linker between GW and AgNP are large hydrophobic organic molecules that may have improved the surface hydrophobicity of the composite.

Several factors influence the choice of adsorbent for water treatment applications, these factors include efficiency,

Table 2 Comparison of different materials used for removal of benzo(a)pyrene from aqueous solutions

Adsorbent	Dosage (g/L)	Removal efficiency (%)	Adsorption capacity (mg/g)	Reference
Wood ash	10.0	> 99	-	Pérez-Gregorio et al. (2010)
Activated carbon derived from coconut shells	0.5	88	-	Amstaetter et al. (2012)
Iron oxide nanoparticles (IONPs)	0.13	99	0.029	Hassan et al. (2018)
Granular activated carbon (GAC)	50.0	-	2.176	Minkina et al. (2021)
Biochar	50.0	-	5.881	Minkina et al. (2021)
Activated carbon derived from plastic waste	0.8	85	6.494	Ilyas et al. (2021)
Graphene wool (GW)	1.0	94.8	0.590	This study
GW-αAgNPs	1.0	98.7	13.670	This study

non-toxicity, availability of material, flexibility, reusability, etc. (Adeola et al. 2021). However, the wool-like form and porosity of GW-αAgNP, in addition to the potential antibacterial activity (discussed in Sect. 3.6), are advantages to the use of GW-αAgNP as a packing material for water treatment applications.

Effect of initial pH on BaP adsorption

The mineral, organic and biotic composition of surface waters depends on the source and geographic location, which in turn affects the water pH and influences the adsorption of chemical pollutants (Kulthanan et al. 2013). Solution pH affects the net charge of the adsorbent and adsorbate, and the alterations are more impactful in compounds and materials with protonated moieties (–OH, –COOH, $–NH_2$ group, etc.) because they tend to form deprotonated groups/complexes under variable pH conditions (Ahmed & Gasser 2012). In principle, at pH < point of zero charge (PZC), the surface of the adsorbent is positively charged and at pH > PZC, sorbents become negatively charged (Liikanen et al. 2006; Ololade et al. 2018). The results obtained in this study revealed that the optimum adsorption of BaP by GW-αAgNP occurred under basic pH conditions. This is in contrast to GW adsorption of PAHs that was slightly favored under acidic pH (Adeola & Forbes 2019).

Figure 3 reveals that the adsorption is favored to the right side of the pH scale due to the nature of the oleylamine-capped AgNP-GW complex, the surface modification, and the abundance of hydroxide ions in basic pH that potentially facilitates hydrogen bonding as discussed in Sect. 3.2. Furthermore, excess hydroxide ions at pH > 7 could potentially lead to the formation of silver hydroxide, which is hydrophobic and thus enhances the more hydrophobic interactions with BaP, which often governs the adsorption and partitioning of hydrophobic organic compounds (HOC) in water (Vasileva et al. 2009; Apul et al. 2013; Bai et al. 2017; Adeola & Forbes 2020, 2021b).

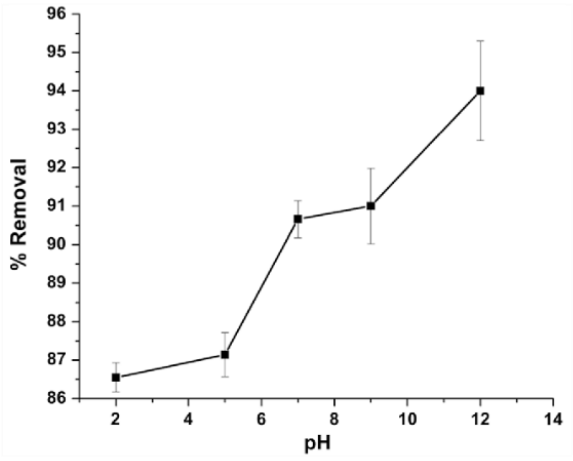

Fig. 3 Effect of pH on BaP adsorption onto GW-αAgNP (Experimental conditions: $C_o = 300$ µg/L; dosage = 5 mg per 5 mL, mixing rate = 200 rpm, T = 25 ± 1 °C, contact time: 24 h). Error bars ± relative standard deviation (RSD), n = 3

Influence of NOM on sorbent-sorbate interaction

Natural organic matter (NOM) is a complex matrix of organic materials which are present in aquatic environments, including drinking water, due to the interconnectivity between the hydrologic cycle, biosphere, and geosphere within the ecosystem (Sillanpää et al. 2018). The composition of NOM is influenced by biogeochemical processes that have occurred within the environment (Myneni 2019). In this study, NOM was isolated from stream sediment collected from the University of Pretoria sports campus, South Africa (latitude E28° 14′ 46″ and longitude S25° 45′ 10″) using established procedures (Ran et al. 2007; Ololade et al. 2018; Adeola & Forbes 2021a). The mineral phase was removed from bulk samples via treatment with 1 N HCl for 45 min at ambient temperature, followed by three consecutive treatments with 1 N HCl and 10% HNO_3 for 12 h

NOM Property	Value
pH	4.5
CEC (M_{eq}/100 mg)	1.3
OC (%)	9.4
ICP-OES elemental analysis (ppm ± std)	
Aluminum (Al)	9.29 ± 0.37
Iron (Fe)	12.67 ± 0.02
Phosphorus (P)	2.48 ± 0.07
Silicon (Si)	3.49 ± 0.97
Manganese (Mn)	0.06 ± 0.0
Lead (Pb)	< 0.09 ± 0.01
Sodium (Na)	2.01 ± 0.05
Potassium (K)	4.81 ± 0.10
Calcium (Ca)	2.64 ± 0.05
Magnesium (Mg)	0.65 ± 0.01

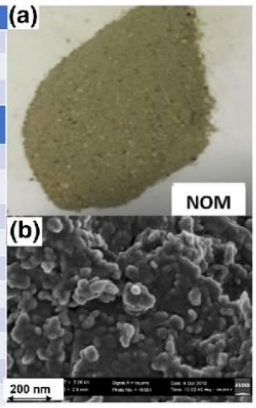

Fig. 4 Physicochemical properties and morphology of NOM isolate. Elemental composition was determined using ICP-OES. **a** Optical image and **b** SEM image of NOM (200 nm)

(Gelinas et al. 2001). The residue was washed each time with DI water, centrifuged at 6000 rpm for 10 min, decanted, and freeze-dried at − 4 °C for 24 h prior to use. Morphological and basic characterization of the NOM was carried out as presented in Fig. 4 (see Adeola and Forbes 2021b for more details). The NOM isolate had an irregular, spherical grain structure with heterogeneous and porous surface morphology (Fig. 4).

The effect of NOM on the adsorption of BaP by GW-αAgNP was evaluated using a preloading batch experiment (Adeola & Forbes 2021a; Ersan et al. 2016). Figure 5 suggests that significant competitive interactions took place between the NOM, BaP molecules, and the adsorbent leading to the comparative decline in removal efficiency, Freundlich adsorption capacity (K_f), partition coefficient (K_d), and maximum adsorption capacity (q_{max}). NOM has been reported to cause fouling of membranes, and retention of hydrophobic compounds and metals in solution, thus limiting the efficiency of conventional water treatment plants (Mehta et al. 2017; Kurwadkar et al. 2019; Adeola & Forbes 2021b). Essentially, NOM often alters the solution's chemistry such as pH, ionic strength, and the presence of leachable trace and heavy metals (Fig. 4), providing a plausible explanation for the inhibitory role of NOM (Ersan et al. 2016; Lamichhane et al. 2016; Adeola & Forbes 2021a).

Effect of temperature and thermodynamic studies

Several physicochemical and biological processes are influenced by temperature. Therefore, the role of temperature on the adsorption of BaP by pristine GW and doped GW-αAgNP was studied at 35, 45, and 55 °C, respectively. The adsorption data were fit to a linear and Sips isotherm models (Eq. 3 and 6), and it was observed that the maximum adsorption capacity (q_m) significantly reduced for GW-αAgNP with an increase in temperature, while the reverse was observed for GW (Table 3, Fig. 6). The free energy change (ΔG°), enthalpy (ΔH°) and entropy (ΔS°) were calculated using the Van't Hoff plot and equations

Fig. 5 Influence of NOM on the removal efficiency and adsorption capacity of benzo(a) pyrene by GW-αAgNP. (Experimental conditions: $C_{o\ (BaP)}$ = 100—500 µg/L; sorbent dosage = 1 g/L, NOM dosage = 1 g/L, mixing rate = 200 rpm, T = 25 ± 1 °C, contact time: 24 h)

Natural organic matter (NOM)	Adsorption parameters		
	K_d	K_f	q_{max} (µg/g)
Without NOM	2.75	1.12e-3	13670.7
Addition of NOM	0.21	9.40e-6	1928.4

K_d: partition coefficient (adsorption capacity), K_f: Freundlich adsorption capacity, q_{max}: maximum adsorption capacity (Langmuir)

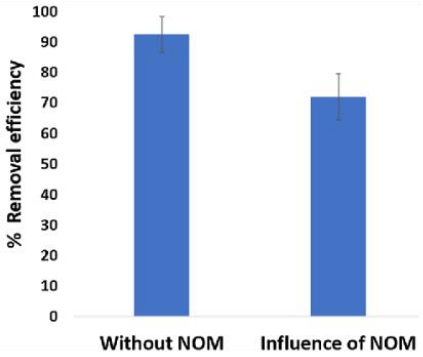

Table 3 Thermodynamic parameters for adsorption of BaP onto graphene wool and doped graphene wool

Temp. (K)	GW				GW-αAgNP			
	ΔG° (J/mol)	ΔH° (kJ/mol)	ΔS° (kJ/mol.K)	*q_m (µg/g)	ΔG° (J/mol)	ΔH° (kJ/mol)	ΔS° (kJ/mol.K)	*q_m (µg/g)
298	50.02			59.75	−2507.55			97.62
308	−2560.71	94.42	0.32	63.09	−1636.57	−24.04	−0.07	84.14
318	−6296.06			66.36	−1065.57			76.88

q_m: maximum adsorption capacity derived from Sips model

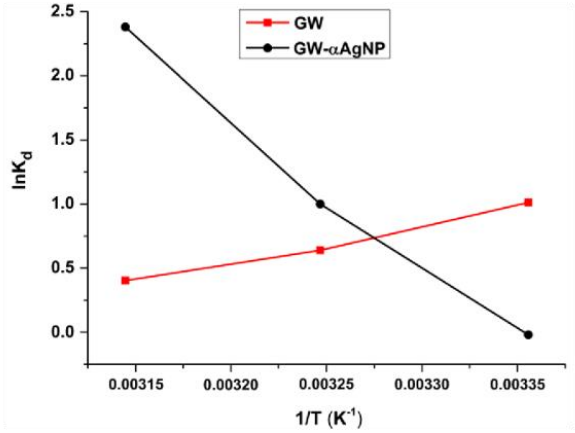

Fig. 6 Van't Hoff equation for BaP adsorption onto GW and GW-αAgNP from aqueous solution

(eqs. 8 and 9) (Fig. 6), in order to elucidate the thermodynamic nature of adsorption of BaP as a function of temperature (Yakout & Daifullah 2013; Adeola & Forbes 2019).

$$\ln K_d = \frac{\Delta S^\circ}{R} - \frac{\Delta H^\circ}{RT} \tag{8}$$

$$\Delta G^\circ = \Delta H^\circ - T\Delta S^\circ \tag{9}$$

where ΔG is the change in the Gibbs free energy (cal/mol); ΔH is the change in enthalpy (cal/mol), and ΔS is the change in entropy (kJ/mol.K), R = gas constant (8.314 J/mol.K), T = thermodynamic temperature (K) and K_d is adsorption capacity determined from the linear isotherm model.

Table 3 revealed positive values of adsorption enthalpy (ΔH°) and entropy (ΔS°), and a negative value of ΔG for GW-BaP interaction, which indicates a spontaneous endothermic process as the temperature increased (Ahmed & Gasser 2012). This result is in agreement with a previous study on the adsorption of phenanthrene and pyrene by GW (Adeola & Forbes 2019). In contrast, GW-αAgNP-BaP interaction is a spontaneous exothermic process (negative ΔH° and ΔG), with a reduction in system chaos (negative ΔS°) and adsorption capacity as the temperature is increased. While GW is more efficient at elevated temperatures, doping GW with oleylamine-capped AgNPs improved the adsorption capacity and ensured optimum removal efficiency at ambient temperature, which is better in terms of energy economics and industrial application.

Antibacterial activity of GW-αAgNP

Silver nanoparticles and composites have attracted scientific attention due to the continuous upsurge of drug-resistant bacteria (Bezza et al. 2020; Cobos et al. 2020). Bacterial strains are classified as Gram-positive (G + ve) or Gram-negative (G-ve) based on film assemblage with layers of peptidoglycan (PG) (Proft and Baker 2009). G − ve microbes have a thin PG (1–5 nm) between the cytoplasmic film and external layer, while G + ve microbes have a thicker PG layer (~ 30 nm) without an external film (Kim et al. 2007). The mechanism of action of silver-containing materials is described in Fig. 7. Silver damages the cytoplasmic membrane of microbes, creates oxidative stress with the cells, damages DNA, denatures cell proteins and has a lethal effect on microorganisms, including drug-resistant bacteria (Ahmad et al. 2020).

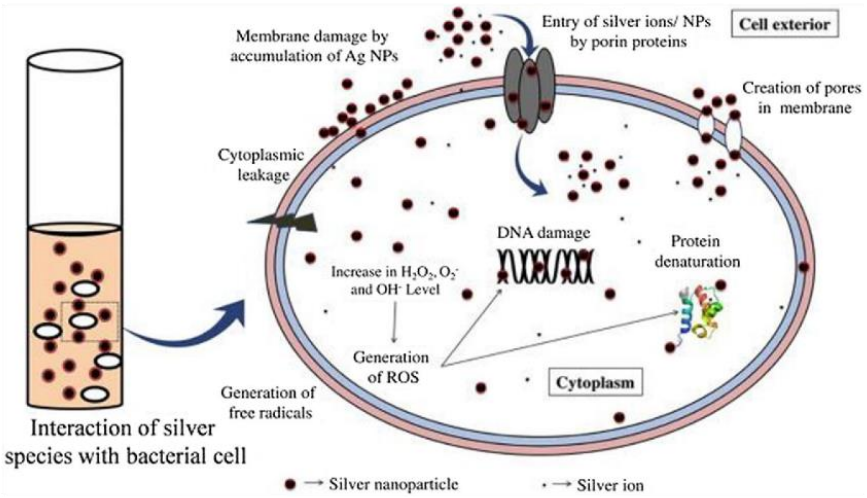

Fig. 7 A plausible mechanism for the antimicrobial action of silver nanoparticles. (Reproduced with permission from Ahmad et al. Copyright 2020, Elsevier)

Several studies have established the antibacterial action of AgNPs and composites, with different minimum inhibitory concentrations against some drug-resistant microbes (Table 4). The minimum inhibitory concentration (MIC) is regarded as the lowest concentration of an antimicrobial agent that inhibits the growth of microbes, recorded in mg/L or µg/mL (Cobos et al. 2020). The literature suggests that AgNPs and bimetallic nanocomposites (such as Au–Ag, Fe-Ag) are more effective against microorganisms based on MIC values; however, the potential adverse effects of AgNPs on human health have been a major concern, hence research into stabilizing AgNPs using capping agents and entrapment within a bulky substrate to limit its release potential/ contamination in aqueous media has gained vast attention (Liu et al. 2011; Loan Khanh et al. 2019; Bezza et al. 2020).

The antibacterial activity of GW-αAgNPs and pristine AgNPs was tested against the Gram-negative *Pseudomonas aeruginosa* CB1 and Gram-positive *Bacillus subtilis* CN2 strains by the standard micro-dilution method. Earlier reports suggest that *P. aeruginosa* and *B. subtilis* strains are capable of adaptive resistance to antibiotics such as penicillin and tetracycline (Araya et al. 2019; Pang et al. 2019). Figure 8 reveals a dose-dependent reduction in the concentration of Gram-negative *Pseudomonas aeruginosa* CB1 and Gram-positive *Bacillus subtilis* CN2 strains after 24 h incubation period as a decrease in turbidity was recorded

Table 4 A brief summary of silver-containing composites and microorganisms inhibited along with their minimum inhibitory concentrations (MIC) as reported in the literature (mg/L)

Composite	Microbes	Minimum inhibitory concentration (mg/L)	References
AgNPs/starch/sodium alginate/lemongrass oil	*Escherichia coli*	Not reported	Maizura et al. (2007)
Sodium Alginate/AgNPs	[a]*Staphylococcus aureus*, [b]*Escherichia coli*	[a]80, [b]40	Mohammed Fayaz et al. (2009)
Silver nanocomposites	[a]*Staphylococcus aureus*, [b]*Escherichia coli*, [c]*Candida albicans*, [d]*Aspergillus niger*	[a]250, [b]62.5, [c]125, [d]2000	Egger et al. (2009)
Bimetallic Au@Ag core–shell nanoparticles	[a]*Escherichia coli*, [b]*Pseudomonas aeruginosa*, [c]*Enterococcus faecalis*	[a]1.56, [b]1.88, [c]2.5	Banerjee et al. (2011)
AgNP-Bovin serum albumin (BSA)	*Staphylococcus aureus*, *Escherichia coli*, *Enterococcus faecalis*	469.2	Espinosa-Cristóbal et al. (2015)
Polycaprolactone-silver composites (PCL-AgNPs)	*Escherichia coli*, *Staphylococcus aureus*, *Pseudomonas aeruginosa*	12.5	Pazos-Ortiz et al. (2017)
Ag-microfibrillated cellulose biocomposite	[a]*Escherichia coli*, [b]*Staphylococcus aureus*, [c]*Pseudomonas aeruginosa*	[a]125, [b]1500, [c]125	Garza-Cervantes et al. (2020)
Chitosan-AgNP	*Staphylococcus aureus*	32.98	Quintero-Quiroz et al. (2020)
Ag–Fe bimetallic nanoparticles	[a]*Staphylococcus aureus*, [b]*Escherichia coli*, [c]*Candida albicans*, [d]*Pseudomonas aeruginosa*	[a,b]125, [c]62.5, [d]31.23	Padilla-Cruz et al. (2021)
Graphene oxide-AgNP	[a]*Staphylococcus aureus*, [b]*Escherichia coli*, [c]*Candida albicans*, [d]*Pseudomonas aeruginosa*	Not reported [b,d]64, [a,c]32	Jaworski et al. (2018) Cobos et al. (2020)
AgNP	[a]*Staphylococcus aureus*, [b]*Escherichia coli*, [c]*Candida albicans*, [d]*Pseudomonas aeruginosa*	< 8.0 10–12 [abc]125, [d]62.5	Gurunathan (2019); Loo et al. (2018) Dong et al. (2019); Vazquez-Muñoz et al. (2019) Padilla-Cruz et al. (2021)
Gelatin-stabilized AgNPs and curcumin	*Staphylococcus aureus*, *Pseudomonas aeruginosa*	125	Loan Khanh et al. (2019)
Lipopetide-capped AgNP	*Pseudomonas aeruginosa*, *Bacillus subtillis*	15.63	Bezza et al. (2020)
Graphene wool doped with oleylamine-capped AgNPs	*Pseudomonas aeruginosa*, *Bacillus subtillis*	1000	This study

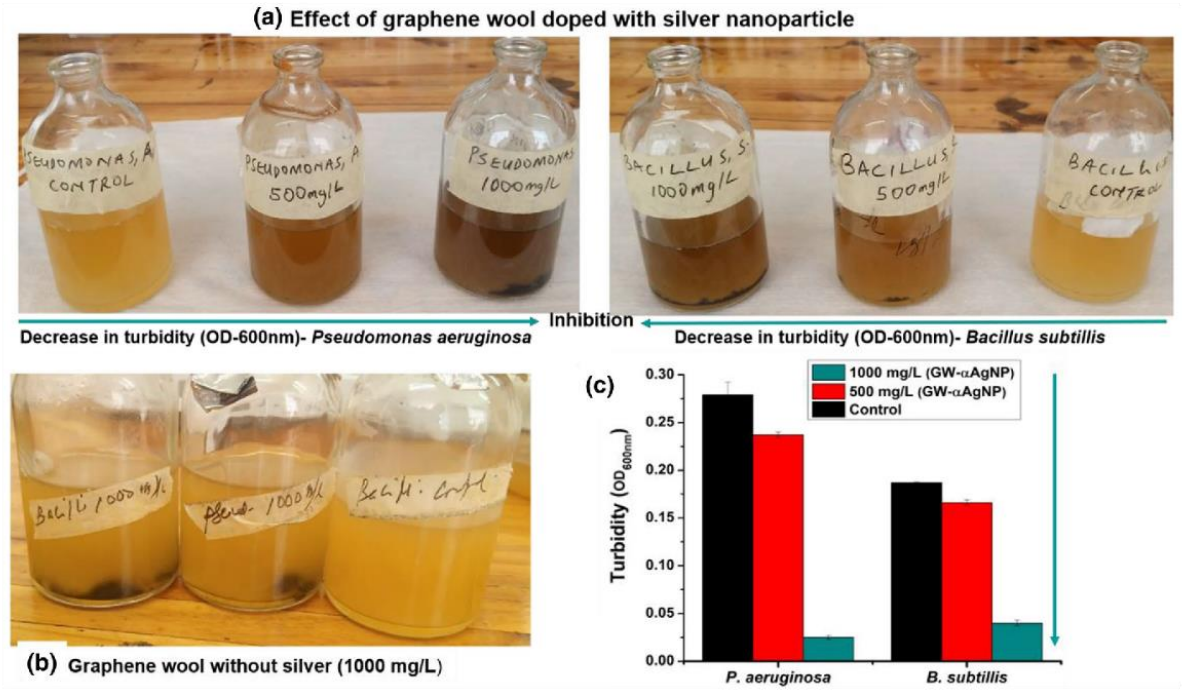

Fig. 8 Visible antibacterial activity of composites **a** 500 and 1000 mg/L of GW-αAgNP in 100 mL TSB nutrient medium inoculated with *P. aeruginosa (left)* and *B. subtilis (right)* **b** 1000 mg/L of GW in 100 mL TSB nutrient medium inoculated with *P. aeruginosa* and *B. subtilis* **c** Variation in concentration of respective bacteria determined spectrophotometrically at an optical density of 600 nm (OD_{600nm}), n = 2. (100 mL TSB nutrient medium inoculated with *P. aeruginosa* and *B. subtilis* without GW or GW-αAgNP were included as controls)

spectrophotometrically at an optical density of 600 nm. The decline in turbidity is a function of bacteriostatic/bactericidal activity of the composite, relative to control experiments. The reduction is most significant at 1000 mg/L (GW-αAgNP) and was more visible in doped GW than pristine GW. Factors such as particle size, stabilizing agent, composition of culture media and bacteria type, inoculum size, and leachability of silver ions from the composite, play a critical role in determining the MIC values. Optical density measurement is the most common technique for determining bacteria concentration and efficacy of antibacterial agents (McBirney et al. 2016; Huang et al. 2017). The agar disk diffusion test is another method often used for nanoparticles that are dispersible in water to form a uniform solution, however, due to the macroscopic and fibrous nature of GW, it was impossible to obtain a uniform dispersion of the material in the solution. When such experiments were attempted, the release and mobility of silver ions from the macrostructure through the semi-solid agar were significantly limited, thus constricting the inhibition zone to the site of deposition on the plate (Fig. 9), a similar finding was reported for large-sized AgNPs (Xiu et al. 2012; Bezza et al. 2020). However, the texture, fibrous nature, antibacterial and adsorptive properties of GW-αAgNP suggest that the material may be suitable for the fabrication of adsorbent layer(s) in water filtration or purification devices.

Conclusion

Facile synthesis of GW doped with oleylamine-capped AgNPs was achieved in this study. The effect of concentration, pH, and temperature on the adsorption of benzo(a) pyrene, a human carcinogen, was evaluated using the doped graphene wool. Isotherm data suggest that GW-αAgNP-BaP interaction is a spontaneous exothermic process (negative ΔH° and ΔG), characterized by a decline in system chaos (negative ΔS°) and adsorption capacity as temperature increases. This study suggests that the adsorption capacity of GW improved and will be more efficient at ambient temperature (ΔG and q_{max}), when doped with AgNPs as a result of improved surface hydrophobicity and heterogeneity, leading to the creation of more binding sites for BaP to adhere to. Results revealed a high degree of desorption hysteresis and irreversible sorption, suggesting a strong binding strength between the doped GW and pollutant, thus limiting

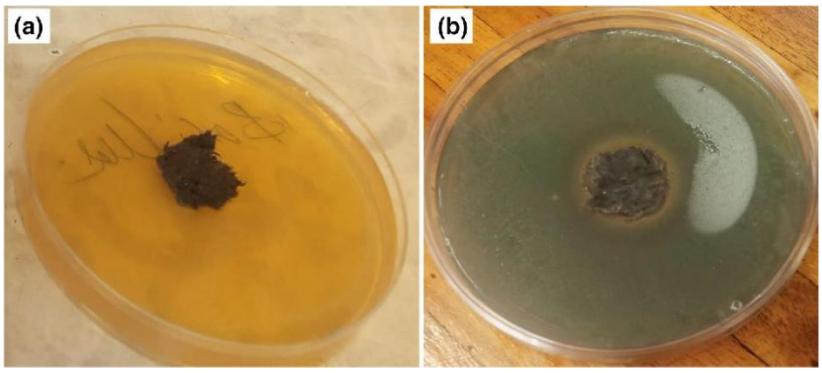

Fig. 9 Agar disk diffusion test **a** Before incubation- 100 mg of GW-αAgNP was placed on agar disk with growth medium and *Bacillus subtilis* culture spread over uniformly, **b** After 24 h incubation- visible growth of the bacteria around GW-αAgNP with inhibition zone limited to the site of deposition

the ease of recontamination. Results also show that the presence of NOM in the aqueous matrix is undesirable for the application of the synthesized adsorbent due to competitive adsorption. Several studies have established the cytoplasmic toxicity and antimicrobial properties of silver-containing nanomaterials and in this study, preliminary results also revealed that there was a dose-dependent reduction in the concentration of Gram-negative *Pseudomonas aeruginosa* CB1 and Gram-positive *Bacillus subtilis* CN2 strains tested in the presence of GW-αAgNP.

Furthermore, unlike most composites that are generated in the form of flakes or powder, GW-αAgNP provides a wool-like form that may be more suitable as a packing material for filters and other water polishing tools due to its lightweight and porous nature. The synthesis of graphene wool is facile and eco-friendly without extensive use of chemicals. Therefore, under appropriate operating conditions, the graphene-based composite can potentially be utilized as a water polishing tool for the removal of emerging organic chemical pollutants. With further studies and suitable fabrication, this hybrid material has the potential to serve as a smart solution to chemical and microbial pollution in water.

Acknowledgements Authors acknowledge the assistance provided by Dr F. A. Bezza during the antibacterial testing of the composite, the University of Pretoria Commonwealth Doctoral Scholarship funding (AA) and the Rand Water Professorial Chair program (PF and EC) for providing funding for the research.

Funding This study is supported by University of Pretoria Commonwealth Doctoral Scholarship funding (AA) and the Rand Water Professorial Chair program (PF and EC).

Declarations

Conflict of interest The authors declare that there is no conflict of interest.

Ethical approval This article does not contain any studies with human participants or animals performed by any of the authors.

References

Adeniji AO, Okoh OO, Okoh AI (2019) Levels of Polycyclic aromatic hydrocarbons in the water and sediment of buffalo river estuary, south africa and their health risk assessment. Arch Environ Contam Toxicol 76(4):657–669

Adeola AO, Forbes PBC (2019) Optimization of the sorption of selected polycyclic aromatic hydrocarbons by regenerable graphene wool. Water Sci Technol 80:1931–1943

Adeola AO, Forbes PBC (2020) Assessment of reusable graphene wool adsorbent for the simultaneous removal of selected 2–6 ringed polycyclic aromatic hydrocarbons from aqueous solution. Environ Technol. https://doi.org/10.1080/09593330.2020.1824024

Adeola AO, Forbes PBC (2021a) Influence of natural organic matter fractions on PAH sorption by stream sediments and a synthetic graphene wool adsorbent. Environ Technol Innov 21:101202

Adeola AO, Forbes PBC (2021b) Advances in water treatment technologies for removal of polycyclic aromatic hydrocarbons: existing concepts, emerging trends, and future prospects. Water Environ Res 93:343–395

Ahmad HB, Yasmin GE, Arain SA, Bhatti IA, Hussain M (2015) Synthesis of some novel adsorbents for antimicrobial activity and removal of arsenic from drinking water. Korean J Chem Eng 32:661–666

Ahmad SA, Sachi Das S, Khatoon A, Tahir Ansari M, Afzal M, Saquib Hasnain M, Kumar Nayak A (2020) Bactericidal activity of silver nanoparticles: a mechanistic review. Mater Sci Energy Technologies 3:756–769

Ahmed IM, Gasser MS (2012) Adsorption study of anionic reactive dye from aqueous solution to Mg-Fe-CO_3 layered double hydroxide (LDH). Appl Surf Sci 259:650–656

Amari A, Elboughdiri N, Ghernaout D, Lajimi RH, Alshahrani AM, Tahoon MA, Rebah FB (2021) Multifunctional crosslinked chitosan/nitrogen-doped graphene quantum dot for wastewater treatment. Ain Shams Eng J. https://doi.org/10.1016/j.asej.2021.02.024

Amstaetter K, Eek E, Cornelissen G (2012) Sorption of PAHs and PCBs to activated carbon: coal versus biomass-based quality. Chemosphere 87:573–578

Anthony KJP, Murugan M, Gurunathan S (2014) Biosynthesis of silver nanoparticles from the culture supernatant of Bacillus marisflavi and their potential antibacterial activity. J Ind Eng Chem 20:1505–1510

Apul OG, Wang Q, Zhou Y, Karanfil T (2013) Adsorption of aromatic organic contaminants by graphene nanosheets: comparison with carbon nanotubes and activated carbon. Water Res 47:1648–1654

Araya G, Benites J, Reyes JS, Marcoleta AE, Valderrama JA, Lagos R, Monasterio O (2019) Inhibition of Escherichia coli and Bacillus subtilis FtsZ Polymerization and Bacillus subtilis Growth by Dihydroxynaphtyl Aryl Ketones. Front Microbiol 10:1225. https://doi.org/10.3389/fmicb.2019.01225

Bai H, Zhou J, Zhang H, Tang G (2017) Enhanced adsorbability and photocatalytic activity of TiO_2-graphene composite for polycyclic aromatic hydrocarbons removal in aqueous phase. Colloids Surf, B 150:68–77

Banerjee M, Sharma S, Chattopadhyay A, Ghosh SS (2011) Enhanced antibacterial activity of bimetallic gold-silver core-shell nanoparticles at low silver concentration. Nanoscale 3:5120–5125

Bezza FA, Chirwa EMN (2016) Biosurfactant-enhanced bioremediation of aged polycyclic aromatic hydrocarbons (PAHs) in creosote contaminated soil. Chemosphere 144:635–644

Bezza FA, Tichapondwa SM, Chirwa EMN (2020) Synthesis of biosurfactant capped silver nanoparticles characterization and their potential application for bactericidal purposes. J Hazard Mater 393:122319

Bushra R, Shahadat M, Ahmad A, Nabi SA, Umar K, Oves M, Raeissi AS, Muneer M (2014) Synthesis, characterization, antimicrobial activity and applications of polyanilineTi(IV)arsenophosphate adsorbent for the analysis of organic and inorganic pollutants. J Hazard Mater 264:481–489

Çınar S, Gündüz G, Mavis B, Çolak U (2011) Synthesis of silver nanoparticles by Oleylamine-Oleic acid reduction and its use in making nanocable by coaxial electrospinning. J Nanosci Nanotechnol 11:3669–3679

Cobos M, De-La-Pinta I, Quindós G, Fernández MJ, Fernández MD (2020) Graphene oxide-silver nanoparticle nanohybrids: synthesis, characterization, and antimicrobial properties. Nanomaterials 10(2):376

Cornelissen G, Gustafsson Ö, Bucheli TD, Jonker MTO, Koelmans AA, van Noort PCM (2005) Extensive sorption of organic compounds to black carbon, coal, and kerogen in sediments and soils: mechanisms and consequences for distribution, bioaccumulation, and biodegradation. Environ Sci Technol 39:6881–6895

Dana E, Taha A, Afkar E (2018) Green synthesis of iron nanoparticles by acacia nilotica pods extract and its catalytic, adsorption, and antibacterial activities. Appl Sci 8:1922

Dong Y, Zhu H, Shen Y, Zhang W, Zhang L (2019) Antibacterial activity of silver nanoparticles of different particle size against Vibrio Natriegens. PLOS ONE, 14, e0222322

Egger S, Lehmann RP, Height MJ, Loessner MJ, Schuppler M (2009) Antimicrobial properties of a novel silver-silica nanocomposite material. Appl Environ Microbiol 75:2973

Eltugral N, Simsir H, Karagoz S (2016) Preparation of nano-silver-supported activated carbon using different ligands. Res Chem Intermed 42:1663–1676

Ersan G, Kaya Y, Apul OG, Karanfil T (2016) Adsorption of organic contaminants by graphene nanosheets, carbon nanotubes and granular activated carbons under natural organic matter preloading conditions. Sci Total Environ 565:811–817

Espinosa-Cristóbal LF, Martínez-Castañón GA, Loyola-Rodríguez JP, Niño-Martínez N, Ruiz F, Zavala-Alonso NV, Lara RH, Reyes-López SY (2015) Bovine serum albumin and chitosan coated silver nanoparticles and its antimicrobial activity against oral and nonoral bacteria. J Nanomater, 420853

Fayaz AM, Balaji K, Girilal M, Kalaichelvan PT, Venkatesan R (2009) Mycobased synthesis of silver nanoparticles and their incorporation into sodium alginate films for vegetable and fruit preservation. J Agric Food Chem 57:6246–6252

Garza-Cervantes JA, Mendiola-Garza G, de Melo EM, Dugmore TIJ, Matharu AS, Morones-Ramirez JR (2020) Antimicrobial activity of a silver-microfibrillated cellulose biocomposite against susceptible and resistant bacteria. Sci Rep 10:7281

Gelinas Y, Prentice KM, Baldock JA, Hedges J (2001) An improved thermal oxidation method for the quantification of soot/graphite carbon in sediments and soils. Environ Sci Technol 21:3519–3525

Gurunathan S (2019) Rapid biological synthesis of silver nanoparticles and their enhanced antibacterial effects against Escherichia fergusonii and Streptococcus mutans. Arab J Chem 12:168–180

Hardonnière K, Saunier E, Lemarié A, Fernier M, Gallais I, Héliès-Toussaint C, Mograbi B, Antonio S, Bénit P, Rustin P, Janin M, Habarou F, Ottolenghi C, Lavault M-T, Benelli C, Sergent O, Huc L, Bortoli S, Lagadic-Gossmann D (2016) The environmental carcinogen benzo[a]pyrene induces a Warburg-like metabolic reprogramming dependent on NHE1 and associated with cell survival. Sci Rep 6:30776

Hassan SSM, Abdel-Shafy HI, Mansour MSM (2018) Removal of pyrene and benzo(a)pyrene micropollutant from water via adsorption by green synthesized iron oxide nanoparticles. advances in Natural Sciences. Nanosci Nanotechnol 9(1):015006

Huang W, Wang J-Q, Song H-Y, Zhang Q, Liu G-F (2017) Chemical analysis and in vitro antimicrobial effects and mechanism of action of Trachyspermum copticum essential oil against Escherichia coli. Asian Pac J Trop Med 10:663–669

IARC, International Agency for Research on Cancer, (2010) IARC Monographs on the Evaluation of Carcinogenic Risks to Humans. (Lyon: World Health Organization) 92, 1–853

Ilyas M, Ahmad W, Khan H (2021) Utilization of activated carbon derived from waste plastic for decontamination of polycyclic aromatic hydrocarbons laden wastewater. Water Sci Technol 84:609–631

Ishihara M, Nguyen VQ, Mori Y, Nakamura S, Hattori H (2015) Adsorption of silver nanoparticles onto different surface structures of chitin/chitosan and correlations with antimicrobial activities. Int J Mol Sci 16:13973–13988

Jaworski S, Wierzbicki M, Sawosz E, Jung A, Gielerak G, Biernat J, Jaremek H, Łojkowski W, Woźniak B, Wojnarowicz J, Stobiński L, Małolepszy A, Mazurkiewicz-Pawlicka M, Łojkowski M, Kurantowicz N, Chwalibog A (2018) Graphene oxide-based nanocomposites decorated with silver nanoparticles as an antibacterial agent. Nanoscale Res Lett 13:116

Jyoti K, Baunthiyal M, Singh A (2016) Characterization of silver nanoparticles synthesized using Urtica dioica Linn. leaves and their synergistic effects with antibiotics. J Rad Res Appl Sci 9:217–227

Khan E, Khaodhir S, Rotwiron P (2007) Polycyclic aromatic hydrocarbon removal from water by natural fiber sorption. Water Environ Res 79:901–911

Kim JS, Kuk E, Yu KN, Kim J-H, Park SJ, Lee HJ, Kim SH, Park YK, Park YH, Hwang C-Y, Kim Y-K, Lee Y-S, Jeong DH, Cho M-H (2007) Antimicrobial effects of silver nanoparticles. Nanomed Nanotechnol Biol Med 3:95–101

Kulthanan K, Nuchkull P, Varothai S (2013) The pH of water from various sources: an overview for recommendation for patients with atopic dermatitis. Asia Pac Allergy 3:155–160

Kurwadkar S, Hoang TV, Malwade K, Kanel SR, Harper WF, Struckhoff G (2019) Application of carbon nanotubes for removal of emerging contaminants of concern in engineered water and wastewater treatment systems. Nanotechnol Environ Eng 4(1):1–16

Lamichhane S, Bal Krishna KC, Sarukkalige R (2016) Polycyclic aromatic hydrocarbons (PAHs) removal by sorption: A review. Chemosphere 148:336–353

Li H, He N, Cheng C, Dong H, Wen J, Wang X (2020) Antimicrobial polymer contained adsorbent a promising candidate with remarkable anti-biofouling ability and durability for enhanced uranium extraction from seawater. Chem Eng J 388:124273

Liikanen R, Yli-Kuivila J, Tenhunen J, Laukkanen R (2006) Cost and environmental impact of nanofiltration in treating chemically pretreated surface water. Desalination 201:58–70

Liu L, Liu J, Wang Y, Yan X, Sun DD (2011) Facile synthesis of monodispersed silver nanoparticles on graphene oxide sheets with enhanced antibacterial activity. New J Chem 35:1418–1423

Loan Khanh L, Thanh Truc N, Tan Dat N, Thi Phuong NN, van Toi V, Thi Thu HN, Ngoc Quyen T, Thi Thanh LT, Thi Hiep N (2019) Gelatin-capped composites of silver nanoparticles and curcumin: characterization, antibacterial and antioxidant study. Sci Technol Adv Mater 20:276–290

Loo YY, Rukayadi Y, Nor-Khaizura M-A-R, Kuan CH, Chieng BW, Nishibuchi M, Radu S (2018) In vitro antimicrobial activity of green synthesized silver nanoparticles against selected gram-negative foodborne pathogens. Front Microbiol. https://doi.org/10.3389/fmicb.2018.01555

Maizura M, Fazilah A, Norziah MH, Karim AA (2007) Antibacterial activity and mechanical properties of partially hydrolyzed sago starch-alginate edible film containing lemongrass oil. J Food Sci 72:C324–C330

McBirney SE, Trinh K, Wong-Beringer A, Armani AM (2016) Wavelength-normalized spectroscopic analysis of Staphylococcus aureus and Pseudomonas aeruginosa growth rates. Biomed Opt Express 7:4034–4042

Mehta R, Saha NK, Bhattacharya A (2017) Pretreatment of agriculture field water for improving membrane flux during pesticide removal. Appl Water Sci 7:3281–3290

Minkina T, Vasilyeva G, Popileshko Y, Bauer T, Sushkova S, Fedorenko A, Antonenko E, Pinskii D, Mazarji M, Ferreira CSS (2021) Sorption of benzo[a]pyrene by Chernozem and carbonaceous sorbents: comparison of kinetics and interaction mechanisms. Environ Geochem Health. https://doi.org/10.1007/s10653-021-00945-8

Miren J, Aurora M-B, Ulrich K, Tomas G-A (2018) Smart and multifunctional materials and their possible application in façade systems. J Facade Des Eng 6:19–33

Mojahed F, Dehghanpour S, Alizadeh M, Mahmoudi A (2011) Wet chemical synthesis of oleylamine-capped silver nanoparticles by a fast and facile reproducible method. Synth React Inorg, Met-Org, Nano-Met Chem 41:664–670

Munyeza CF, Osano AM, Maghanga JK, Forbes PBC (2020) Polycyclic aromatic hydrocarbon gaseous emissions from household cooking devices: a kenyan case study. Environ Toxicol Chem 39:538–547

Myneni SCB (2019) Chemistry of natural organic matter—the next step: commentary on a humic substances debate. J Environ Qual 48:233–235

Nguyen TH, Sabbah I, Ball WP (2004) Sorption nonlinearity for organic contaminants with diesel soot: method development and isotherm interpretation. Environ Sci Technol 38:3595–3603

Ololade IA, Adeola AO, Oladoja NA, Ololade OO, Nwaolisa SU, Alabi AB, Ogungbe IV (2018) In-situ modification of soil organic matter towards adsorption and desorption of phenol and its chlorinated derivatives. J Environ Chem Eng 6:3485–3494

Padilla-Cruz AL, Garza-Cervantes JA, Vasto-Anzaldo XG, García-Rivas G, León-Buitimea A, Morones-Ramírez JR (2021) Synthesis and design of Ag–Fe bimetallic nanoparticles as antimicrobial synergistic combination therapies against clinically relevant pathogens. Sci Rep 11:5351

Pang Z, Raudonis R, Glick BR, Lin T-J, Cheng Z (2019) Antibiotic resistance in Pseudomonas aeruginosa: mechanisms and alternative therapeutic strategies. Biotechnol Adv 37:177–192

Pazos-Ortiz E, Roque-Ruiz JH, Hinojos-Márquez EA, López-Esparza J, Donohué-Cornejo A, Cuevas-González JC, Espinosa-Cristóbal LF, Reyes-López SY (2017) Dose-dependent antimicrobial activity of silver nanoparticles on polycaprolactone fibers against gram-positive and gram-negative bacteria. J Nanomater. https://doi.org/10.1155/2017/4752314

Pérez-Gregorio MR, García-Falcón MS, Martínez-Carballo E, Simal-Gándara J (2010) Removal of polycyclic aromatic hydrocarbons from organic solvents by ashes wastes. J Hazard Mater 178:273–281

Prakash P, Gnanaprakasam P, Emmanuel R, Arokiyaraj S, Saravanan M (2013) Green synthesis of silver nanoparticles from leaf extract of Mimusops elengi, Linn. for enhanced antibacterial activity against multi drug resistant clinical isolates. Colloids Surf B 108:255–259

Proft T, Baker EN (2009) Pili in Gram-negative and Gram-positive bacteria—structure, assembly and their role in disease. Cell Mol Life Sci 66:613. https://doi.org/10.1007/s00018-008-8477-4

Quintero-Quiroz C, Botero LE, Zárate-Triviño D, Acevedo-Yepes N, Escobar JS, Pérez VZ, Cruz Riano LJ (2020) Synthesis and characterization of a silver nanoparticle-containing polymer composite with antimicrobial abilities for application in prosthetic and orthotic devices. Biomater Res 24:13

Ran Y, Sun K, Ma X, Wang GH, Grathwohl P, Zeng EY (2007) Effect of condensed organic matters on solvent extraction and aqueous leaching of PAHs based in soils and sediments. J Environ Poll 43:111–123

Schinwald A, Murphy FA, Jones A, MacNee W, Donaldson K (2012) Graphene-based nanoplatelets: a new risk to the respiratory system as a consequence of their unusual aerodynamic properties. ACS Nano 6:736–746

Schoonraad G, Madito MJ, Manyala N, Forbes PBC (2020) Synthesis and optimisation of a novel graphene wool material by atmospheric pressure chemical vapour deposition. J Mater Sci 55:545–564

Sears GW (1956) Determination of specific surface area of colloidal silica by titration with sodium hydroxide. Anal Chem 28:1981–1983

Sha L, Guanying C, Paras NP, Mark TS (2011) Synthesis of Monodisperse Au, Ag, and AuAg alloy nanoparticleswith tunable size and surface plasmon resonance frequency. Chem Mater 23:4098–4101

Sillanpää M, Ncibi MC, Matilainen A (2018) Advanced oxidation processes for the removal of natural organic matter from drinking water sources: a comprehensive review. J Environ Manage 208:56–76

Tran M-H, Jeong HK (2015) Synthesis and characterization of silver nanoparticles doped reduced graphene oxide. Chem Phys Lett 630:80–85

Vasileva SY, Olenin AY, Romanovskaya GI, Krutyakov YA, Pogonin VI, Korotkov AS, Zuev BK (2009) Adsorption preconcentration of pyrene by silver nanoparticles and its determination in aqueous solutions. J Anal Chem 64:1214–1220

Vazquez-Muñoz R, Meza-Villezcas A, Fournier PGJ, Soria-Castro E, Juarez-Moreno K, Gallego-Hernández AL, Bogdanchikova N, Vazquez-Duhalt R, Huerta-Saquero A (2019) Enhancement of antibiotics antimicrobial activity due to the silver nanoparticles impact on the cell membrane. PLOS ONE, 14, e0224904

Wang L, Niu J, Yang Z, Shen Z, Wang J (2008) Effects of carbonate and organic matter on sorption and desorption behavior of polycyclic aromatic hydrocarbons in the sediments from Yangtze River. J Hazard Mater 154:811–817

Wang W, Wang Z, Liu J, Zhang Z, Sun L (2017) Single-step one-pot synthesis of graphene foam/TiO2 nanosheet hybrids for effective water treatment. Sci Rep 7:43755

Wang S, Li X, Liu Y, Zhang C, Tan X, Zeng G, Song B, Jiang L (2018) Nitrogen-containing amino compounds functionalized graphene oxide: Synthesis, characterization and application for the removal of pollutants from wastewater: a review. J Hazard Mater 342:177–191

Xiu ZM, Zhang QB, Puppala HL, Colvin VL, Alvarez PJ (2012) Negligible particle-specific antibacterial activity of silver nanoparticles. Nano Lett 12:4271–4275

Yakout SM, Daifullah AAM (2013) Removal of selected polycyclic aromatic hydrocarbons from aqueous solution onto various adsorbent materials. Desalin Water Treat 51:6711–6718

Yang K, Chen B, Zhu L (2015) Graphene-coated materials using silica particles as a framework for highly efficient removal of aromatic pollutants in water. Sci Rep 5:11641

Yerushalmi L, Nefil S, Hausler R, Guiot SR (2006) Removal of pyrene and benzo(a)Pyrene from contaminated water by sequential and simultaneous ozonation and biotreatment. Water Environ Res 78:2286–2292

Yuan P, Li X, Wang W, Liu H, Yan Y, Yang H, Yue Y, Bao X (2018) Tailored design of differently modified mesoporous materials to deeply understand the adsorption mechanism for polycyclic aromatic hydrocarbons. Langmuir 34:15708–15718

Zhang C, Wu L, Cai D, Zhang C, Wang N, Zhang J, Wu Z (2013) Adsorption of polycyclic aromatic hydrocarbons (fluoranthene and anthracenemethanol) by functional graphene oxide and removal by ph and temperature-sensitive coagulation. ACS Appl Mater Interf 5:4783–4790

Zhang W, Yang Z-Y, Cheng X-W, Tang R-C, Qiao Y-F (2019) Adsorption, antibacterial and antioxidant properties of tannic acid on silk fiber. Polymers 11(6):970

Zhao G, Jiang L, He Y, Li J, Dong H, Wang X, Hu W (2011) Sulfonated graphene for persistent aromatic pollutant management. Adv Mater 23:3959–3963

Chapter 9 Conclusions and Future work

This chapter presents the main findings of this study and some proposals that can be considered for future work.

Polycyclic aromatic hydrocarbons (PAHs) and antiretroviral drugs (ARVDs) are environmental pollutants with potential toxic effects for both aquatic fauna and humans. Chronic exposure to these pollutants may reportedly result in endocrine disruption, carcinogenic effects, organ failure, and life-threatening effects. Anthropogenic activities play a major role in the release of these contaminants into the environment. Their toxicity at low concentrations and the need for decontamination at various concentrations present a challenge to water treatment professionals and environmental chemists. Robust and ecofriendly techniques for the removal of these pollutants are required. Therefore, this research project sought to use the adsorption technique for the removal of PAHs and ARVDs from water using synthesized graphene wool (GW) composites. To gain useful insights, extensive reviews were first conducted on the existing and emerging techniques for the removal of PAHs from water. The status of antiretroviral drugs in African surface water and potential remediation approaches was thoroughly reviewed and recommendations were suggested towards pollution control.

Graphene wool was synthesized by means of a bottom-up approach using a chemical vapour deposition (CVD) system and was characterized using various techniques for structural and morphological elucidation. This material was used to remove PAHs and ARVDs in batch adsorption experiments considering various concentrations and other process variables for optimal efficiency. The electronic structure, surface moieties and hydrophobic nature of the adsorbent enhanced its performance towards the removal of the targeted compounds. Generally, adsorption of PAHs by GW is best described by the Sips (Freundlich-Langmuir) model and the Freundlich multilayer adsorption mechanism for single-solute and competitive batch adsorption studies, and is mainly controlled by hydrophobic and π-π interactions. Thermodynamic studies of PAH adsorption revealed that the process is spontaneous and endothermic, with a negative value of Gibb's free energy (ΔG) and a positive value of adsorption enthalpy (ΔH). On the contrary, the

adsorption of antiretroviral drugs, specifically efavirenz (EFV) and nevirapine (NVP), is slightly more complex and the nature of interaction may vary for different types of ARVD due to the variations in chemical structure thereof. Similar to PAHs, ARVD adsorption onto GW was best described by Sips (EFV) and Freundlich (NVP) models. However, while GW-EFV interaction was spontaneous and endothermic, GW-NVP was spontaneous and exothermic. Several mechanisms such as hydrophobic, π-π, covalent, van der Waal's, and hydrogen bonding interactions are possible, depending on the molecular properties and conformations of the ARVD as revealed by supporting computational studies.

Furthermore, the study carried out on the influence of natural organic matter (NOM) on adsorption of pyrene revealed that the mineral-rich fraction (MRF) of NOM significantly diminished the removal efficiency of graphene wool, as both adsorption capacity (K_d) and efficiency reduced from 16.9 L g^{-1} and 95.4% to 0.3 L g^{-1} and 18.5%, respectively. Fractions with higher % organic carbon (natural sediment, black carbon and mineral deficient fractions) had higher maximum adsorption capacities for several PAHs. Aromaticity and hydrophobic moieties of the different PAHs and NOM significantly influenced the π-π and hydrophobic–organophilic interactions between sorbates and sorbents that may have occurred, which led to some degree of irreversible sorption as shown by hysteresis indices.

Adsorption isotherm parameters suggested that GW adsorbed NVP slightly better with stronger binding strength than EFV under optimum conditions, with removal efficiencies and adsorption capacities (K_d) of 84% and 2.54 L g^{-1} for nevirapine, and 80% and 1.48 L g^{-1} for efavirenz respectively. There is positive correlation between the adsorption capacities, hydrophobicity and molecular weight of PAHs investigated under the same process conditions. The adsorption capacities (K_d) of GW for adsorption of naphthalene (NAPH), anthracene (ANT), benzo(a)anthracene (B(a)ANT), benzo(a)pyrene (B(a)P) and benzo(g,h,i)perylene (PERY) under the similar process conditions are 0.17, 1.92, 3.62, 5.73 and 12.50 L g^{-1}. The overall GW removal efficiencies of the target compounds (PAHs and ARVDs) in this project ranged from 81 – 100% under optimum conditions. It was reported that the removal efficiency is dependent on the choice of operational parameters, such as concentration of adsorbate and adsorbent dosage, etc.

Graphene wool doped with stabilized silver nanoparticles (GW-αAgNP) was synthesized and its adsorption capacity was evaluated using benzo(a)pyrene contaminated water. The Sips maximum adsorption capacity (q_m) of GW-αAgNP was 97.62 μg g^{-1}, much higher than GW with 59.76 μg g^{-1}. Furthermore, GW-αAgNP and GW were tested against Gram-negative and Gram-positive bacteria (*Pseudomonas aeruginosa* and *Bacillus subtilis*). While GW showed no significant inhibition at the concentrations tested, 1000 mg L^{-1} dosage of GW-αAgNP significantly inhibited the growth of both bacteria. This hybrid material thus has the potential to serve as a smart solution to chemical and microbiological water pollution.

In conclusion, with the right fabrication, this novel form of graphene (GW and GW-αAgNP) can be used to make packing materials for filters and adsorbents for water purification and polishing purposes due to their wool-like structure, good water permeability, high volume-to-mass ratio (low density), and porosity. This work has demonstrated that the graphene wool composite is a viable adsorbent for the removal of emerging chemical pollutants, such as PAHs and ARVDs, from water.

9.1. Future work

The reviews and experimental articles presented in this project have undoubtedly added to the body of scientific knowledge. However, potential directions for expansion and future studies are summarized below:

- Investigation of the competitive adsorption of antiretroviral drugs (ARVDs) using graphene wool (GW) and GW-αAgNP composites, and the impact of natural organic matter (NOM) on the adsorption of antiretroviral drugs. This will provide further insight into the role of variation in the molecular structure of different antiretroviral drugs on adsorption thereof by GW particularly in a complex mixture, as is often the case in environmental samples. Natural organic matter exists in different forms in the aquatic environment and its role in the retention and mobility of organic compounds is widely investigated. Therefore, similar to Chapter 7, it could be useful to evaluate ARVD adsorption in relation to the presence of NOM, and to determine the overall impact thereof on the removal efficiency of the synthesized material.

- Fabrication of a column using the synthesized adsorbents for adsorption of organic chemical pollutants and antimicrobial studies using flow-through experiments should be investigated. Fixed-bed column adsorption experiments can be carried out to provide useful insight into parameters such as optimum flow rate, bed height, breakthrough time, and other operational conditions. This is the next essential step towards the field- or industrial-based application of the composite, although fixed-bed column adsorption has its challenges, such as poor temperature control, pressure control requirements, difficulty in uniform packing and regeneration of adsorbent, etc. However, fixed-bed column experiments are relevant in filling the gaps in understanding of process variables between pilot- and industrial-scale application of synthesized adsorbents.

APPENDIX

Table 1: List of antiretroviral drugs approved by the United States Food and Drug Administration (US FDA)

Drug Class	Generic Name	Brand	FDA Approval Date DD-MM-YYYY
Nucleoside Reverse Transcriptase Inhibitor (NRTIs)	abacavir	Ziagen	17-12-1998
	emtricitabine	Emtriva	02-07-2003
	lamivudine	Epivir	17-11-1995
	tenofovir disoproxil fumarate	Viread	26-10-2001
	zidovudine	Retrovir	19-03-1987
Non-Nucleoside Revers Transcriptase Inhibitor (NNRTIs)	doravirine	Pifeltro	30-08-2018
	efavirenz	Sustiva	17-09-1998
	etravirine	Intelence	18-01-2008
	nevirapine	Viramune	25-03-2011
	rilpivirine	Edurant	20-05-2011
Protease Inhibitors (PIs	atazanavir	Reyataz	20-06-2003
	darunavir	Prezista	23-06-2006
	fosamprenavir	Lexiva	20-10-2003
	ritonavir	Norvir	01-03-1996
	saquinavir	Invirase	06-12-1995
	tipranavir	Aptivus	22-06-2005
Fusion Inhibitors	enfuvirtide	Fuzeon	13-03-2003
CCRS Antagonists	maraviroc	Selzentry	06-08-2007
Integrase Inhibitors	dolutegravir	Trivicay	13-04-2013
	raltegravir	Isentress	12-10-2007
Post-Attachment Inhibitors	ibalizumab-uiyk	Trogarzo	06-03-2018
Pharmacokinetic Enhancer	cobicistat	Tybost	24-09-2014
Recent Combination Medicine	abacavir, dolutagravir and lamivudine	Triumeq	22-08-2014
	atazanavir and cobicistat	Evotaz	29-01-2015
	duranavir and cobicistat	Prezcobix	29-01-2015
	efavirenz, lamivudine and disoproxil fumarate	Symfi	22-03-2018
	bictegravir, emtricitabine and tenofovir	Biktarvy	07-02-2018
	doravirine, lamivudine and tenofovir disoproxil fumarate	Delstrgo	30-08-2018

Extracted from National Institute of Allergy and Infectious Diseases; United States Food and Drug Administration.

Table 2: Surface water sampling location for detection of antiretroviral drugs in various parts of South Africa (Wooding et al., 2017)

Sample numbe	LOCATION	ANTIRETROVIRAL DRUG DETECTED
	ROODEPLAAT DAM SYSTEM	
1	Pienaars River Inflow	Nevirapine, zidovudine, lamiduvine, tenofovir and stavudine
2	Zeekoegat WWTW Outflow	Zidovudine
3	Angling Area	Nevirapine, zidovudine, stavudine
4	S.E Bank	Nevirapine, zidovudine, lamiduvine
5	Motorboat Launch	Nevirapine, zidovudine
6	Rowing Club	Nevirapine, zidovudine, lamiduvine
7	Roodeplaat Outflow	Nevirapine, zidovudine, stavudine
	RIETVLEI DAM	
8	Southern Bank	Zidovudine, lamiduvine
9	Northern Bank	Nevirapine, zidovudine, lamiduvine
	ORANGE RIVER SYSTEM	
10	Orange River (Bethulie)	Zalcitabine, tenofovir
11	Gariep Dam Oviston	Didanosine
12	Gariep Dam (N.E)	Tenofovir
13	Vaal confluence	ND
14	Orange confluence	ND
15	Confluence	ND
	CAPE REGION	
16	Eerste Rivier	ND
17	Theewaterskloof Dam	ND
	VAAL DAM	
18	Dam wall	ND
19	Oranjeville	ND
20	Vaal Dam Inflow	Zidovudine
21	Vaal Dam Out Flow	ND
	SINGLE SYSTEM SAMPLES	
22	Hartebeesfontein WWTW Outflow	Zidovudine, lopinavir
23	Ditholo	Nevirapine
24	Hartbeespoort Dam, Meerhof (201	Nevirapine, zidovudine, lopinavir
25	Hartbeespoort Dam, Meerhof (201	Zalcitabine, Didanosine, nevirapine, lopinavir
25	Hartbeespoort Dam, Tap Water Sample	Zalcitabine, zidovudine
26	Renosterkop	ND
27	Inanda Dam	ND
28	Inanda Dam offshore	ND

ND-Below Detection Limit. Adapted from (Wooding et al., 2017) with several modifications.

The Faculty of Natural and Agricultural Sciences newsletter featured achievements of students (page 14), which included an article in this thesis that was chosen as editor's choice in March 2021.

https://www.up.ac.za/media/shared/11/ZP_NewsImages/up_nas_squaredupnewsletter_june-2021_final.zp205677.pdf

UNIVERSITEIT VAN PRETORIA
UNIVERSITY OF PRETORIA
YUNIBESITHI YA PRETORIA

SQUARED² UP

Newsletter of the Faculty of Natural and Agricultural Sciences

June 2021

www.up.ac.za/nas

In this edition:

Humans, predators and prey

By Meredith Thornton (MRI)

Large mammals shape their environment and are of great importance to the tourism and conservation industry. Research done by the Mammal Research Institute (MRI) in the Faculty of Natural and Agricultural Sciences provides invaluable information to help manage both wild and captive populations.

Researchers involved with the MRI produced some interesting research on large mammals over the last year.

Lions are apex predators that experience multiple threats due to human activity and are classified as vulnerable (IUCN Red List). Analysis by Dr Peter Lindsey and co-authors (Bauer et al, 2020) teaches us more about their distribution and numbers. Eleven threats were identified in total, with human-lion conflict and depleted food supply (resulting from the bush meat trade) emerging as the top threats. Lion conservation is a complicated problem, with many threats interacting simultaneously, which can easily result in the complete eradication of a lion population. A problem tree and root-cause analysis was used to visualise this complex situation. According to Dr Lindsay, 'The results of this study will aid conservation managers, social scientists and politicians in teasing apart the underlying issues before lion conservation can be tackled efficiently.'

...continues on page 3.

STUDENT ACHIEVEMENTS

Discovery of a rare gas-rich galaxy group with the MeerKAT telescope

Shilpa Ranchod

Ms Shilpa Ranchod, who recently graduated with a master's degree in Physics from the University of Pretoria (UP) leads an international team that reports the discovery of a large, unusual group of galaxies with South Africa's MeerKAT telescope. This result is a component of her MSc thesis, supervised by Prof Roger Deane.

Her research is focused on understanding atomic hydrogen's role in star-formation in the younger universe, and dense regions within it. To do this, she uses the 64-antenna MeerKAT telescope, the South African precursor to the Square Kilometre Array. The observations that led to this serendipitous discovery form part of the MeerKAT International GHz Tiered Extragalactic Exploration (MIGHTEE) Survey, a large collaboration of international scientists. The survey produces hundreds of terabytes of data, which are processed on the cloud computing facility hosted by the Inter-university Institute of Data-Intensive Astronomy (IDIA), a partnership between the universities of Pretoria, Cape Town and the Western Cape.

This galaxy group was identified through the detection of 21cm atomic hydrogen (HI) emission, an important component of galaxies and a key ingredient in star formation. Within galaxies, HI is diffuse and extends far beyond the extent of the stars, making HI a sensitive tracer for the dynamics of galaxy evolution, particularly how the group environment affects this.

Twenty of these HI-rich galaxies were detected, and through HI spectral line observations were identified as a large galaxy group for the first time. Some of the member galaxies have disturbed morphologies, clearly influenced by the group environment. These include an interacting pair of galaxies that will potentially merge, and a "jellyfish galaxy" exhibiting a long tidal tail. The results suggest that the group is rare and in the early stages of assembly due to a large number of HI-detected galaxies and its unsettled velocity distribution. This discovery will be published in the Monthly Notices of the *Royal Astronomical Society* journal.

Journal paper selected as Editor's Choice

A recent publication by Adedapo Adeola, a PhD student in Chemistry and Prof Patricia Forbes from the Department of Chemistry, published in *Water Environment Research* (a Wiley publication) was selected as the Editor's Choice in March 2021.

The article titled is titled "Advances in water treatment technologies for removal of polycyclic aromatic hydrocarbons: Existing concepts, emerging trends, and future prospects" (https://doi.org/10.1002/wer.1420) and is highly acclaimed.

In his Editorial entitled "The water industry toolbox" (https://doi.org/10.1002/wer.1528), Prof Baeza noted that "this article is a comprehensive review of existing and emerging technologies for remediation of PAH-polluted water... the great variety of existing alternatives for water treatment and the efforts of many researchers to advance water treatment with new proposals".

Adedapo Adeola, PhD student and first author of the paper, said that "this is a great honour, as it is recognition of the hard work put into the gathering of data and information on this subject".

Adeola is a UP-Commonwealth Scholarship holder and his research focuses on the synthesis and application of a graphene wool composite for the removal of selected organic pollutants from water. His project is also supported by Rand Water and he is supervised by Prof Patricia Forbes, who holds a Rand Water Research Chair in the Department of Chemistry.

Adedapo Adeola

Adeola has four publications from his PhD work to date. He commented that "we should be encouraged to continue to make a difference irrespective of global and regional challenges. I would like to acknowledge my supervisor, funders as well as the Department of Chemistry and University of Pretoria for providing enabling environment for my studies".